Systems for the automated 3D assembly of micro-tissue and bio-printing of tissue engineered constructs

A thesis submitted in partial fulfilment of the
requirements for the degree of

Masters of Engineering

in

Mechanical Engineering
University of Canterbury
Christchurch, New Zealand

by

Michael Lang

2012

To Annie and Leonardo.

Abstract

Tissue engineering is a field devoted to the design and creation of replacement tissues with the ultimate goal of one day providing replacement organs. Traditional strategies to accomplish this through the bulk seeding of cells onto a single monolithic porous bio-scaffold are unable to realise a precise architecture, thus the inability to mimic the cells natural micro-environment found within the body.

Bio-printing approaches are the current state of the art with the ability to accurately mimic the complex 3D hierarchical structure of tissue. However, a functional construct also requires high strength to provide adequate support in load bearing applications such as bone and cartilage tissue engineering, and to maintain the open geometry of a large intricate channel network, which is crucial for the transport of nutrients and wastes. Typical approaches utilise materials which have processing parameters more amendable for cell incorporation, thus they can be simultaneously deposited with scaffolding material. However, the resulting construct is typically of low strength.

This thesis explores the automation of a printing and "tissue assembly" process with the ability to incorporate delicate cell aggregates or spheroids within a high strength bio-scaffold requiring harsh processing parameters, at precise locations. The 3D printed bio-scaffold has a lattice architecture which enables a frictional fit to be formed between the particle and scaffold, thus preventing egress. To achieve this the pore must be expanded before the delivery of a single ϕ1mm particle. Novel subsystems were developed to automate this process and provide the ability to achieve scalable, flexible, complex constructs with accurate architecture.

A system architecture employing the benefits of modularity was devised. The main subsystems developed were the singulation device, to ensure the separation of a single particle; the injection device, to deliver and seed particles into the scaffold, and the control system, to facilitate the operation of the devices.

Three generations of singulation devices have been developed ranging from mechanical to fluid manipulation methods alone. The first prototype utilised mechanical methods, with simple control methods. However the inability to correctly position the lead particle within the singulation chamber, resulted in damage to the test alginate particles. In the second prototype a fully fluidics based device utilised two trapping sites to capture the leading particles. Singulation success rates of up to 88% was achieved. Higher rates were limited by the trapped particle's interaction with the lagging particles during capture. In a similar concept to the second prototype, the third prototype utilised only a single trapped particle, and achieved much higher throughput, and 100% singulation accuracy.

The injection device, utilised a conical expanding rod within a thin outer sheath. It was able to expand the pore, with minimal damage to the scaffold, providing an unobstructed path for the delivery of the particle into the pore.

A decentralised control system was devised to integrate the process operation for the electro-mechanical devices. Separate microcontrollers were able to sense, interact and communicate with one another, and the master control PC, to execute specific tasks to automate the process.

The development of systems to automate the process has addressed the ability to accurately incorporate delicate cells with a high strength bio-scaffold, and will enable the realisation and investigation of intricate complex constructs, unachievable with current manual processes. Thus features found within the body may be more closely mimicked and functionalised, which may provide the necessary signals, micro-environment and infrastructure to correctly regulate the formation of complex functional tissue, supported by the adequate mass transport of nutrients and wastes. This may one day lead to 3D printing or assembly of viable replacement tissue, accurate in vitro model systems for laboratory testing, or even whole organs.

Acknowledgements

The work presented in this thesis was completed and written during a period where the foundations of the beautiful city of Christchurch were scathed to say the least, by the forces of nature. There were times when other than the immediate concerns for human life, there were concerns over whether the equipment, built from scratch had survived, and whether after all the after-shocks there was enough redundancy in systems to prevent the corruption of the enormous sequences of 1s and 0s trapped within a hard drive, that was my data.

It was an experience having gone through both the large earthquakes, on 4 September 2010 and the more disastrous 22 February 2011 earthquake. It highlighted the many fragilities of life, and the foundations and essential services given to us, in which we easily take for granted. It allowed an interesting perspective, striped of distractions, focusing on the necessities of life and placing the mind back into an almost instinctive primitive state. I would like to thank however, all of the emergency workers for their tremendous efforts and utility workers for quickly restoring the lifelines of the city.

With these ramblings and experiences aside, I would like to thank the people who were more directly involved in this thesis. I would like to thank my supervisors Prof. XiaoQi Chen, Dr. Wenhui Wang and Dr. Tim Woodfield for their insightful comments and guidance, as well as their encouragement and continual challenges for me to step outside my comfort zone. I would like to thank my supervisors again for their time in reviewing and proofreading this thesis, especially Tim who painstakingly went through sections of the initial drafts, corrected my grammatical

errors, and introduced me to the exciting field of Tissue Engineering.

I would also like to thank the technicians for their help in manufacturing the prototypes, especially Jim McLean for tolerating my novice skills while I was working within the mechanical workshop during the early stages. Surprisingly, I would also like to acknowledge the New Zealand governments past and present, for providing financial assistance schemes, and the Mechanical Department for funding during the final stages, without which this work might not have been possible.

I would also like to thank Myrthe van der Ven, Anthony Chan and Ben Schon for supplying the fixed cartilage spheroids, as well as supplies to produce alginate beads. I am sure there were others that I have regrettably failed to mention, but they will know who they are.

Finally, I would like to thank my parents, who have engrained in me the virtues of hard work, and have given me the freedom and support, to enable me to foster my interest and thirst for knowledge. Last, I am grateful to my beautiful and loving partner Annie, for her support and endurance throughout the entire process, and all the events in between.

Contents

Chapter 1

Introduction

Tissue loss or damage in the body is a common occurrence, due to disease or trauma. In some cases the body has repair mechanisms which enable the regeneration of damaged tissue such as bone. However in other cases significant loss of tissue exceeding the bodies regenerative capabilities, especially in old age, may result in severely reduced tissue function, greatly impacting on the quality of life. Medical intervention is thus required.

Current surgical approaches for the treatment of tissue loss involve the replacement of tissue from either a biological or man-made source such as the replacement of joints, mechanical heart valves or vascular prostheses [1]. However current replacement approaches have limitations which inhibit the long term success of the treatment, such as the need for periodic revision of implants due to wear, loosening, growth of paediatric patients, or the severe side-effects of immunosuppressive drugs required for organ transplants. Furthermore there is a growing shortage for replacement organs. To address these issues, the field of tissue engineering and regeneration has emerged.

Tissue engineering is a growing area involving a wide multidisciplinary field encompassing engineering, biology and medical sciences [2]. It is a field which focuses on the development of techniques and strategies for the regeneration of functional tissue and may offer significant advantages over current surgical

methods to repair or replace damaged tissue [3]. Although tissue engineering may be focused on applications for replacement tissue, the impact is far broader and could greatly accelerate drug development [4], providing highly accurate model systems for study, reducing the gap between cell cultures and physiological tissue [5].

The general strategy is to promote cells to undergo healing processes and synthesise new repair tissue, by combining cells and a 3D porous degradable bio-material [6]. Traditional methods inoculate a prefabricated porous structure (scaffold) with patients cells, which are then cultured along with growth factors, to regulate and promote tissue formation in the lab [7].

The common approach is to seed suspended cell onto a scaffold before implantation back into the patient. Other strategies are the implantation of cells into the damaged site alone, or the implantation of a scaffold alone for cell recruitment within the body [4]. Challenges for the success of the approach, include the methods of assembling cells and scaffolding material, the sourcing of sufficient number of appropriate cells and the integration of the construct into living systems [6].

An important aspect to tissue engineering are the methods and techniques for integrating and controlling cells, scaffolding and bio-molecular materials, which are known as "construct technologies" [6]. Construct technologies deal with the methods which assemble the cells, to produce an environment to promote healing, thus cells can undergo effective synthesis of new repair tissue.

Tissue within the body is a structured and hierarchical 3D arrangement of cells and extracellular matrix (ECM). Cell function within the body is orchestrated by a highly complex, and dynamic spatial and temporal interaction with physical and bio-molecular stimulus. Thus it is reasonable to assume that promotion and support for the desired level of cell function, require certain aspects of the micro-environment to be initially established and recreated, that is bio-mimicry to occur.

Traditional approaches utilising bulk cell suspension seeding methods onto a monolithic bio-scaffold, which rely on cell adhesion dynamics are unable to realise

the precise spatial locality of cells within the construct. Thus the inability to mimic the desirable natural micro-environment. Numerous other approaches to the assembly of constructs attempting to mimic certain aspects of natural tissue have been investigated, however none have achieved a fully successful outcome [8].

A novel tissue engineering construct technique currently being explored by the Christchurch Regenerative Medicine and Tissue Engineering (CReATE) group address a number of limitations over the traditional approaches, including the potential to mimic the precise spatial locality of cells. However, biological studies are currently limited by manual assembly methods to small simple plain constructs. For larger more complex constructs to be realised, a concurrent printing and cell incorporation process most suited for robotic systems is needed.

In this thesis the automation process to realise the tissue engineering construct technique currently being investigated is explored. A state of the art investigation is conducted on tissue engineering construct technologies to determine the major limiting themes across the various construct techniques, and how they relate to the current automation process and construct technique under investigation. The development, testing and evaluation of the subsystems necessary for the automation process are also described.

The following publications have resulted from this work:

- M. Lang, X. Chen, W. Wang and T. Woodfield, "Injection System for Cellular Assembly of 3D Bio-Tissue Engineered Constructs", in *2012 IEEE Conference on Automation Science and Engineering (CASE)*. (Accepted for publication and presentation. Nominated for Best Student Paper).

- M. Lang, W. Wang, X. Chen, and T. Woodfield, "Integrated system for 3D assembly of bio-scaffolds and cells", in *2010 IEEE Conference on Automation Science and Engineering (CASE)*. IEEE, Aug. 2010, pp. 786-791.

- T. B. F. Woodfield, M. Lang, X. Chen and W. Wang, *New Zealand provisional patent*: 587478, "System and method for 3D tissue assembly", Aug. 2010.

1.1 Thesis Objectives

The primary objectives of the thesis are:

(I) To develop proof of concept for individual subsystems to automate the novel tissue engineering construct technique.

(II) To validate the systems and gain insight into the processes including such aspects as the throughput and accuracy of the systems and possible limitations of the concept.

1.2 Thesis Overview

Chapter 1 presents an introduction and a brief background into the field of tissue engineering.

Chapter 2 presents a literature review into the state of art in tissue engineering construct technologies and aspects which currently need addressing.

Chapter 3 presents the construct technique for integrating cells and scaffolding material, and the envisioned fabrication processes. Followed by the design and architecture of the systems, to implement the requirements of the processes.

Chapter 4 presents the development of the instrumentation and electrical systems for the control of individual electro-mechanical subsystems, and integration of system and process.

Chapter 5 presents the first prototype for the singulation of spherical particles. A device using mechanical separation mechanisms is investigated.

Chapter 6 presents the second singulation prototype with a fully fluidics based singulation device, through fluidic flow path manipulation and the trapping of two particles.

Chapter 7 presents the third vastly improved prototype, utilising a simpler fluidic flow path manipulation sequence and the trapping of a single particle.

Chapter 8 presents the development and validation of the novel injection device which expands a pore to provide an unobstructed path for the delivery of a single particle into the pore. After which the device is retracted and the particle becomes confined within the pore.

Finally a conclusion of the work is given in Chapter 9 and the direction for future work is discussed and suggested.

Appendices A-B provide the different mechanical drawings, electrical worksheets, and software outlines for the systems.

Chapter 2

Tissue Engineered Construct Technologies Literature Review

2.1 Introduction

The development of construct technologies for tissue engineering is an important aspect and challenge in the success of tissue engineering, among many cell technological challenges, such as the selection of cell types, the availability and sourcing of sufficient number of cells, followed by the eventual integration with living systems [6]. Construct technologies deal with the methods and technologies of assembling and integrating cells, bio-molecular, and scaffolding material into a construct which promote cells into the synthesis of new repair tissue.

Tissue within the body is a highly complex micro-environment with a vast supporting infrastructure. Each tissue type comprises of many different cell types and extracellular matrices (ECMs), which are assembled into a highly organised three dimensional architecture at different length scales [9]. The form and function of each tissue type is cooperative, hierarchical and highly optimised to achieve its physiological function.

The function of cells within tissue is regulated by a symphony of dynamic and interacting stimulus, both physical and bio-chemical, in both spatial and temporal

dimensions in their specific micro-environment [4]. The ultimate decision of a cell to differentiate, proliferate, migrate, apoptose or perform other cell specific functions is an orchestrated response to the stimulus [10], as well as the bidirectional or dynamic reciprocity of interaction between the cells and their environment [11].

In addition to the signalling processes, cellular function is supported by a vast interwoven infrastructure, ensuring adequate mass transport rates of waste and nutrients in and out of the micro-environment are meet [12]. Cells within the body are typically found no more than 100-200μm from the nearest support network or capillary [13]. This spacing provides the adequate balance between the nutrient and waste diffusion limited transfer rates, to support and maintain viable tissue [14]. However some cell types such as cartilage cells, which have low metabolic requirements, represents the extreme case and can remain viable in constructs over 1mm.

The ability to mimic and manufacture such a complex and dynamic cellular environment in the regulation and support of cellular function is a challenging task *in-vitro* thus it is not surprising to date that simple, traditional, construct techniques have had limited success.

In this review construct technologies beginning with traditional approaches as well as emerging technologies, will be reviewed against the ability to recreate and mimic aspects of the complex 3D micro-environment such as the ability to recreate the 3D hierarchical spatial distribution of cells, construct strength and the main limiting factor, the ability to realise a vast interwoven conduit network to improve the mass transport of nutrients, oxygen and water soluble metabolites through convective mass transport.

2.2 Top Down Construct Technologies

Traditional top down methods rely on the inoculation of cells onto the scaffold surface. They are classified as top down due to the design principles where the most abstracted high level view of the construct is described as the construction of a single monolithic scaffold, and subsequent bulk seeding of cells, as opposed

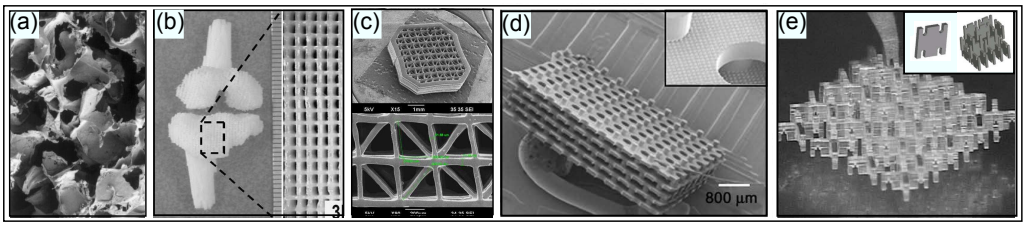

Figure 2.1 – *Bio-scaffold fabrication approaches: (a) SEM micrographs scaffold cross-section fabricated by particle-leaching [16]. (b) Scaffold fabricated with fused deposition modelling showing anatomically shaped structure and controlled pore architecture [17]. (c) Scaffold fabricated using µSLA technologies [18]. (d) Microfabrication of scafold through the stacking of planar layers [19]. (e) Robotic microassembly of micro-modules [20]. Adapted from [21].*

to methods which build the construct from smaller individual modules. Top down designed scaffolds are typically porous bio-degradable structures on which suspended cells can adhere, proliferate and infiltrate; where the cells self assemble or remodel the entire structure into the desired functional tissue [15].

2.2.1 Top Down Scaffold Fabrication

Methods of fabricating porous scaffolds have included simple techniques such as porogen leaching and gas foaming approaches [16], to more sophisticated and controlled architectural approaches (Fig. 2.1), utilising additive manufacturing methods such as fused deposition modelling (FDM) [17], laser sintering, stereo lithography (SLA) [22], μSLA [18], laser micro-machining, micro-fabrication [19], [23] and robotic micro-assembly [20]. The use of computer controlled technologies enable much greater accuracy over the internal and external architecture, where the porosity and interconnectivity of the construct can be precisely controlled. This is beneficial as the orientation, interconnectivity, size, and surface chemistry of the pores have been reported to affect proliferation, migration and differentiation, which are all desirable properties for tissue engineering [24]. The control also enables constructs which resemble the external geometry of the tissue to be replaced, enabling a template for tissue formation in addition to the benefits of controlled pore distribution.

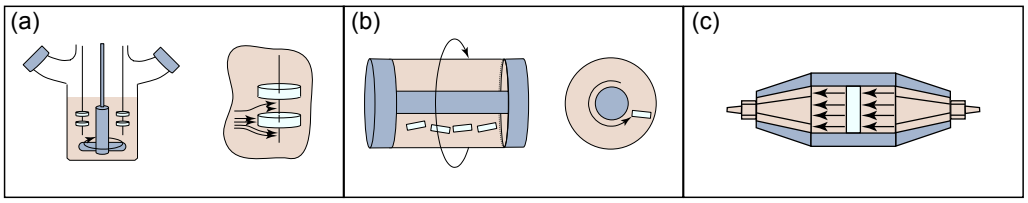

Figure 2.2 – *Dynamic bio-reactor based seeding methods - (a) Spinner-flask. (b) Rotating-wall vessel. (c) Direct perfusion where medium flows directly through the pores of the scaffold. Adapted from [25].*

Cell Seeding After the process of scaffold fabrication cells need to be incorporated with the scaffold. Top down approaches rely on bulk seeding methods and typically rely on the adherence of cells onto the scaffold surface for integration. The constructs can be seeded and cultured in the same device known as a bio-reactor, which provides a physiologic environment to correctly regulate tissue formation [26]. The seeding methods can be classified as static seeding, where the construct is placed in a cell suspension with no fluid flow, or dynamic seeding where fluid flow is introduced. Various methods have been explored to introduce fluid flow including, spinner-flask, rotating wall and direct perfusion methods (Fig. 2.2) [25]. However the seeding approaches do not enable precision control over the spatial distribution of cells and seeding efficiency remains relatively low, thus limiting the ability of the construct to mimic the hierarchical structure of native tissue.

2.2.2 Top Down Vascularisation Methods

A critical aspect for the success of clinically relevant functional tissue is the vascularisation of the construct. Without the adequate mass transport network throughout the construct to support cellular function, cell necrosis within the interior of the construct will occur. The aforementioned top down methods have utilised interconnected pores as a form of pseudo vasculature to increase the perfusability, however realisation of a more complex channel network has been limited. Vascularisation of scaffolds have traditionally relied on the spontaneous vascularisation of the scaffold once implanted, however the natural healing pro-

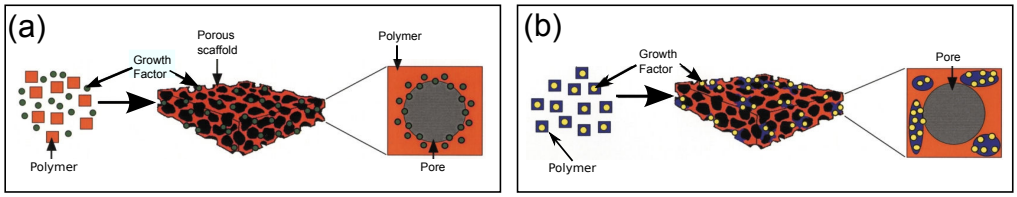

Figure 2.3 – *Schematic of scaffold fabrication with growth factor release - Growth factors can be incorporated into the polymer by either mixing with polymer particles before processing (a), or the pre-encapsulation of factors into polymer micro-spheres, used to form scaffolds (b). Adapted from [28].*

cesses are generally too slow to create the necessary vasculature needed to support the adequate mass transport to the interior of the construct [27]. Thus other strategies to increase the rate of vascularisation and pre-vascularisation of initial conduits have been investigated.

Indirect vascularisation methods

In-vivo vascularisation One strategy to increase the rate of vascularisation is to enhance the ingrowth of host vasculature [27]. This is typically achieved through the introduction of pro-angiogenic factors which stimulate blood vessel formation [28]. A number of approaches to introduce this into the construct have been investigated. One simple approach is to coat or bulk load the scaffold with growth factors during the scaffold processing (Fig. 2.3(a)) [29]. However there are limitations with this approach in targeting the drug to areas of need and the lack of control over the temporal release profiles [30]. Another approach which address these issues, is through the encapsulation of growth factors within micro-sphere bio-materials (Fig. 2.3(b)), which can be subsequently incorporated into the final tissue construct [28]. With this approach the temporal release profiles can be tailored through the degradation of the encapsulating material, and the micro-spheres can provide more selective localisation. An example of this is a multiple staggered growth factor release scheme, where the drug loaded micro-spheres were compacted and processed into a continuous scaffold before implantation into the

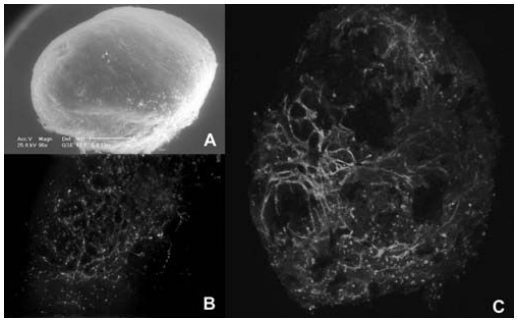

Figure 2.4 – *Endothelialisation without artificial angiogenic factor introduction - SEM image of a co-culture spheroid. Scale bar = 200μm. (b)-(c) Immunostained spheroid, showing the formation of a 3D prevascular network. Images were made using conventional fluorescent microscope (b), or a convocal fluorescent microscope (c). Adapted from [33].*

incemic hind-limbs of mice [31]. A high blood vessel density and high level of stabilised mature vessels within the scaffold were reported. The formation of mature stabilised vessels is important in creating a functional vascular network as immature vessels have been found to be disorganised, leaky and hemorrhagic, where loss of blood through the vessels occurs [32].

In-vitro pre-vascularisation Enhancement of vascularisation through the release of pro-angiogenic factors are typically in-vivo strategies which rely on the ingrowth of vessels from the host after implantation. Another strategy is to pre-vascularise the construct in-vitro after adding endothelial cells (ECs) to other tissue [33]. It has been demonstrated that ECs have the ability to self organise into mature stabilised vessels without the introduction of artificially introduced pro-angiogenic factors (Fig. 2.4) [33, 34, 35]. Pre-vascularisation is beneficial as the construct can be vascularised in a much shorter time span, due to the ingrowing vasculature of the host requiring only to reach the pre-existing network and not to the interior. Furthermore the approaches typically avoid the artificial introduction of unregulated pro-angiogenic factors, which may negatively influence other cell types within the construct.

Both the introduction of angiogenic factors and in-vitro pre-vascularisation through the introduction of EC's have proven the ability to enhance vascularisation and form high levels of both immature and stabilised mature blood vessels within

the construct, however the lack of control over the process, result initially in a non functional perfusable vasculature. For the network to become functional further remodelling of the construct is required, where the time required for the process may not adequately maintain cell viability throughout the entire construct and cells in the interior undergo necrosis.

Direct Vascularisation Fabrication Methods

A more directed and instantaneous approach to forming vasculature is to directly pre-fabricate the required conduits and network, however such an approach is a huge challenge and is viewed as one of the greatest challenges in the formation of large functional tissue [13]. Although the aforementioned methods improve perfusion of the construct and to some extent form a pseudo vasculature through the introduction of interconnected pores, the non-physiological fluid flow conditions through the network [36] may not provide the appropriate biological and physical 3D gradient field for the proper remodelling or function of cells. It has been reported that even when induced stabilised vessels are formed, they regress in time in the absence of true physiological demand [37].

To recapture more bio-mimetic features such as channel profile, and the hierarchical networks such as the reduction of channel diameters to fine intricate structures of capillaries, micro-fabrication approaches have been employed [38, 39]. The channels are typically fabricated by casting the desired material into high resolution micro-fabricated moulds [36, 40, 41, 42].

In a simple micro-fabrication approach, investigation of cell laden hydrogels have been explored with a single straight channel [36, 43, 44, 45]. In one example Ling et al. [43] employed agarose, a thermally reversible hydrogel material to encapsulate cells. Agarose is a naturally derived polymer whose cell encapsulation characteristics have been demonstrated in a variety of applications. It is bio-compatible in-vivo and furthermore cells continue to secrete their own ECM in the encapsulated state. Ling et al. [43] bulk seeded hepatocytes into agarose while a single channel was formed from casting into a micro-fabricated silicon

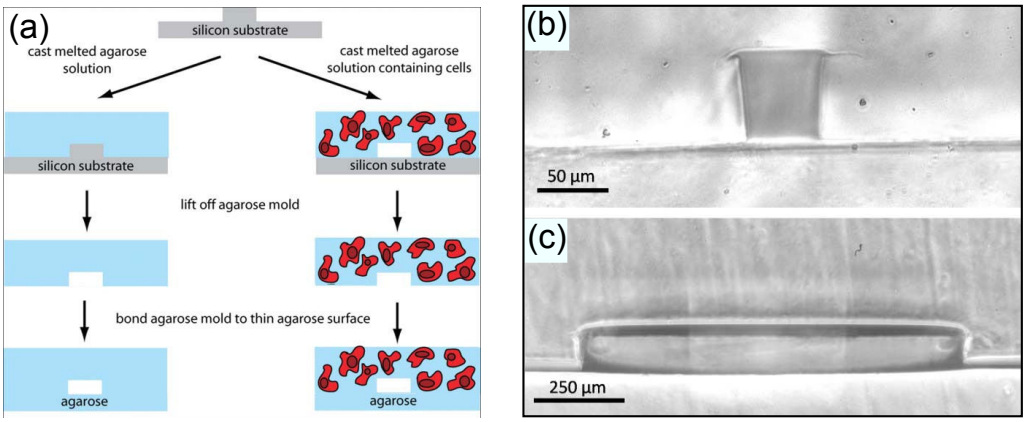

Figure 2.5 – *Single Channel Micro-fabrication. (a) Schematic of fabrication process for agarose micro-fluidic device with (right) and without (left) embedded cells. (b-c) Light micrograph cross-sectional images of agarose channels with small aspect ratio (b) and wide aspect ratio (c). Adapted from [43].*

mould (Fig. 2.5). When medium was perfused through the channel the viability of cells were reported to remain high up to 200μm from the channel, with viability decreasing moving further away from this region. Significant decreases in cell viability after 3 days of perfusion in regions ~1000μm from the channel were reported. The non perfused construct faired badly in maintaining high cell viability over time. The simple experiment demonstrated the ability for a perfused channel in maintaining high cell viability within the interior of the construct and the ability to grow ECs to confluent layers within a 3D environment. However a single channel is not sufficient to maintain a large construct, and instead a branching interwoven network is required.

To achieve complex branching channel networks, another micro-fabrication approach has been employed by Fidkowski et al. [42]. A novel bio-material poly(glycerol sebacate) (PGS) was cast from a micro-fabricated silicon mould to form interconnected branching channels (Fig. 2.6(a)). The rectangular channels formed ranged from 3mm at the connection points, to 45μm at the finest channel with a constant channel height of 35μm. The dynamically seeded endothelial cells grew to confluence in some regions within 14 days (Fig. 2.6(b)). Cells were reported to remain viable under culture conditions for at least 4 weeks. Another investigation into the creation of a vascular network by Borenstein et al. [36]

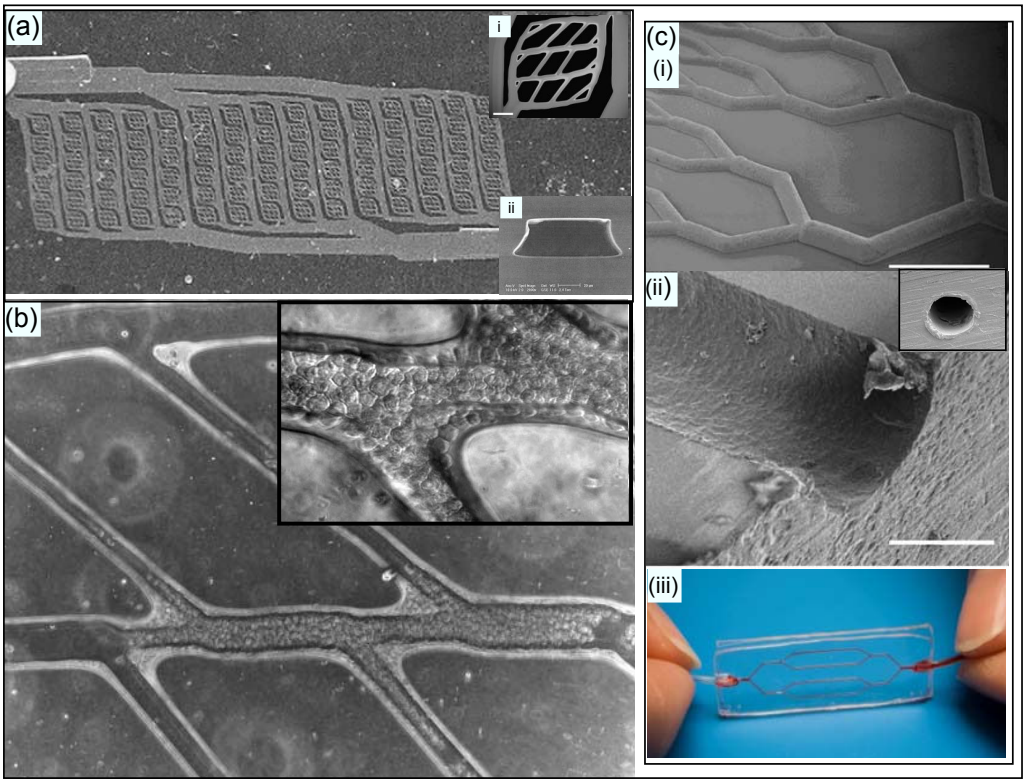

Figure 2.6 – *Micro-fabricated channel network. (a) The patterned PGS film channel network device with external connections to external circulation. (ii) Fluorescent microscopy of capillary network. Scale bar = 500μm. (ii) Cross-sectional view of bonded capillary after cure. (b) Photomicrograph of endothelialised capillary network. Adapted from [42]. (c) Micro-fabricated channel network enabling smooth fluid flow. (i) SEM image of Cu electroplated mould on a silicon substrate, showing four levels of smooth vessel bifurcations. (ii) SEM image of polystyrene film hard-embossed using the mould. Inset showing the sealed circular cross-section with no bond interface. (iii) Photo of device with integrated external tubing. Adapted from [36].*

was also explored. However channels with circular cross sections and smooth transitions at the point where the channels split (bifurcations) were fabricated in polystyrene (Fig. 2.6(c)). This was pursued to enable smooth flow conditions within the channel, providing more physiologically relevant signals for vascular remodelling. Both the approaches demonstrated the ability for cells to grow to confluence within the channel and remain viable for a long period of time, however a number of limitations were highlighted. These included the inability to embed cells into the bulk of the scaffold, due to the harsh processing parameters, the lack of control over seeding procedures resulting in inhomogeneous seeding densities,

and the inflexibility of the process.

2.3 Modular Bottom Up Methods

The assembly of modular units has emerged to address the critical limitation of spatially positioning different cell types at specific locations. These approaches known as bottom up methods of assembly, approach the problem of construct realisation through the assembly and integration of small discrete modules. While that of top down approaches typically utilise a single monolithic scaffold structure, subsequently inoculated with cells in a secondary bulk process. Bottom up approaches can address the issue of scalability and heterogeneous cell distribution, due to the possible combination and arrangements of modules and module types. Thus the potential for constructs to mimic the 3D hierarchical structure.

The modules can consist of single cells, scaffolding material or both. A typically utilised scaffold material or delivery vehicle for cells are hydrogels. Hydrogels have mechanical and structural similarities to many tissues in the body and the ECM [46] and can be sourced naturally or synthetically. They are hydrophilic polymers in a 3D cross-linked network [47] and in general are highly permeable to oxygen, nutrients, and other water soluble metabolites, which give them excellent characteristics for cell encapsulation [48]. In addition to the investigation of material types, several aspects to modularity have been investigated such as the size, shape, processing of modules, and techniques for the assembly of the modules [8, 49, 50].

Such investigations have resulted in the emergence of technologies such as modular cell-laden hydrogels, and bio-printing.

2.3.1 Modular cell-laden hydrogels

One approach to achieving modularity is through the assembly of macro-scale blocks. These blocks consist of cells which are encapsulated in scaffolding material [51, 52]. A variety of approaches have been investigated for the assembly of these hydrogel blocks into constructs, from random methods [53], directed assembly of

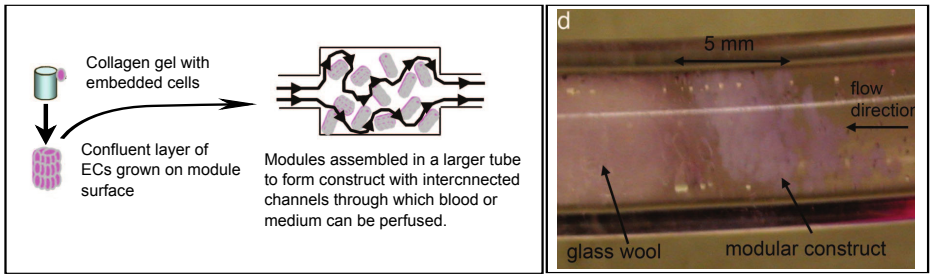

Figure 2.7 – *Modular construct fabrication. (a) Collagen rods with or without encapsulated HepG2 cells are seeded with HUVEC cells until complete coverage of the collagen rod surface with HUVEC is complete (2-3days). The rods are then assembled into a cavity shown as a tube, where the construct is perfused. Assembly of the modules created a network of interconnected channels throughout the construct. Blood or medium is perfused to supply appropriate mass transport of waste and nutrients. (b) Modular construct within the fluidic circuit being perfused with PBS. Adapted from [55].*

modules into solid free-standing constructs [54], or the containment of modules within a conduit [55].

An early attempt to assemble hydrogels into a macro-scale construct by McGuigan and Sefton [55] involved the packing of modules into a cavity. Individual rod shaped modules were confined into a perfusable cavity (Fig. 2.7). Endothelial cells (ECs) were cultured to confluence on rod surfaces and model cells (hepatoma cells) were encapsulated within the rod. The construct was perfused with both whole blood and culture medium for comparison. High cell viability up to one week, with delayed blood clotting was reported. The approach demonstrated the ability to perfuse and maintain a scalable interconnected porous construct, with relatively high cell density, however limitations exist in the ability to achieve more complex constructs. These include the random placement of the individual modules, and the difficulty in realising more intricate constructs using a packed cavity approach.

To address the issue of the random assembly and to achieve more complex 3D structures, the approach described as “directed assembly” have been investigated [52]. Directed assembly enables greater control over both the external and internal architecture of the modules. Modules are typically directed to assemble into various configuration, before a secondary bonding process.

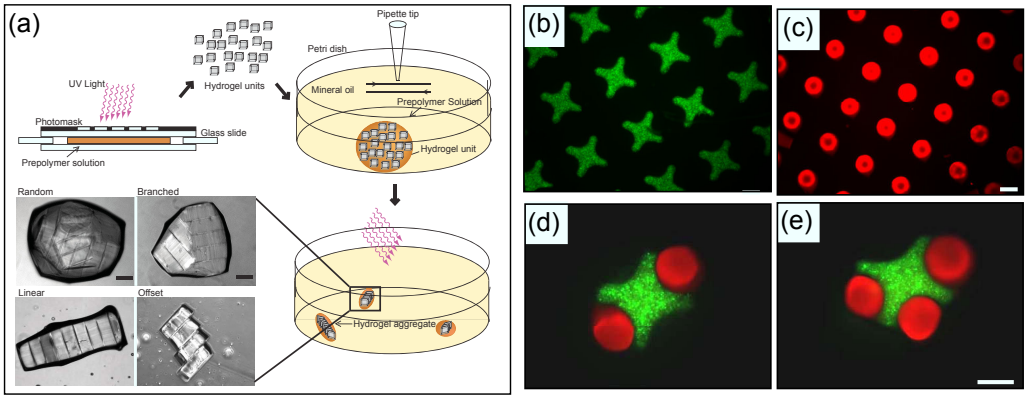

Figure 2.8 – *Schematic diagram of assembly process. (a) Micro-gels were fabricated using photo-lithography, transferred into mineral oil then subjected to agitation through the manipulation of a moving tip. Four micro-gel assembly structures were observed: linear, branched, random and offset. (b-c) Fluorescent images of lock (b) and keys (c). (d-e) Directed assembly of lock and key - Fluorescent images of two rods per cross (d) and three rods per cross (e). Adapted from [56].*

An early investigation into free-standing directed assembly, involved the mechanical agitation of solution to promote aggregation, where the modules would aggregate and pack in various arrangements (Fig. 2.8(a)) [56, 57]. The modules were reported to pack in a more structured fashion, however the positioning of the individual modules were still random. Progressing from this approach modules of two different shapes which were inter-lockable, were fabricated (Fig. 2.8(b-c)), resulting in more structured alignment, and mechanical packing of the modules, described as the "lock and key" method (Fig. 2.8(d-e)). The geometric constraints enabled a more structured internal architecture but only small structured regions were reported (∼10%), in addition it would be difficult to control the external geometry from a random agitation based method alone.

In a similar method, improvement in the porosity of the construct was explored through the utilisation of modules which did not geometrically fit together [58]. The geometry of the modules resulted in gaps or pores forming between adjacent modules (Fig. 2.9). Different module shapes were investigated including squares, circles and star modules (Fig. 2.9(a)). These were randomly assembled within a mould and bonded before perfusion (Fig. 2.9(b)). The star shaped modules were reported to have the greatest porosity and interconnectivity (Fig. 2.9(c)).

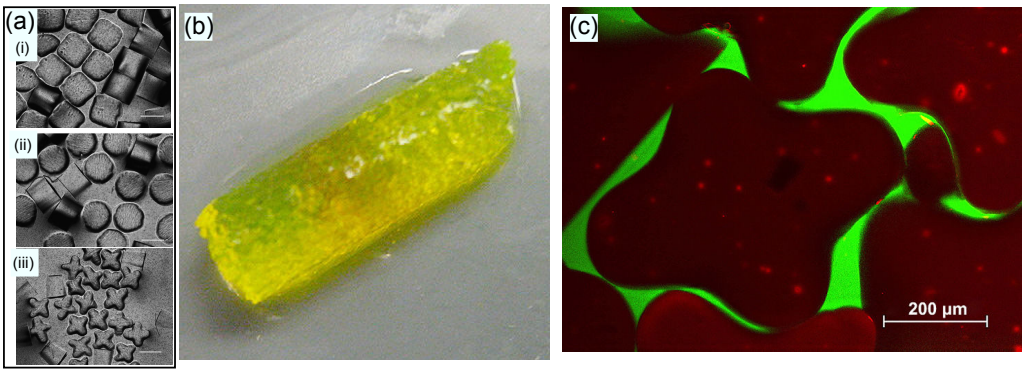

Figure 2.9 – *Directed Assembly of porous micro-gels. (a) Investigated module shapes, rectangles (i), circles (ii) and stars (iii). (b) Assembled and bonded constructs. (c) Fluorescent image of star modules showing porous structure. Adapted from [58].*

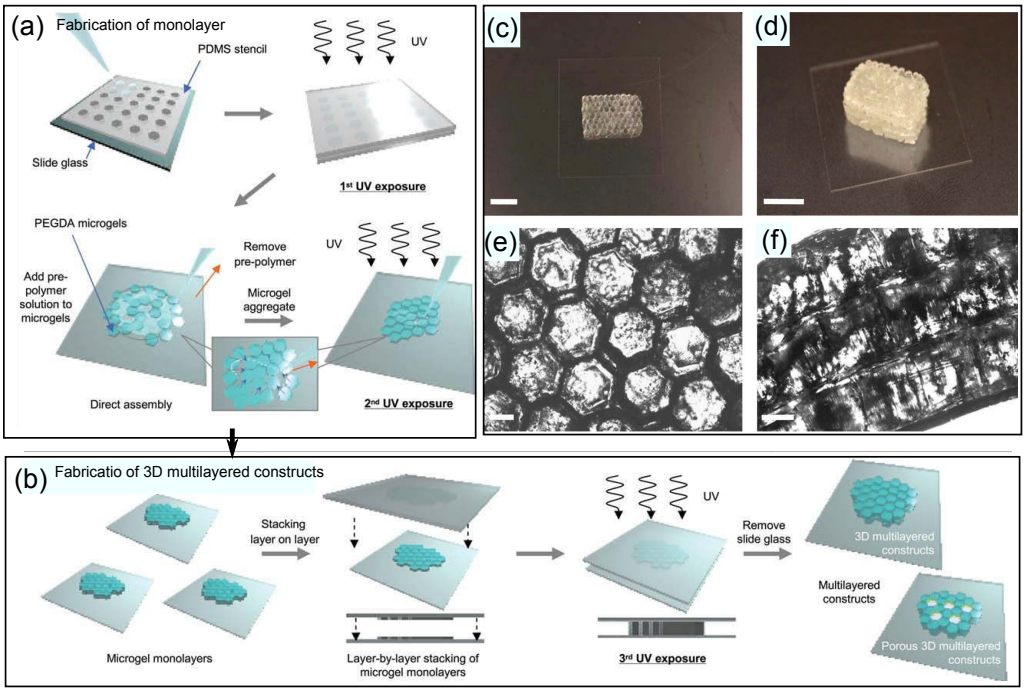

Figure 2.10 – *Schematic diagram of template based method of assembly. (a) Micro-gels and micro-gel monolayers were fabricated by photo-lithography. Monolayers were assembled by placing micro-gels onto a slide with pre-polymer solution. Removal of the solution would result in the aggregation of modules. A subsequent cross-linking process was performed to bond modules. (b) 3D constructs were fabricated by stacking monolayers layer by layer on a glass slide. Pre-polymer solution was added between layers and stabilised though cross-linking by exposing the entire construct to light. (c) Photograph of assembled construct. (d) Perspective photograph of assembled construct. (e) Microscope images of construct top view. (f) Microscope images of construct side view. Adapted from [54].*

To achieve higher levels of module alignment, placement and increased mass transport, the use of templates have been explored, enabling constructs with greater control over the internal cell distribution and controlled porosity (Fig. 2.10) [54]. Templates were utilised to fabricate monolayers and position the hydrogel modules accurately, where the removal of excess pre-polymer solution caused the modules to aggregate (Fig. 2.10(a)). A secondary photo-initiated cross-linking process was used to bond the modules together. To realise the pores, sacrificial alginate modules incorporated into the construct was utilised. The process is repeated layer by layer to achieve a free-standing 3D construct. Although the process enabled higher control over the placement of modules, a degree of uncertainty remained in the process. This is the potential for the modules to disorganise during the removal from templates. Thus once aggregated the module position may be different to the template.

To achieve complex three dimensional shapes the use of moulds or physical template surfaces have been explored in the assembly of modules [53] . The approach described as "micro-masonry" utilises a PDMS mould to confine and restrict the subunits to produce defined 3D structures (Fig. 2.11). Polyethylene glycol (PEG) micro-gel subunits were formed form a solution of PEG-dimethacrylate with a photo-initiator and exposure to UV light. These were spread over a PDMS template surface, where upon the removal of the solution, capillary forces would bring the blocks into a densely packed arrangement. This would result in a "brick wall" like structure forming around the template. The assembly is then exposed to UV for a second time, cross-linking the remaining solution and bonding the units together.

Cell laden approaches described thus far, have typically addressed the issue of controlling the modules internal and external architecture, and have increased perfusability through the introduction of pores and pore interconnectivity. However the realisation of a bio-mimetic branching vasculature network has not been addressed. An approach which attempts to address this issue, involves the assembly of torus shaped micro-units [59]. The units were assembled through the manual swiping of a needle which induced the aggregation of the modules into

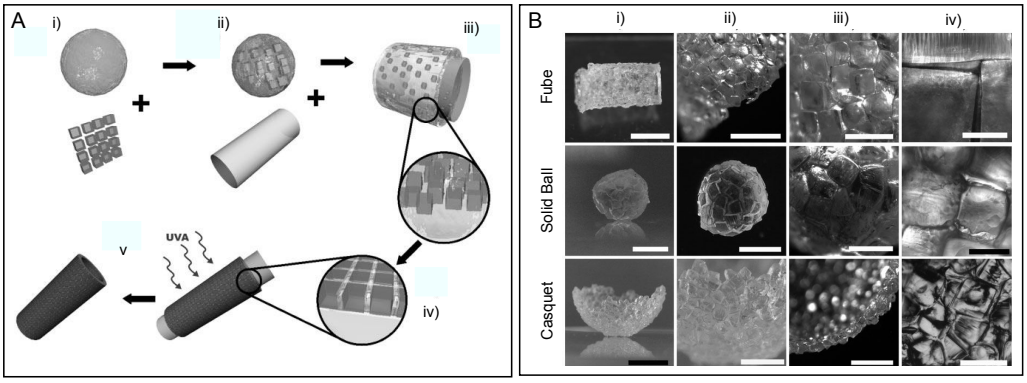

Figure 2.11 – *Micro-masonry. (a) Schematic diagram of the assembly process. Microgel modules of desired shapes were produced using photo-lithography and mixed with a solution containing pre-polymer (i). The solution with the micro-gel units was poured on a PDMS mould (ii) where it spread on the PDMS surface (iii). The removal of excess per-polymer solution induced the aggregation and packing of the modules (iv). The assembly was exposed to light to cross-link the pre-polymer on the units, followed by the subsequent separation of the PDMS template (v). (b) Structures constructed by micro-masonry. Each row presents different structures, with columns presenting increasing magnification. Adapted from [53].*

tubes (Fig. 2.12(a)). A range of tube lengths were assembled, with the maximum length reported to be 6mm. Branched tubes were achieved by the introduction of modules containing multiple lumen (Fig. 2.12(b-c)). The possibility of assembling more complex structures was pursued, where multiple tubular structures in a single construct was demonstrated through the introduction of the "lock and key" concept once more (Fig. 2.12(d)). The approach assembled constructs comprising of a series of linear tubes arranged around the key, however branching between the linear tubes was not achieved. Branching between these structures would require a branching module connecting one linear tube to the other. Such an aligned branching element maybe difficult to achieve with the described needle swiping assembly approach.

2.3.2 Bio-Printing

Approaches utilising robotic systems in the assembly of discrete modules have emerged to address the limitation in achieving precision defined modular internal and external architecture. These approaches have been referred to as bio-printing, utilising computer aided processes for the deposition and assembly of living and

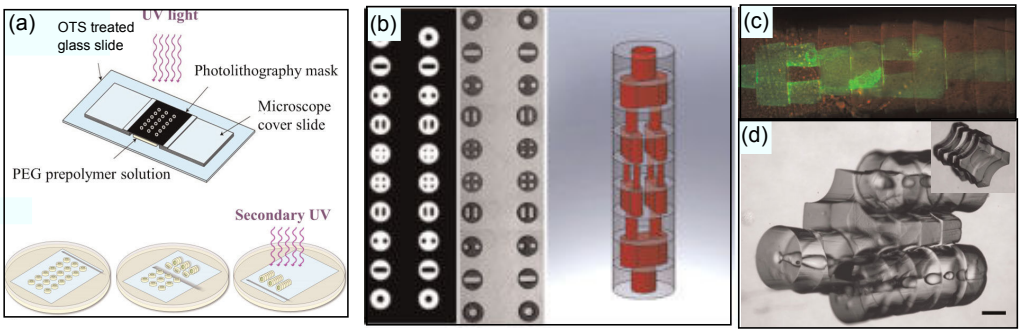

Figure 2.12 – *Sequential assembly of cell ladin hydrogels to form lumen channels. (A) Schematic of the micro-gel assembly process: Glass slides containing a prefabricated array of micro-gels was immersed in mineral oil and the micro-gels were assembled into structures by swiping a needle underneath. The assembly is subsequently stabilised by a secondary cross-linking. (B) Design and microscope images of the micro arrays which can be assembled into tubular structures with branching lumens. (C) Phase microscope images of the micro-gel assembly with branching lumen.(E) Perfusion of bonded tubular micro-gel assembly with branching lumens by a suspension of green fluorescent micro-beads in Dulbecco's Phosphate Buffered Saline (DPBS). (F) Microscope image of lock and key assembly after secondary assembly. Inset: Microscope image of cross shaped micro-gel primary assembly. Adapted from [59].*

non-living materials with an organised 2D or 3D architecture [60]. 3D printing approaches have included the precision placement of modules ranging from the macro-scale, with the extrusion of cell aggregates and scaffold encapsulated cells, to the jetting of single cells onto scaffolding material [50, 61, 62, 63].

Micro-scale Bio-Printing Technologies

Micro-scale bio-printing such as inkjet and laser jet printing technologies, approach modular assembly at the lowest resolution, attempting to mimic the construct on the cell level. The approach utilises the jetting of a carrier fluid containing cells onto a flat substrate [61, 62]. The carrier fluid may also contain a scaffold pre-cursor, in which case scaffold material is simultaneously deposited [64, 65]. To date the most prevalent micro-scale bio-printing technologies are inkjet and laser based approaches.

Inkjet Inkjet approaches to the placement of cells, utilise and modify conventional inkjet printer cartridges. In bio-printing, ink from the cartridges have been replaced with solutions containing a cell suspension, or "bio-ink" where droplets

are deposited onto a substrate [66]. The bio-ink may also contain a polymer pre-cursor resulting in the simultaneous deposition of cells and scaffolding material [67]. Two predominant mechanisms have been utilised for the formation of the jet, these are thermal and piezoelectric approaches [68]. The mechanism for thermal ink jetting utilises the generation of an expanding bubble, generated by a heating element. The temperature of the heating element is quickly raised to several hundred degrees Celsius, where bubble generation occurs in appropriate conditions. This expanding bubble forces fluid out of the orifice where a jet is generated. Heating of the surrounding fluid is minimised by the short heating pulse, thus cells are not exposed to the high temperatures.

In piezoelectric jetting mechanisms, a piezoelectric element deforms, causing the contraction of the fluid reservoir. This induces the jetting of the fluid from the orifice. Relaxation of the element then causes the fluid reservoir to return to its original volume drawing in more fluid.

Inkjet methods have the potential to deposit small volumes of fluid and single cells with high accuracy, without the need for an overly complicated setup, however there are a number of issues that limit its application. These include the tendency of the orifice clogging with high cell suspension concentrations, and the limited range of viscous solutions that can be jetted through the orifice [69].

Laser Jetting To address a number of inkjet related issues, the use of highly focused lasers to generate jets, requiring no orifices, have been investigated for the deposition of cells. The approach enables higher throughput potential compared with inkjet approaches with no clogging potential of the nozzles, and the ability to jet more viscous materials [68].

A number of approaches to apply a pulsed laser to jet or direct cells have been investigated. The most common laser based direct write approaches for cellular applications are laser-induced forward transfer (LIFT), absorbing film-assisted laser induced forward transfer (AFA-LIFT), biological laser processing (BioLP), matrix-assisted pulsed laser evaporation direct writing (MAPLE DW) and laser guided direct write (LG DW) [70].

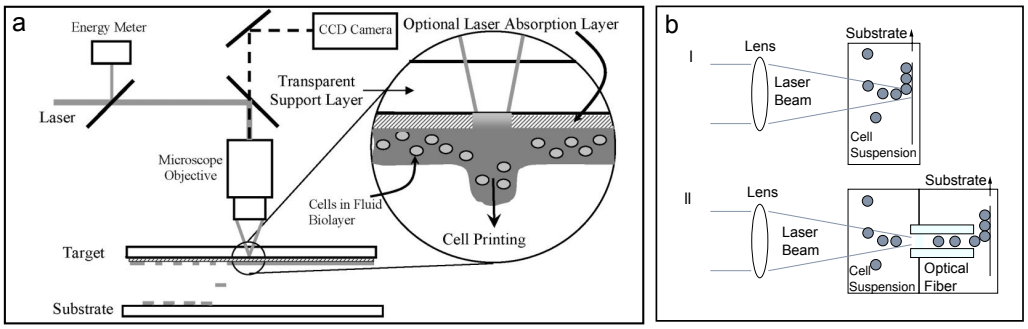

Figure 2.13 – *Laser based jetting and guidance appraoches - (a) Schematic of modified-LIFT based methods of jetting. Adapted from [68]. (c) Laser guided direct write method (i) and LGDW coupled with a hollow optical fibre (ii). Adapted from [70, 71].*

In all modified-LIFT variants and MAPLE DW based approaches, a bubble is generated to produce a cell encapsulating jet [69]. The approach typically focuses a pulsed laser beam through a laser transparent print ribbon. This ribbon has a laser transparent support layer and a bio-ink layer containing at least one side of material with suspended, or adhered cells (Fig. 2.13(a)). A secondary layer may also be employed to protect the cells from high power laser pulses. This secondary layer may consist of a thin metal layer, or a bio-compatible polymer to enable the initial attachment of cells to the underside, away from the laser source. To propel fluids, the focused laser vaporises either the sacrificial layer or the first molecular level of the bio-ink, generating a bubble where the expansion and collapse induces the formation of a jet.

In LG DW the laser beam is weakly focused into a liquid suspension of cells where the optical forces propel the cells from the suspension onto the translating substrate (Fig. 2.13(bi)). However the working distance is typically less than 300um. To extend this range, the laser beam can be coupled to a hollow optical fibre to carry cells up to centimetre distances (Fig. 2.13(bii)). By introducing computer control and a CCD camera, specific cells can be targeted and precise patterns can be achieved.

Laser based approaches to bio-printing have advantages in achieving a high level of accuracy with single cell precision and its inherent ability to achieve high throughput jetting (5kHz speeds have been reported [61]). Furthermore

the throughput can be greatly increased by employing parallel arrangements. Compared with inkjet methods which utilise a small diameter orifice, clogging is not an issue, enabling the jetting of higher cell concentrations and higher solution viscosities.

Laser jetting approaches to bio-printing is relatively new, and the majority of investigations conducted to date have been on determining the affects of processing parameters on cell viability. Thus investigations have typically focused on the jetting of cells onto a simple single planar surface, rather then applications for the fabrication of thick constructs.

Micro-scale Construct Technologies

The use of micro-scale deposition technologies to assemble and fabricate tissue constructs enable the greatest level of precision over the spatial distribution of cells within the construct. The majority of micro-scale construct investigations have utilised inkjet technologies. This may be due to the low cost associated with the equipment and the ease of setup compared with relatively sophisticated laser based approaches. Functionally both these technologies are jetting material onto a substrate with high resolution, thus construct approaches developed for inkjet based constructs, may be easily transferred to laser based approaches.

An early investigation into biological inkjet printing with the goal of creating tissue constructs was conducted by Wilson Jr. and Boland [66]. Modified inkjet printers and cartridge heads were custom built to dispense cells in a controlled manner (Fig. 2.14(a-b)), however the process was limited to 2D patterning. This may have been due to the lack of jetable scaffolding material at the time, and the need to dispense a large number of layers to achieve a construct with an appreciable thickness using such small modules.

To achieve 3D constructs with shorter construction times, and thicker constructs, the same setup was used to dispense larger cell aggregates onto either a thermo-reversible gel or collagen [72]. Thermo-reversible gels are fluid like at 20°C and gel above 32°C enabling the jetting of the material which would solidify

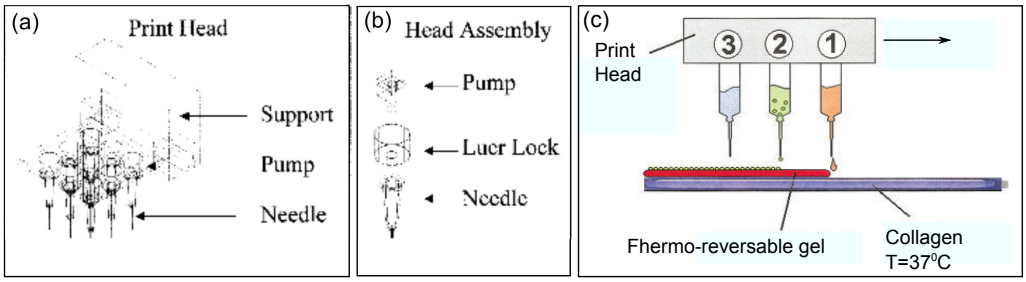

Figure 2.14 – *Inkjet Printer - (a) Custom print head, comprising of nine independently operated piezoelectric pumps each with an outlet connected to a luer locked needle (b). (c) 3D printing process - The same modified print head (a) is loaded with collagen or hydrogel where a thin layer of either material is deposited, followed by a layer of bio-ink. The sequential deposition sequence is repeated to achieve a multi-layered construct. Adapted from [66].*

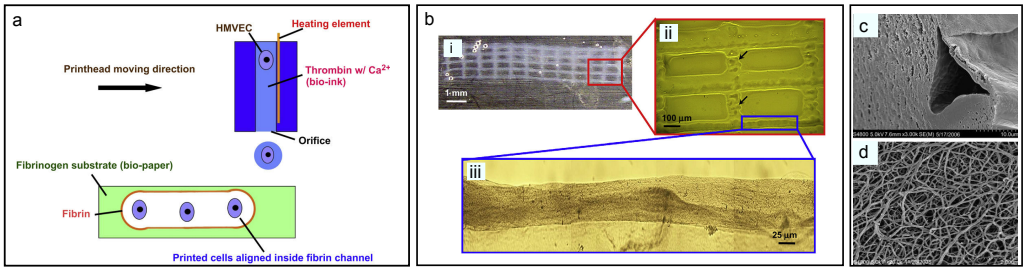

Figure 2.15 – *Simultaneous inkjeting of cells and scaffolding material - (a) Schematic of deposition process. Thrombin and endothelial cells (bio-ink) are deposited into fibrinogen, where an outer fibrin skin or layer forms after polymerisation. (b) Incubated patterned structure, in increasing magnification (i-iii). (c) SEM image of channel cross section and scaffold surface showing nano sized fibres (d). Adapted from [64].*

without the need for additional processes. The approach was described as "organ printing" with the scaffolding material called "bio-paper" and the cell suspension "bio-ink". Sequential layering of the bio-paper and bio-ink enabled a 3D construct to be achieved (Fig. 2.14(c)). The deposited cell aggregates ($\sim \phi 500 \mu$m) were reported to fuse with adjacent aggregates which were in close proximity. Fusion was reported for aggregates deposited in both collagen and the thermal-reversible gel, with a higher effectiveness of aggregates fusing within collagen. Further results on the interlayer aggregate fusion of the construct were scarce, as it was a feasibility study.

Simultaneous deposition of scaffolding precursors and cells have also been explored in various studies to achieve a structured 3D construct. In one example

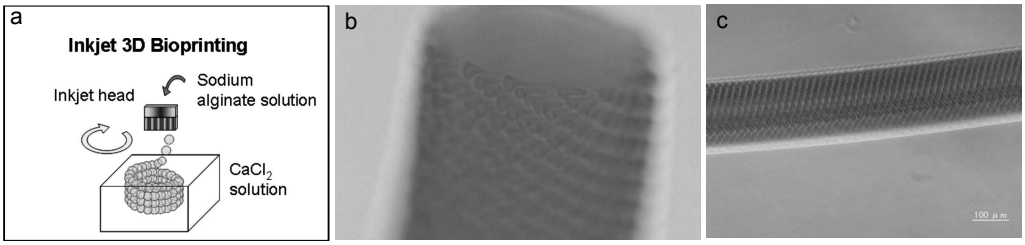

Figure 2.16 – *Digital construct scheme - (a) Alginate droplets are accurately dispensed into a calcium chloride solution for cross-linking. Sequential positioning and stacking of modules enable complex and accurate structures to be achieved. (b) Photo of resulting 200μm diameter tube. (c) Lower magnification of constructed tube. Adapted from [67].*

Cui and Boland [64] deposited thrombin solution, a fibrin precursor, with endothelial cells (bio-ink), into fibrinogen (Fig. 2.15(a)). The cartridge was loaded with bio-ink before being dispensed onto the substrate in a regular cross hatched pattern (Fig. 2.15(b)).

The construct was later incubated (5mins) to complete polymerisation, forming an outer fibrin skin or channel, in which the encapsulated cells subsequently adhered to. The formation of open micro-channels were reported (Fig. 2.15(c)) with attachment and proliferation of ECs. Characterisation of the mechanical properties of the printer fibrin fibres, enabled estimation of the burst pressure of the channel which was found to be comparable to those experienced within the body. However actual perfusion of the channels was not performed.

In another example a digital scheme of fabrication has been utilising with alginate [65, 67]. Sodium alginate solution was jetted into a solution of calcium chloride where cross-linking occurred (Fig. 2.16(a)). Droplets with mean sizes of 39μm and 26μm were produced with two different orifices, and the deposition of a tube having a diameter of $\sim \phi 200\mu$m was reported (Fig. 2.16(b-c)). However encapsulation of cells was not investigated, where the orifice would need to be modified to accommodate for the larger size of cells. The perfusion ability of the structure was also not mentioned, which may have been due to the weak bond forces between modules.

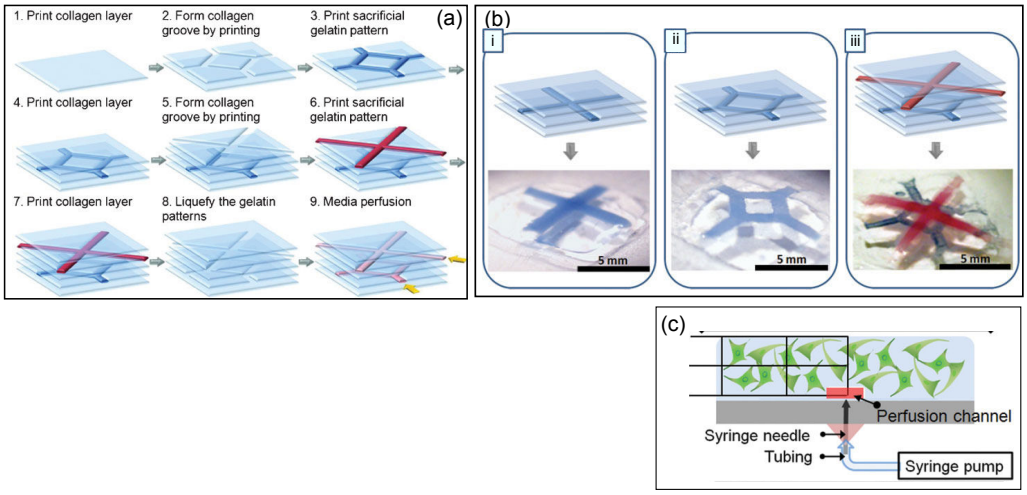

Figure 2.17 – *Pneumatic Bio-printing - (a) Schematic of the construction procedure. Collagen hydrogel were printed and gelated by cross-linking with $NaHCO_3$. Sacrificial gelatin patterns are printed into the grooves and cooled to gel. Another collagen layer is printed to cover the gelatin pattern. The construct is placed in an incubator where the gelatin liquefies before being removed by perfusion of warm medium. (b) Five different channel designs were constructed, where blue coloured and red micro-spheres were injected into the fluidic channels for visualisation. Patterns of a cross (i), and more complex rotary patterns (ii) were printed along with a five multi-layered construct with cross and rotary pattern (iii). (c) Schematic of perfused cell encapsulated construct used in viability tests, showing investigation zones. Adapted from [73].*

Pneumatic Droplet Free Form Fabrication Utilising another micro-scale deposition technique in which nL fluid volumes are dispensed, compared with pL volumes produced by inkjet and laser technologies, a 3D construct with perfusable channels was reported [73]. The technique uses a pressurised reservoir and electromechanical micro-valves to control the flow through to orifices of $\phi 150\mu$m, accommodating for the deposition of larger cells. Fabrication of a vascular network was investigated through the utilisation of a sacrificial gel material. Lee et al. [73] fabricated a construct which contained a collagen hydrogel precursor cross-linked with sodium bicarbonate, and a temperature sensitive gelatin sacrificial layer. The space previously occupied by the gel would form the channel. The gelatin layer is removed by raising the temperature of the construct in an incubator where the gel would liquefy, before being removed through gentle perfusion (Fig. 2.17(a)). Channels with widths of $\sim 400\mu$m and various cross patterns (Fig. 2.17(c)) were reported and perfusion tests on a simple single channel construct were able to

tolerate upto 2 Psi. However this is not comparable to the burst pressures experience by blood vessels in-vivo [74]. The viability of cells within the non perfused control and perfused construct were also reported, with the viability of fibroblasts in the control construct exhibited greatly decreased viability in the centre of the construct, while in the perfused construct (Fig. 2.17(d)), there was a uniform distribution of high cell viability. A number of features enabled greater flexibility in the method, including the ability to dispense higher viscosity fluids compared with inkjet and laser based approaches and the direct formation of perfusable channels. Inter-planar connections between layers was not reported, however it was suggested that it is conceivable. The weak mechanical strength of the collagen construct was also highlighted as a limiting factor in supporting and achieving larger constructs.

2.3.3 Extrusion

Extrusion based bio-printing methods constitute the macro-scale of bio-printing approaches, although there is potential to scale some techniques towards the micro-scale. Unit length of modules are typically in the order of μm, thus a thick construct can be achieved with fewer modules being deposited, compared with pL and nL volumes of micro-scale technologies. Materials are typically extruded via mechanical means, with a plunger setup or pneumatic methods.

Hydrogel extrusion One method of constructing 3D free-standing structures utilises technology from additive manufacturing process of free form fabrication [75], where the deposition of an extruded fibre is precisely controlled under computer control. Extruded materials have typically been hydrogel materials, which have relatively mild processing parameters such as low processing temperatures and high bio-compatibility. These properties are amendable to cells encapsulation ensuring high cell viability after deposition [63].

In an early example of hydrogel extrusion Smith et al. [76] investigated the deposition of fibroblasts in Pluronic® F-127 a thermo-reversible hydrogel, and bovine endothelial cells (ECs) encapsulated in collagen type I solutions. Free-

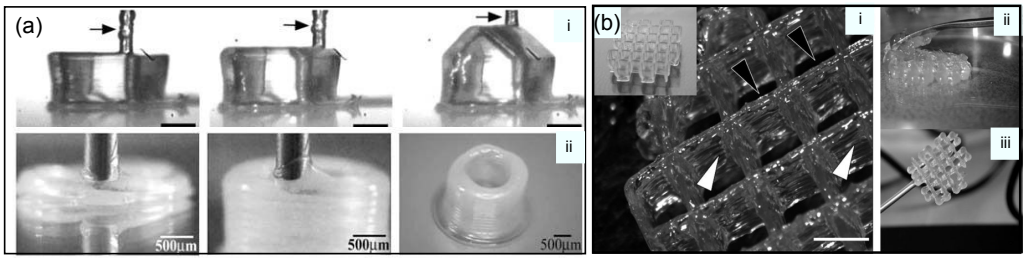

Figure 2.18 – *Cell laden hydrogel extruded construct - (a) Representation of a house fabricated from Pluronic® F-127 in a layer by layer fashion, with walls and an inclined roof. Arrows indicate the pen tip. Scale bars: 1 mm. (b) Printed modified Lutrol hydrogel scaffolds - (i) Patterned 3D structure. Black arrows show vertical pores while the white arrows horizontal pores. (Scale bar = 2.5mm). Printed structure and handling of non photo-polymerised structure (ii), and photo-polymerised structure (iii). Adapted from [76].*

standing 3D structures were deposited (Fig. 2.18), as well as regular patterned porous structures with wall thickness no more than 200μm to stay within diffusion limits. High viability of the ECs in collagen were reported after a 24h incubation period, while ∼60% of the fibroblast in P-F127 remained viable immediately after deposition.

Although collagen is a more bio-compatible material, the weak mechanical strength of the material created a challenge when processing into a solid structure. In addition the dissolution of collagen during incubation in culture medium were also an issue. To address theses issues, the gelling period was increased between successive layers. Similarly the construct was left to further gel after the printing process before introduction into the culture medium, however overly long time periods would result in the dehydration of the hydrogel, in which case cell viability was almost zero.

To further address the weak mechanical properties of hydrogels, additional additives and processes have been introduced to increase the mechanical properties. Fedorovich et al. [77] modified Lutrol F127 (Pharmaceutical grade of Pluronic F127) with a photo-initiator (Irgacure® 2959) to increase the mechanical properties of the hydrogel through photo-polymerisation. The printed constructs (Fig. 2.18(b)) were able to prevent the dissolution in culture conditions for up to 3 weeks and the processing parameters were able to maintain cell viability comparable to previous studies conducted without photo-polymerisation. Although

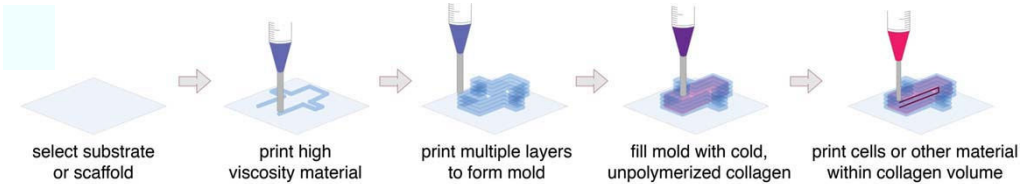

Figure 2.19 – *Construct integrating higher strength support material - Schematic of bio-printing and combining two scaffolding materials. First a Pluronic F127 mould is printed and filled with low temperature unpolymerised collagen. Next the biological materials such as a cell-collagen suspension are then dispensed into the desired shape within the existing collagen. Adapted from [63].*

the process was able to produce a more stable material during incubation, a number of additional concerns were introduced, such as the cytotoxicity of the photo-polymerisation processes from the addition of the photo-initiator and UV exposure on the cells.

Another method to increase the mechanical strength of the construct is through the utilisation of a combination of materials having different mechanical and bio-compatibility properties. In one example Chang et al. [63] utilised collagen I and Pluronic F127 to take advantage of the useful properties of the materials. Pluronic F127 having a higher strength, but lower bio-compatibility is deposited and combined with a low mechanical strength, high bio-compatible material collagen. Investigation with collagen as a scaffolding material was used due to its excellent in-vitro and in-vivo compatibility with previous cellular and micro-vascular experimental systems. However the collagen solution was weak and did not maintain its structural geometry before sufficient gelation occurred. To overcome this, moulds were first printed using P-F127, followed by the deposition of collagen (Fig. 2.19).

In another example Shim et al. [78] utilized a high strength polymer typically employed in top down fabrication methods for load bearing applications [17]. The harsh processing parameters of the polymer are not amendable for cell encapsulation due to the high processing temperatures. The polymer was integrated with two hydrogel materials, gelatin and atelocollagen. Co-polymer polycaprolactone (PCL) and poly(lactic-co-glycolic acid) (PLGA) were deposited as troughs before being filled with the hydrogel materials. A criss-cross pattern was fabricated layer

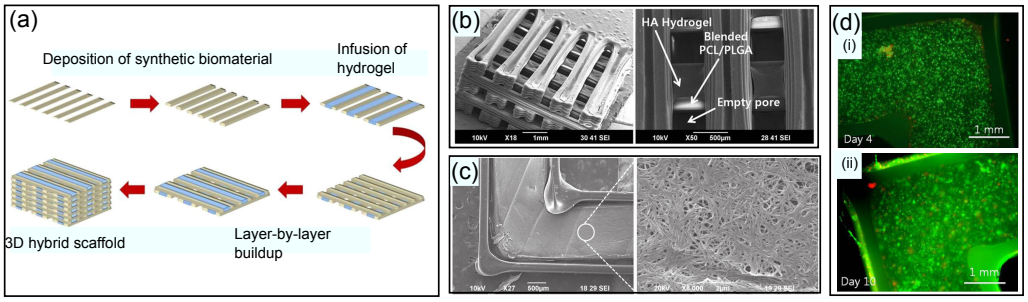

Figure 2.20 – *Biological Assembled Tissue- (a) Schematic of the hybrid scaffold fabrication using solid free form technology. First a mould is constructed with three layers of synthetic bi-material. Next a cell laden hydrogel is deposited into the mould. The procedure is repeated, layer by layer, in different orientations to achieve a 3D hybrid construct. (b) SEM image of fabricated hybrid (c) SEM image of cell encapsulated in atelocollagen construct, with magnified image showing the fibrous surface of the collagen area . (c) Fluorescent microscope image of live dead assay on encapsulated cells after 4 days (i), and 10 days (ii). Adapted from [78].*

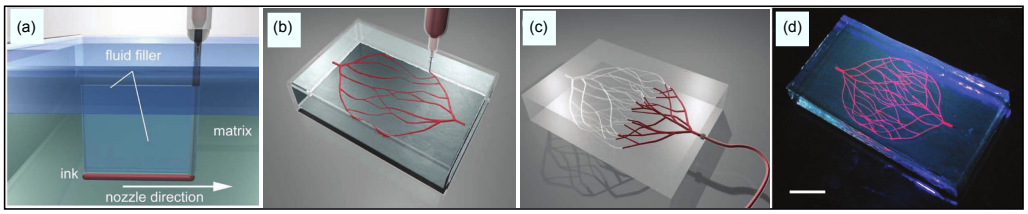

Figure 2.21 – *Omnidirectional printing of micro-vascular networks - (a) Translating the nozzle through the material matrix while printing the sacrificial material, induces voids which are filled with the liquid from the capping layer. (b) Schematic depicting the omnidirectional deposition of the sacrificial material, enabling hierarchical, branching networks to be patterned. (c) After photo-polymerisation of the entire construct, the sacrificial material is liquefied and removed with a modest vacuum to expose the channels. (d) Fluorescent image of resulting 3D micro-vascular network fabricated via omnidirectional printing (scale bar = 10mm). Adapted from [79].*

by layer to achieve the 3D construct (Fig. 2.20). The periodic criss-cross lay-up pattern ensured that contact between the molten polymer with the hydrogel was reduced and only limited to small areas at the intersection. The described methods which combine and lay-up two different materials, yields a construct with advantages of both materials, however the lay-up patterns, specifically the need to form a mould in order to incorporate the two, may hinder the construction of more intricate features, such as a vascular network.

In the aforementioned hydrogel extrusion approaches, focus was on the deposition of cell laden hydrogel into free-standing structures. Although interconnected

porous structures were achieved, the formation of a true 3D vasculature was not explored and maybe difficult with such lay-up methods. Wu et al. [79] investigated the fabrication of omnidirectional channels into a block of Pluorinc-F127, through the deposition of a sacrificial ink. The sacrificial ink is extruded and deposited into the semi gelled block with the desired omni-directional path (Fig. 2.21). This created a cavity or a void where the nozzle had previously passed (Fig. 2.21(a)). A low viscosity reservoir on top of the block filled the voids as they were created. After depositing the sacrificial material, the entire construct was exposed to light for photo-polymerisation, before the subsequent liquefaction, and removal of the ink through a vacuum (Fig. 2.21(c)). The approach demonstrated the ability to achieve intricate sealed channels comparable to the intricate vasculature in a rapid fashion. However it addressed only a single issue and suffers the same fate as micro-fluidic top down approaches, with the inability to spatially incorporate cells at desired locations.

Spheroid Extrusion The extrusion of spheroids or micro-tissue in combination with a collagen scaffold has also been explored as an extrusion module [80, 81]. Cell aggregates or spheroids of approximately 300μm diameter, or bioink particles are extruded into a layer of biopaper, a collagen hydrogel (Fig. 2.22(a-b)). The process is repeated layer by layer to fabricate a thick construct (Fig. 2.22(c)). The embedded spheroids were reported to undergo fusion where spheroids in direct contact with each other form a continuous cohesive structure. A recent review by Jakab et al. [50] described the limitations and issues encountered with the process. One limitation with the process was the strong dependency on the properties of the collagen hydrogel layer. Uneven gelation would effect the delivery of the spheroid, thus spatial accuracy. This problem would compound as each additional layer would progressively distort the overall construct. Another issues with the collagen scaffold was the solution concentration, which was required to be finely tuned to ensure fusion of the spheroids, so as not to hinder cell migration. Other issues included the logistics associated with the large number of spheroids required, and long time periods for complete fusion of the construct.

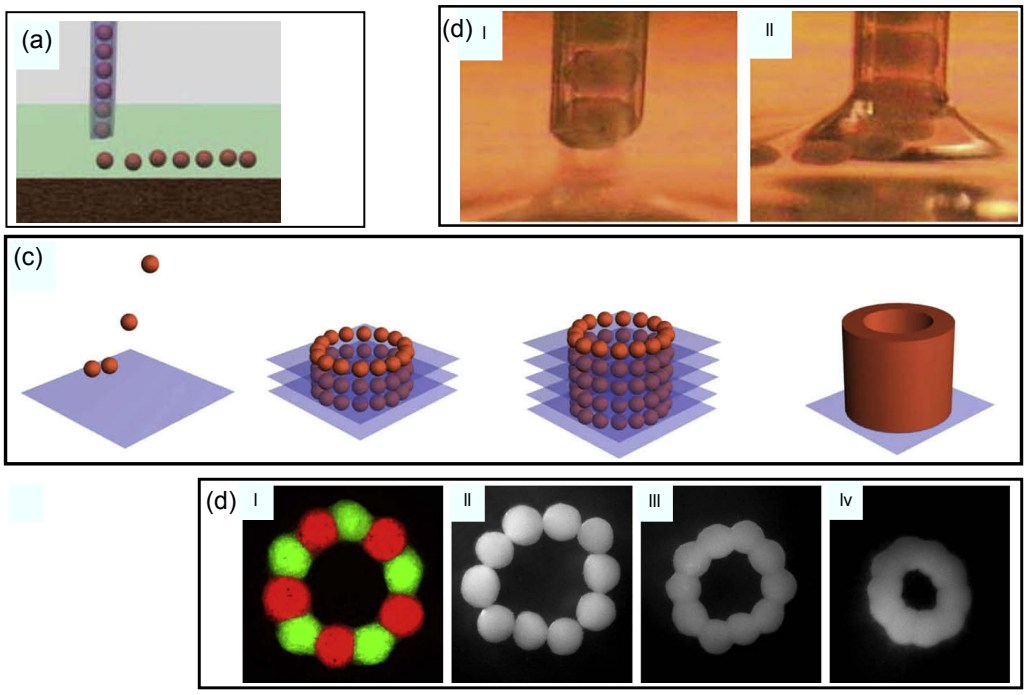

Figure 2.22 – *Spheroid based tissue printing - (a) Diagram of digital dispensing of spheroids in fluid (b) Tissue spheroids in loaded micro-pipette before dispensing (i) and during (ii). (c) Scheme for the bio-assembly of tubular tissue construct. Illustration showing the sequence of deposition and layer by layer construction, followed by the subsequent fusion of spheroids. (d) Assembled ring like structure and tissue fusion process. (i) Labeled spheroids showing absence of cell mixing during the fusion process. (ii-iv) Sequential steps during tissue fusion process. Adapted from [80].*

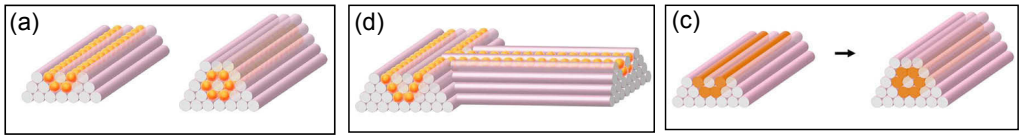

Figure 2.23 – *"Scaffold free" tissue assembly- (a) Deposition scheme of spheroids (orange) for the smallest diameter tube that can be constructed from agarose rods (pink), using discrete spheroids into agarose. (b) Design of more complex structures. (c) Deposition scheme using cell embedded cylinders and agarose cylinders. Adapted from [82].*

To address a number of these issues a processes where multicellular rods or spheroids are deposited into a mould or template has recently been explored [82]. The approach which has been described as a "scaffold free" approach utilizes agarose hydrogel moulds (Fig. 2.23), a material typically used as scaffolding to provide temporary support during the fusion process. This approach is similar to previously described hydrogel approaches utilising cylindrical structures. Construction into the moulds have included spheroids and cell encapsulated rods down to $\phi 300\mu$m. Preference was suggested towards the construction with rods due to the number of deemed advantages over the small discrete spheroids, including faster construction time, less logistical handling of smaller units, and faster fusion times. The described "scaffold free" approach may solve a number of issues associated with depositing modules into a hydrogel, however the rod based approach is now no longer a purely digital scheme, built upon small discrete units and instead a more continuous scheme similar to other methods previously explored. Although the scheme gains several advantages outlined, the process is no longer as flexible in achieving complex internal architectures, which would have otherwise been easily obtained from a digital scheme.

2.4 Construct Technologies Fabrication Specifications

Construct technologies have made great progress in reaching the potential to fabricate complex functional tissue. From the early approaches of fabricating a construct whose structure comprised of a random pore architecture, and random cell distribution. To modular approaches, where a tissue construction is realised through the positioning of discrete modules of different types, in defined locations. Thus enabling heterogeneous structures mimicking 3D structures found within the body. A large number of approaches have been investigated to assemble these modules into a unified construct each having their associated strengths and weaknesses. It is generally accepted that a level of bio-mimicry is required to ensure the formation of functional tissue, as the premise on the ability of cells to remodel an entire large foreign environment, is a largely ambitious task. However

the accuracy or resolution in which the level of mimicry is required has yet to be answered.

Construct Spatial Accuracy The spatial locality of cells, bio-chemical materials and scaffolding material within the construct, is an important feature in providing a tissue mimetic micro-environment for cells. Top down techniques may enable the creation of high resolution scaffolds for tissue formation, however the accuracy of the scaffold is only one aspect. Cells also need to be accurately located within the construct.

The incorporation of cells with top down methods are typically bulk methods with imprecise control over the locality of cells. Modular approaches have addressed this through the assembly of discrete units of modules containing cells or scaffold material assembled into the desired spatial arrangement. Micro-fabricated cell laden blocks have the potential to recreate accurate structures with modular blocks typically in the 500-900μm range. However, the bulk manual assembly methods typically explored, do not enable the high level of precision and accuracy over the placement of individual modules. Despite these limitations they may still provide a good modular technique for fabrication in environments where sophisticated and costly systems are not available. To achieve the highest level of precision and accuracy over the placement of modules, robotic assembly systems have been employed in bio-printing approaches. They offer an inherently flexible recreation of complex patterns and arrangements through modifications in the digital domain. Jetting approaches offer the highest spatial resolution in the range of 20-100μm. However, the cell density is typically low, with the delivery material occupying the majority of the droplet volume. Extrusion based bio-printing methods typically deposit materials widths in the range of 100-500μm. However the mechanical strength of most printed construct remains an issue. This problem influences the ability to satisfy the other aspects in tissue fabrication, including the practical issues with realising large, stable constructs, and the ability to realise an intricate and extensive open channel network.

Construct Vascularisation The vascularisation of constructs is of great importance to the success of integrating the final construct within a living system, in addition to the ability to maintain high cell viability, during the incubation period before implantation. Successful vascularisation requires the formation of a channel network which can be perfused and can span the entire construct, especially to the interior. Methods relying on accelerating the ingrowth of host vasculature through the artificial introduction of pro-angiogenic factors have had success at increasing the number and density of vessels. However, it is the network functionality and perfusability that is important. The current methods of artificially introducing growth factors typically do not release dynamically, and do not respond to cell demand. Thus they may not provide the proper regulatory signals for the formation of functional vasculature, with the release of appropriate signals at the appropriate time. The resulting vasculature thus requires a further remodelling period of the disorganised network, which is still a slow process, even with pre-vascularisation methods.

The direct fabrication of channels is one method of instantaneous realisation of a perfusable channel network. Top down methods with micro-fabrication techniques can address the issues with the structural strength, and the high geometric replication of intricate enclosed channels, however they suffer from the inability to achieve accurate cell spatial distribution. While modular approaches can address the spatial accuracy of cells, but typically have issues with the construct strength and preventing the collapse, or the integrity of open channels in large structures. A readily perfusable vasculature supporting a mimetic construct, may thus be achieved once techniques can be integrated satisfying the criteria of high construct strength, cell spatial accuracy and the realisation of an enclosed channel network.

Construct Mechanical Strength The strength of the construct is another important aspect to the success of achieving functional constructs. This is especially true for load bearing applications such as bone and cartilage and extends to the success in achieving channels and large structures. High mechanical properties of the

construct ensure the structural integrity of larger constructs more than a few layers and fine intricate channels remain open and can sustain the required pressures during perfusion.

Top down methods offer examples of constructs with good structural strength, due to the use of high strength scaffolding material. This is made possible with the separation of the cell seeding process from the processing of the scaffold requiring harsh processing parameters, typical for materials of high strength. These high strength constructs found in cartilage and bone tissue applications typically have a stiffness in the magnitude of MPa. However they suffer from a major limitation with the lack of spatial control during cell incorporation.

Modular approaches typically utilising hydrogel materials have inherently weak mechanical properties, with typical stiffness in the kPa magnitude ranges. Thus it is difficult to scale the construct to several layers, before the likely collapse of the construct or the fine internal channel network. Processes to increase the strength of hydrogels, through additives and photo-cross-linking may introduce additional factors where the careful characterisation of the process is required to prevent cytotoxic effects. However the strengths gained are still not comparable to the strengths of other bio-compatible scaffolding materials. Other approaches to increase the strength of the construct though the integration of a high strength material enable a construct with good overall strength, while maintaining the use of high bio-compatible materials. However, the current methods of introducing the structural component may interfere and spatially obstruct the realisation of an extensive channel network. Further investigation into methods to best incorporate the material without obstruction will need to be investigated.

Construct Technique Throughput The fabrication time of constructs on a single machine may also need to be addressed. When cells with high metabolic requirements are utilised, the process may not be able to realise the entire construct with a supporting infrastructure, before cell necrosis occurs. This is similar to the situation with top down approaches, where the natural remodelling process does not occur fast enough.

The problem is further compounded when high resolutions are required and smaller units are deposited. This requires the handling of more units to fabricate a given volume, dramatically increasing construction time with the same deposition speeds. Throughput on a single machine may be substantially increased, however this may reach a physical limit before a practical output can be meet. Modular approaches such as cell laden block techniques, is a highly modular concept and offers the potential for the fabrication of units with high cell accuracy in parallel machines, before finally being assembled into a larger tissue construct. However such modular units will bring with it inherent issues associated with modularity. These will include such factors as the ability to accurately align modules to its neighbour and the ability for a low leakage join between modules, when channels are created.

2.5 Construct Technologies Summary and Identified Challenges

The different technologies that have emerged are able to address a single specific aspect of the cell micro-environment well, capturing and mimicking the specific features of the micro-environment in-vivo, such as the spatial locality of cells, cell density, construct strength, temporal and spatial bio-chemical environment and vascularisation. However none have been able to capture all these aspects in a unified manner. This is summarised in Table 2.1 where the various construct technologies excel at a certain aspect but not across others.

The various approaches have typically focused on one technique or deposition technology. This may have been to minimise complexity, or due to the infancy of the field, however technologies may have now progressed to a point where the combination of technologies is warranted. Thus the Holy Grail of construct techniques may not exist by the utilisation of only one technology or approach, but a manufacturing process, where the various methods are combined in a novel combination, in an efficient and cost effective manner. Such an approach may integrate the top down scaffold construction for its ability to achieve high res-

Table 2.1 – *Summary of technologies.*

Construct Specifications	Microfluidic top-down	Conventional top-down	Modular cell-laden hydrogels	Micro-scale bio-printing	Macro-scale bio-printing
Ability to control cell position within construct	-	-	+ [54]	+++ [83]	++ [50]
Strength of the construct	+++ [36, 42]	+++ [17]	+	+	+ (exception hybrid printing [78] +++)
Potential to achieve perfusable channels	+++ [36, 42]	-	+ [59]	+ [73]	+ [82]
Potential to achieve a complex channel network	+++ [36, 42]	-	++ [59]	+++ [73]	+++ [50]
Construct cell density	-	-	+	+	++ [82] (exception, methods which utilise spheroids, +++ [50])
Time required to achieve perfusable channel	+++ [36, 42]	+++ [84]	+ [59]	+ [73]	+ [82]
Time required to fabricate construct of practical size	-	+++ [85]	++ [53]	-	++ [82]

olution features, maintaining the structural accuracy over several layers with high construct strengths, extrusion based approaches for its ability to deposit high strength material and jetting approaches for the deposition of bio-chemical materials. Finally modular approaches can be integrated to promote parallel construction, reducing the construction time, leading to more time for the cells to undergo remodelling, before the accumulation and onset of negative processes. Thus a truly bio-mimetic platform where the construct comprises of an infrastructure supporting cell function, and a micro-environment provides appropriate signals for the correct remodelling of functional tissue may be provided. This may enable longer term investigations of the numerous dynamics orchestrated influences on tissue formation, which may ultimately lead to the creation of complex tissue such as organs.

In the next chapter a bio-assembly or tissue-assembly method is described, whereby a top down method utilising a high strength bio-compatible material, is integrated with discrete modules of cells encapsulated within natural bio-material assembled in a digital manner.

Chapter 3

Systems Design

A system can be defined as "a set of interrelated components working together toward some common objective" suggesting that there are multiple interacting parts that collectively perform a significant function [86]. These interacting parts can be represented by a hierarchical structure with varying levels of abstraction. Such a structure is composed of subsystems, components, subcomponents and finally parts. The interactions between the entities are of important concern, and defined interfaces are required for the successful integration of the entities.

The system engineering process is commonly viewed as the decomposition (or design) followed by the re-composition (or integration) process [87]. In the decomposition process the requirements are analysed, defined in engineering terms and partitioned or allocated into several segments, elements or components. The partitioning of the entities is typically based on heuristics, thus it can be referred to as including elements of art as well as science [88].

In this chapter the requirements for the system are described, followed by the systems architecture and finally the combined overall view of the system.

3.1 Tissue Construct Technology

The current state of the art in bio-tissue construct technologies is to utilise robotic positioning systems to place or deposit modular units to build and assemble a

continuous 3D structure. Current issues that need to be addressed are the precision of the overall construct while assembling modules, and strength of the construct, which has implications in the realisation of a construct with a pre-existing vascular channel network and construct size.

3.1.1 Novel Tissue Assembled Constructs

To promote cells into the formation of functional tissue it is generally accepted that a mimetic environment is required. For this to be achieved the 3D hierarchical structure of cells, bio-molecular materials, scaffolding material must be arranged in a precise and defined manner. Current techniques maybe able to deposit materials in a highly accurate and precision manner, however the materials typically deposited are of low strength.

A method that is currently being explored by the CReATE group is a construct process called "Tissue Assembly" a hybrid approach utilising both top down and bottom up approaches with spheroids. The main advantages of a top down approach include the ability to use high strength materials. This has been shown to be required if large constructs are to be constructed, and fine intricate channels are to maintain their geometry. Furthermore, there is greater accuracy over the overall dimensions of the construct, as the technique is not subjected to the accumulative errors that can occur when depositing material one on top of another.

The bottom up approaches enable much flexibility in depositing different materials at differing locations, in a digital manner.

The utilisation of spheroids instead of single cells is also highly advantageous. Each of the spheroids are micro-tissue that have been formed after an initial incubation period (Fig. 3.1(c)). Thus each spheroids is a module of pre-formed natural tissue in a micro-environment of natural ECM, which is more robust then single cells alone. The process however is not only limited to spheroids, and other processes of forming spherical micro-tissue may be possible. This may include the use of synthetic spherical porous scaffold which have been bulk seeded with cells

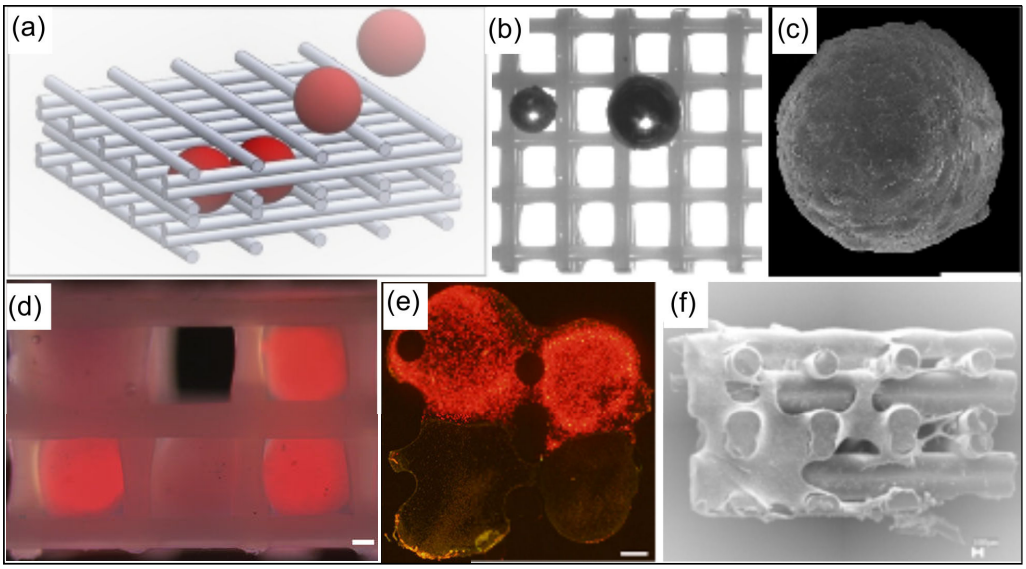

Figure 3.1 – *Tissue Assembled Construct. (a) Computer rendering of the assembled 3D construct comprising of free-form fabricated scaffold and spheroids. (b) Top view of printed scaffold with a test particle and scale particle (ϕ1.59mm) placed on top. (c) SEM image of example spheroids formed from human skin fibroblasts [82]. (d) Fluorescent and light imaging of spheroids within the construct. (e) Histological fluorescent images of construct section, showing fusion of spheroids. [21]. Cultured construct showing cartilage formation on the surface after a 14 day incubation period.*

and incubated for a period of time. This may allow for the control over both the density and size of the spherical micro-construct.

Figure 3.1 illustrates the basic concept of the technique where spheroids are encapsulated within the scaffold matrix to prevent the egress of particles. Initial biological studies of simpler, small scale constructs have shown the potential of the approach, with studies showing spheroid fusion (Fig. 3.1(e)) [21], and tissue formation (Fig. 3.1(f)).

Figure 3.2 illustrates a number of parameters which can be altered with this approach illustrating the high flexibility in the internal architecture, including control over the spatial arrangement of the spheroids and scaling of the process.

3.1.2 Assembly Schemes

There are a number of methods to assemble the presented construct. One such scheme is through the sequential deposition of scaffolding material followed by

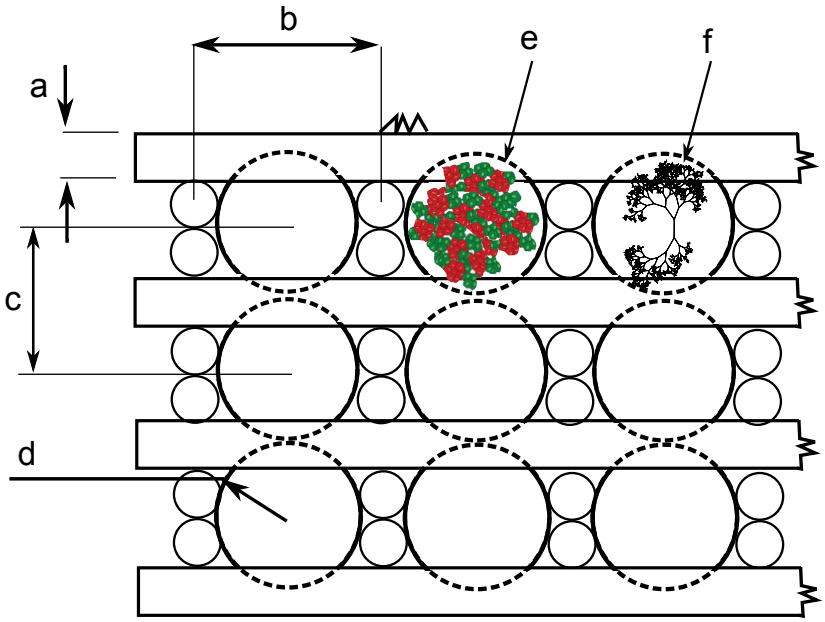

Figure 3.2 – *Schematic diagram showing flexibility of the approach. A number of parameters can be changed, but are not only limited only by those shown: (a) diameter of fibres, (b) width of pore, (c) spacing between spheroids, (d) spheroid diameters, (e) co-cultured spheroids and (f) vascularised spheroids.*

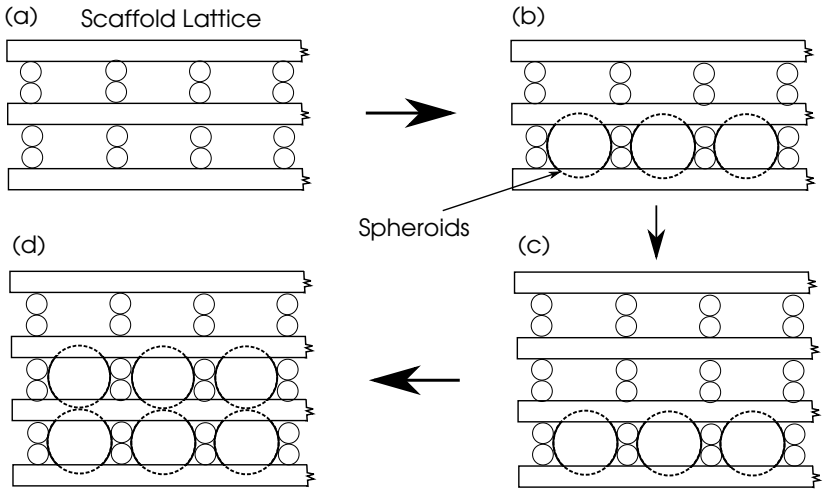

Figure 3.3 – *Schematic diagram showing an exemplary assembly scheme. Multiple layers of fibres are first deposited forming a two layer pore space (a). Next spheroids are delivered into the bottom layer (b), followed by the deposition of the next pore layer (c). Spheroids are once again delivered into the lowest possible layer (d). This ensures that a single buffer layer exists between the molten polymer and spheroids.*

the delivery of the spheroids. However such an approach may not be suitable, as the spheroids will be at a close vicinity to the molten polymer as it is deposited. Another scheme is where a buffer layer is formed (Fig. 3.3). Here a single offset buffer layer will exist providing an insulative effect.

Due to the flexibility of the approach a number of different permutations of the assembly scheme are possible. Furthermore the construct is not limited to only cubic type structures, and constructs resembling the external 3D structure of their biological counterparts are possible.

3.2 System Requirements

The main scope of the research is to develop prototypes which provides proof of concepts for the device functionality as well as system functionality. Performance requirements are not included in the requirements listing, as the functionality is of most importance.

3.2.1 Mechanical Functional Requirements

In general terms the requirements are to construct a predetermined, porous 3D scaffold structure in a rapid fashion, and to insert spherical particles into specific pore locations. The pores must be sufficiently small to prevent the egress of spheroids, and handling methods must minimise damage to the spheroids.

To clarify and decompose these functions, the system must:

- Uniformly deposit fibres of molten polymer.
- Transport or deposit a single spherical particle to the required pore site.
- Ensure that spheroids are held securely to prevent egress of spheroids from scaffold during incubation.
- Numerically control the deposition of the molten fibres and delivery of the spherical particles.

- Assemble the construct with schemes listed in Sect. 3.1.2.

- Provide a simple, highly level, abstracted interface to the system.

3.2.2 Biological Functional Requirements

In addition to the mechanical functional requirements of the system, biological compatibility requirements are also critical. The biological particles that are handled by the system contain living cells, and for high quality tissue regeneration, the particles should not be subjected to overly large stresses which may increase the risk of damage and lead to cell fatalities.

Cartilage spheroids due to the nature of their function are more forgiving to harsh handling methods than other tissue types. However less resilient tissue types may be handled in the future. Thus a gentle handling method must be developed, which exhibits relatively low mechanical stresses to the spheroids.

The surrounding environment of the spheroids where they are stored and transported through, must also be considered. Sterility will be a requirement in the future when the device is depositing live cells, however this lies outside the scope of the current project. Other environmental requirements include hydration, and possibly a nutrient supply if the cells are in the assembly process for long periods of time. In addition fluidisation[1] requirements may also be advantageous, ensuring proper uniform distribution of nutrients and preventing the spheroids from adhering or fusing to one another.

3.2.3 Desired Functions

The desired functions are outside the scope of the project, but will be considered when developing the system architecture to aid in extending features in the future and include:

[1] Process of levitating solid particles against gravity by shear-drag of a moving fluid, resulting in a solid-fluid mixture which behaves as a “fluid“ [89].

- High level control of the system being commanded through the translation of a solid CAD model,
- Sterile operating conditions.

3.3 System Architecture

The architecture of a system can be defined as "The structure (in terms of components, connections, and constraints) of a product, process or element" [86]. It is this structure that is developed in the following section, providing a guide for the engineering of the system components.

The partitioning schemes to achieve a desired structure are primarily based on heuristics. A major goal in partitioning is to define boundaries between the subsystems and components, which minimizes their interdependence. The same principles of modularity to minimize interdependence in software are also applicable to hardware. This can be achieved through low coupling, and high cohesion [86]. High cohesion is where related items are grouped together, and loose coupling is where the interdependence of one module to another is low. With tight coupling, changes in one modules cause changes to one or more other modules. Good modularity in the systems architecture offers the following desired features:

- Each component can be specified, developed, designed, manufactured and tested as a self-contained unit.
- A faulty component can be replaced directly by an equivalent interchangeable component.
- A component can be upgraded without affecting the design of other components.

A system architecture typically deals with abstracted high level concepts and functionality, such that the complexity of the system can be reduced and more readily analysed. For abstraction to exist, a model representing the system is required. Such models have traditionally been based on informal block diagrams augmented with supplementary textural documentation [90]. The block diagrams represent system components, and lines connecting them represent exchange of information, energy, or physical entities. This informal representation can be

viewed as a more creative, flexible approach as there are no constraints imposed on the notations used in expressing ideas. On the other hand the informal representation can be ambiguous, and misinterpretation can occur.

Architecture description languages (ADLs) are formal approaches for architectural modelling, providing a set of notations. One notable language is the Management Group's Systems Modelling Language (OMG SysML) which is adopted from the unified modelling language 2.0 (UML 2.0) [86]. The language provides notations and methods to describe the system in a number of views with varying levels of abstraction, all of which are desirable in the design of a system. In addition the formalised approaches enable automated methods in checking for consistency and architectural analysis, such as the validation of requirements.

In the following section the traditional methods of representing a system architecture are used, as the degree of complexity in the system is not considered to be high, and the advantages gained from an ADL may not be significant. Following the guidelines of achieving good modularity, the following sections describe the system architecture of the automated system.

3.3.1 Highest Abstracted View

The system is split into the subsystems of the master controller, polymer dispensing system, spheroid delivery system, and the three-dimensional positioning systems as illustrated in Fig. 3.4. The combination of these subsystems satisfies all of the functional requirements for the system. Interfaces between the subsystems are accomplished through a shared bus. The development of each subsystems will be discussed in greater detail in the later chapters. A graphical overview of subsystems is shown in Fig. 3.5.

3.3.2 Master Controller

The main control module sends high level commands via the bus to the corresponding units. It is the supervisor that initiates communications, directing the high level process flow. The main controller is implemented on a personal

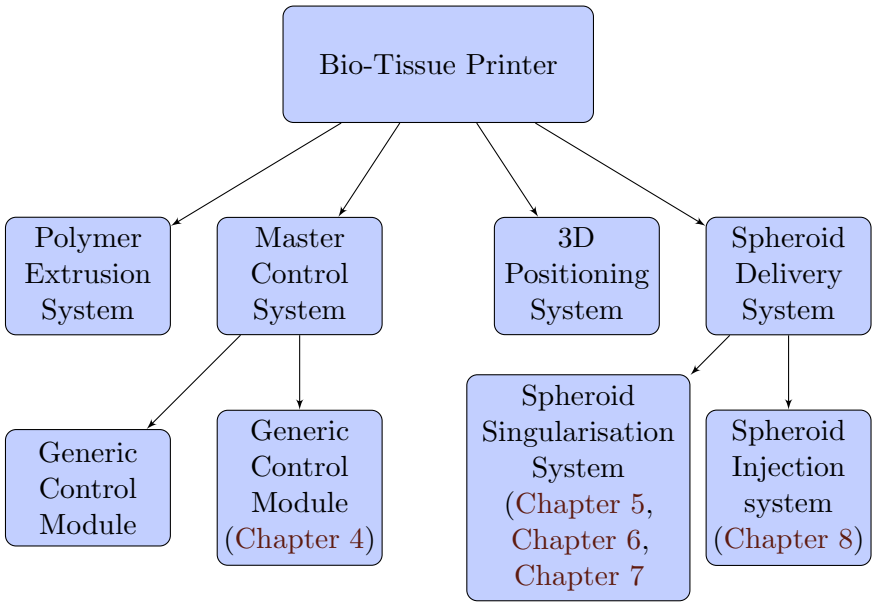

Figure 3.4 – *Structural architecture of combined subsystems.*

computer and transmits G codes to the motion control board for the control of the three stepper motor drivers, to achieve precision positioning of the stage. The master controller in the future will potentially include software systems to convert a CAD model into the required control signals, controlling the overall process.

3.3.3 Three-Dimensional Positioning System

The three-dimensional positioning system is responsible for the functional requirement of numerically controlling the positioning of the two dispensing heads. The most cost effective solution for this subsystem was to purchase an off-the-shelf system. The XJ3030 (XYZ Tech, Shandong, China) was selected for this task due to the low cost, control through non propriety G-code and motion parameters within the requirements. The machine with G-code control enables numerical control of the dispensing head in 3 axes, allowing precision positioning of both the polymer dispensing system and the spheroid deposition system.

3.3.4 Polymer Deposition System

The polymer deposition subsystem is responsible for the functionality of extruding a fine polymer filament. A system previously developed by the final year students and subsequent modifications by summer interns at The University of Canterbury was used. The system is simply mounted onto the positioning platform.

3.3.5 Spheroid Delivery System

The spheroid delivery system was further partitioned into two subsystems accomplishing two different functions. These were the singularisation system and the injection (embedding) system. In the spheroid delivery system, a single particle is first separated by the singularisation system, as manipulation of a single particle has many advantages. These include the independent control of a single particle for delivery into a single pore while being independent of the locations or movements of the other particle, simplifying the control processes. The development of a singularisation system is described in Chapter 5 through to Chapter 7.

The second subsystem, the spheroid injection system is responsible for the delivery of the singulated spheroid into the pore site. As this is a specialized task, off-the-shelf components do not exist, and in house research and development was required. The development of this system is detailed later in Chapter 8.

3.3.6 Generic System Control Modules

In maintaining the principles of modularity, a generic control module for each of the systems was developed. The microcontroller along with the supporting peripheral circuits, form the control and communications backbone of the systems. Each board contained various peripheral circuits required to successfully control the required sub-system.

The control arrangement is a decentralised control network where each of the control boards handled the local control algorithms. A hub was required to connect the various control modules. Along with a communications network converter, providing compatibility between the PC serial interfaces and the subsystems

network.

Detailed development of the generic control modules is described in the next Chapter 4.

3.4 High Level Overall System Schematic

The combined interfaces and structure of the subsystems as previously described individually, are illustrated in Fig. 3.6. In the master controller or PC, it is envisioned that solid models will be automatically translated into G Code. The generated G Code is passed to NC Studio which interfaces with the motion controller card over the PCI bus. The motion control sends the control signals to drive both the stepper motors and sends additional control signals onto the network bus. A bus converter is required to translate these signals into the required bus protocol. Both the polymer deposition system and spheroid delivery system are controlled by separate microcontrollers that executes specific tasks.

3.5 Summary

The developed systems architecture is highly modular, enabling independent development, testing and manufacturing of the modules. With the implementation of a network bus and protocol, future upgrades can be made without major changes to the system. As the control modules are generic, they are highly reusable, and new features can be easily added to the system. In the following Chapter 4 the development of the generic control modules will be described.

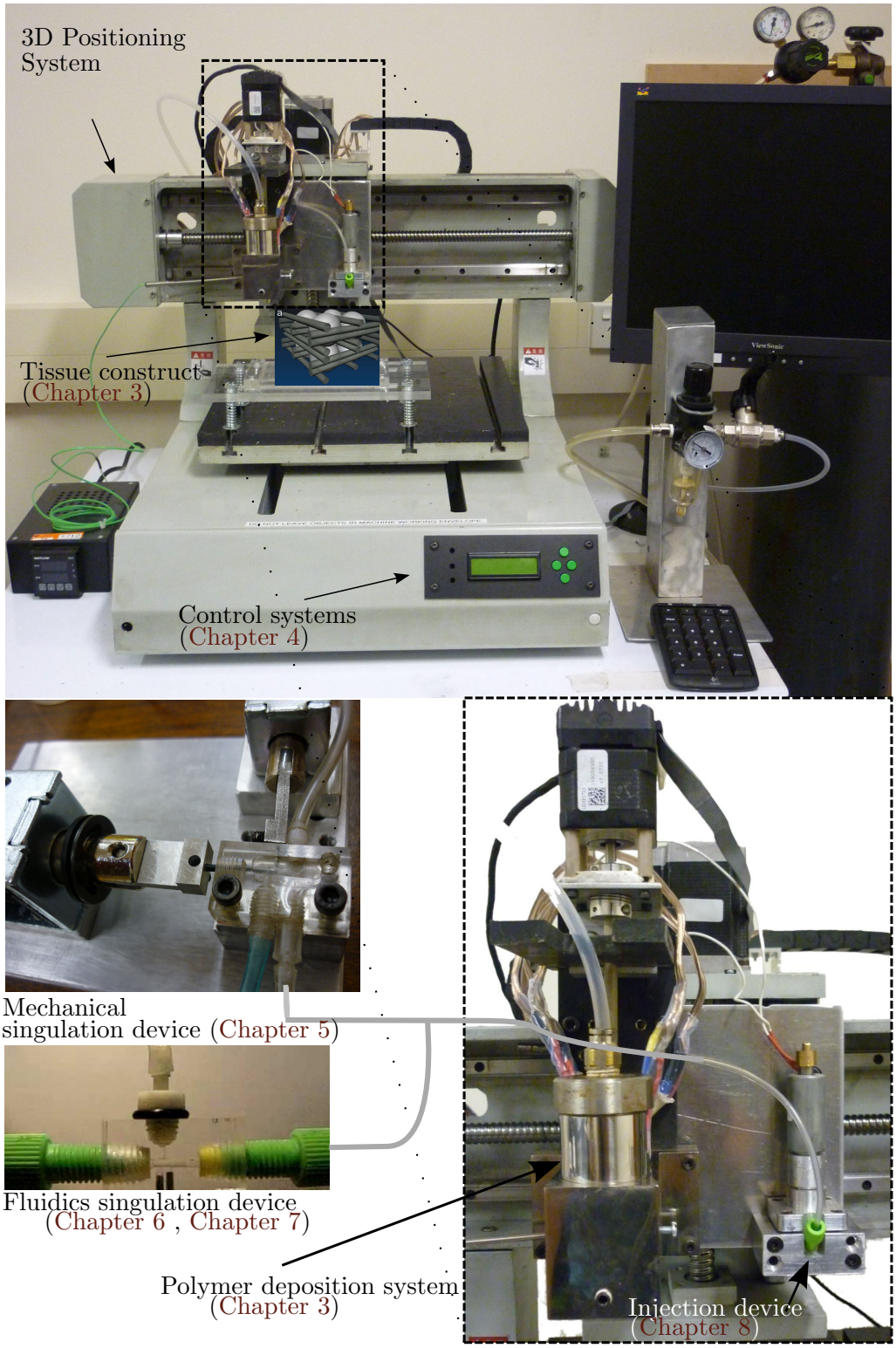

Figure 3.5 – *Subsystems overview.*

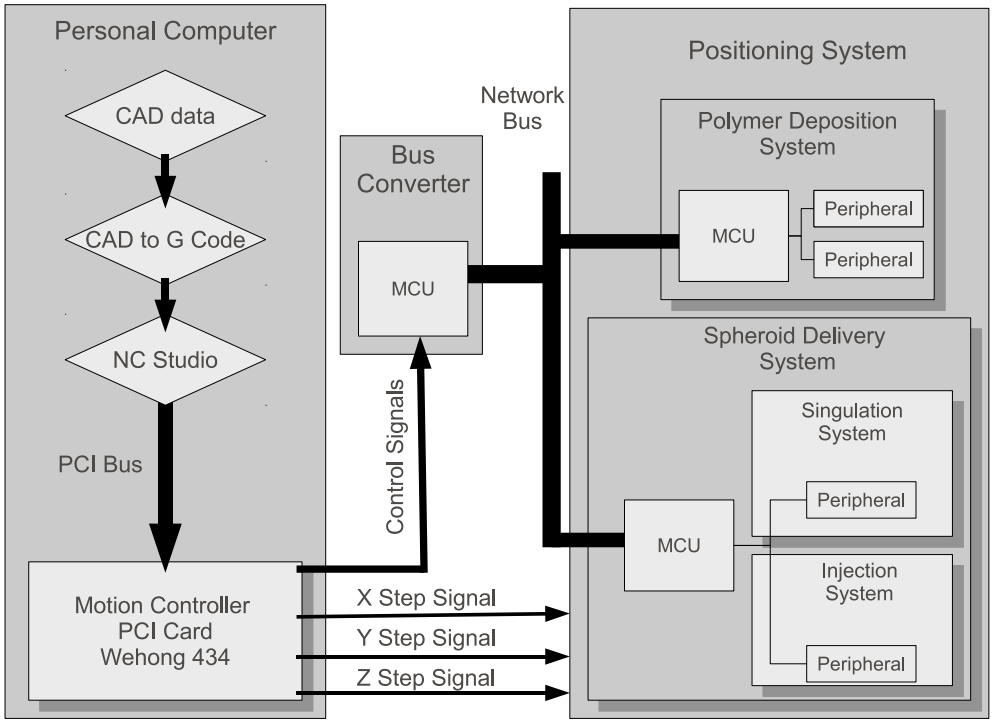

Figure 3.6 – *Structural architecture of combined subsystems.*

Chapter 4

Development of Generic System Control Modules

4.1 Introduction

A control system can be generally defined as a combination or network of subsystems and processes that are assembled for the purpose of obtaining desired output with desired performance, given a specified input [91]. In the case of a tissue assembly process, a number of inputs and corresponding outputs are required. In order to reduce the complexity of the problem, each of these input/output requirements are partitioned and grouped into more manageable functional partitions as described in Chapter 3.

To realize the control system, programmable microcomputers or microcontrollers are used as they are highly flexible and versatile in the realisation of control algorithms through software. The partitioning of the control systems into distributed modules, required an electrical communications method to coordinate them. In addition, for the electrical controller to sense the physical analog quantities, transducers are interfaced to signal conditioning circuity, and an analog to digital converter is required. This enables the conversion of analog physical quantities into the digital domain for manipulation and processing.

This chapter describes the development of the generic control module. Sec-

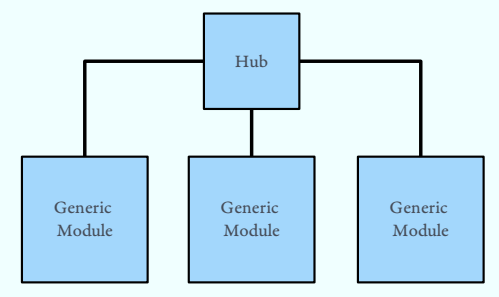

(a)

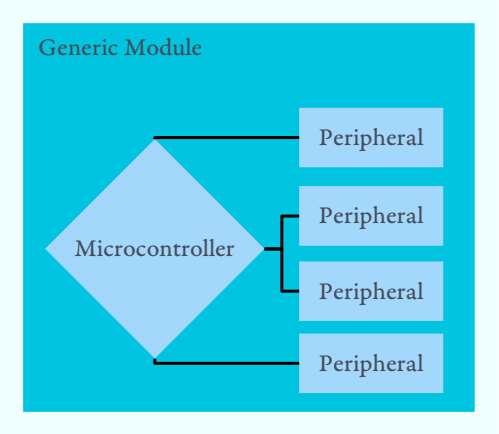

(b)

Figure 4.1 – *High Level System Connections:(a) High level connections of generic control boards, (b) Generic board architecture.*

tion 4.2 describes the control system architecture. Section 4.4 describes the development of a communications protocol and finally Sect. 4.5 describes the development of the support circuity or signal conditioning circuits required before the analog to digital conversion stage. Developments of the control algorithms, are left to later chapters relating to the specific devices.

4.2 Generic Control Board Systems Architecture

Generic modules connect to each other through a network sharing a common bus. Each of the generic board will connect at a central hub providing the physical interconnects (Fig. 4.1a).

Each of the generic control modules comprises a micro-controller, interfacing to

peripheral circuits (Fig. 4.1b). These peripherals include combinations of lowpass filters, amplifiers, solid-state high power switches, network transceivers and user input. This enables modular additions to the generic control module, to meet requirements and functionality appropriate for specific tasks.

4.3 Communications

Communication between the individual modules are an essential component for the successful control and operation of the process. This is an inherent requirement resulting from modularity. As each of the devices is modularised, a method is required for each module to communicate reliably, and successfully carry out the process function.

For communication to occur, there must be a common method of understanding or the decoding of bits. Procedures are also required to ensure that the successful transmission and reception of messages have taken place through error detection. This is where protocols are used. There is a critical requirement of low latency in industrial networks compared to that of data networks used to link PC's. In an industrial network there must be a level of "determinism" where a critical message is guaranteed to be sent within a certain time period [92].

The Modbus standard of communication has been the "de-facto" standard for industrial communication networks for the last 15 years, with some estimates indicating that 40% of industrial communications networks still use Modbus [93]. This can be attributed to the range of multiple vendor devices that can connect to each other. The main limitation is the predominant point to point communications, and multiple masters in a multipoint topology are not supported. Thus decentralised control can not be implemented.

A network standard which is multipoint and used in connecting the low level field devices to the higher level controllers and terminals is the IEC 61158 standard also known as the Fieldbus standard. The network provides determinism or real-time communications. There are numerous fieldbus implementations but the two most prominent standards are Profibus and Foundation Fieldbus. Ethernet based

Fieldbuses also have great potential owing to their dominance in the office and home environments, which helps to accelerate development of the standard [94]. In addition the Ethernet chips are relatively inexpensive. The major shortcoming of Ethernet is the "non determinism". Although there are several proposals for an "industrial Ethernet", the solution may come from the consumer market with the need for quality of service (QoS)[1] to support streaming media, voice and images.

According to the OSI/ISO standard the functions of data communication can be divided into seven similar interacting but separate abstracted layers [94]. Where each layer relies on the services of the lower layer, performing its specific functions on a message, before passing the message up or down the layers. These layers are called the physical, data link, network, transport, session, presentation and application layers (Fig. 4.2). One or more protocols implements each of these layers and the sequential order forms the protocol stack.

At the lowest layer, the physical layer handles the transmission of raw bits over the communications link. The data-link layer is concerned with the formatting of the raw bit stream into larger aggregates called a frame. The data link layer also handles the data flow control. That is the process control to ensure that the frames have been correctly sent and received at each end of the physical link as well as a frame error check such as a cyclic redundancy check (CRC) [95]. The network layer combines a number of separate data-links into a chain, thus forming a complete path across a network consisting of multiple nodes. At this layer the unit of data exchanged among nodes is typically called a packet, and it is the handling of these packets, and packet switching which this layers is concerned with [96]. The transport layer is responsible for providing network-independent communication services between computer applications running in the end-users terminals. This is required as data may need to traverse different networks in route. The layer also ensures the coordination and control of all the various networks and arranges a communication path end to end. The most commonly used transport protocols nowadays are TCP (transmission control protocol) and UDP (user datagram protocol).

[1] Network with the ability to control the data flow of messages with different priorities

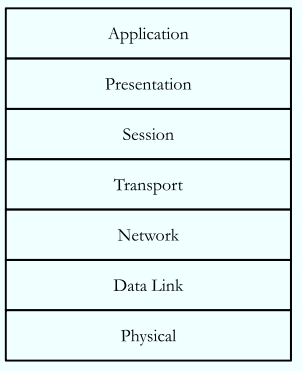

Figure 4.2 – *The model of the open systems interconnection (OSI) showing the stacking of 7 layers implementing a protocol stack.*

Layer	OSI/ISO Model	Modbus Stack
7	Application	Modbus Application Protocol
6	Presentation	Empty
5	Session	Empty
4	Transport	Empty
3	Network	Empty
2	Data Link	Modbus Serial Line Protocol
1	Physical	EIA-TIA-485 or EIA-TIA-232

Table 4.1 – *The Modbus RTU frame.*

The higher level protocols 5 to 7 commonly run on the end device and the strict functions of the separate layers is typically less defined. These are software programs running on the operating system and at the application level. Thus they are usually determined by the operating systems manufacturer and rarely adhere to the strict OSI layering model [96]. However in an abstracted view, the application layer may be defined as performing input and output sub-routines on behalf of more complicated end user applications.

The strict implementation of the layers are defined by standards. A widespread, simple and robust communications protocol standard used in industrial automation is the Modbus standard described in the following section.

MODBUS Message

Start	Address	Function	Data	CRC check	End
≥ 3.5 char	8bits	8bits	Nx8bits	16bits	≥ 3.5 char

Figure 4.3 – *The Modbus RTU frame.*

4.4 Communication Prototcol - Modbus

4.4.1 Introduction

Modbus is a communications protocol that was developed by Modicon (now part of Schneider Electric) for process control systems. It had been a "de-facto" standard in the integration of multi-vendor devices for many years. It is considered a open standard and many of the standards publications are openly available. The standard only specifies the data-link and application layers, thus any physical transport layer can be used. The data-links are inherently master-slave [1] and support up to 247 slaves. An overview of the Modbus RTU (remote terminal unit) communication stack compared with the OSI model is illustrated in Table 4.1. It can be seen that only three of the layers in the OSI model are implemented in the Modbus RTU standard, as inter-network communications are not required, further increasing the simplicity of the standard. The Modbus standard of communication was chosen as the model for the development of the network. Owing to its simplicity and tested robustness, which is important in reducing the developmental times required for the prototype.

4.4.2 Data Link Layer

In the Modbus RTU mode each 8-bit byte in the message contains two 4-bit hexadecimal characters. This allows greater throughput than ASCII mode for a given baud-rate. The message frame is split into 4 different fields (Fig. 4.3) [97]. The address field is used to address the slave that has been assigned the specific address. Address location 0 is a broadcast message targeting all slaves. The

[1] One device (master) can talk to a group of slave devices only.

function code indicates to the server the kind of action to perform. It is followed by a data field that contains the request and response parameters. The error check field is the result of a redundancy checking calculation that is performed on the message contents. In RTU mode the check is a cyclic redundancy check (CRC).[1]

The protocol for the sending and receiving of frames by the master and slave representing both data and applications layers is illustrated in Fig. 4.4 and Fig. 4.5. From the master's point of view, after the power up of the device, it enters the 'idle' state where neither emission nor reception is active. A request can only be sent in the 'idle' state. When a unicast[2] request is sent to a slave, the master enters into 'Waiting for reply' state and a 'Response Time-Out' is started which prevents the master from staying indefinitely in the waiting state. When a reply is received the master checks the reply before processing the reply. The check may result in an error where the reply is from an unexpected slave or an error in the received frame. In the case where the reply is from an unexpected slave the Response time-out is kept running. In the case of a frame error, a retry may be performed, which is the responsibility of the application layer. In the case where no reply is received, the Response time-out expires and an error is generated. The master then goes back into the 'Idle' state.

The state behaviour of a slave is illustrated in Fig. 4.5. At start-up the device enters the 'idle' state. When a request is received, the slave checks the frame for errors before performing and processing the action requested in the frame. Even if the frame is error-free, errors may still occur during the processing of the request for example, format error, invalid action. When this occurs a reply is sent back to the master. If the slave detects errors in the received frame, no reply is returned to the master. If no error is detected the message is echoed back to the master.

The listed diagrams (Fig. 4.4, Fig. 4.5) are a simplification of the actual communications process, and in the actual protocol additional factors such as

[1]The cyclic redundancy code is generated from the remainder of a polynomial division of the data. By comparing the code that was originally generated (and sent) for the data with the calculated code of the received data, errors can be detected. [98]

[2]Sending of messages to a single network destination.

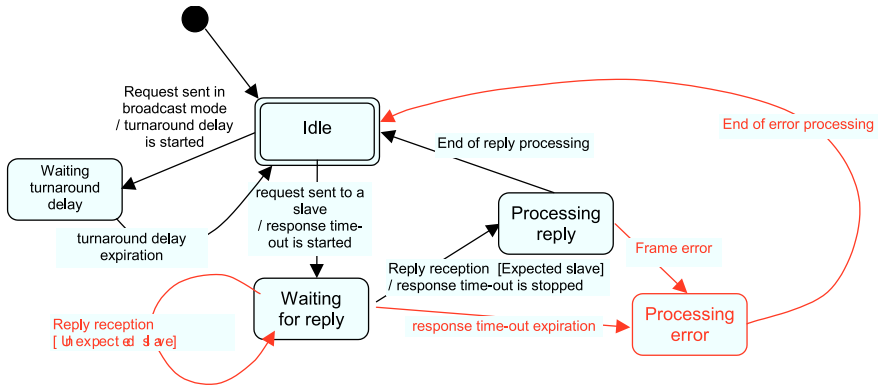

Figure 4.4 – *The MODBUS masters states [97].*

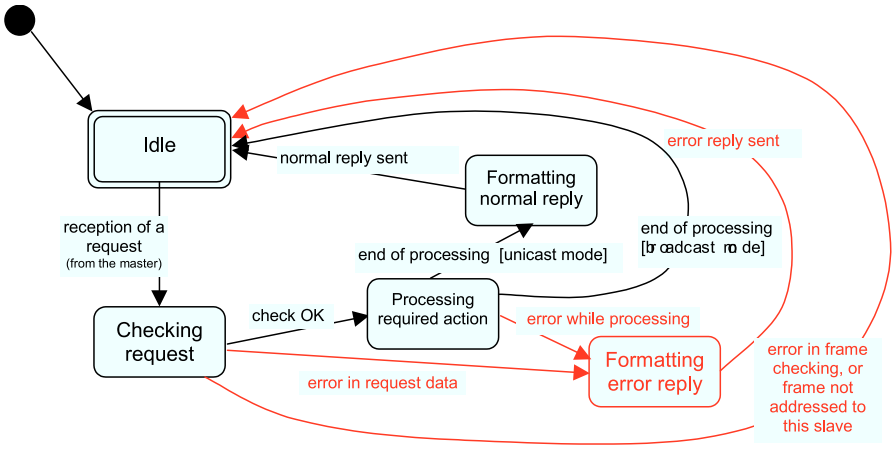

Figure 4.5 – *The MODBUS slave states [97].*

timing of character reception, access to the line, retransmission following and error, and framing need to considered.

Details of the data-link that was developed and adapted from the Modbus standard for the communications protocol can be referenced in Appendix B.0.4.

4.4.3 Application Layer

The application layer lies closest to the end user, and handles the higher level communications, which include high level error handling. The Modbus application protocol defines a simple protocol data unit (PDU) that consists of the function code field and data field. This is independent of the underlying communication

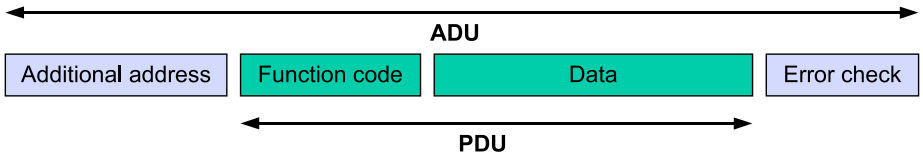

Figure 4.6 – *The Modbus simple protocol data unit (PDU) and application data unit (ADU) [99].*

layers [99] (Fig. 4.6). The mapping of the Modbus protocol on specific buses or networks introduces additional fields on to the application data unit (ADU) which may include the address field and error checking field (Fig. 4.6).

The application data unit is formed by the client that initiates a Modbus transaction. The function code field ranges from 1-127, with 128-255 reserved and used for exception responses. When a message is sent from the client to the server, the function code field specifies to the server the type of action to perform. The data field contains additional information that is required to perform the action.

The Modbus protocol defines three PDUs. Where the function code field determines the PDU type. They are:

- Modbus Request PDU.
- Modbus Response PDU.
- Modbus Exception Response PDU.

When a client initiates a request (Transmission of a request PDU), the server responds by echoing the same function code field, followed by any data that is requested (Fig. 4.7). In an event that an error occurs during the processing of the function, the server returns a code that is equivalent to the functional code from the request PDU, but with its most significant bit set to logic 1. This is accompanied by the exception code in the data field (Fig. 4.8).

Details of the application layer that was developed and adapted from the Modbus standard can be referenced in Appendix B.0.5.

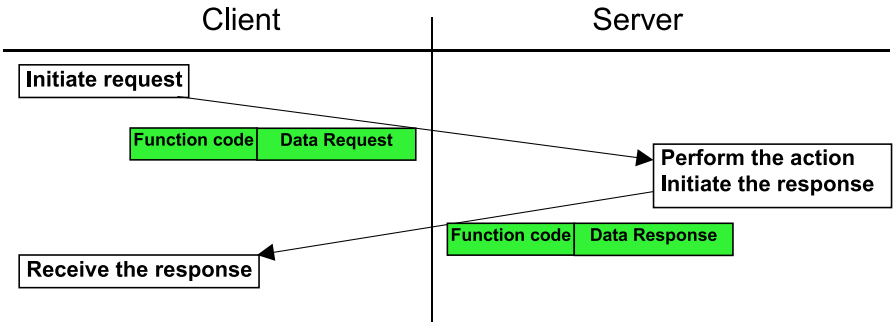

Figure 4.7 – *The MODBUS slave states for a valid transaction [99].*

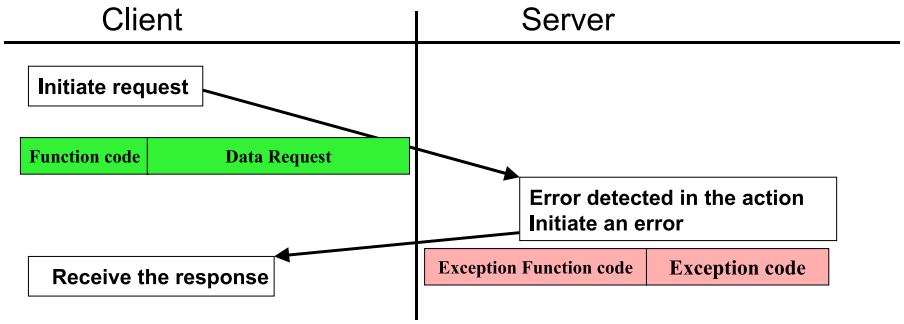

Figure 4.8 – *The MODBUS slave states for an invalid transaction. [99].*

4.4.4 Physical Layer - RS485

Introduction

RS-485 formally known as the EIA-485 standard was chosen as the physical layer to the communications network. There were a number of advantages for selecting this as it supported a multipoint[1] communication method and half duplex[2] mode of communication, as well as balanced differential lines.

The EIA-485 standard defines the electrical characteristics of the line and the receivers and drivers, but there is no discussion of a software protocol. The standard defines that the bus can have up to 32 load units which is equivalent to an input impedance of $12k\Omega$. If higher impedance transceivers are used this number can be increased further. The use of repeaters can increase the network

[1] multiple masters and slaves

[2] Data flow where information can be transmitted bidirectional by taking terms as opposed to full duplex where both sending and receiving occurs concurrently

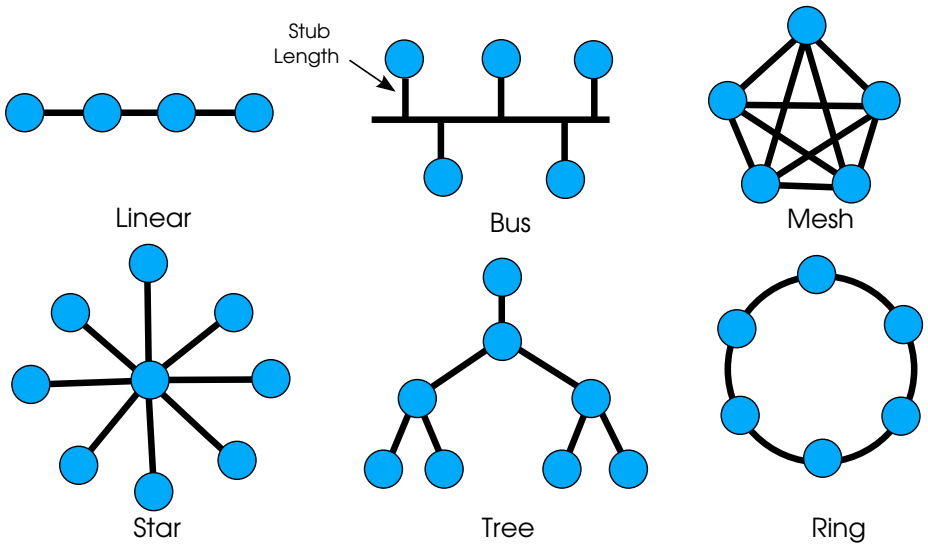

Figure 4.9 – *Common network topologies.*

size well over the load limits. The standard uses a balanced, differential pair to transmit data. The use of a balanced pair greatly increases its immunity to noise, as noises that couple to the wires are usually common to both input terminals and cancel out. In RS-485 the driver can go into three states; logic high, logic low, and the key feature of high impedance. The high impedance enables the network to be multipoint. The receiver only needs to see a voltage difference at its differential input greater than 200mV to determine a logic high or low. A voltage greater than 200mV is a high, while a voltage difference less than -200mV is a low. For input levels between +200mV and -200mV the output is undefined, and the output logic behaviour is highly implementation specific of the connected circuit. This situations can occur in half-duplex operation when all devices are in the high impedance mode, and the line is not driven. Such a situation is undesirable as noise may appear as data transitions, however this can be solved with line biasing.

Network Topology RS-485 is typically best arranged in a linear network topology with proper line termination. Termination is required to minimize the reflections that occur when a signal is transmitted through a transmission medium and reaches a point of abrupt impedance mismatch. Other arrangements are possible (Fig. 4.9), including bus, ring, star, and tree. However reflections may occur and

corrupt the signal. The level of impact that the reflections cause to the signal is dependent on both the data rate and the length of the electrical lines. Lines connected to the linear bus (Stubs) are acceptable if the length of the lines are kept to a minimal length and the data rates are not high.

Implementation To implement the receiver and driver for the RS484 standard, the transceiver chip ST485C (STMicroelectronics) is selected. The driver is able to enter a high impedance state essentially placing no load on the bus, enabling half duplex communications. This state is controlled by a signal from the micro-controller. The network topology is arranged in a star network, where devices connect to a central hub. Although it is not the ideal arrangement, the length of each of the stubs are short to minimize reflections. The hub also provides conversion from RS-485 to RS-232 for communication with a PC. The schematic and layout of the hub can be referenced in Appendix A.0.2.

4.5 Signal Conditioning

Signal conditioning is required to manipulate the analog input signals to produce an output that better meets the requirements of the device in the next stage, that is, the analog to digital converter (ADC). A signal conditioning system commonly performs any of the following functions: amplification, level shifting, filtering, impedance matching, modulation, demodulation and isolation [100].

An ADC requires a low source impedance to minimize signal distortions during sampling, while the transducer under instrumentation require high impedance inputs. The ADC's dynamic range in amplitude is limited, thus for greatest sensitivity the signal should span the whole range. While that of the signals from a transducer is typically in the millivolt range. As the ADC is a sampling device the bandwidth of the frequency spectrum also needs to be limited to prevent aliasing.

Aliasing of a signal occurs where there is an ambiguous representation of a sampled signal. Sampling is the representation of a continuous-time signal by a

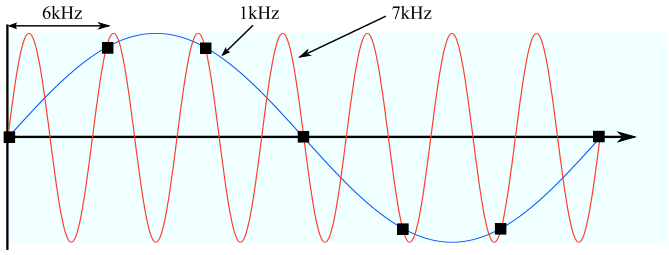

Figure 4.10 – *Aliasing effect of sampling 7kHz sinewave at 6kHz generating a 1kHz alias.*

sequence of continuous-valued signals at discrete time intervals [101]. The main requirement of sampling is to collect sufficient data to accurately represent a continuous-time signal. This can also be stated as determining the sampling frequency that enables precise reconstruction of the signal. When insufficient samples are taken the representation of the signal is ambiguous and an alias of the signal results. This is illustrated in Fig. 4.10 where a sine-wave of 7kHz is sampled at discrete times of 6kHz represented by dots. The reconstruction of the discrete values generate an alias of 1kHz. The sampling frequency at which aliasing is eliminated, occurs when the Nyquist-Shannon sampling theorem is satisfied. The theorem states that a band limited signal can be reconstructed exactly, if the sampling frequency is greater than the Nyquist frequency (defined as twice the signal bandwidth). Thus if the signal is band-limited by a filter, aliasing will not occur. When a filter is designed to prevent aliasing it is called an anti-aliasing filter.

The incompatibilities of impedance, signal bandwidth and amplitude requires that signal conditioning be performed for optimal performance. In this section the focus will be on the signal conditioning of a Wheatstone bridge, incorporated in a pressure sensor in order to meet the requirements of the subsequent ADC stage.

4.5.1 Amplification

Transducer signals are typically small differential signals in the presence of a high common mode signal. For the desired signal to be extracted and span the full scale range of the ADC, amplification of the differential signal as well as attenuation of the common signal is required. Although a number of amplification topologies can

be implemented to amplify the signal, a differential amplifier is most appropriate for the task.

Differential amplifier

A differential amplifier can be implemented in a number of topologies. Where each one may be more appropriate for one design than the other. Referring to Fig. 4.11a under the conditions where the resistances form a balanced-bridge, that is,

$$\frac{R_4}{R_3} = \frac{R_2}{R_1} \tag{4.1}$$

The output for an ideal differential amplifier is expressed as:

$$v_o = \frac{R_2}{R_1}(v_2 - v_1) \tag{4.2}$$

Which shows that the output is linearly proportional to the difference between the two input voltages. The equation can be expressed in terms of a differential mode (DM) input and common mode (CM) input components, which highlights the functionality of the amplifier,

$$v_{DM} = v_2 - v_1 \tag{4.3a}$$

$$v_{CM} = \frac{v_1 + v_2}{2} \tag{4.3b}$$

where the input voltages can be expressed as,

$$v1 = v_{CM} - \frac{v_{DM}}{2} \tag{4.4a}$$

$$v2 = v_{CM} + \frac{v_{DM}}{2} \tag{4.4b}$$

where Fig. 4.11a can now be expressed in terms of the new components as shown in Fig. 4.11b.

A high impedance input of the amplifier is important to prevent loading effects on the instrumented circuit, resulting in non linearities in the output. Referring to Fig. 4.12. The following input impedance can be expressed as:

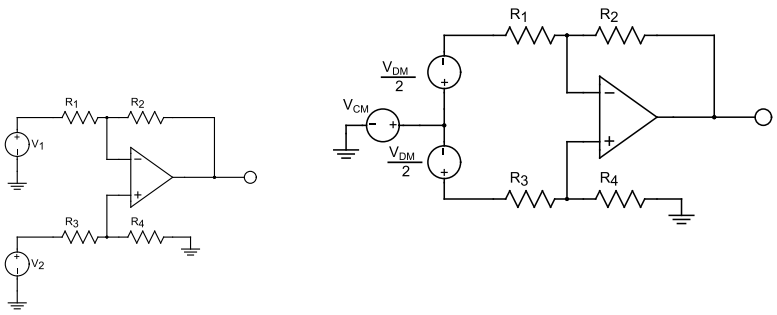

(a) **(b)**

Figure 4.11 – *Differential single op-amp implementation*

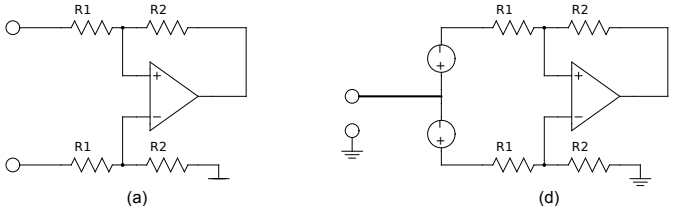

Figure 4.12 – *Differential-mode and common-mode input resistances.*

$$R_i d = 2R_1 \tag{4.5a}$$

$$R_i c = \frac{R_1 + R_2}{2} \tag{4.5b}$$

Both showing finite input resistances.

Another feature of the differential amplifier is in its ability to reject the signals common to both inputs. A typical scenario in instrumentation. This ability is quantified by the common mode rejection ratio (CMRR). This is defined as the ratio between the differential mode gain (A_{dm}) and the common mode gain (A_{cm}) , A_{dm}/A_{cm}. Typically it is expressed in decibels (dB),

$$CMRR_{db} = 20log_{10}\left|\frac{A_{dm}}{A_{cm}}\right| \tag{4.6}$$

For an ideal differential amplifier the $A_{cm} \to 0$ and therefore $CMRR \to \infty$, but in reality the tolerances of the resistors result in resistor bridge mismatch.

This along with non ideal op-amps lead to a finite CMRR [102]. To achieve high CMRR the resistor bridge must be balanced[1], thus requiring high tolerance resistors. Integrated monolithic approaches where the resistors and the op-amp are contained on a single chip can achieve high CMRR through the precise trimming of the resistors.

Although the differential amplifier is effective in the amplification of a differential signal, and offers a high CMRR, its shortcoming is in the input resistances from each input which is very limited [100].

Instrumentation amplifier

An instrumentation amplifier (IA) is a type of differential amplifier that simultaneously yields high input impedance and high common mode rejection ratio. In addition, it usually offers high stable gain and low output impedance [102]. The IA is used to amplify a small signal in the presence of a large common mode signal, which is a typical scenario in instrumentation. Compared with the differential amplifier, IAs have extremely high input impedances which minimize loading of the circuit. The mentioned features are advantageous in interfacing to a Wheatstone bridge network where loading of the circuit results in non-linearities. The instrumentation amplifier can be implemented as a two op-amp implementation or the traditional three op-amp implementation.

Three op-amp The three op-amp instrumentation amplifier (Fig. 4.13) is the traditional implementation of the IA. It can be partitioned into the "input stage" comprising of OA_1, OA_2 and the "output stage" OA_3 which is a differential amplifier. The input stage can be viewed as an amplifier with a differential input and output.

The equation for the input stage is,

$$v_{O1} - v_{O2} = \left(1 + \frac{2R_3}{R_G}\right)(v_1 - v_2) \tag{4.7}$$

[1] A balanced resistor bridge is one that satisfies the condition of, $\frac{R_4}{R_3} = \frac{R_2}{R_1}$

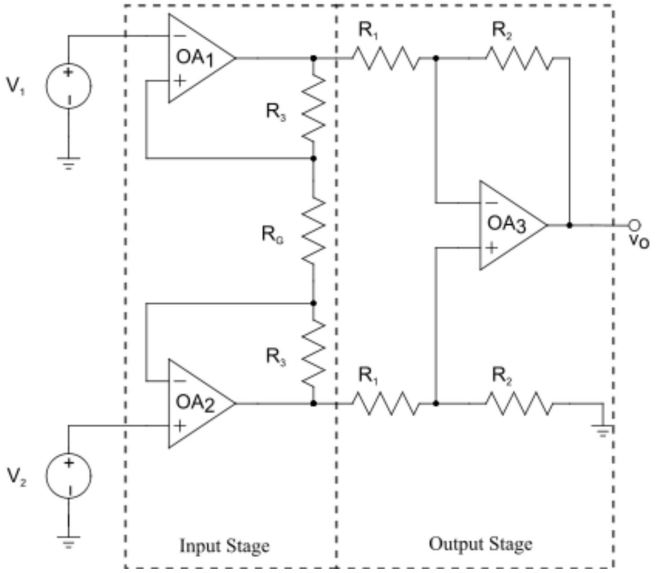

Figure 4.13 – *Three op-amp instrumentation amplifier.*

The output stage is given by,

$$v_O = \frac{R_2}{R_1}(v_{O2} - v_{O1}) \tag{4.8}$$

Combining the last two equations gives the output for an ideal 3 op-amp IA.

$$v_O = \left(1 + \frac{2R_3}{R_G}\right)\frac{R2}{R1}(v_2 - v_1) \tag{4.9}$$

Adjustment of the gain for the amplifier is achieved by altering the value of R_G, as it does not need to be matched to other resistors to maintain high CMRR.

The three op-amp implementation offers the best performance of the mentioned differential amplifier and two-opamp IA. The symmetric loading of the signals ensures that the CMRR does not premature roll off, as in the case with the two op-amp method, and it has a lower risk of saturation due to the lower gain at the input stage.

Two op-amp The two op-amp method of implementing an IA (Fig. 4.14) enables higher performing op-amps to be used more cost effectively then the three op-amp implementation, as there is one less amplifier. This is significant when costly high quality op-amps are used to achieve superior performance [102].

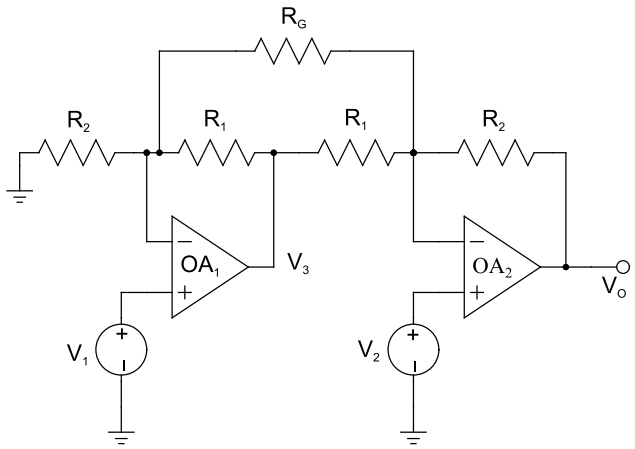

Figure 4.14 – *Two op-amp instrumentation amplifier.*

The output from the first amplifier is given by,

$$v_3 = (1 + \frac{R_1}{R_2})v_1 \tag{4.10}$$

and the output for the two op-amp instrumentation amplifier with adjustable gain is,

$$v_O = \left(1 + \frac{R_2}{R_1} + \frac{2R_2}{R_G}\right)(v_2 - v_1) \tag{4.11}$$

A disadvantage of this amplifier is the possibility of saturation in the presence of a high common mode voltage. With reference to Eq. 4.10 (the output voltage of the input stage) and assuming the case where $v_C M \gg v_D M$, saturation is avoided when,

$$v_C M \left(1 + \frac{R_1}{R_2}\right) < V_{sat} \tag{4.12}$$

where V_{sat} is the op-amp saturation voltage. The scenario of saturation for a three op-amp IA is of less risk as it has unity gain at the input stage [100]. A further disadvantage is the inputs asymmetrical path. The delay created by the asymmetric path causes the CMRR to degrade prematurely at high frequencies compared with that of the symmetric three op-amp IA.

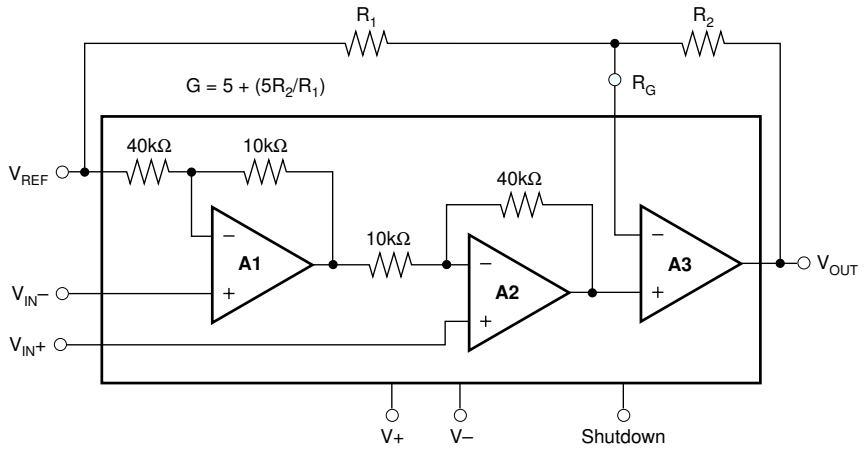

Figure 4.15 – *Schematic of INA2331 monolithic integrated circuit [103].*

Even with the shortcomings, the two op-amp implementation is an attractive solution for the implementation of an instrumentation amplifier and is well suited for designs where the common mode voltage is low, preventing saturation, and where the CMRR performance at high frequencies is not significant.

4.5.2 Selection

The two op-amp instrumentation implemented in a monolithic chip was selected for the instrumentation board due to the higher quality op-amps that could be obtained when compared with the three op-amp IA. The monolithic approach ensures that the resistors are matched sufficiently to ensure high CMRR compared with a discrete implementation. The two op-amp IA features high input impedance and a high CMRR and meets design requirements. The internal schematic of the selected integrated chip INA2331 (Burr-Brown) is shown in Fig. 4.15.

The INA2331 is a modified two op-amp instrumentation amplifier with an additional gain amplifier. As with all two op-amp implementations there is an increased risk of saturation of the first amplifier and the conditions need to be considered. The schematic diagram implemented in the circuit board can be referenced in the Appendix A.0.1.

4.5.3 Filtering

Introduction

Electrical circuits which handle or process signals are inherently susceptible to the introduction of unwanted signals. Especially in the case where the signals are required to travel a long distance, such as a remote transducer [104]. Examples where such signals may arise from include, poor shielding, thermal noise sources and cross talk through signal coupling. Hence filtering is required to remove the undesired signals so that the desired signal is prominent and can be accurately determined.

An electrical filter is a network that transforms an electrical signal applied to its input such that the signal at the output has specific characteristics. Filters are required to attenuate the unwanted signals to a satisfactorily low level. In applications where the signal is interfaced to a analog to digital converter, as is the case in this section, an anti-aliasing filter is required. This is a low pass filter which restrict the bandwidth of the signal, ideally attenuating all signals above the Nyquist sampling rate.

A filter can be classified broadly by the function that it performs, in terms of the pass bands and the stop bands which are frequency ranges [105]. The pass band is the frequency range where there is little or no change to the amplitude of the signal, effectively letting it pass through. The stop band is the frequency range where the signal is attenuated and is effectively prevented from passing. The arrangement of the pass bands and stop bands, defines the four most common filters. These are:

- Lowpass, allowing low frequency signals to pass (Fig. 4.16a)
- Highpass, allowing high frequency signals to pass (Fig. 4.16b)
- Bandpass, allowing a band of signal frequencies to pass (Fig. 4.16c)
- Band-stop, stopping signals within a frequency band (Fig. 4.16d)

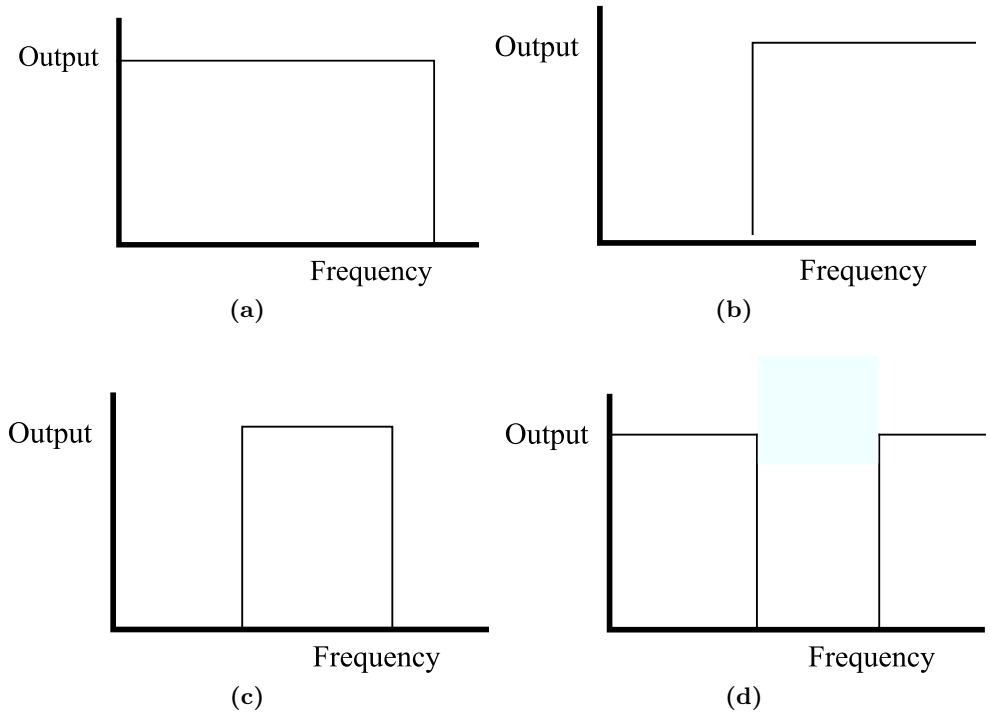

Figure 4.16 – *Characteristics of ideal filters: (a) Lowpass. (b) Highpass. (c) Bandpass. (d) Bandstop.*

A low-pass (LP) filter will be described as this is the filter that is required. The low-pass filter more specifically passes frequencies from DC to ω_c, (cut off frequency) and attenuates the frequencies beyond the cut off (SB). In an ideal LP filter the gain is constant from zero to ω_c and zero beyond this. The frequency band from DC to ω_c is called the passband. This ideal "brick wall" filter is difficult to realise in practice with analog components, but in the digital discrete domain the realisation of this comes close to ideal [106]. This comes with a trade-off of greatly increased components count and processing power (depending on the order of the filter). Due to the non idealistic performance of components, the specifications for the LP filter include other parameters to characterise response (Fig. 4.17). This is given by its cut off frequency ω_c, a stop band frequency ω_s, maximum loss in (A_p) allowed in the pass band, the minimal SB attenuation (A_s) and the slope of the transition band (TB)[1] [106]. These few specifications alone

[1]The frequency range from ω_c to ω_s

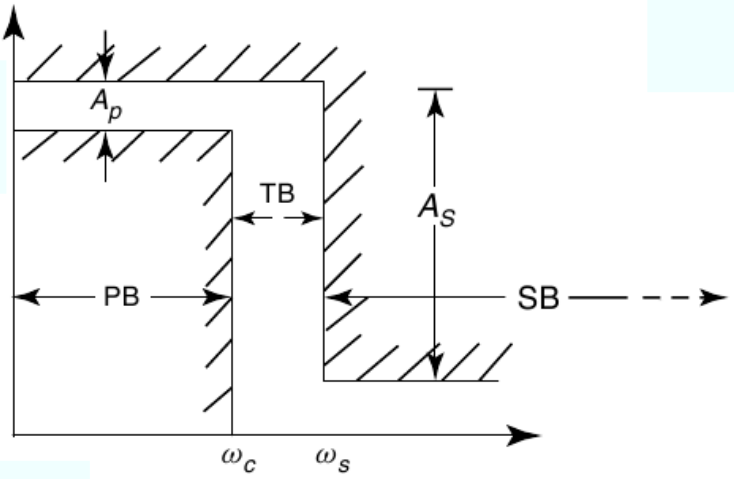

Figure 4.17 – *Typical specifications for a low pass filter [106].*

enable the characterisation of a reasonably good filter for a particular application.

A filter's response or the output of the system can be approximated by a transfer function, and its response can be determined by the locations of the zeros and poles. In general the more poles and zeroes that the filter approximation has, the more components that will be required to realise it. There are a broad range of filter approximations, but the basic types are Bessel, Butterworth, Chebyshev, Inverse Chebyshev and Elliptic(Causer) [107]. Each filter approximation exhibits a unique output response. Examples of a selection of these responses are shown in Fig. 4.18.

Butterworth The Butterworth has a completely flat passband and is often described as having a maximally flat response in the passband as there is essentially no ripple in the passband. The attenuation rate in the transition region is higher than that of the Bessel but slower than the other mentioned filters.

Chebyshev The Chebyshev filter exhibits ripples in the passband. Its attenuation rate in the transition region is higher than that of the Bessel, Butterworth and Inverse Chebyshev.

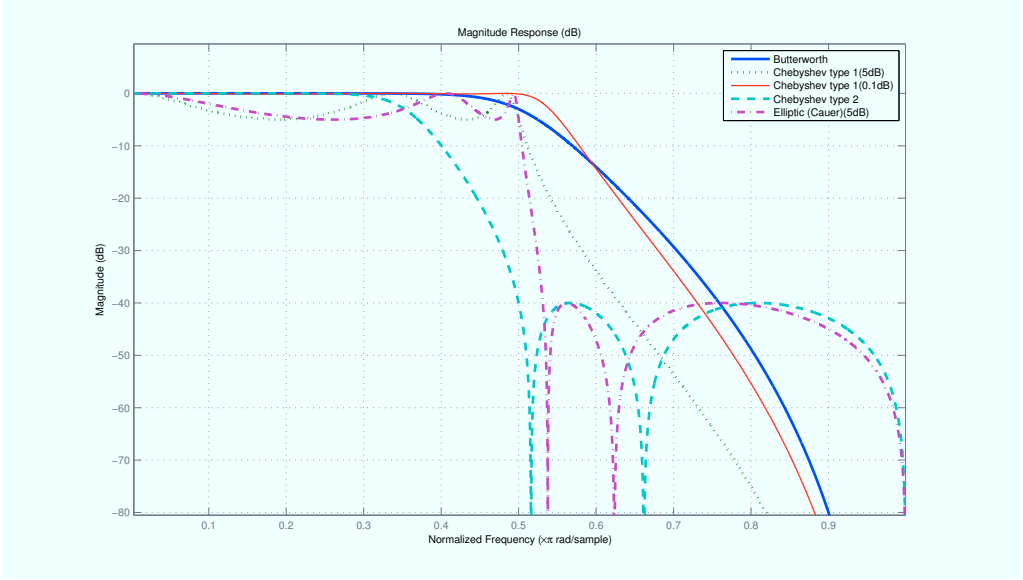

Figure 4.18 – *Diagram showing a different output responses of a selection of the basic filters types. The filters are 5th order with the ripple amplitude labelled.*

Inverse Chebyshev The inverse Chebyshev filter exhibits ripples in the stop band but essentially flat in the pass band. The attentuation rate in the transition region is higher than that of the Bessel and Butterworth but less then Chebyshev.

Elliptic The Elliptic (Cauer) filter has the steepest attenuation rate in the transition band of the mentioned filters. But it exhibits ripples in both the stop-band and the passband.

To realise the desired transfer function, the filter is implemented into an electrical network. The implementation can be classified broadly into passive and active filters. Passive filters are implemented from inductors, capacitors and resistors and require no additional power other than the signal. Due to this, signal attenuation occurs in the passband. The main disadvantage is the physical size of the components and the attenuation in the passband, although they have a large dynamic range and are able to handle high frequencies.

The active filter is one where there is an active component within the electrical network, requiring additional power. The active components typically has been

an operational amplifier (OA), although other methods are available such as switched capacitor[1], operational transconductance amplifier (OTA)[2] [106]. In addition monolithic, integrated systems on a chip are common, which feature all components necessary to implement a filter on a single substrate, typically with a switched capacitor active component. This is due to the space savings associated with implementing a capacitor rather than a resistor.

The introduction of an active component to the network also introduces additional factors that need to be considered compared to that of the passive implementation. The active component can be a source of significant noise, and in op-amps, dynamic range and bandwidth requirements need to be considered [102].

Anti-aliasing Filter Implementation

A low pass filter with the purpose of preventing aliasing called an anti-aliasing filter is described below. In a data acquisition system it is highly desirable to sample the signal without the addition of distortion. This minimises the amount of processing required to correct for it. The Butterworth filter has one of the flattest undistorted responses in the passband, thus additional processing of the signal is not required. The Butterworth filter approximation is also simple to design and implement and is appropriate for the anti-aliasing filter as the requirements are not too demanding.

Ideally the filter should attenuate the high frequency components above the Nyquist rate to a level below that of the ideal SNR of the ADC. With a 10 bit resolution, as in the case of the ATmega8, the SNR is 62dB. Thus at the stop-band frequency an attenuation of at least 62dB should ideally be provided. This assumes the worst case scenario where full scale noise is present at frequencies above the stop band. The maximum sampling rate limited by the transfer rate of the communications interface to the PC is 450 samples/sec each, for two channels.

[1]The switched capacitor is a device which emulates a resistor through the rapid charging and discharging of the capacitor

[2]The OTA closely follows the structure of an OA but the low impedance output stage is replaced with a high impedance output stage [106]

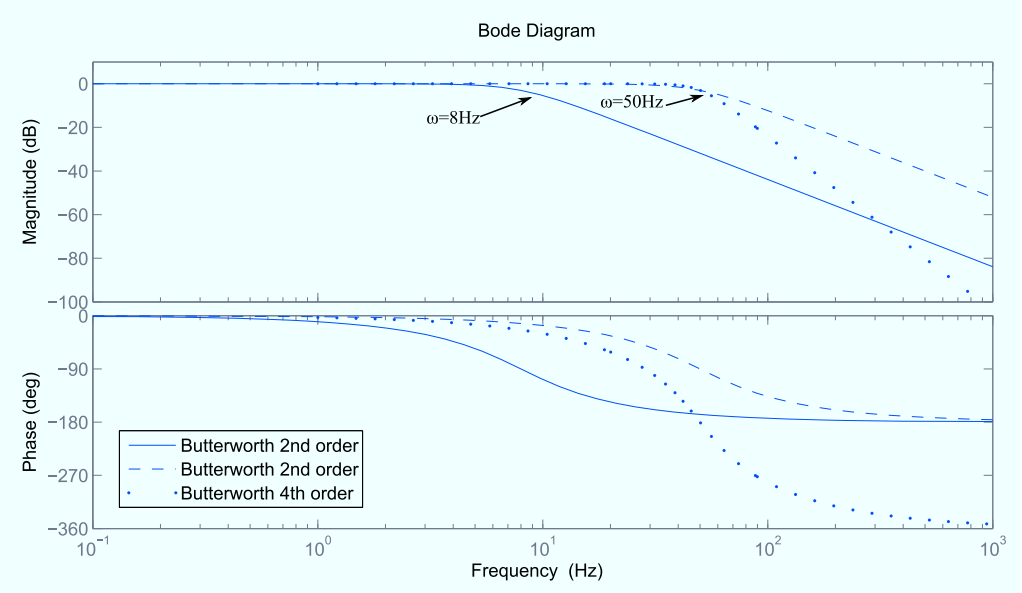

Figure 4.19 – *Bode plot showing response for three Butterworth low pass filters of varying order and cut-off frequency.*

This dictates that the highest signal frequency that can be sampled is 225Hz. Thus the attenuation should be below 62dB at 225Hz. The chosen filter approximation was a second order Butterworth low pass filter. The response of the filter can be seen in Fig. 4.19, three filters are shown for comparison. The second order filter with a cut-off frequency of 50Hz has an attenuation of 25dB at 225Hz while the same order filter with a cut-off frequency of 8Hz has an attenuation of 57dB. A fourth order filter is also shown with a cut-off frequency of 50Hz achieving a greater attenuation of 51dB at 225Hz. For a second order filter to achieve an attenuation of 62dB the cut-off frequency must be approximately no higher than 8Hz. This severely restricts the bandwidth of the signal and important information may be lost. The second filter with the 50Hz cut-off frequency was selected on the assumption that the high frequency components above the stop band is not expected to be full scale and that the attenuation levels shown is assumed to be adequate.

Oversampling- An alternative solution to improve the attenuation at the stop band while maximising bandwidth, is to apply the process of oversampling. Over-

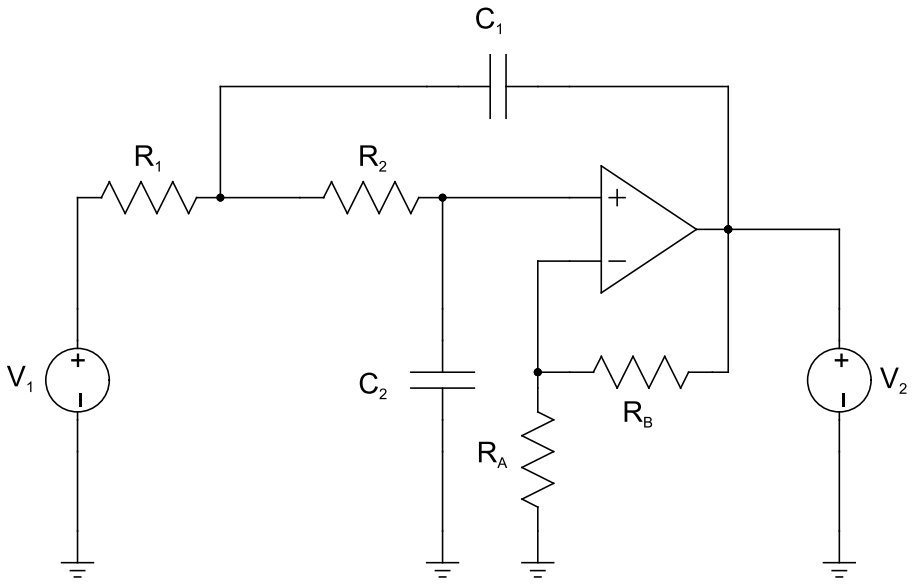

Figure 4.20 – *Sallen-Key Lowpass filter*

sampling is simply the process of sampling the signal at a frequency significantly higher then that of the Nyquist frequency. Oversampling reduces the demands of the low-pass filter as it is now transferred to the digital domain. In addition the ADC quantisation noise is reduced [108]. Once sampled at the higher frequency the signal can be digitally filtered with a significantly higher order filter, then down-sampled to the desired frequency. There is a trade-off with this technique, as a significant load can be placed on the processor while performing signal processing, as well as the need for a faster ADC.

Sallen-Key Circuit To realise the previously described Butterworth filter, (Fig. 4.19) a simple network topology known as Sallen-Key[109] is used. An example of a typical second order low pass filter implementation is shown in Fig. 4.20. This is a popular topology as it has the ability to cascade to achieve higher filter orders, and requires a minimal number of parts.

The transfer function of the low pass Sallen-Key arrangement shown in Fig. 4.20 is,

$$T(s) = \frac{V_2}{V_1} = \frac{\frac{K}{R_1 R_2 C_1 C_2}}{s^2 + \left(\frac{1}{R_1 C_1} + \frac{1}{R_2 C_1} + \frac{1-K}{R_2 C_2}\right) s + \frac{1}{R_1 R_2 C_1 C_2}} \tag{4.13}$$

where $K = 1 + \frac{R_B}{R_A}$.

This equation can be seen as a transfer function of the general form,

$$T(s) = \frac{K{\omega_o}^2}{s^2 + (\omega_o/Q)s + {\omega_o}^2} \tag{4.14}$$

where,

$$\omega_o = \frac{1}{\sqrt{R_1 R_2 C_1 C_2}} \tag{4.15}$$

$$Q = \frac{\frac{K}{\sqrt{R_1 R_2 C_1 C_2}}}{\frac{1}{R_1 C_1} + \frac{1}{R_2 C_1} + \frac{1-K}{R_2 C_2}} \tag{4.16}$$

which is an all pole low-pass filter. This enables the implementation of a filter with a specific response type by specifying ω_o and Q.[1]

The final schematic of the filter can be referenced at Appendix A.0.1.

4.6 Software

The software for the embedded processor was developed in C. No real-time embedded operating system is run on top of the processor and all tasks are run in a single threaded fashion. All routines have direct low level access to the microprocessor.

Software that runs in the PC terminal was developed in Visual C++ with .NET framework under the Windows operating system. This provides a graphical user interface (GUI) for sending request to the various devices on the bus.

[1] The denominator of the transfer function which is a quadratic polynomial, $s^2 + b_1 s + b_0$ is often written in the general form of $s^2 + (\omega_o/Q)s + {\omega_o}^2$ where $Q = \sqrt{b_0}/b_1$ and $\omega_0 = \sqrt{b_0}$ [106]. In control theory the denominator of the transfer function is often written as $s^2 + 2\zeta\omega_n s + {\omega_n}^2$ where ζ is the dampening ratio and ω_n the undamped natural frequency. For large values of Q there is typically a peak in the neighbourhood of ω_o.

High Level Generic Module Description The function of each of the control modules can be described generally as receiving a request from a device on the network and carrying out this request. This behaviour is illustrated in Fig. 4.21.

The device first enters an idle state where it awaits a valid request from a device on the bus. The request is processed for validity in the communication application layer, before invoking a function to carry out the request. The general process of a typical request involves acquisition of data, which may involve the ADC, processing of the data, and performing some action based on the processed data. This can be a repetitive process, or a single operation process. Once the process is finished a message is sent back on the bus to inform the requester of the finished process. The handling of ADC conversions and the communications layers are interrupt based to enable efficient use of the processor.

For specific diagrams for other devices refer to Appendix B.

4.7 Specific Boards

4.7.1 Singularisation Board

The singularisation board handles the control of the singularisation subsystem for the singularisation process which will be described in later chapters. For detailed implementations of the singularisation board refer to Appendix A.0.1 for hardware and Appendix B.0.7 for software.

4.7.2 Pressure Regulator Board

The pressure regulator board forms a component of the singularisation subsystem, enabling regulated pressures to be delivered to the system. For detailed hardware implementations of the pressure regulator board refer to Appendix A.0.3.

4.7.3 Communications Hub

The communications hub in addition to connecting the separate devices on the network together, performs physical layer translation. The board provides

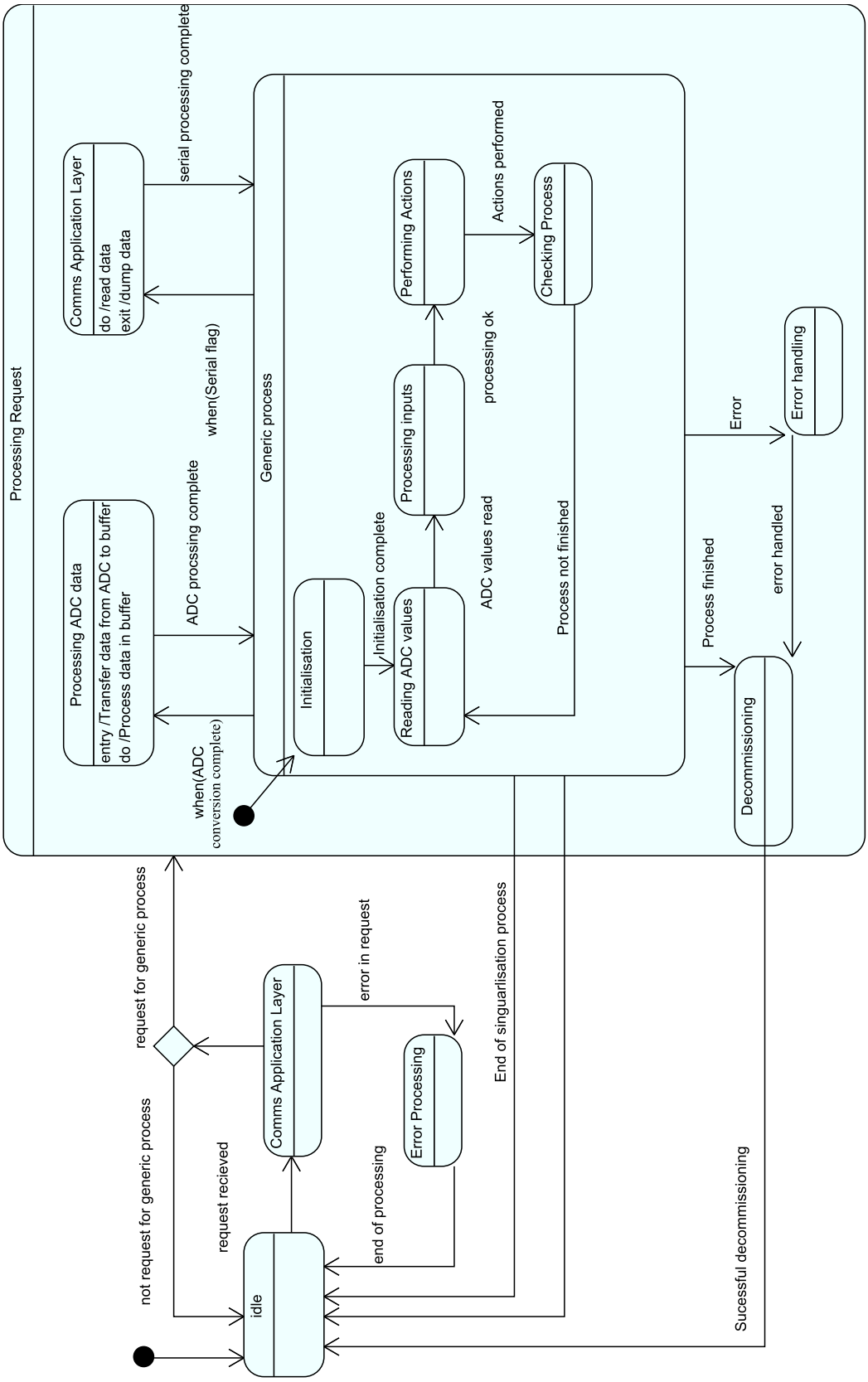

Figure 4.21 – *High level state diagram of the software in a generic module.*

translations from the RS-485 standard used for the system components, to RS-232 for interfacing to the PC. Detailed implementation of the hardware can be referenced in Appendix A.0.2.

4.8 Summary

The development of generic control modules used in the control of the process has been described. The implemented communications protocol is modelled heavily on the Modbus open standard with an EIA-485 physical layer. The signal conditioning circuits have been developed to enable effective interfacing of the transducers to the analog to digital converter for digitisation. Finally state diagrams of the behaviour of the control modules have been described.

The development of the generic module provides a highly flexible control solution which can be adapted to meet a number of requirements through implementing the combination of peripherals. The modularity of each of the systems, eases testing and promotes high reuse of components and code. In addition modularity greatly simplifies extensibility in the future, as additional modules can be added to the network with ease. The following chapters will focus on the development of singularisation devices based on various concepts.

Chapter 5

Mechanical Singularisation

5.1 Introduction

In Chapter 3 (system architecture), an architecture was described where a required module is the spheroid delivery system. The architecture describes a further partitioning of the system into the singularisation system and the spheroid injection system. In this chapter a simple singularisation system is presented which utilises both fluid flow and the mechanical actuation of rods. Enabling the separation of a single particle from a particle train. In Sect. 5.2 the experimental methods are presented along with the concept of how the device achieves singularisation. Section 5.3 presents the results of a manual and automated test. Section 5.4 presents a discussion of the results and finally Sect. 5.5 presents a summary of the presented mechanical method of singularisation.

5.2 Methods and Materials

5.2.1 Experimental Setup

The key components to the singularisation system consists of a transparent fluidics block (containing the fluidic chambers), pressure injection system, the shunting and trapping rods, and solenoids for the actuation of the rods, as shown in Fig. 5.1

The singularisation fluidic device consists of three main chambers: The loading chamber, the singularisation chamber and the injection chamber. The loading chamber is responsible for confining the particles so that a single particle train is formed. The separation chamber is where the leading particle is separated from the particle train, which is then transported into the injection chamber for further manipulation. The pressure injection system (Dagan PMI-200) is responsible for supplying the pressure burst for the automated loading of the beads. In the initial manual tests, a manually operated syringe is used instead. A further description of the singularisation method is described later in Sect. 5.2.3.

The trapping rod is located so that its outer surface on one side is in line with the surface of the loading chamber. This is to ensure that the leading particle is kept in line with the particle train. Fittings to couple the tubing to the device are custom manufactured to ensure a seamless connection to the device chambers.

Control of the two solenoids which actuate the rods is acomplished through a custom developed control board previously described in Chapter 4.

For detailed mechanical drawings of the setup refer to Appendix Fig. C.1.

5.2.2 Device Fabrication

For ease of machining and prototyping, the singularisation block containing the chambers is made from poly(methyl methacrylate) (PMMA). The block chambers are realised through conventional machining techniques.

The shunting rods are high speed drill bits shanks which have been ground. These are the same drill bits which have been used to drill the chambers. Although the material is prone to rust, it provides a simple method for realizing the rods. After each test the rods are thoroughly cleaned to minimize corrosion. The custom fittings are also machined from PMMA.

5.2.3 Particle Separation Method

Separation of a particle was achieved through the movement of mechanical rods. Figure 5.2 provides an illustration of the key sub-processes. First, the leading

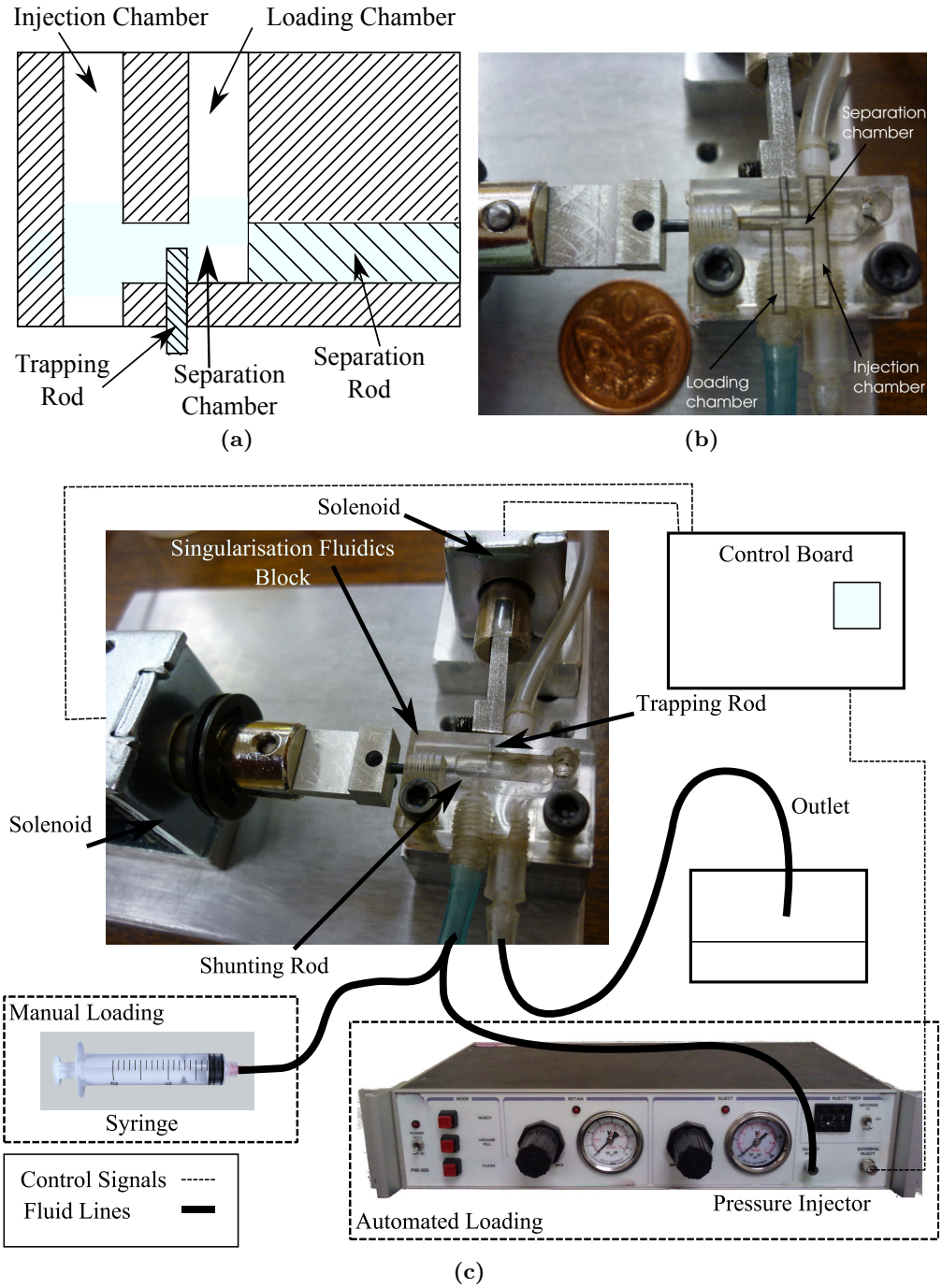

Figure 5.1 – *Diagrams of schematic setup of mechanical singularisation setup. (a) Layout of fluidic chambers within the singularisation block. (b) Photograph of prototype with fluidic chambers highlighted (c) Schematic of system components.*

particle in the particle train is transported into the separation chamber from the loading chamber via fluid flow. The particle train is prevented from progressing further through to the injection chamber due to the obstruction from the extended trapping rod (Fig. 5.2a). The diameter of the separation chamber was sized appropriately so that a single particle is presented into the separation chamber at a single time. Secondly, with the particle in the singularisation chamber the trapping rod is retracted (Fig. 5.2b) and moments later the shunting rod is extended. The fluid flow generated, along with physical movement of the shunting rod transports the leading particle through to the injection chamber (Fig. 5.2c). The extended shunting rod further isolates the injection chamber from the rest of the chambers, so that manipulation of the single particle within the injection chamber is independent to that of the system. Once the particle is in the injection chamber, pressure is applied and the particle is transported downstream for further manipulation or analysis (Fig. 5.2d).

5.2.4 Experimental Procedure

Due to the low availability and difficulty in obtaining cartilage spheroids, alginate beads were used as a simulant. They were made by mixing a 2% alginate solution (Sigma-Aldrich) with $CaCl_2$. Additionally, red dye was added to the alginate solution to improve visualisation. The beads used in the trials had an average diameter of 1.30mm$\pm$0.05. The working fluid within the device was water although in the actual device Phosphate Buffered Solution (PBS) or cell culture media will likely be used.

At the beginning of each trial, chambers were fully purged to remove large bubbles that may have accumulated within the chambers during setup. This was accomplished simply by flushing the chambers with a high flow rate of fluid.

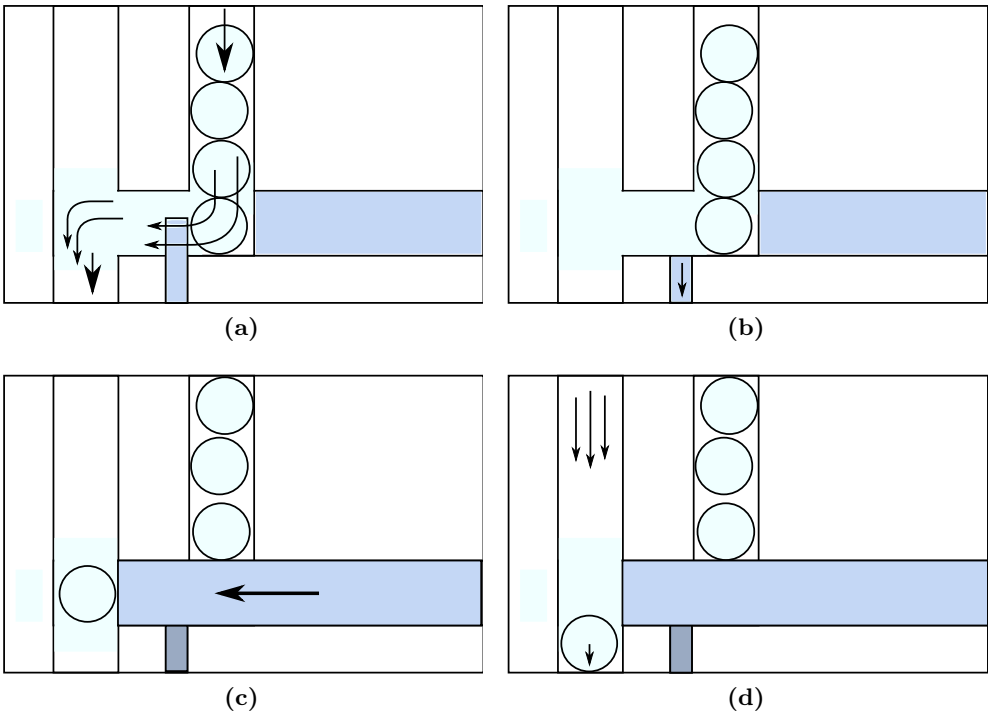

Figure 5.2 – *Diagrams of singularisation process. (a) The transport of the leading particle to the singularisation chamber. (b) The retraction of the trapping rod. (c) Separation of the particle and transport to the injection chamber. (d) Transport of the separated particle downstream for further analysis.*

5.3 Results

5.3.1 Manually Loaded Tests

Manual tests conducted involved an operator manually controlling fluid flow into the loading chamber via a syringe. The operator would provide flow until the required bead was positioned within the loading chamber. Once correctly positioned, the operator would commence the singularisation sequence as described in Sect. 5.2.3.

In the trials where the manual method of loading was conducted, the beads were observed to separate correctly, although only a maximum of 10 beads were used. The state of the beads after singularisation was not thoroughly characterised or investigated under higher magnification, however no obvious signs of tearing or breakage were observed to have occurred to the beads.

5.3.2 Automated Loaded Tests

In the automated tests, the manual loading of particles into the loading chamber was replaced with a pressure pulse, followed by the singularisation sequence. This predetermined pressure pulse enabled pressure driven fluid flow into the loading chamber, thereby transporting the particle train and the leading particle down into the singularisation chamber. The experiments showed that the open loop method of transporting the particles through a pressure pulse was an unreliable method. Singularisation cycles would predominately damage the beads, resulting in large tears, depending on the location of the particle relative to the singularisation chamber. The tears were the result of the particle pressing against the juncture of the singularisation and loading chamber as the shunting rod was extended. Video analysis confirmed that the damage was due to the improper positioning of the beads during the loading process. This was observed to occur due to three scenarios:

- Partial transport of leading particle into separation chamber (Fig. 5.3a).
- Deformation of the leading particle where the second particle was partially inside separation chamber(Fig. 5.3b).
- Particle blockages (Fig. 5.3c).

The partial transport of the particles occurs where the fluid flow time was not sufficient to fully transport the leading particle into the singularisation chamber. Instead, the leading particle was partially in the chamber. At the other end of the spectrum was when the fluid flow rate was high, and the leading particle was observed to deform, resulting in the second particle becoming partially inside the singularisation chamber. In both these cases, the partial presence of the particle was sufficient for the bead to catch on the chamber junctures, resulting in the bead being severed once the shunting rod was extended. Lastly, particle blockages result in singularisation failure as the system assumes that a particle has been separated, but damage does not occur to the beads.

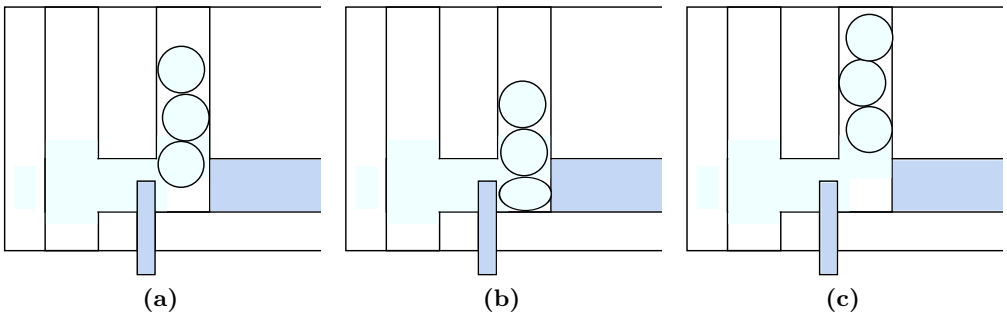

Figure 5.3 – *Diagrams illustrating failure modes: (a) Failure due to the partial transport of the leading particle. (b) Deformation of the leading particle. (c) Blockages.*

Due to the difficulty and problems in obtaining consistent singularisation results, and the inherent limitations of this method, no further characterisation of the device was performed.

5.4 Discussion

The presented device was able to separate a single particle with high probability when manual loading of the particles was conducted, however a high probability of failure resulted with the automated methods. The manual tests conducted showed proof of concept for the device's ability to separate the particle with no obvious signs of damage to the beads. Whereas in the automated loading case, a high proportion of the trials resulted in severe damage to the beads.

The results showed that the failure in singularisation was due to the inability of the automated system to accurately position the leading bead in the singularisation chamber (Fig. 5.3). In these tests, a set burst of pressure was supplied to the loading chamber to transport the leading particle into the singularisation chamber. This was an open loop process where there was no feedback of any parameters from the system. In these tests, the set pressure burst alone was not enough to guarantee the successful positioning of the particle as there are many other random process responsible for the transport of the lead particle. This can be seen in the results where the same set pressure burst resulted in scenarios where the flow was not sufficient (Fig. 5.3a), leading to partial transport, or high (Fig. 5.3b),

leading to particle deformation. The variations showed that without a method of feedback from the system, the level of accuracy required to position the particle could not be accomplished. Furthermore, this task was difficult with the use of alginate beads as they were tear shaped rather than spherical, leading to more complex stacking of the beads within the loading chamber.

In the case of the manual tests, there was a high possibility that a closed loop control system exists with the operator. The operator was able to use visual feedback to control the actuation of the syringe which provided the fluid flow. This enabled the particle to be correctly positioned within the singularisation chamber, thus greatly increasing the probability of successful singularisation.

With the current setup for the system to operate correctly, there must be feedback of the particle position. One method of providing localisation data for the control system is through computer vision. A computer algorithm could be developed where the lead particle's position is tracked. A vision approach is highly flexible and has the potential of providing high positional accuracy of the beads, but the time required to process the image may be a bottleneck of the system throughput. Tracking of spherical particles through computer vision is a common task and several commercial and open-source packages are available [110]. Along with several custom in-house developed algorithms which have been reported [110, 111, 112, 113].

The experiments have also highlighted the limitations of a mechanical mechanism based method of particle manipulation. The failure to correctly position the particle in the singularisation chamber would result in damage to the alginate test beads. In the actual application cartilage spheroids used will be relatively more robust, and may not suffer from the same fate. However since the potential to damage the particles remains, more gentle methods of particle manipulation will need to be sought after. The small precision moving parts used in the device is also a disadvantage which increases complexity, manufacturing costs, reduced durability with wear and difficulty in scaling down. An example of more gentle manipulation methods is through the use of hydrodynamic forces alone, generated from fluid flow. This would also have the added advantage in eliminating the

direct need for custom moving parts.

5.5 Summary

In this chapter a device was presented which was proven to have the ability to separate alginate beads when manual loading of the beads into the singularisation chamber was performed. When an automated method was introduced, the lead particle was unable to be successfully positioned in the singularisation chamber and failure occured. The failure of singularisation caused either damage to the lead particle or the second lagging particle, as the shunting rod was extended, severing the bead.

There were also limitations with the mechanical method of singularisation, including the harsh method of manipulation compared with other methods. The use of small moving parts was also problematic and difficult to scale down if required.

The difficulties and unreliable operation of open loop control positioning of the lead particle within the separation chamber, and the inherent harsh manipulation methods, along with the small mechanical moving parts within the device, limits the device's usefulness in the successful separation of fragile particles. The prototype has shown that a device utilizing gentler manipulation methods, along with feedback of the particle position would provide a better solution. The next chapter will describe the development of such a singularisation device, which utilises less harsh hydrodynamic forces for manipulating spheroids, along with a feedback system for detecting spheroid positioning.

Chapter 6

Dual Trap Method of Particle Singularisation

6.1 Introduction

Previous developments of a device (Chapter 5) to singulate the spheroids were unsuccessful and highlighted the many shortcomings of a mechanical based method for singularisation.

In this chapter, a device which utilises hydrodynamic forces alone for manipulation and trapping of particles to achieve singularisation is presented. In Sect. 6.3, an investigation of fabrication methods for a macro fluidics device, as well as the methods used in the fabrication of the prototype is presented. Section 6.2 describes the concept of manipulating the fluid flow and trapping site to achieve singularisation. Section 6.4 describes the experimental setup and general procedures, and Section 6.5 presents the results and discussion from the characterisation of all the sub-processes in the singularisation process. Finally Sect. 6.6 provides a discussion of the overall results and Sect. 6.7 summarises the fluidics singularisation prototype utilising dual trapping sites.

6.2 Functionality - Singularisation concept

The concept to separate a single particle utilise a particle train, with sequential manipulation of fluidic flow paths and trapping sites. Particles are trapped at fixed locations acting as temporary barriers to impede the flow of particles. By trapping the first two particles in the particle train, and releasing the first particle while the second particle acts as a barrier, singularisation is achieved.

The arrangement of chambers is illustrated in Fig. 6.1a. The device consists of four chambers, main chamber M, and three smaller side channels C1 and C2 and F. Channels C1 and C2 were at a lower pressure relative to the main chamber while that of channel F was higher. The main chamber is sized relative to the diameter of the particles to prevent horizontal stacking. The side channels were sized smaller than the diameter of the particles so that they can be held at the fixed locations. Relative placement of the side channel F and side channel C1 were important to ensure the volume near channel C1 was fully swept, and that occurrences of dead volume where particles may become trapped were minimised.

The singularisation process progresses through a sequence of five key steps (Fig. 6.1). They are,

1. Capture of the leading particle - Fluid path from chamber H to C1 is established (Fig. 6.1b).

2. Transport of the untrapped particles back upstream - Fluid path from chamber F to H is established (Fig. 6.1c).

3. Capture of the second particle - Additional fluid path from chamber H to C2 is established (Fig. 6.1d).

4. Release and transport of leading particle. Additional flow is established from chamber F to D. Chamber C1 is closed (Fig. 6.1e).

5. Termination of all flows and transport of lagging particles upstream - Burst of flow from F to H to transport particles upstream (Fig. 6.1f).

The process is repeated for each particle required to be separated.

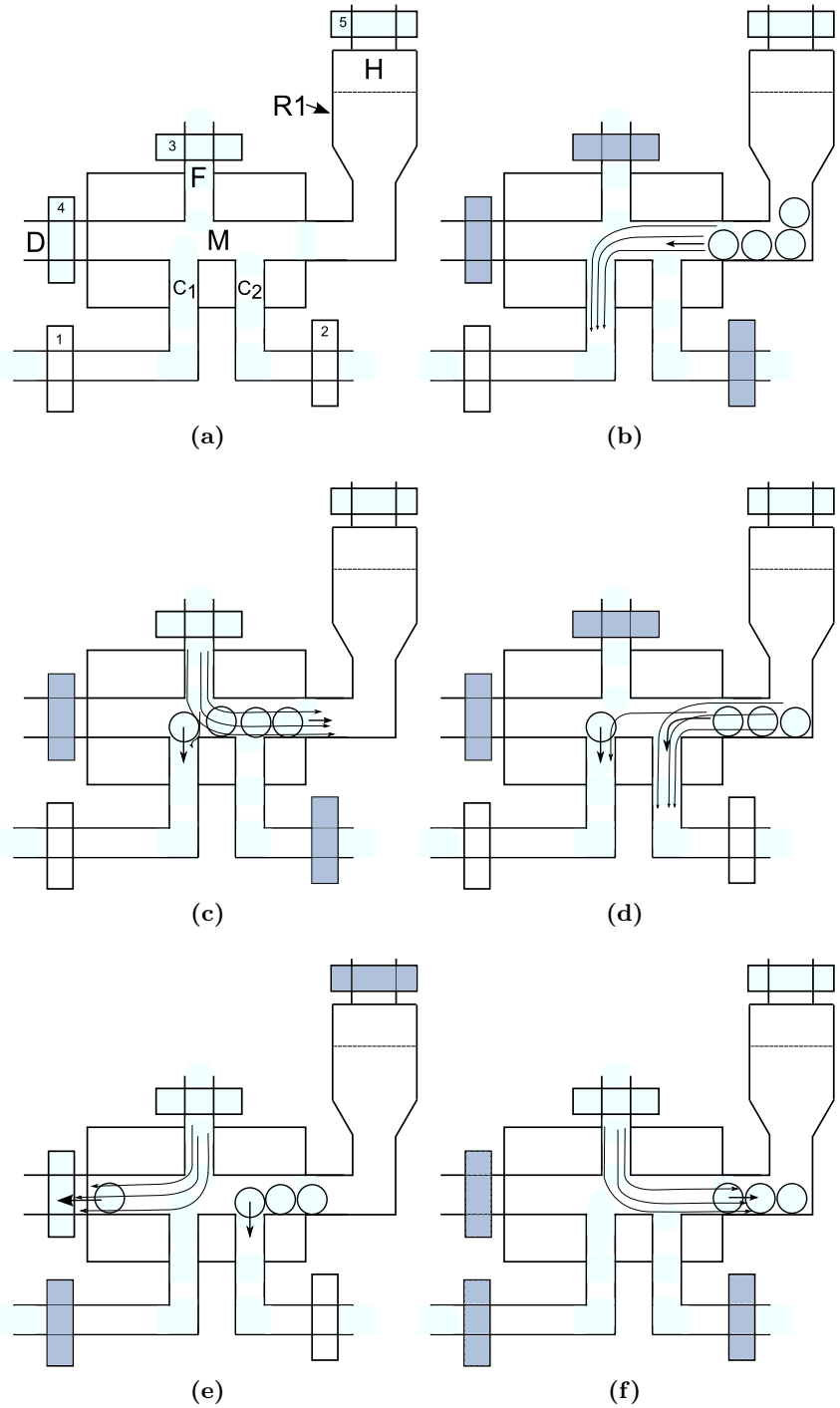

Figure 6.1 – *Dual capture site singularisation method- (a) Name and location of the fluidic chambers. A single particle is separated through the sequential steps of; capturing the leading particle (b), separation of lagging particles (Flush back) (c), capture of second particle (d), the transport of leading particle downstream (e) and finally the termination of the fluid flows (f).*

6.3 Fabrication

A prototype was required to be manufactured which contained millimetre and sub-millimetre scale circular channels within a clear fluidics block. Appropriate material and manufacturing methods were selected for the device.

6.3.1 Material Selection

The selection of the material was governed by the requirements of the application. As the device was a prototype, the requirements were less on the life cycle, and more on the ease of development. Required properties of the material include transparency, enabling imaging techniques to be employed, and good chemical resistance to high concentrations of ethanol. This resistance was required for the sterilisation of the device without damaging the material.

Poly(methyl methacrylate)(PMMA) and polycarbonate were good candidates for meeting the requirements. They belong to the thermoplastic class of synthetic polymers, which become molten or rubber-like above the glass transition temperature (T_g). They can also be easily worked using conventional machining techniques, and are relatively inexpensive, which are important in the development of a prototype.

PMMA is commonly used in microfludic devices but solvent crazing will occur with prolonged expose to high concentrations of ethanol, used for the sterilsation of the fluidics device. Crazing is the crack like structures in a glassy polymer when subjected to a tensile stress prior to failure [114]. These structures severely degrade the optical performance of the material preventing successful imaging of the underlying objects. Polycarbonate is more resistant and does not exhibit solvent crazing to ethanol, so was selected for the device.

6.3.2 Fabrication Method

The method of manufacturing the prototype could influence the design of the prototype by placing limits on the level of detail that can be attained. For prototyping, the two methods which were suitable for a quick turnover are,

additive manufacturing and in-house conventional machining techniques. There was also the possibility of using micro-fabrication techniques, if the device was to be scaled down. This would enable unprecedented levels of accuracy and small features, however the process was limited to the creation of structures on much smaller scales.

Additive manufacturing techniques, offer one possible method of manufacturing the device. This would enable detailed complex internal features and enclosed chambers.

The remaining methods of fabrication was through conventional machining methods. This method places a limit to the design as only simple internal features can be realised through the drilling of holes. There was also the possibility of manufacturing the device in two halves, which would enable the realisation of more intricate chamber paths, and access to internal features. The creation of two parts necessitates bonding to enclose and form sealed channels.

There are a number of methods available for manufacturing the prototype, with the required accuracy and resolution, but ultimately the turn around time would be a major factor. μSLA may be appropriate for manufacturing the prototype, and offers a relatively fast turnaround time, but relative to in-house manufacturing, the turnaround time of each prototype may become a problem. As the development would inevitably involve many iterations, in-house manufacturing would enable the fastest turn-around time, early on in the development stage. At the later stages, after more knowledge is gained, rapid prototyping techniques may provide a better choice.

6.3.2.1 Overview of Bonding Techniques for Polycarbonate

To implement the intricate features within a device using conventional machining methods in-house, the block must be fabricated in two halves. Bonding of the device was necessary to achieve the enclosed chambers. The bonding method was a challenge as conventional methods of direct bonding where a liquid solvent is applied has a high probability of blocking the chambers.

An initial literature search showed that bonding of plastics is a common step in the fabrication of microfluidic devices when thermoplastics are involved. PMMA is the most common plastic used in microfluidic devices, thus most bonding techniques are for PMMA, however the techniques may also be relevant for PC. Bonding techniques used in microfluidics can be categorised as either direct or indirect methods [115]. Indirect bonding involves the use of an adhesive layer to bond the surfaces, whereas direct bonding methods mate the surfaces without any additional material added to the interface.

The indirect method of bonding where an adhesive is used, has limitations that need to be considered when sealing micro-channels. The application of an adhesive will result in channel side-wall properties which are altered from that of the bulk material. It was important that the adhesive did not degrade the performance of the channel. The application of the adhesive also poses a challenge whereby the micro channels can become blocked. These issues may limit the usefulness in micro-fluidics applications.

The prevalent direct bonding methods are thermal fusion bonding and solvent bonding [115]. Thermal fusion bonding involves elevating the material to the glass transition temperature (T_g) with a constant applied pressure. Prior to thermal bonding the surface can also be treated to achieve higher bond strengths. Thermal bonding is relatively simple, inexpensive and does not require the use of sophisticated equipment. Raising the temperature to the T_g point enables the polymers to interlock at the interface forming a strong bond. This process is highly dependent on the temperature, pressure and application time. Undesired channel deformation will occur with unoptimised processes, therefore optimisation of the process was required to obtain the desired bond strength, while minimising channel deformation.

In solvent bonding the process utilises the solubility of the polymer in selected solvents [116]. Once solvated the polymer chains become mobile and can diffuse across the solvated layer, leading to the entanglement with other similarly dissolved chains from another polymer surface. This results in exceptionally strong bonds. Ogonczyk et al. [117] described a concept employing both a solvent and thermal

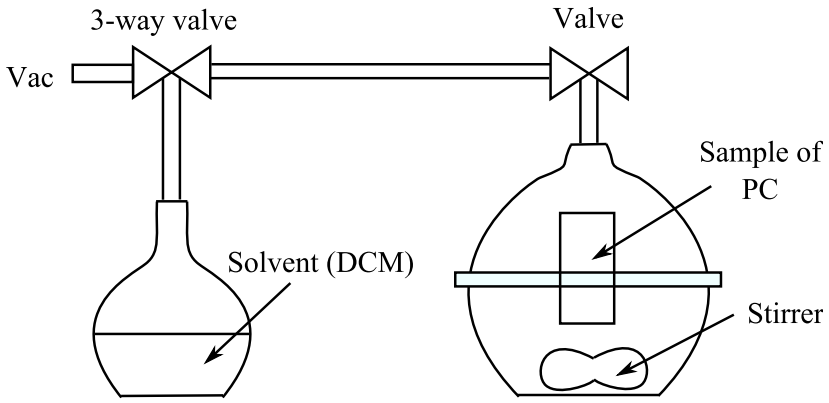

Figure 6.2 – *Bonding experimental setup consisting of a vacuum pump, stirrer, a desiccator and a flask with dichloromethane (DCM) [117].*

based method of bonding. The method relied on the controlled diffusion of solvent into the material, as well as a thermal bonding process. The depth of solvent diffusion was controlled through the controlled exposure to solvent vapours. The addition of a solvent enabled a much lower temperature to be employed compared to that of the thermal fusion bonding methods alone. The combination yields stronger bonds than what can be achieved with either process alone, while minimising channel deformation. The setup was relatively simple and the results have shown good bond strengths with low channel deformation. Due to these factors, this method of bonding was a good candidate for the bonding of the macro-fluidic device.

6.3.2.2 Bonding Experiment

The approach taken by Ogonczyk et al. [117] was investigated to determine the suitability in the manufacturing of the prototype. The setup (Fig. 6.2) consists of: a round bottom flask for the solvent, a glass desiccator and a vacuum pump. Briefly, bonding samples were placed in a desiccator where it was evacuated to 10mbar. Solvent vapour was then introduced through the three-way valve from the flask.

6.3.2.3 Results and Discussion

The preliminary tests showed that the combination of solvent vapours, and elevated temperatures for bonding did successfully bond the device, however there were variations in the results. This was due to the inability to accurately characterise the solvated layer, resulting in situations where a much deeper solvated layer occurred. This would result in significant deformation to the channels.

This method has potential when the solvent layer was thoroughly characterised to achieve consistent bond results. In addition, the characterisation parameters would need to be repeated for each batch of plastic, as there may be variability between batches.

This bonding process was not pursued further, as the degree of gains from achieving the smaller features with the two piece fabrication method was unknown. Instead the conventional method of manufacturing would provide a more effective solution for the fabrication of the initial prototype. If it was found that intricate details were required, then this method of construction provides an attractive solution.

6.3.3 Fabrication summary

Fast turnaround times are highly advantageous when prototyping, as there will inevitably be many iterations involved. In-house manufacturing was decided as the most appropriate solution at the early stages of development where the requirements of the device are not fully understood and are likely to quickly change as knowledge is gained from the preliminary experiments.

Manufacturing of the device in two parts was investigated where bonding was the major challenge. Attempts were made to bond the device using solvent vapour deposition, in combination with a thermal fusion bonding method. The results were inconsistent and no further investigations were considered, as it was unknown whether significant gains would be achieved by the ability to realise finer details. After revisiting the design, modifications were made to enable the device to be manufactured using simple conventional machining operations.

Although this method was selected, the fabrication using two parts and bonding along with a μSLA method may provide an attractive solution for the production of the prototype, once more specifications of the problem are defined though experimentation.

6.4 Experiment

6.4.1 Experimental Setup

A schematic of the experimental setup is shown in Fig. 6.3. The singularisation system consists of a fluidics block, valves to manipulate fluid flow within the block, pressure regulated reservoirs and control boards.

Fluidic connections were made through flexible tubing (Tygon) with an ID of 1.6mm. Tubing was coupled to the device through a flangeless connection system (VICI JOUR). This system ensured that a concentric, relatively seamless, constant ID connection occurs from the tubing to the device to minimize obstructions.

System pressure was supplied through electronically regulated pressure reservoirs (Chapter 4). For the positive pressure reservoir, pressure was regulated at a point in the fluidic line to eliminate pressure variances caused by the decrease in the height of water, within the reservoir. The pressure at the regulation points were maintained constantly throughout the experiments.

Fluidic path actuation The fluidic paths within the device were controlled by various types of valves. Valves 1-3 were hydraulic valves (ASCO 067) and valve 2 was a pneumatic valve (ASCO 188). Valve 4 was a pinch valve (ASCO 284) to ensure particles could flow unobstructed through the tube.

System control Control of the valves and instrumentation was performed with a custom developed control board (Chapter 4). This was responsible for sequential control of the valves, as well as instrumentation of the pressure data from chambers C1 and C2, and system status feedback. The control board was attached to a personal computer (PC) and sent a constant stream of pressure values to the PC.

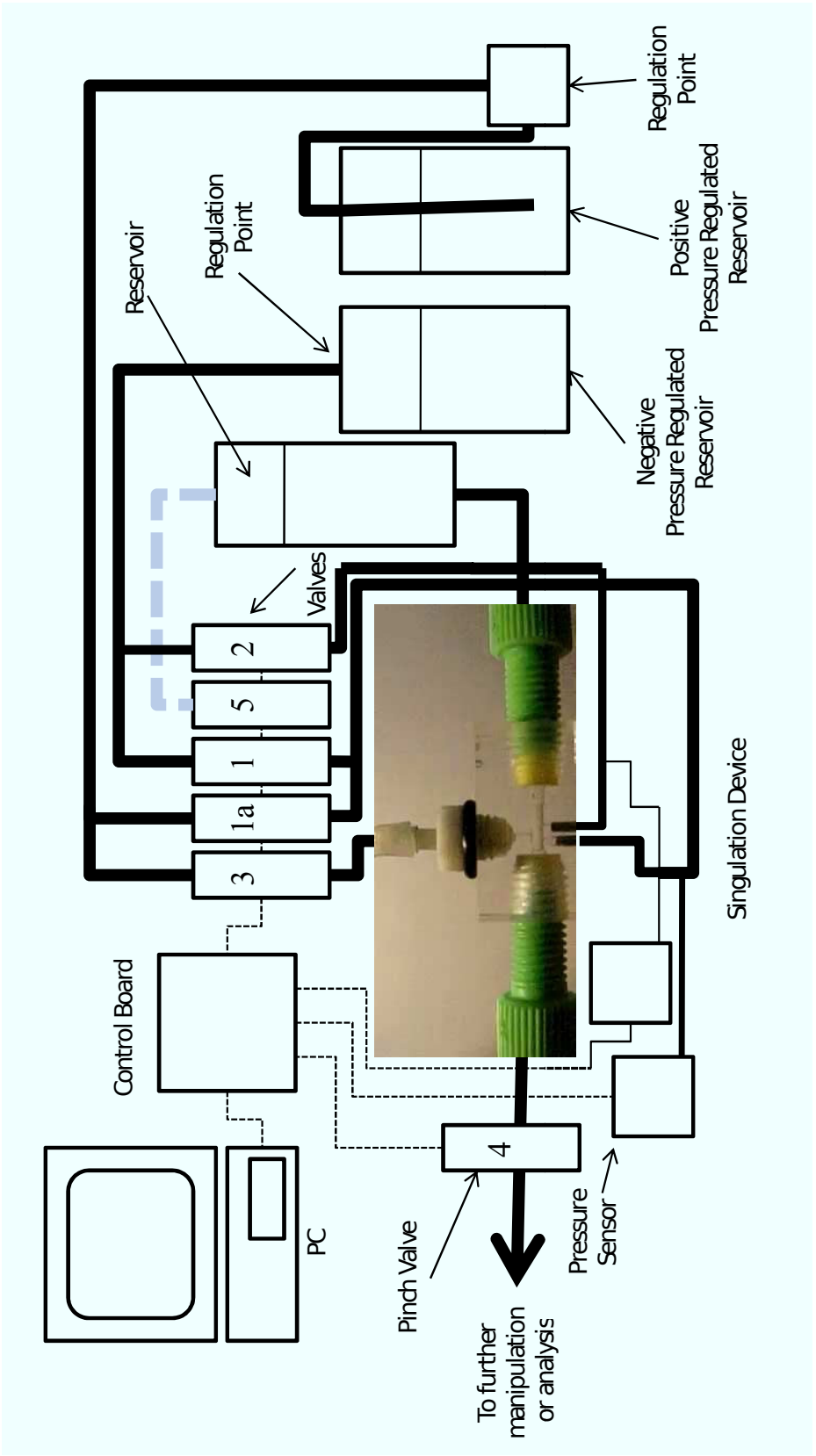

Figure 6.3 – *Schematic of the experimental setup used in testing of the singularisation device. The system comprised of a transparent block containing the fluidics chambers, valves for the actuation of fluid paths, regulated pressure reservoirs and control systems.*

This data was indexed by software on the PC to allow for synchronisation with video data. Interface from the PC to control board was through custom software developed in C++.

6.4.2 Experimental Procedure

The following general procedure was followed for each test. The height of water in reservoir 1 was maintained at 10cm from the centreline of the main chamber M in each trial. Glass beads (Meyer Imports) with an average diameter of 0.9mm were used to simulate pellets.

Custom control algorithms were programmed into the control board for each of the trials of different algorithms. During each trial, pressure data and synchronised video data was streamed to the PC for later analysis.

Prior to each trial, fluid was flushed at high pressure to minimize bubbles that may have become trapped within the system. In general, 15 beads were loaded into the main chamber, unless otherwise specified in the experiment.

6.5 Results and Discussion

The singularisation device presented in this chapter utilised two holding sites in combination with fluid flow manipulation to separate particles in a queue. There were a number of factors that affected the reliability of the dual trapping site method of singularisation. The method of singularisation relied on the successful capture of a particle at chamber C2 so that it acts as a barrier. Early release of the particle resulted in singularisation failure, as the lagging particles were no longer prevented from moving downstream.

6.5.1 Capture of Leading Particle

The capture of the leading particle simply involves the opening of chamber C1 and chamber H. The results show that the probability of successfully capturing and holding the leading particle is unaffected by the range of parameters that were tested (Table 6.1). In all cases 100% capture success was recorded.

Table 6.1 – *Parameters of each trial for the capture of the leading particle.*

Case	Pressure at regulator (Pa)	Head of Reservoir (mm)	Number of beads
1	-3100	130	3
2	-6700	130	3
3	-3100	130	15
4	-6700	130	15
5	-3100	65	15

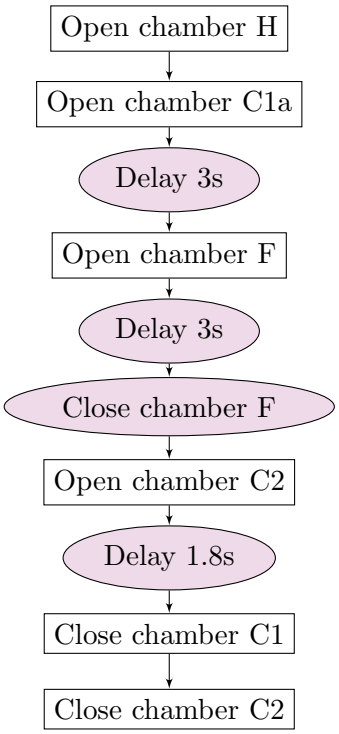

Figure 6.4 – *Intial algorithm for the capture of lagging particle.*

6.5.2 Capture of Lagging Particle after Leading Particle Capture

After the successful capture of the leading particle, the lagging particle must be captured in the second trapping site C2. A number of dynamics can effect the capture of the lagging particle, and significant contributing parameters have been investigated, including, leakage flow from the first holding site, collisions from lagging particles, fluid development time and particle holding forces.

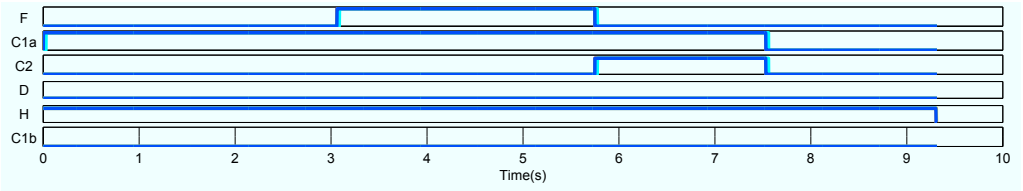

Figure 6.5 – *Timing diagram of the valves showing the initial algorithm valve sequence for the capture of the leading particle.*

6.5.2.1 Initial Capture Algorithm

The initial algorithm illustrated in both state form (Fig. 6.4) and timing diagrams (Fig. 6.5) show how the valves were sequentially manipulated to control the fluidic paths within the device. The algorithm first captures the leading particle through the development of flow from chamber C1 and chamber H. This should transport the particles towards chamber C1 where the leading particle will become trapped. Chamber F was opened allowing an additional flow to develop from F to H. The chamber is activated for 3s. This results in particles which have not been captured to be transported upstream. Chamber C2 was then opened to recapture the lagging particle.

Figure 6.6 shows the pressure response of the system, for four trials, during the capture algorithm. As expected the pressures in both of the chambers decreased as they were opened and in fluid commutation with the negative pressure regulator. The capture of the particles in either of the chamber was observed by the abrupt drop in the pressure. After which the pressure began to level as steady state was reached. It could also be seen that there was a distribution in time, of the lagging particle capture, due to the random distribution of the particle spacing.

The parameters used for the trials and results are summarised in Table 6.2. The results show that there was a high probability of capturing the second bead when only two beads are in the chamber, but this probability was significantly lower once more particles were introduced. Video analysis of the cases that failed, showed the particle was temporarily held until the momentum of particles behind the trapped particle caused it to release. An example of this is shown in Fig. 6.7. The leading particle can be seen to be temporarily held (Fig. 6.7a) before the

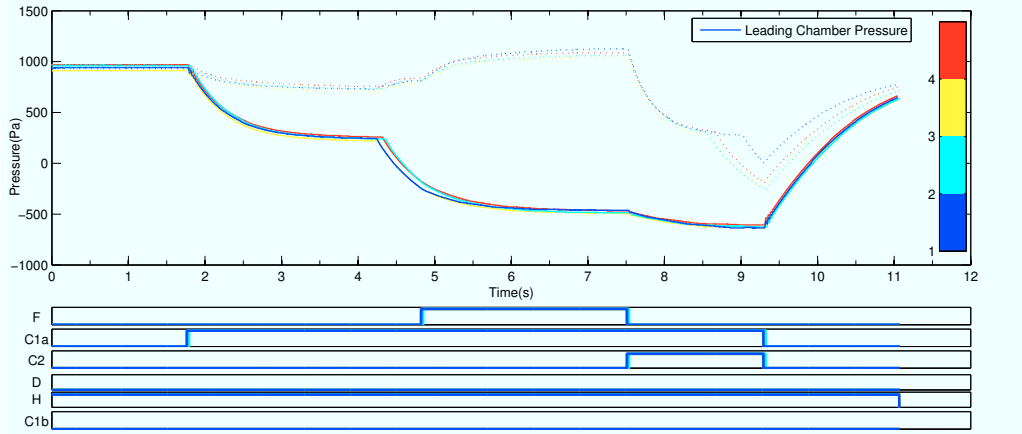

Figure 6.6 – *Simple Capture Algorithm.*

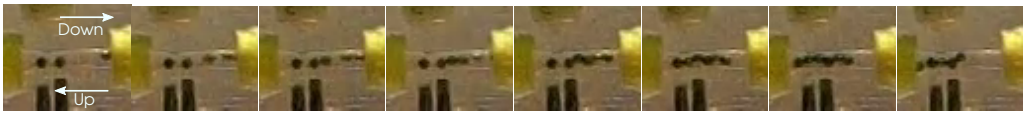

(a) **(b)** **(c)** **(d)** **(e)** **(f)** **(g)** **(h)**

Figure 6.7 – *Frames showing the capture and release of the second particle. The second particle is temporarily captured (a), before the lagging particles begin to accumulate (d)-(e). At (f) the second particle has already released where lagging particles are no longer obstructed and begin flowing downstream (f)-(g). This is until a lagging particle is recaptured (h).*

Table 6.2 – *Parameters and success rate for each case in the capture of the second particle.*

Case	Pressure at regulator (Pa)	Number of beads	Success Rate (%)
1	-6700	2	91
2	-3100	2	73
3	-6700	10	10
4	-3100	10	0

release of the trapped particle due to interactions from the oncoming lagging particles (Fig. 6.7e - Fig. 6.7h).

The success in capturing the lagging particle confirms that the fluid flow paths have sufficient force to transport and capture the second lagging particle alone, but this holding force is insufficient once additional particles are introduced. The additional particles may be interacting with the trapped particle introducing

additional forces. These interactions can be the result of both particle collisions, or from the drag force of the lagging particles. Both of these examples seem to be supported from observations. Examples have been observed where a large group of lagging particles collide in a group with the trapped particle causing it to release. Other examples were observed where the particles collide one by one with the trapped particle, but release was not observed until more than three particles were in contact. This suggests that the force from the collisions alone was not the only cause of release, and that the combined drag force may also be the cause.

The high velocity of the particles at the point of collision, as well as the lagging particles continued velocity once the second particle was captured was unexpected. The assumption was that once a particle was captured, no further flow into the chamber should occur. This should result in the rapid decrease in the velocity of the fluid approaching zero, where the drag forces will rapidly decelerate the particle. Although the particles are not expected to immediately stop due to momentum, the distances travelled were more than expected.

The distances suggested that there was still a relatively significant amount of fluid flowing. The fluid flow was likely to be due to leakage flow moving into chambers C1 and C2. Leakage flow can be due to the mismatch of geometry between the holding surfaces and the held particle. As both the model particle and the holding site are inelastic, a seal can not be formed. This problem should be greatly reduced once real bio-particles are used as they are more deformable, and will conform better to the holding site surface better than the glass beads used in this experiment. The presence and degree of leakage can be verified by capturing a bead and measuring the flow rate. This is characterised in the later Sect. 6.5.2.3.

The leakage flow was responsible for the magnitude of the force the lagging particles exerted on the captured particle. Although leakage flow exists when the leading particle is captured, it was the magnitude and path of the leakage flows, and the resultant angle of the force, which maybe important. When the leading particle was captured, it was only the leakage flow from chamber C1 which is contributing to the fluid flow in the main chamber. This main fluid flow provides

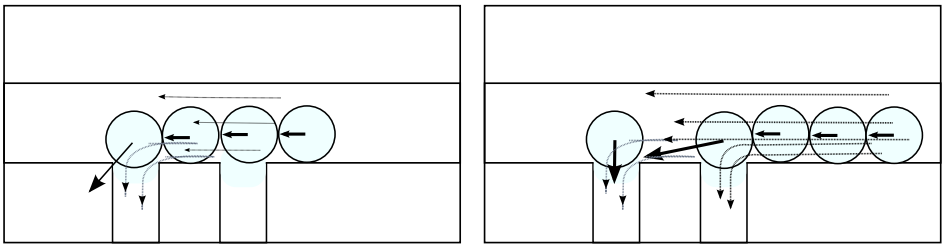

Figure 6.8 – *Fluid flow paths during the capture of the leading particle only (a), and the capture of the second particle once the leading particle is trapped (b).*

the drag on the lagging particles. Assuming the holding forces are equal for each chamber, then the particle trapped in chamber C2 must resist a much larger force. These larger forces are the result of there being more fluid flow in the main chamber than in the first case. The reason for this is that the main chamber flow now consists of both the leakage flow to C2 as well as an additional flow into C1. This would result in a resultant force angle which is much shallower than that of the first case. This is further illustrated in Fig. 6.8, where the illustration shows the differences between the two cases.

In addition to considering the steady state flows, transients must also be considered. The leakage flow which has had sufficient time to establish into chamber C1, may be quite large compared to the flow into chamber C2, at the moment of capture. This is due to the systems constant state of transition, where flows are established and disestablished. This was supported in the trials (Fig. 6.6) where the pressure in chamber C1 can be seen to be relatively constant (more developed flow), than that of the pressure in chamber C2, at the moment of capture. This may further reduce the probability of capture as the leakage flow relative to the capture flow into chamber C2 may be quite large.

The analysis and discussion has indicated that the underlying factor in determining the probability of capturing the second particle was the ratio of the fluid flow into chamber C2 versus the leakage flow into chamber C1, at the moment of capture. A high flow rate into chamber C2 should result in higher capture probabilities. With the current setup this was not easily achieved as both chamber

C1 and C2 are connected at a common point (Fig. 6.3). Decreasing the pressure, or increasing the vaccuum in both chambers by equal amounts may not significantly effect the flow ratio. Although the holding pressures are higher, the leakage flows may also be proportionally higher. This may suggest why the probability of capture is not significantly increased when higher vacuum pressures are used (Table 6.2).

To alter the flow ratio, a number of approaches can be taken. Leakage flow into C1 can be reduced if the capture site geometry is altered to match closer to that of the held particle, or additionally the glass beads are replaced with deformable beads more closely resembling that of the bio-particles. Secondly, the pressure in C2 may be altered, by regulating the pressure within this chamber so that its pressure is significantly higher than that of C1. Of these options the independent regulation would provide the fastest method to implement. This independent regulation of pressure in the two chambers will be investigated in the later Sect. 6.5.2.4.

6.5.2.2 Transient Analysis and Developed Flow

The experiments conducted in the previous section have indicated the fluid flow ratio between C1 and C2 as a possibility, for effecting the probability of successfully capturing the lagging particle. This ratio was not constant and fluctuates as flows develop when chambers are opened. The ratio of the flow at the point of capture may be an important factor. Although the flow rates are expected to be significantly different due to the large difference in the pressure, if insufficient time is given for the flow to develop, the flow ratio at the moment the lagging particle is captured may not be as large.

The transient effects of the system was investigated via monitoring of the pressures. When the valve was opened, there was a period of time required for the fluid to develop to steady state. The determination of this steady state was important as the fluid velocity and flow rate determines the holding force of the bead against the side channel. The algorithm to test this is shown in Fig. 6.9.

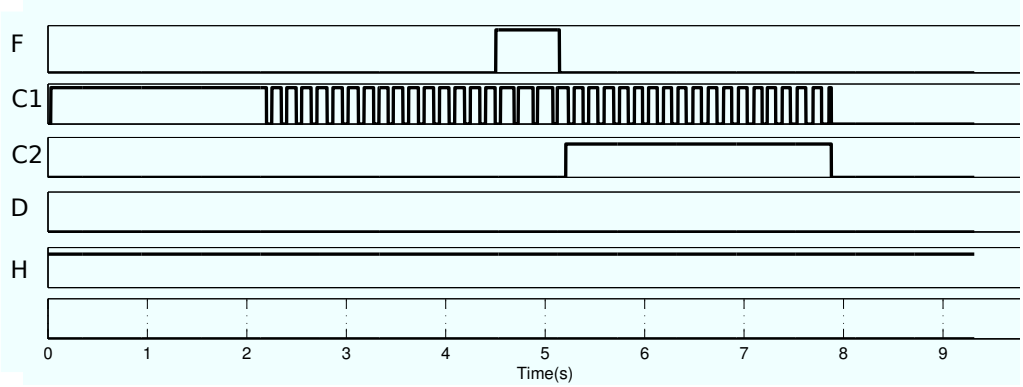

Figure 6.9 – *Timing diagram of the valve sequence for the testing of transients within the device.*

Chamber C1 was toggled regulating around the set pressure point, drawing the leading particle. Chamber F was briefly opened to flush un-trapped particles upstream before chamber C2 was opened, capturing the second particle. It can be seen in the figure that chamber C1 was switched rapidly to regulate the pressure, while that of chamber C2 was left opened as it was regulated by the pressure regulator.

Figure 6.10 shows the pressure response within the two chambers during capture with two different pressure settings. Corresponding timing diagrams are also displayed. The pressure settings were -6000Pa and -3200Pa. It can be seen that both the pressure settings reaches steady state (SS) velocity within ≈1s, with the higher pressure setting reaching SS slightly earlier. In addition, the gradient of the pressure profile was larger for the higher vacuum setting.

It was desirable to capture the particle after the flow was developed so that the flow rate into C2 was at its greatest. Therefore the beads needed to be captured after 1s for this to occur. To achieve this, one method was to flush the beads upstream to a distance where the resulting traverse time is over 1s. This may not be a practical solution as the distances required may be quite large. Another solution was to open chamber C2 while the beads are still being flushed upstream. The particles will be prevented from reaching chamber C2 if the pressure within chamber F was larger than that of the pressure from the reservoir head, while flow is developed into chamber C2.

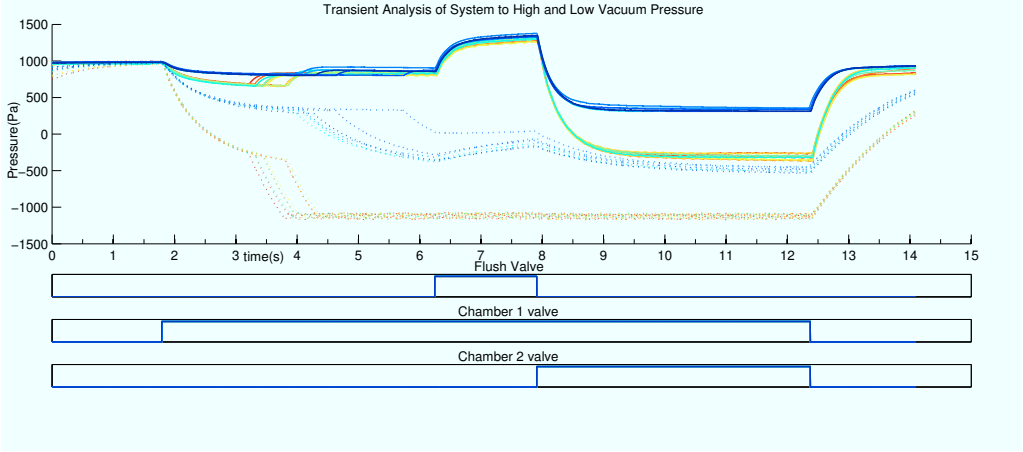

Figure 6.10 – *Pressure profiles for two different regulation pressures.*

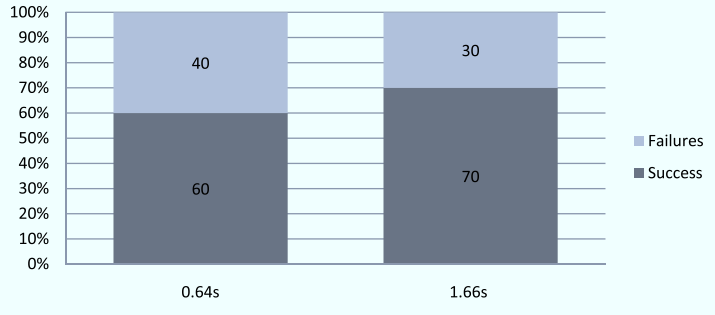

Figure 6.11 – *Probability of capturing the second particle due to various flush back durations and thus various capture delays.*

To test the effects of developed flow on the probability of capture, the duration that chamber F was open was varied. Two different periods for this duration was tested. The open duration of chamber F would determine the distance the particles were flushed upstream. This in turn will determine how much time was allowed for the flow to develop, before the capture of the particle as it nears C2. The results showed that controlling the time from when chamber C2 was opened to when the particle was captured does effect the probability of capturing the second bead. Figure 6.12 and Fig. 6.13 shows the pressure profile for a short (0.64s) and long (1.67s) flush back period respectively. The results (Fig. 6.11) showed that there was a 10% higher probability of capturing the second particle with a long flush back period than compared to that of the shorter period.

The higher probability can be explained by the different flow rates at the point

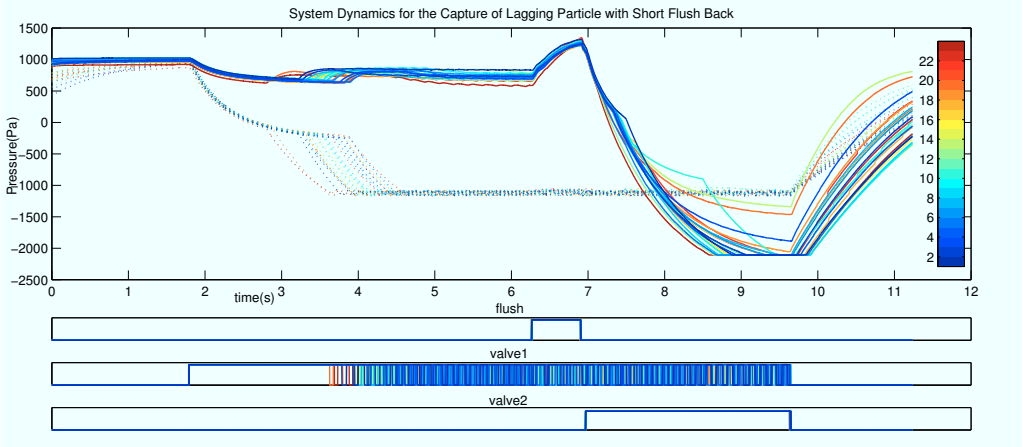

Figure 6.12 – *System Pressure Response to 0.64s flush back period.*

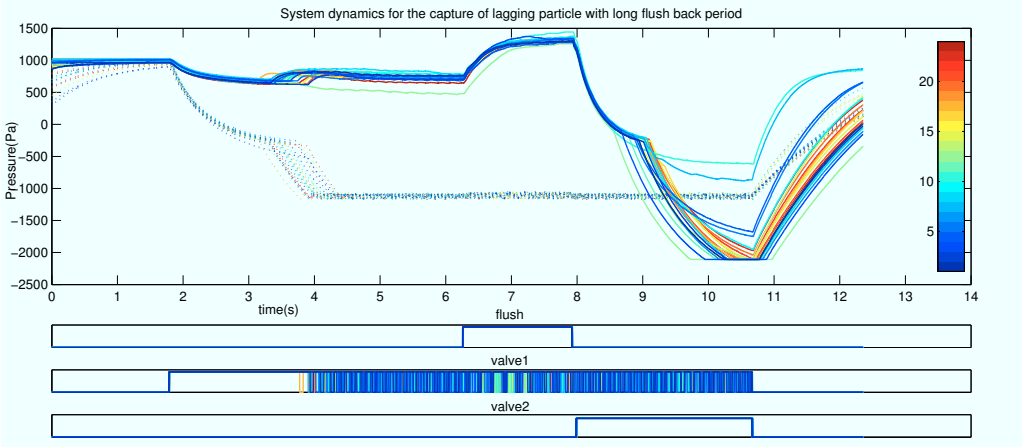

Figure 6.13 – *System Pressure Response to 1.66s flush back period.*

of capture. By flushing the particles further upstream, greater time was allowed for the fluid flow to develop and, therefore, the flow rate at the point of capture was higher than that of the short flush back. This could be seen in the pressure profiles within chamber C2 in Fig. 6.13 where, at the point of capture, the rate of change in the pressure within chamber C2 is less than that of Fig. 6.12, indicating that the flow was more developed. These results further support the concept that the different flow rates into each of the chambers effect the probability of capturing the second particle.

6.5.2.3 Leakage flow characterisation

The leakage flow rate into chamber C2 has been identified in the previous experiments as a factor in determining the probability of successfully capturing the second particle. Characterisation was performed to determine the degree of leakage for each pressure setting. This was characterised by investigating the velocity of the particle due to the leakage flow. The velocity of the particle as a result of flow into chamber C2 was also determined so that a comparison could be made.

To determine the velocity of the particle caused by the leakage flow alone, a particle was first captured at chamber C1, after 1s a single particle was introduced into the main chamber. To determine the velocity due to the flow into chamber C2, chamber C2 was opened and a single bead was introduced 1s after. The velocity was determined through high speed video analysis.

The results indicate the leakage flow does contribute a significant amount to the main flow. Figure 6.14 shows the velocity of a particle that resulted from leakage flow. A linear relationship was found to exist between the pressure within the chamber and the particle velocity for the range of pressures tested. At a pressure of -1500Pa, the leakage flow caused the particles to move at a velocity of 37mm/sec, which was a significant amount. Figure 6.15 shows the relationship between the velocity of the particle and the pressure setting of chamber C2. It could be seen that a linear relationship also exists in the range of tested pressures.

The results show the assumption of the flow being blocked by the particle was incorrect, and significantly high leakage flow rates are present. As the velocity of the particle is linearly proportional with the pressure in the chamber, if a higher pressure setting (lower negative pressure) was used in the capture of the first leading particle, particle velocity and thus the leakage flow could be significantly reduced, thus contributing less to the flow in the main chamber.

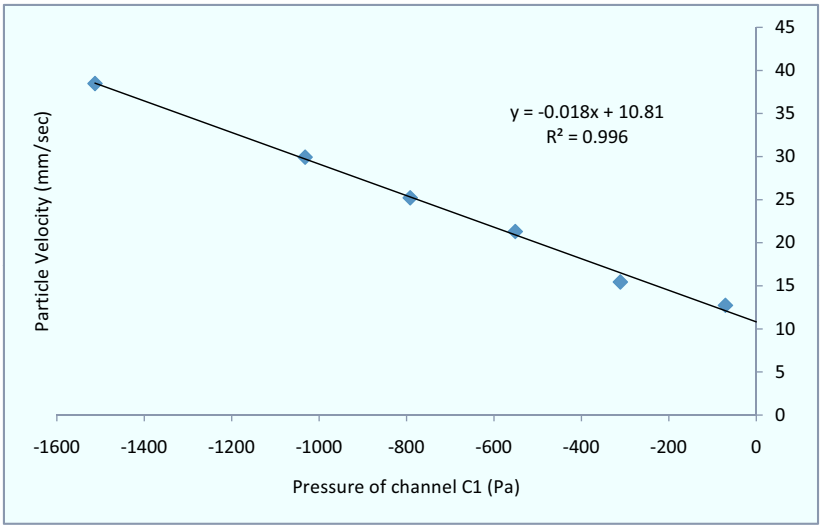

Figure 6.14 – *Velocity vs pressure of chamber C1 for a single bead due to leakage flow from channel C1.*

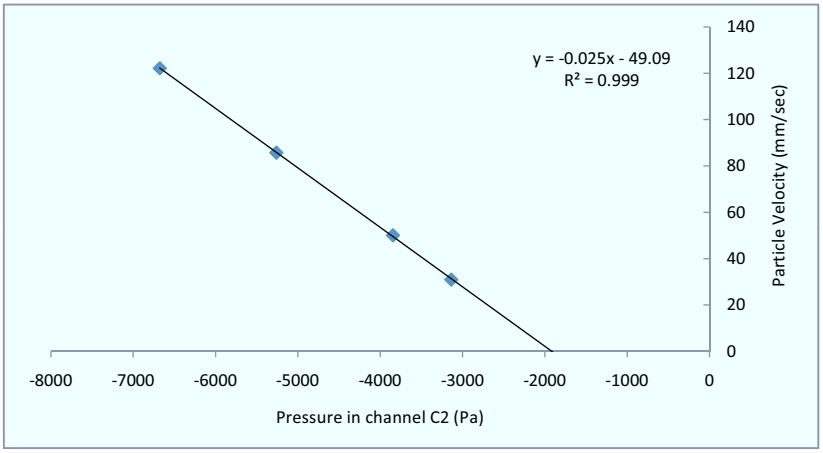

Figure 6.15 – *Velocity vs pressure of chamber C2 for a single bead due to flow into chamber C2 alone.*

6.5.2.4 Independent Fluid Flow Flux Algorithm

Previous experiments have identified that the probability of successfully retaining the second particle may be dependent on the fluid flow ratio. This is the ratio between the leakage flow into chamber C1 and the flow into chamber C2. This ratio will be investigated in the following section.

To obtain independent flow ratios within the device, the valve connected to chamber C1 was rapidly switched to regulate the pressure in the chamber, while that of chamber C2 was left open to the connected pressure regulator. The regulation of the chamber was performed by a simple on-off algorithm. The algorithm to capture the two particles for the experiments was shown in Fig. 6.16. The system first opens chamber H, followed by the activation of the regulation process in chamber C1. After the pre-set time has elapsed allowing for the capture of the leading particle, chamber F is opened, flushing the lagging particles upstream. Chamber C2 was opened a pre-set time before chamber F was closed. During the establishment of flow into chamber C2, the second particle was captured. After the chamber C2 was opened for a pre-set time, the process is finished. In each experimental case the pressure within the chambers was varied so that various flow ratios could be obtained.

The pressure profiles during the experiment for two pressure ratios is illustrated in Fig. 6.17a and Fig. 6.17b. In both figures, the pressure within chamber C1 was regulated to 316Pa, but the second chamber was varied. In Fig. 6.17a, chamber C2 was regulated to -4.5kPa, while chamber C2 in Fig. 6.17b was regulated to -6.7kPa. It could be seen that, in both the experiments (Fig. 6.17a, Fig. 6.17b), chamber C1 was correctly regulated around the set point of 316Pa. As expected the pressure rises and falls as the various chambers were opened and closed. The pressure decreased as chamber C2 was opened, then abruptly drops as a particle is captured in the chamber. Instances could also be seen where a particle was not captured and the pressure continued to smoothly decrease. Comparing the two experiments, the -6.7kPa case captures a lagging particle much earlier than the case where chamber C2 was set to -4.5kPa, in addition at the point of capture,

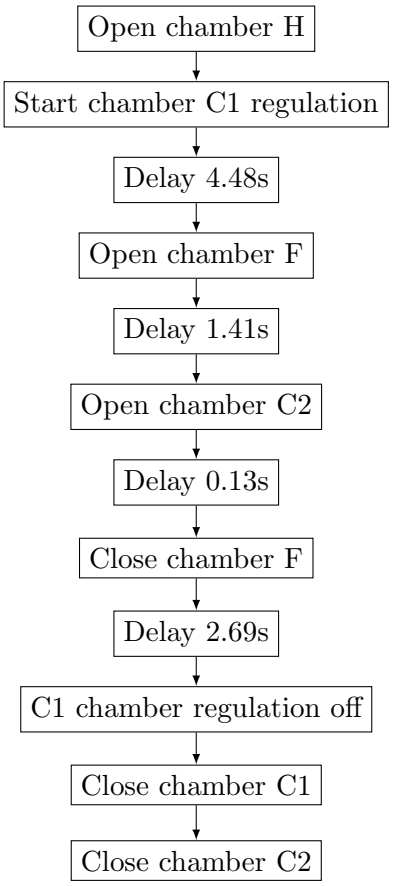

Figure 6.16 – *Independent fluid flow algorithm.*

the static pressure within the chamber was lower.

The probability of capturing and successfully retaining the second lagging particles for all tested pressure ratio pairs is summarised in Fig. 6.18. The results show that a weak trend exists, indicating the probability of capture decreases as a higher vacuum pressure is set in chamber C2. This general trend applies until the cases where early release of the leading particle occurs. Early release of the particle was when the trapped particle at chamber C1 releases and becomes captured in chamber C2, before a lagging particle is captured in chamber C2 (Fig. 6.19). Early release occurs when the pressure within chamber C1 was above 410Pa, in combination with high vacuum pressures in chamber C2. The results showed that in general, for a given pressure setting in chamber C2, the probability of capture will increase when the vacuum pressure in C1 is lower.

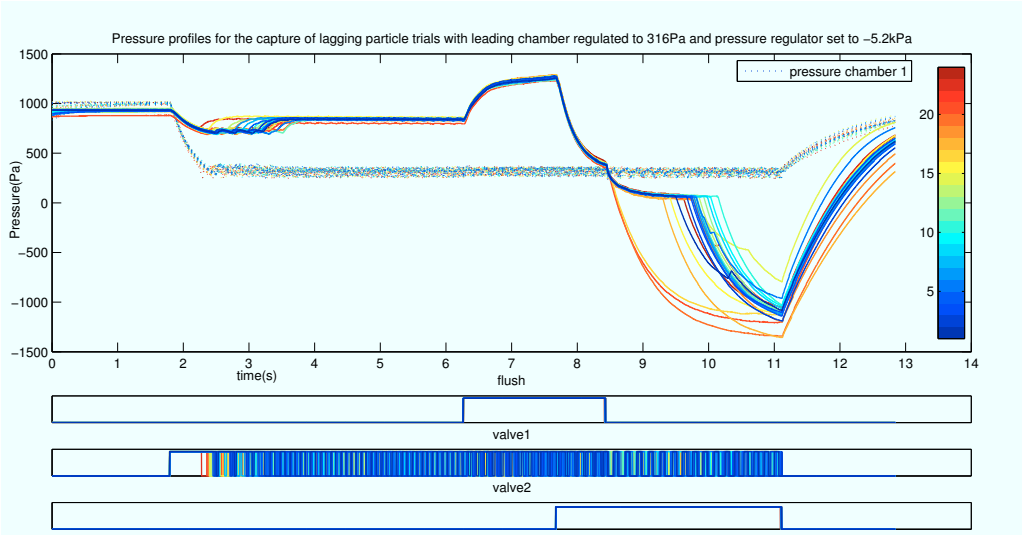

(a)

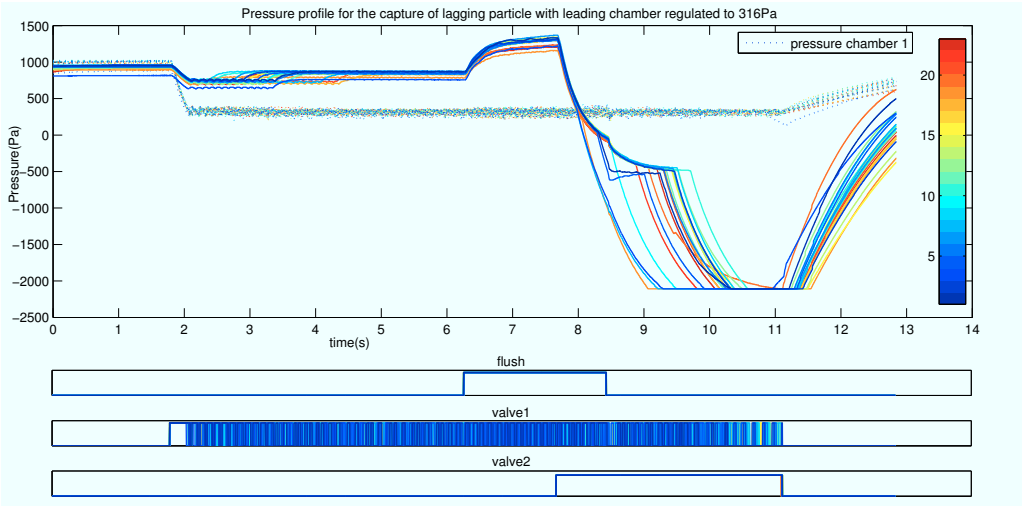

(b)

Figure 6.17 – *Pressure profile of system for the capture of the second particle. Pressures in the two chamber are regulated independently. Chamber C1 is regulated to 310Pa while that of C2 is -4.5kPa (a) and -6.7kPa (b).*

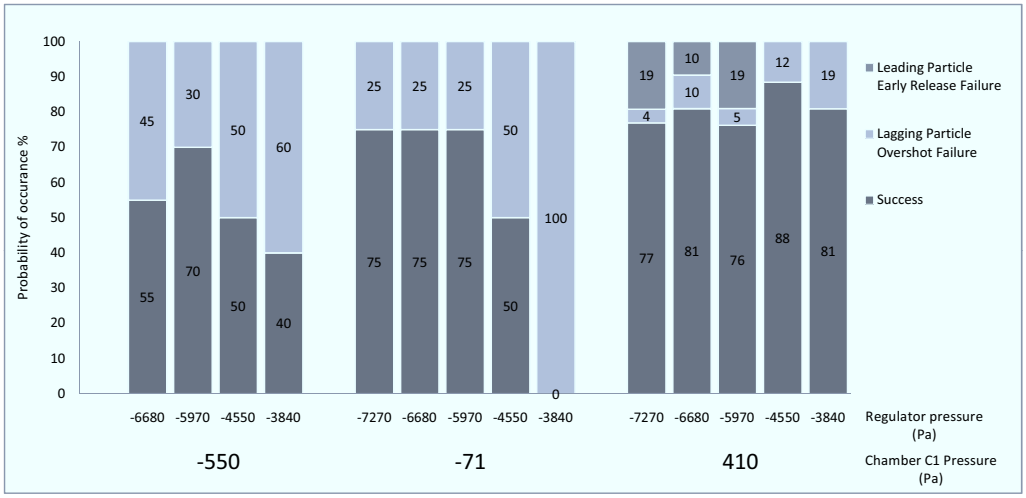

Figure 6.18 – *Probability of capturing the second particle for various pressure pairs.*

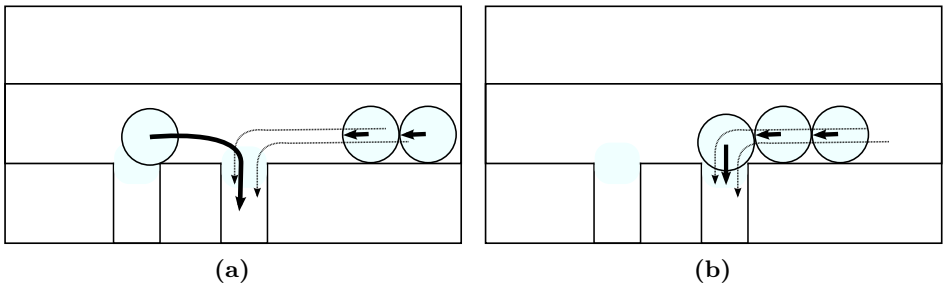

Figure 6.19 – *Illustration of the early release of the leading particle. When chamber C2 is activated the particle trapped at chamber C1 releases (a) and becomes trapped at chamber C2 (b) before the lagging particles can be captured.*

When the probability of capture was expressed in terms of the particle velocity, (obtained from the previous Sect. 6.5.2.3) instead of system pressure, a clearer general trend could be observed (Fig. 6.20). The results showed that generally the probability of capture increases, when the contribution from the leakage velocity was lower compared with the velocity of side channel C2. This was before the leading particle begins to release. The highest probability of capture occurred when particle velocity contribution from chamber C1 was 5% of the particle velocity contribution from channel C2.

The results showed that a general trend exists, and that the flow ratio was a significant factor in determining the probability of capturing the second par-

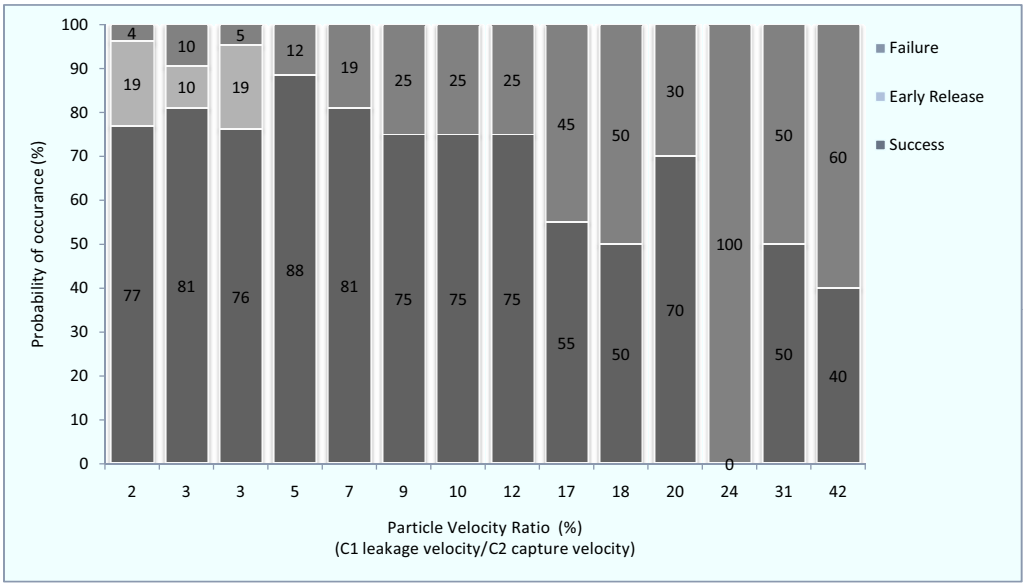

Figure 6.20 – *Second particle capture probability vs the velocity ratio of C1/C2. This velocity ratio is characterised in Sect. 6.5.2.3.*

ticle. However the weak trend suggests that there are other factors involved in determining this probability. One likely explanation could be attributed to the particle train spacing distribution. The spacing between particles can be difficult to control, and the seemingly random distribution of particles can result in particles clustering together. These clusters could be formed during the many transitions in the process as the particles are flushed up and downstream over the course of the process. The clustering results in trials where; at one end of the spectrum the trapped particle was subjected to a large group of particles that collided with it, or when there was only one particle. Both of which have different outcomes for the release of the trapped particle. The result is that each of the trials conducted with the controlled parameters are not subjected to the same condition. In order to minimise the effects of this, the trials were repeated at least 20 times. Although the distribution of the particles was difficult to control, the conditions is representative of what will occur, if this algorithm was adopted.

The general trend indicates that the probability of capture will increase with a decreasing velocity ratio, however there was a limit. As the ratio reaches lower than 5%, early release begins to occur. This places a limit to the probability of

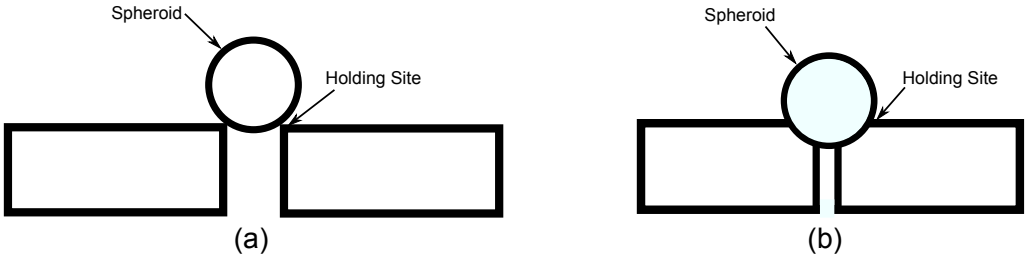

Figure 6.21 – *Current holding site geometry (a), formed from the intersection of two cylindrical channels and improved spherical like holding site (b).*

capture as the ratio can not go to zero, thus, singularisation is unlikely to ever reach 100% with the current setup. The release of the particle from chamber C1 to chamber C2 was expected, as at the lower ratio, the flow rates into chamber C1 was relatively low, and therefore holding forces were low. When chamber C2 was opened, the combination of the low holding force and a high flow rate into C2 was likely to cause the release of the particle.

The results have confirmed that the proportion of leakage flow into chamber C1 can effect the probability of capturing the particle in chamber C2. However a maximum probability of 88% for the capture of the second particle was achieved in the specific setup, there are still a number of methods for increasing the capture probability even further if the system is altered. As discussed in Sect. 6.5.2.1, the leakage flow could be further reduced if a proper seal is formed. This would enable the leading particle to be held with a greater force, while minimising leakage flow, unlike the linear relationship seen in the results (Sect. 6.5.2.3). In the real application, this is likely to occur, as the particles are more deformable. In addition, the holding sites could be manufactured with surfaces matching closer to that of the particles. This would be a spherical cup like surface, unlike the elliptical geometry current formed from the intersection of the two cylindrical channels (Fig. 6.21).

6.5.3 Transport of leading particle downstream and termination of flow

The last step in the singularisation cycle was the transport of the leading particle to the systems further downstream, and the termination and resetting of the system. The system was required reset back to the initial state so the lagging particles could be recaptured.

Termination occurs after the trapped particle at chamber C1 is released and flushed downstream. The valves are in the following states at termination:

- Chamber D Open
- Chamber F Open
- Chamber H Closed
- Chamber C2 Open
- Chamber C1 Closed

For termination to be successful, the particle trapped at chamber C2 must remain held while the flows terminate. This section will investigate the switching sequence of the valves in order to obtain the desired flows during termination, as well as the conditions for the successful transport of the leading particle out of the device.

6.5.3.1 Release and transport of leading particle

For successful transport of the leading particle to occur, the trapped particle at chamber C1 must release while the particle held at chamber C2 remains trapped, or is prevented from moving downstream. Particle C1 was transported with the algorithm shown in Fig. 6.22. The first nine seconds of the algorithm utilises the algorithm described in Sect. 6.5.2.4 to capture the two particles in the holding chamber. Transport began with the closure of chamber H, and the opening of chamber F and D. Flow began to develop from chamber F to D before

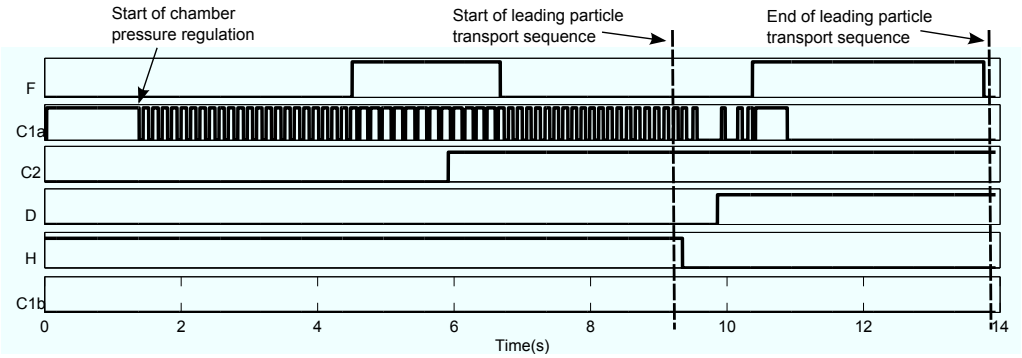

Figure 6.22 – *Timing diagram of chambers, showing the singularisation algorithm leading to the transport of the particle trapped at chamber C1 to systems further downstream.*

chamber C1 was closed. With the closure of chamber C1, the pressure within the chamber began to increase, reaching that of the main chamber, until the particle detached from the holding site. It was then transported by the fluid flow in the main chamber, past chamber D towards the injection device. In all of the trials conducted, problems have not occured in the release and transport of the leading particle downstream. The particle trapped at chamber C2 remained held throughout the process and therefore does not move downstream past chamber C1.

6.5.3.2 Algorithm 1 - Termination sequence 1

The algorithm for the termination sequence is illustrated in Fig. 6.23 and Fig. 6.24. Termination began after the particle was flushed. The algorithm terminates the flow by first closing chamber F, followed by the opening of chamber H, and finally the closure of chamber D. The pressure response of the system during the whole experimental process is shown in Fig. 6.25. It could be seen that the release of the lagging particle, (indicated by the increase in pressure) coincided with the closure of chamber D.

The sequential closure of the valves causes distinct fluidic flow paths to develop which resulted in the movement of the lagging particles. These movement patterns may be responsible for the failure of termination. After the closure of chamber F, lagging particles were observed to accelerate in the direction of chamber C2 and

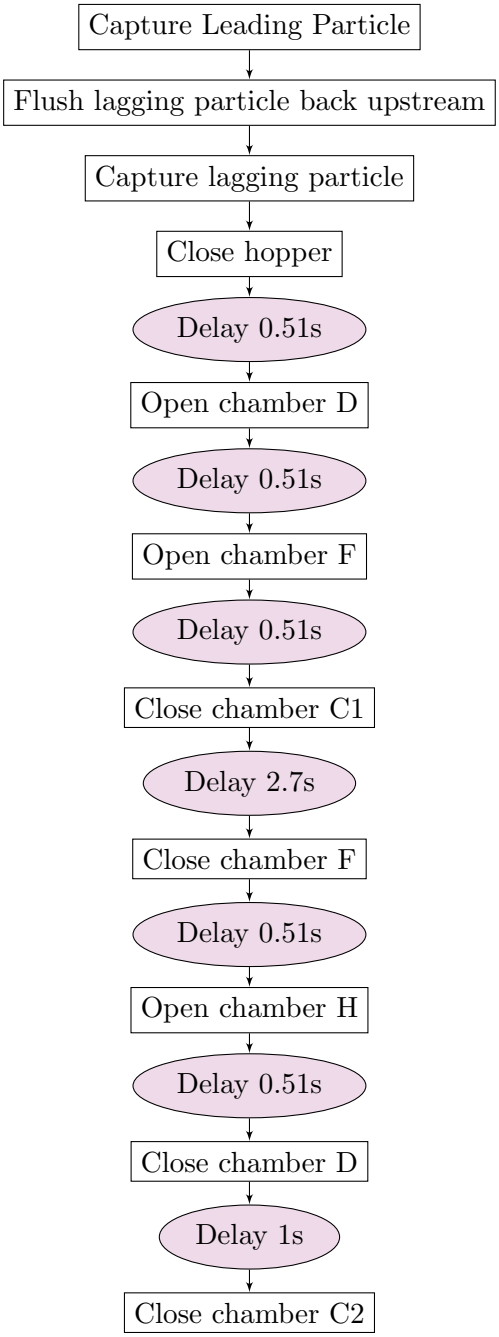

Figure 6.23 – *Flow chart of algorithm 1.*

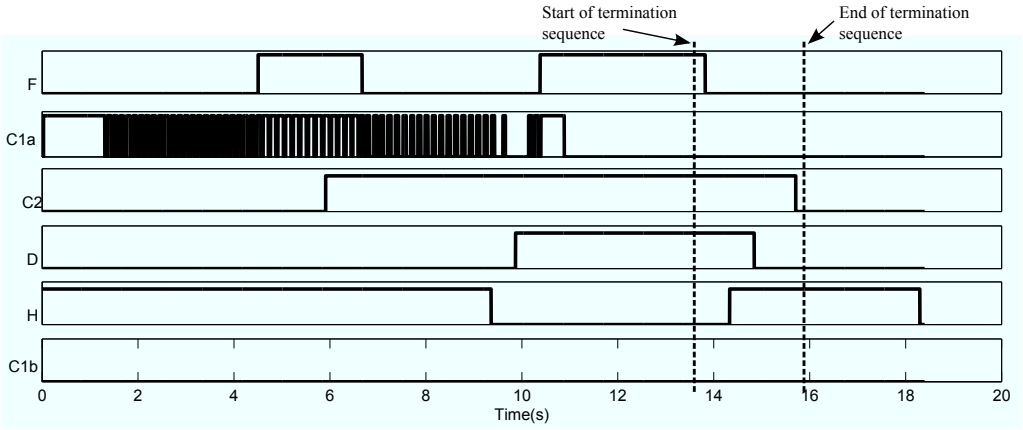

Figure 6.24 – *Pressure vs time response of the system of a single trial for the control method of transporting lagging particle to leading chamber, using an extended flushing sequence.*

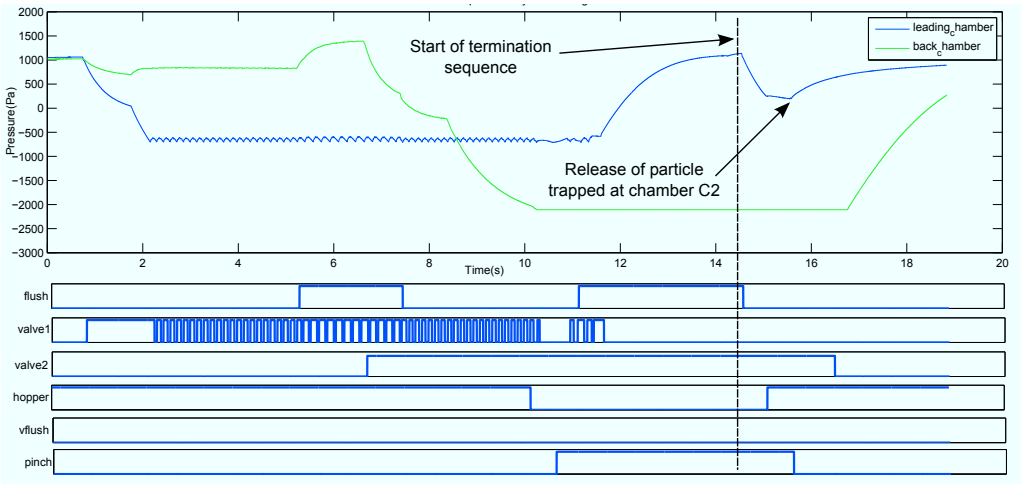

Figure 6.25 – *Control sequence and pressure profile of capture chambers showing a trial for algorithm 1.*

collide with the trapped particle. The collisions have not been shown to release the trapped particle. Furthermore, the opening of chamber H did not significantly change the movement of the particle. The closure of chamber D resulted in the release of the trapped particles. High speed video analysis showed the particle releasing almost immediately after chamber D is closed.

The release of the trapped particle caused multiple particles to overshoot chamber C1 (Fig. 6.26). Although fluid is still flowing into chamber C2 the force was not enough to capture the particle immediately after the trapped particle,

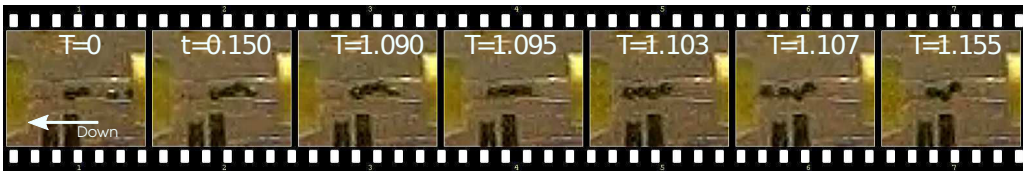

Figure 6.26 – *High speed video showing the key frames during the release of the trapped particle at chamber C2. Particles can be seen to overshoot the trapping chamber followed by the subsequent recapturing of the lagging particles.*

resulting in multiple particle overshooting chamber C2. Once the particles have overshot, no fluidic path is available to flush the particles back upstream and they are left at that position until the next cycle. This was undesirable as multiple particles will be transported in the next cycle instead of the required single particle.

The early release of the held particle at chamber C2 was difficult to explain as the pressure data (Fig. 6.25) showed that moments before the release of the trapped particle a large pressure difference existed between the pressure in the main chamber and the pressure in chamber C2. This suggested that the particle is held with a relatively large force. A possible explanation to the release could be due to the sudden closure of chamber D. The pressure waves that result from the sudden closure, may be large enough within the main chamber to disrupt and decrease the holding force. This may not have been recorded in the data due to the fast transient response of these waves. Although the response of the transducer elements are capable of recording fast transients, dampening and attenuation may have occurred at the higher frequencies due to the interface between the transducer and pressure system (transmitting fluid and connecting tube).

The observation that the particles flow further downstream after release, suggests that an additional flow may exists in the main chamber just before chamber D is released. A possible cause for this flow is due to the high pressure in chamber H. When chamber F is closed, the pressure opposing the pressure in chamber H has now decayed. A large pressure now exists in chamber H as the valve has not been opened to vent to atmosphere. As chamber D is still open there will be a large pressure difference between chamber H and chamber D, which

will create a flow within the main chamber. The large flow coupled with the travelling pressure waves from sudden closure of chamber D, may be sufficient for the particle to release.

Although the cause of the particle releasing when chamber D was closed is not known for certain, failure can still be avoided. If the flow path is moving upstream (instead of downstream as observed) at the point of release, the particles will not overshoot chamber C1. This is possible if the flushing valve is closed near the end of the process, after all other valves have terminated. Chamber F will provide a consistent flow upstream, and as chamber F is at a higher pressure, fluid will not flow downstream. This was investigated in the next algorithm.

6.5.3.3 Algorithm 2 - Termination sequence 2

The early release of the particle held at chamber C1 has been determined as the cause of failure for successful termination. The cause of the release is not known for certain but the problem of failure can be solved. Although the release may not be preventable, the particles can be transported to a recoverable location after release. If the particles flow upstream instead of downstream past chamber C1 the system is able to recapture the released particle.

The algorithm to allow for successful termination is illustrated in Fig. 6.27. The concept was to establish a flow upstream to prevent the particle from moving downstream at the point of release. The timing diagram as well as the pressure response for a single trial is illustrated in Fig. 6.28.

As previously described, the opening and closure of chambers resulted in fluid flow being developed within the device which may result in undesirable effects of releasing the trapped particle. The termination sequence was initiated with the opening of chamber H, and was observed to cause the lagging particles to accelerate and travel back downstream, colliding with the particle trapped at chamber C2 (Fig. 6.29). Although the collisions occur, the trapped particle was not observed to release. Following the opening of chamber H, chamber D was closed. Immediately after the closure, the particles were observed to accelerate

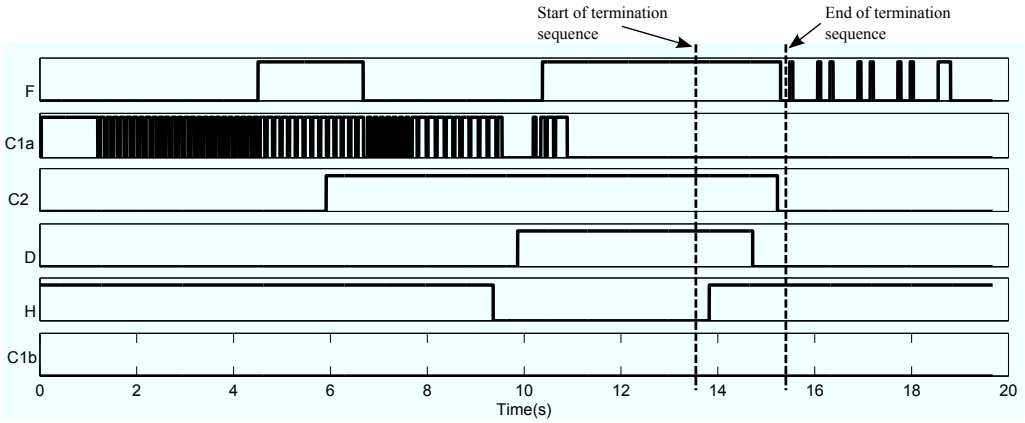

Figure 6.27 – *Timing diagram of the singularisation algorithm 2 to the point of termination. Chamber F is terminated last.*

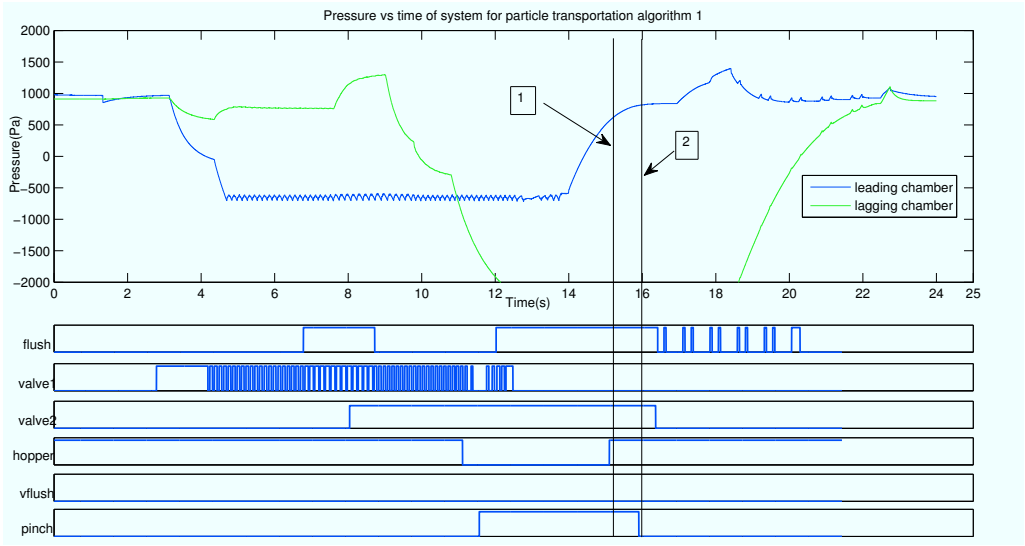

Figure 6.28 – *Pressure vs time response of the system for a single trial during the singularisation process. The process starts from the capture of the two particles through to termination of the flows. At position 1 the lagging particles are observed to accelerate downstream before colliding with the trapped particle. At position 2 the particles are observed to accelerate upstream.*

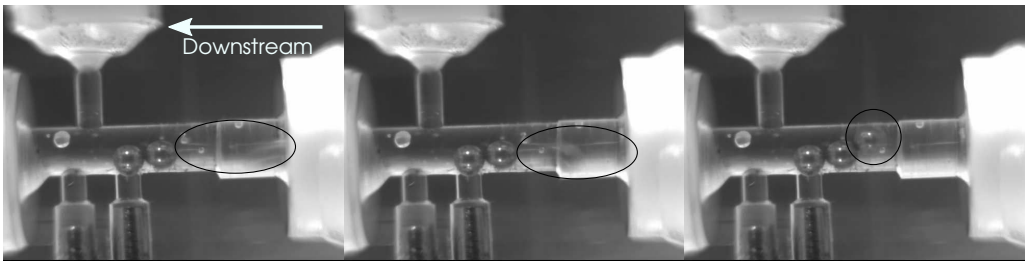

Figure 6.29 – *Example video clip shortly after the closure of chamber H showing particle which had been transported upstream begin to accelerate back downstream before colliding with the captured particle and coming to a halt.*

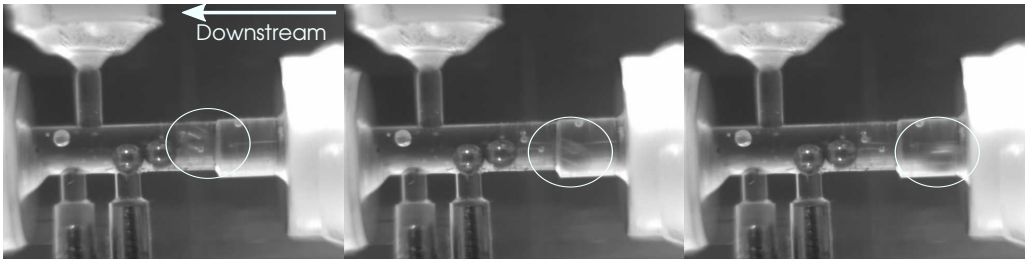

Figure 6.30 – *Example video clip showing the movement of a particle upstream shortly after chamber D is closed.*

upstream before decelerating once chamber F was closed (Fig. 6.30). 100% success was recorded using the algorithm described and the trapped particle was observed to remain held at all times. There were no signs of the particle releasing when chamber D was suddenly closed, such as those observed in the previous algorithm. This could be due to the increase in pressure in the main chamber, as chamber F provides a higher pressure in the main chamber which increases the holding force further.

Although a high success rate was recorded with the described termination sequence, there were still areas in which the sequence could be improved. One area was in the collision that occured at the opening of chamber H. Although no release was recorded, it would be advantageous if this did not occur. The movement of the particles downstream suggests that the pressure at chamber F was not large enough to prevent fluid moving from chamber H. This in turn resulted in fluid moving from chamber H to D. Possible solutions to this are to either increase the pressure in chamber F so that the pressure is larger than the

pressure in chamber H, or to open chamber H after chamber D is closed.

6.6 Discussion

The results have shown the singularisation device was able to successfully separate a single particle from a group of particles. The fully fluidics device utilised hydraulic forces for the manipulation of the particles. This is opposed to the more mechanical methods of singularisation presented in the previous chapter, which was found to have many inherent limitations (Chapter 5). By manipulating the fluidic paths within the device through several chambers, along with the trapping of particles at defined places, singularisation was achieved. Although 100% singularisation success was not recorded, a singularisation success probability of 88% was achieved. This is not the limit of the concept and further modifications to the device can result in higher singularisation success rates. A number of aspects on the singularisation device were investigated to determine where failures occurred and to improve upon them.

The singularisation process can be divided into four distinct stages. These are:

- The capture of the first leading particle,
- The capture of the second lagging particle,
- The transport of the leading particle to the injection device,
- Termination of the flow from the injection device.

There is a probability of failure at each of these stages which will determine the overall probability of success for the device. Failure at any level of the stages will result in the failure of the entire cycle where multiple particles will be delivered for that cycle, until the start of the next cycle. The device has been thoroughly characterised to determine where these failures are likely to occur and to improve upon them.

In the first process, the capture of the leading particle, no failure was reported for the range of parameters that were tested. These parameters were variations in

the pressure setting in chamber C1, number of beads in the particle train, and initial pressure of the main chamber from the head of water in the main reservoir.

In the second process the capture of the second particle at chamber C2 was investigated. A number of parameters were found to effect the probability of successful capture. The cause of failure was due to the high forces from the lagging particles interacting with the single trapped particle. These interacting forces are the impulse force from the collisions, as well as the combined drag force from the lagging particles exerting on the trapped particle. The interacting forces were not consistent and the trapped particle interacted with a varying number of lagging particles in each cycle. The variances were due to the seemingly random distribution of particle spacing which gave rise to random clustering. This resulted in variances of collision force and combined drag force. These forces increase and are more detrimental when leakage flow occurred.

A significant level of leakage flow from chamber C1 and chamber C2 was found to exist. These leakage flows contribute to the flow in the main chamber, which in turn, provides the driving force behind the lagging particles. If the driving force can be decreased and the holding force increased, there is a higher probability that the forces from the lagging particles will be lower than that of the holding force. This would result in a higher probability of capture success. That is if the ratio between the leakage flow from chamber C1 is reduced (reducing lagging particle driving force) while the flow rate into chamber C2 is increased.

It was found that as this ratio (C1/C2) decreases the probability of capturing the second particle increased. At the highest success rate of 88%, the particle velocity from leakage was 5% of the particle velocity into chamber C2. There was however, a limit that exists, where lower ratios resulted in the release of the leading particle, and the relocation into chamber C2 (Fig. 6.19). A possible solution to improve this would be to have the devices holding chamber reshaped so that a better fit occurred between the trapped particle and the holding site. This would significantly improve the leakage flow problem as it is currently an elliptical shape.

Fluid flow within the device is in a constant state of transition as flows establish

and disestablish, with the system never reaching steady state. Time must be considered in the establishment of sufficient flow ratios. Setting the pressure in the chambers with a large pressure difference does not guarantee a large flow ratio, as development time needs to be considered. It was found that allowing more time for the flow to develop and therefore enabling higher flow rates into chamber C2, before the second particle was captured also yielded higher probability of successful capture. This was due to the flow that was already established in chamber C1 versus the developing flow of C2 at the moment of capture.

The last two processes to be characterised were the transport of the leading particle to the injection device, and the termination of the flows resetting the system so that the cycle can start again. No failures were recorded for the transport of the leading particle and the sequential flow control of the chamber was able to successfully deliver a single particle out of the singularisation device each time, assuming the two particle are successfully captured at the beginning.

The termination of the flows required a specific chamber closure sequence in-order to be successful. The termination sequence must be carefully considered, so that the resulting pressures during termination lead to desirable flow paths. The flows are established as the system pressures move towards equilibrium. Termination requires that the flows are closed while the particle trapped at chamber C2 remains held, otherwise release occurs where the particle overshoots chamber C1 and the system is unable to recover the released particle. In the first termination algorithm it was found that the particle would release immediately after the closure of chamber D. Possible reasons may have been due to the sudden closure of the valves as well as the retained pressure within certain chambers, creating a large pressure difference. However this was not confirmed and remains unknown. With the knowledge that the particle released at the closure of chamber D, a solution was found where the flow was established upstream before the closure. This would enable the particle to flow upstream if it were to release, thus enabling the system to recapture the particle. Although, once implemented, the particle was not found to release and remained held throughout the termination sequence.

6.7 Summary

In this chapter a singularisation device utilising hydrodynamic forces alone for gentle manipulation of particles was presented. Fabrication of the prototype in two parts was investigated which requires that bonding take place. A hybrid solvent vapour, thermal fusion process was investigated but difficulty in characterisation of the process resulted in inconsistent results. It was unknown whether significant advantages could be gained from realising the smaller internal feature through fabricating the prototype in two pieces. Instead the design was revisited and conventional manufacturing techniques were employed. The use of a non elastic model for the bio-particles enabled the elucidation of the many dynamics of the singularisation system that may have otherwise been ignored. The controlled, timed, sequential manipulation of the fluidic paths is important in each of the processes so that controlled manipulation of particles within the device was achieved, in order to accomplish successful singularisation. The only sub-process contributing to the probability of failure was the capture of the lagging particle at chamber C2, after the capture of the leading particle. The capture success was found to be predominately effected by the flow ratio into the two capture chambers. This was due to the systems constant state of transition, where the flow ratio is time dependent and methods were required to enable the desired flow ratios to develop before capturing the second particle. The termination sequence of the developed flows at the end of the process must also be carefully considered, enabling the system pressures in various chambers to reach equilibrium without producing undesirable flows, which increases the risk of failure. Although a high singularisation success rate of 88% was recorded for the singularisation of beads, improvements have been outlined which may enable the device to achieve even higher success rates. The presented method is one of many other methods that may exist for manipulating fluidic flow within the device to achieve singularisation. In the next chapter such a concept utilizing a different method of fluid manipulation is presented and was found to achieve a singularisation rate of 100%.

Chapter 7

Single Capture Site Singularisation Device

7.1 Introduction

Singularisation or the separation of biological particles from a group of particles is an important step in the process of printing and assembly of the tissue construct. Singularisation is not only limited to tissue printing applications, but also forms a fundamental step in many biological studies. Automated singularisation enables high throughput manipulation, analysis and screening of single particles, which include single cells and spheroids. Systems which are capable of sorting particles have been commercially available for decades, thus the technology is well developed. These technologies include fluorescence activated cell sorter (FACS), where the suspended particles are focused into the centre of the fluid stream, and individual cells are identified via a fluorescent signal. FACS traditionally achieves sorting through the jetting of liquid droplets containing a single cell, where the droplet is deflected into separate containers through electric fields [118].

FACS provides a standard with which all sorting devices are benchmarked against, but even current commercial bench-top units are large, expensive and the non-enclosed nature of the sorting environment posses problems in terms of

bio-safety due to the generation of aerosols [119]. Furthermore there are differences between sorting and singularisation, namely the start stop conditions required for assembly versus the continuous processes. Fluidic devices, namely micro-fluidic devices, can address many of these issues, when dealing with micron sized particles [120].

Previously in Chapter 6, a singularisation device was presented which utilised hydrodynamic forces alone in a dual trap fluidics arrangement to achieve singularisation. The fluidics approach of manipulation enables gentle handling of the particles. The highest recorded singularisation accuracy of the device was 88%. This was a significant improvement from the mechanical singularisation device presented in Chapter 5, where the beads were easily damaged due to the mechanical shunting of beads during singularisation.

In this chapter a singularisation fluidics device is presented which requires that only a single particle is trapped instead of two. The device is label free, nor relies on the physical properties of the particles, and is able to separate spherical particles with high efficiency. Although the previously developed device (Chapter 6) was able to achieve a relatively high singularisation rate, the optimal printing process requires that 100% is achieved. Singularisation failure will result in multiple particles being delivered to the pore which will distort the assembly process of the surrounding pores, leading to an accumulation of errors in the final construct. In Sect. 7.2 the fabrication and experimental setup will be described, followed by the concept of singularisation. Section 7.3 will present the results and discussion of the device characterisation. Finally Sect. 7.4 will present an overall discussion of the device and Sect. 7.5 will provide a summary of the single trapping site singularisation device.

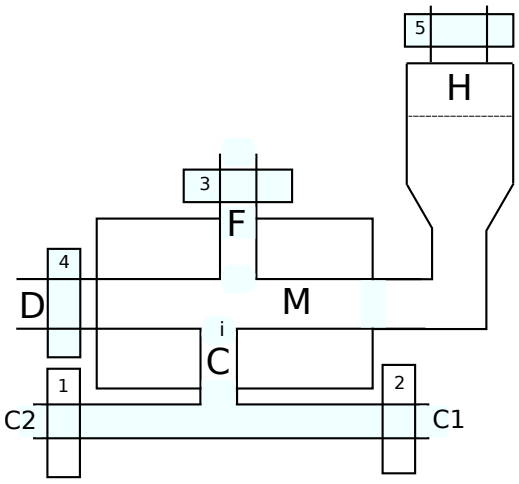

Figure 7.1 – *Diagram of the singularisation block with labelled chambers and valve numbering.*

7.2 Methods and Materials

7.2.1 Device Fabrication

The singularisation block was fabricated from poly(methyl methacrylate), (PMMA) using conventional machining techniques. PMMA was selected, as the prototype was not required to be sterilised via high concentrations of ethanol and thus resistance was not required. The prototype was kept simple and the various injection, loading and separation chambers were realised through conventional machining techniques. Due to the limitations of the manufacturing method, the ratio of chamber diameter to length were kept within the ratio of 1:10 to maintain channel accuracy, by preventing the formation of long channels.

7.2.2 Experimental Setup

The singularisation device consisted of a main loading chamber M with two side channels, F and C (Fig. 7.1). These side channels were used to manipulate the fluid flow paths. Side channel C was positioned offset from chamber F by half the diameter of the expected particle, which ensured the area adjacent to the trapped particle was fully swept, minimising dead volume. Side channel C was split into two chambers itself where positive and negative pressure was introduced.

To control and manipulate the fluid within the device, the device was pressure driven with accompanying system components. The system as illustrated in Fig. 7.1 was actuated through hydraulic, pinch and pneumatic valves. Fluid flow into side chambers C and F were controlled through isolation valves (ASCO 067 US). Fluid flow originating from the reservoir was controlled through a pneumatic valve (ASCO 188) and was in fluid communication with the atmosphere. Side D of the main chamber was controlled through a pinch valve (ASCO 284) to isolate the singularisation system to other systems further downstream.

Fluidic connections to the reservoir and subsequent systems downstream of the device was realised through flexible tubing (Tygon) with a 1.6mm ID. The tubing was coupled to the device using a flangeless ferrules system (VICI JOUR) to ensure a relatively seamless constant ID connection, and to accurately locate tubing to the device.

Pressure regulated reservoirs N and P were coupled through tubing to the device, providing pressure to chamber C1, C2 and F . Regulator N was regulated to a negative pressure relative to atmosphere and regulator P, positive relative to atmosphere. Pressures within the reservoirs were maintained at a set level throughout the experiment.

Control of the valves and monitoring of the pressure levels in chamber C was performed through a custom developed control board and instrumentation circuits (Chapter 4).

Experimental data was recorded through the direct streaming of pressure data back to a PC terminal, synchronised with the image frames captured from a camera (Basler 610). A high speed camera (CASIO EX-F1) was used to capture video for higher accuracy, although this was not synchronised with the pressure data and was instead used in conjunction with the video recorded from the slower camera.

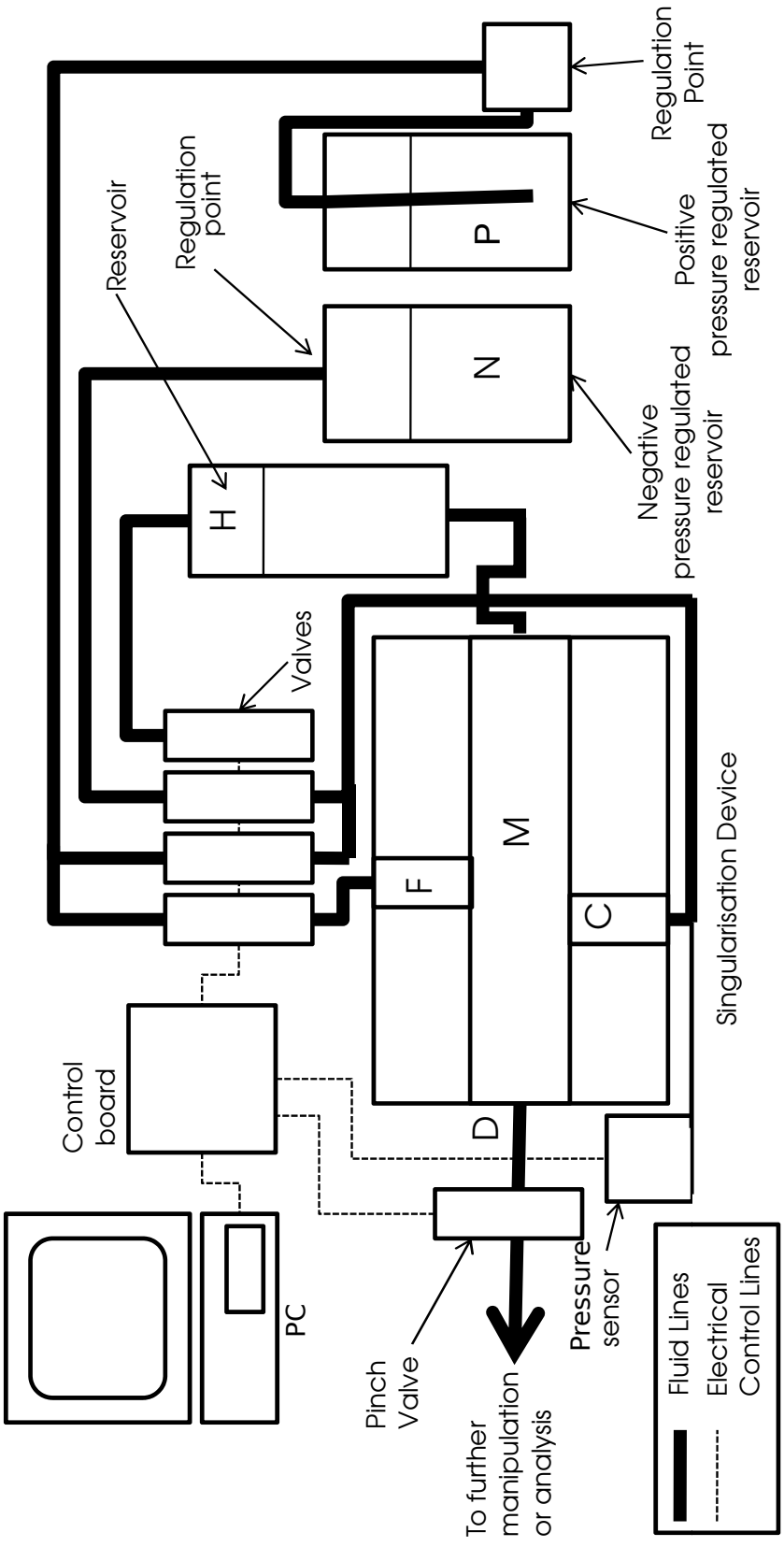

Figure 7.2 – *Schematic of the single capture site singulation system. The system was pressure driven consisting of the singulation fludics block, positive and negative pressure regulators, control board and valves.*

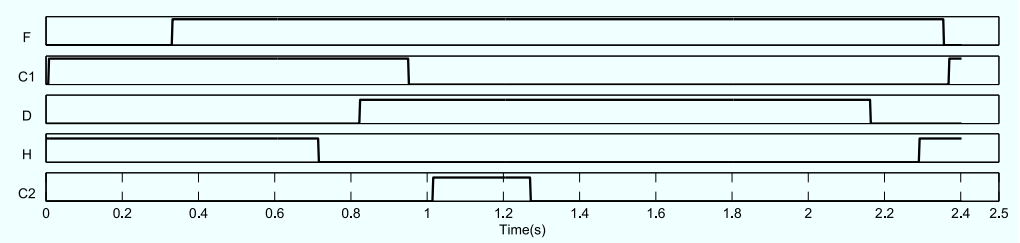

Figure 7.3 – *General timing diagram of valves for the singularisation process. Different algorithms differ only by the delays, but the sequence remains the same.*

7.2.3 Particle Separation Method

The singularisation device separates a single particle from a particle train through sequential manipulation of valves to control the fluid paths within the device in order to separate the leading particle from the particle train.

The concept of singularisation for the single capture site was to first capture a single particle at a predetermined point. A flow was developed which separated the flow between the trapped particle and non trapped lagging particles separating them. Once separated the leading and lagging particles could diverge and were transported to the required locations.

A detailed description of the singularisation process is illustrated in Fig. 7.4. The general sequence and the timing diagrams for the initial singularisation algorithm are illustrated in Fig. 7.3. The following describes a general sequence for the singularisation process, with given delays as an example.

The algorithm begins with the state of all valves being closed. The first step in the process is the trapping of the leading particle at chamber C. Valves connecting to chambers H and C2 were opened, transporting the particles towards the holding site i (Fig. 7.4b) until the leading particle in the particle train was captured. Detection of the capture was signalled by the pressure within chamber C falling below -310Pa. The capture was followed by the opening of chamber F developing an additional flow from F to H (Fig. 7.4c). Particles which were not captured were transported back upstream. During the flush back process, chamber C2 remained open to ensure the leading particle was retained.

To prevent the lagging particle from being transported upstream too far, valve

H was closed 384ms after the opening of chamber C. 128ms after the closure of chamber H, chamber D was opened enabling fluid to develop from chamber F to D forming the main transport flow to the injection device. 128ms after the opening of chamber D, chamber C1 was opened supplying a burst of fluid releasing the captured particle into the main flow, transporting it downstream to other systems (Fig. 7.4d).

To terminate the flow through to the injection device, the pinch valve was first closed, followed by the opening of the hopper valve and finally the closure of chamber C. The method and dynamics of termination have been previously discussed in Sect. 6.5.3.

The whole process described was repeated to separate each individual particle.

7.3 Results and Discussion

A control algorithm was required to ensure the successful establishment and manipulation of fluidic flow paths, thus particle flow paths, in accordance to the singularisation concept presented in Sect. 7.2.3. Two singularisation algorithms are presented. The knowledge gained from the previous dual trap singularisation device (Chapter 6) have aided in the development of the following control algorithms.

7.3.1 Algorithm 1 - Initial singularisation control algorithm

The initial algorithm was developed to investigate the dynamics of the system and delays between the switching of chambers. The length of the delays have been intentionally extended to exaggerate the effects on the particles movement. However this greatly reduces the throughput of the device. A timing diagram shown in Fig. 7.5 illustrates the state of each valve in the initial algorithm 1. In the following sections, the description of the resulting particle flow within the chamber and the time positions, will refer to the key positions labelled in Fig. 7.6. The figure also illustrates the typical pressure response of the system during the singularisation process.

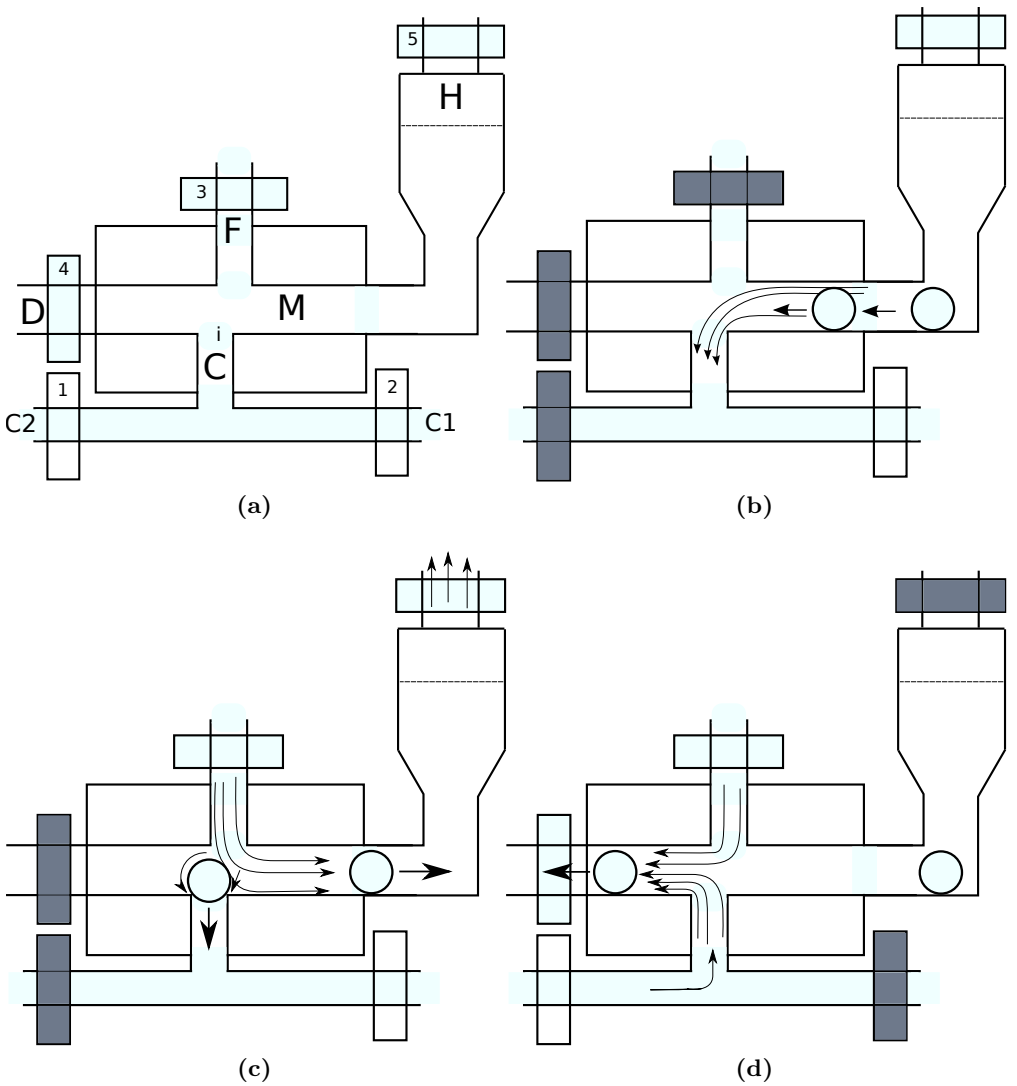

Figure 7.4 – *Diagrams of singulation process. (a) Chambers and valve numbering. (b) The capture of the leading particle. (c) The transport of the lagging non trapped particles upstream. (d) The transportation of the single leading particle to systems further downstream.*

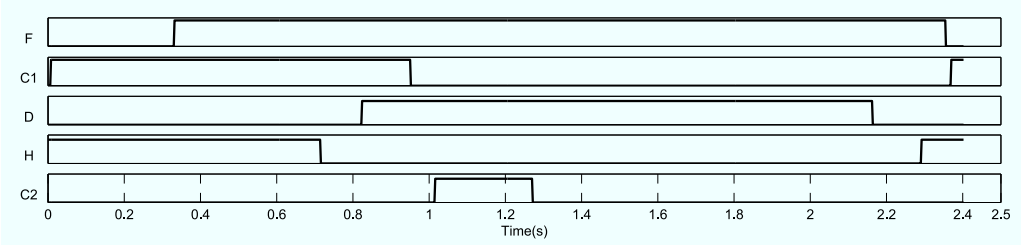

Figure 7.5 – *Timing diagram of valves for algorithm 1 - Singularisation Process.*

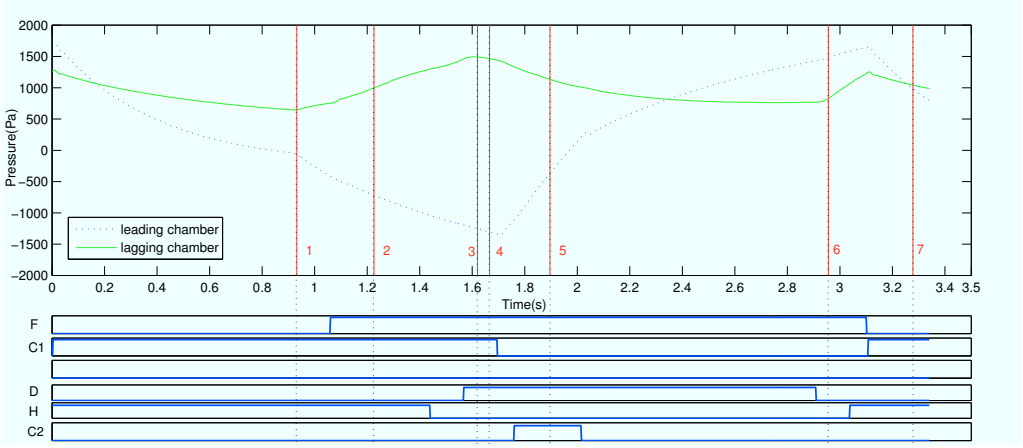

Figure 7.6 – *Typical pressure response of system to singularisation algorithm 1. Key time periods are also illustrated.*

7.3.1.1 Singularisation Process Dynamics and Accuracy

The dynamics of the singularisation device was investigated through pressure response data, and through video analysis of the particles movement. The sequential closure of valves causes fluidic flow paths to develop within the device. These flow paths resulted in the movement of the particles. These fluidic paths may not be predictable and therefore the need to investigate the dynamics. It is these unpredictable flows which are likely to cause singularisation failure.

The initial singularisation algorithm caused the particles to move in a displacement profile pattern for each cycle. A typical particle displacement profile can be seen in Fig. 7.7, where the particles were observed to switch directions, accelerate and decelerate throughout the entire singularisation process. Chronological images of the process can be seen in Fig. 7.8 where the key features of the particles capture, release and transport are illustrated.

The singularisation process can be partitioned into four main sub-processes for analysis, these were:

- The capture of the leading particle.
- The transport of the non captured particles back upstream.

- The release and transport of the leading particle to systems further downstream.

- The termination of the flow.

Capture of leading particle The start of the singularisation cycle begins at time position 0 with the opening of chamber C1 and H . Video analysis showed the velocity of the particle increasing in the direction of the leading chamber (Fig. 7.8(a) - Fig. 7.8(b), Fig. 7.7). The particles traversed until the leading particle was captured in chamber C1 (Fig. 7.8(c)). There was a sudden decrease in the gradient of the pressure within the leading chamber when this capture occurs. The pressure decreased at a steady rate until the threshold pressure of -310Pa was reached. At which point the system considered the particle to be held with sufficient force.

False detection of the captured particle was observed to occur at a threshold pressures above -310Pa, however this was not present in the current algorithm. The probability of false detection increased as the threshold pressure was increased from -310Pa. The threshold pressure must be sufficiently low (high vacuum) to ensure proper immobilisation of the particle, while also preventing early false positive detection of capture. When chamber C1 was opened the pressure within the chamber fell before levelling as it reached steady state. If the threshold pressure was within the steady state region the system would falsely assume a particle was captured. Ensuring the threshold pressure was slightly above the steady state pressure minimised false detection, as the system should capture the particle before steady state is reached. Further detection algorithms which monitor the gradient instead of the absolute pressure values may solve this issue.

In all the trials conducted the leading particle was successfully captured at the capture site (i) and no overshoot was observed. In a single trial where the particles were continuously separated, the longest time recorded for the capture of the leading particle was 1.196s (Fig. 7.9). With an average capture time of 1.109s. The capture time of the leading particle was considered to begin from when

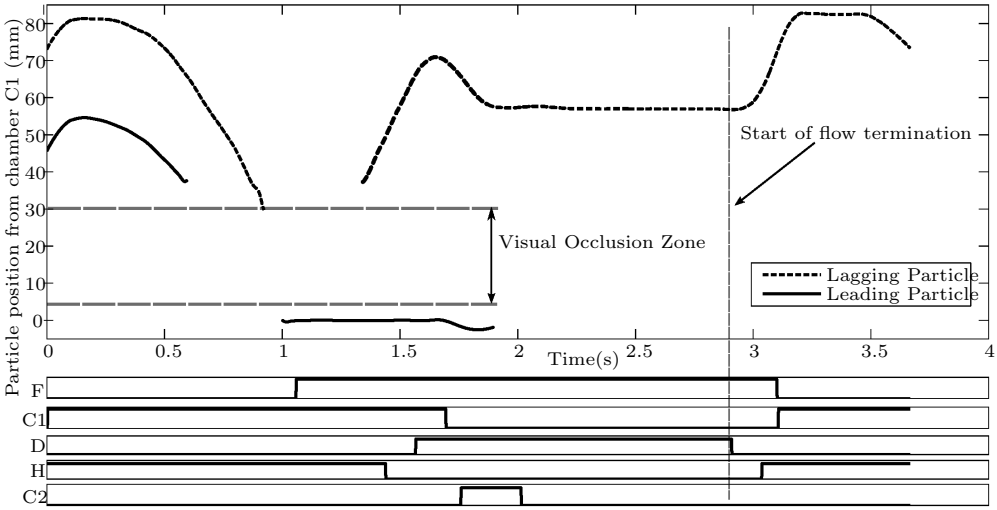

Figure 7.7 – *Particle displacement of a lagging particle and the leading particle during singularisation algorithm 1. The region where no displacement data is presented is due to visual occlusion.*

chamber C was opened and end when the pressure within the holding chamber C had reached the threshold pressure (-310Pa).

Separation and transport of leading particle downstream After the detection of the particle's capture, chamber F was opened transporting the particles which were not captured upstream. The particles were at first stationary, until after time position 2, (0.17s after the activation of the flushing valve) where the velocity of the particles began to increase and the particles were transported upstream of the holding site (Fig. 7.8(d) - Fig. 7.8(e)). Chamber H was closed 0.384s after the first activation of the flushing valve, at which point the particles began to decelerate, until they were stationary at time position 3 (0.17s after the chamber H is closed) (Fig. 7.8(f)). The transport of the particles upstream typically transported the lagging particles 70mm from the holding site (Fig. 7.7).

Leading particle transport After the lagging particles were transported away from chamber C the process of transporting the leading particle was initiated. Chamber D was opened 0.126s after the closure of chamber H to enable flow to develop

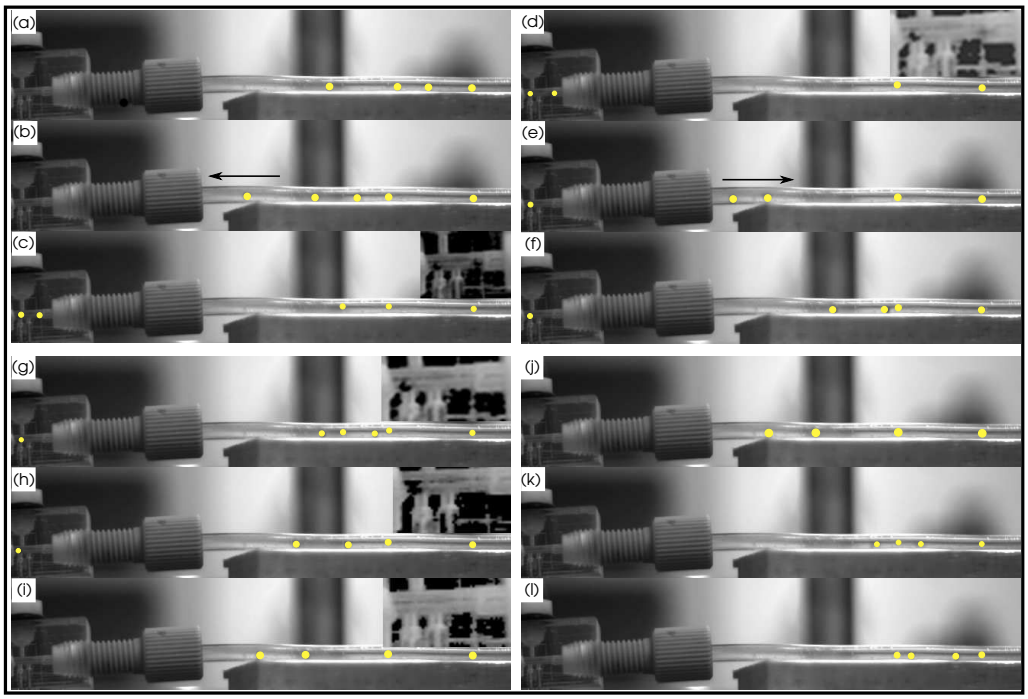

Figure 7.8 – *Image frames showing key processes of the singularisation algorithm. Definite presence of particles have been highlighted. (a)-(c) The capture of leading particle. (d)-(f) The transport of lagging particles upstream. (g)-(i) The transport of the leading particle to systems further downstream. (j)-(l) Termination process.*

from chamber F to D. The leading particle was released into the main chamber M with the opening of chamber C1, where the particle was transported downstream out to a container. During the release of the leading particle the lagging particles was observed to accelerate (downstream direction) then decelerate until stationary at time position 5 (Fig. 7.8(g) - Fig. 7.8(j), Fig. 7.7). After time position 5 the particles were stationary for the remainder of leading particle transport process until the next step of flow termination.

Flow Termination The fluid flow termination sequence which has been previously investigated and discussed in the dual capture chamber prototype, (Sect. 6.5.3) was reimplemented in this prototype. The termination flows resulted in further movements of the particles upstream. Termination began after 1.146s from when C2 was activated. It was assumed at this point that sufficient time has been allowed for the leading particle to be transported to its destination. To terminate

the flow, chamber D was first closed and ≈0.5ms after (position 6), the velocities of the lagging particles rapidly increased upstream before slowing to a halt at time position 7 (Fig. 7.8(j)-Fig. 7.8(l), Fig. 7.7). During termination, chamber H was opened and chamber F was closed. In a typical trial, termination resulted in the particles moving an additional 25mm upstream (Fig. 7.7). The whole cycle was restarted beginning with the capture of the leading particle to repeat singularisation.

Possible failure modes The trials showed 100% singularisation success when no blockages occurred. The occurrence of blockages (caused by the stacking of particles) was the only observed cause of singularisation failure. Blockages were observed to occur at the location where the main chambers transitioned to a larger diameter. The diameter change was required to ensure an almost seamless connection was formed between the fluid lines to the device. The fluid lines used in the experiment have an ID of 1.6mm while the ID of the device main chamber was 1.3mm. The occurrence of blockages resulted in failure, however it was cleared in subsequent singularisation. Theses failures were not recorded as it was caused by the implementation rather than the fundamental concept.

It was found the blockages resulted in singularisation failure as the system was unable to transport the lagging particles upstream sufficiently far from the transport stream. The transport of the leading particle was achieved by the transport stream from chamber F to chamber D. During the flow establishment of this fluid path, transients will occur with a turbulent region. This region may extend upstream of chamber F. Particles lying within this turbulent region (due to blockage) may then be transported downstream along with the leading particle. However, the region of effect was not known for certain, and transport of lagging particles lying close to chamber F (due to blockages) have been observed. In normal operation this would not occur as the lagging particles are transported upstream sufficiently far, and lie outside this region during the leading particle transportation process.

The problem with blockages is common in micro-fluidic devices [121] where a

single particle train is manipulated, relying on physical wall confinement. Kobel et al. suggested that in order to minimise the risk of the particles stacking and blocking the chambers at low flow rates, the chamber diameters of 30% - 40% larger than the cell diameters are used. In the presented device, the larger chamber of 1.6mm was approximately 100% larger than the glass beads, which may explain the much higher occurrence of blockages. The solution to this is to simply select tubing closer to the diameter of the main chambers, thus maintaining a constant ID which is within the low blockage risk range.

7.3.1.2 Throughput Analysis

Throughput of the device is an important factor for the singularisation device as the device will typically handle a large number of particles. Parallelism where multiple devices operate in unison is a simple method of achieving high throughput, if the costs involved in the addition of multiple devices is minimal. In macro devices this is not a cost effective method, but for micro-fluidic devices, units can be easily replicated. If much smaller particles in the micron range are used, micro-fabrication techniques can be applied. As the structure of the chambers was simple, and can be easily scaled down, it lends itself to micro-fabrication techniques. The advantages in moving to a micro-fabrication process are the inherent ease of replicating the structures and therefore the ability to achieve parallel singularisation, which will significantly increase throughput.

Even without the ability to achieve parallelism economically, the throughput of the device itself can be improved. The time required to separate a single particle varied from 3.07s, to 3.22s, with an average of 3.15s (Fig. 7.9). These variations were due to the different times required to capture the leading particle, which itself was a result of the random distribution of the particle spacing as the particles were manipulated. To better understand the singularisation process and its contributing sub-process times, the singularisation algorithm was once again analysed by its four sub-processes. Each of these sub-process contribute to the total overall singularisation time. To effectively improve the throughput of

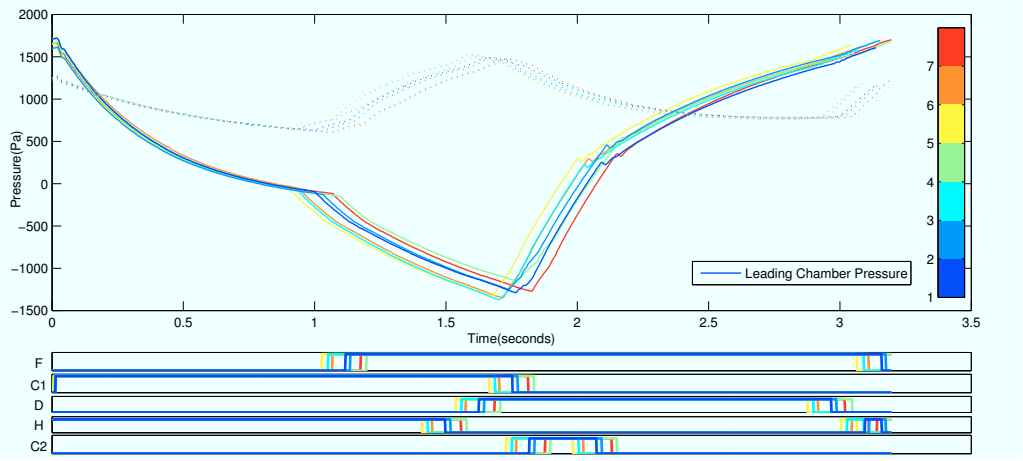

Figure 7.9 – *Pressure response of system during the singularisation cycle algorithm 1. Eight cycles which occurred continuously are illustrated. Varying capture times and cycle times can be seen.*

the device, the sub-processes requiring the longest time was investigated. One general solution which can improve the cycle time for all sub-process was to simply increase overall system pressure. This enabled the fluid flow rates to increase, which in term generated higher particle velocities as well as enabling faster flow development. The higher particle velocities enabled faster switching times while still maintaining the required particle transport profile.

There may be a limit to the speed of the particle velocities, as increased damage may occur to the spheroids. The damage may be greatest in the process of capturing the leading particle as the particle comes to an abrupt stop against a stiff physical surface. The effects of the higher velocities will need to be investigated in relation to the viability of the cells within the spheroids. However the damage may not be as profound, as spheroids are inherently less prone to handling damage then single cells. In addition the system's use of a feedback system for the detection of sufficient holding forces at the holding site, may further limit the damage due to excessive holding pressures. A low holding pressure can be maintained even when there are high overall system pressures. This is a feature that is not easily achieved with passive side channel trapping devices [122].

There are however other methods of reducing the singularisation time when detailed analysis of each process is considered:

Longest Contributing Process - Transport of leading particle to downstream location The process which required the longest time was the transport of the leading particle to the injection chamber. This process on average, required a total of 1.28s from when the positive pressure was first introduced into chamber C1, guaranteeing the release of the particle, until the beginning of termination with the opening of chamber H. This process accounts for 40.6% of the total singularisation time. This period was determined by the need to reliably deliver the leading particle out of the injection device. In this experiment the injection device was not connected and instead the beads were delivered to a container. In the real application the delivery period may need to be further increased. Although the injection device was not used in testing, there are still principles which can reduce the delivery time. These are to either increase the pressure of chamber F or decrease the distance from the capture site to the desired delivery location. The distance can be greatly decreased if the device is placed next to the subsequent downstream system. Both of these solutions can be implemented without too much difficulty.

Second Longest Contributing Process - Leading particle capture The next sub-process contributing a significant amount of time was at the start of the process where the leading particle was captured (Fig. 7.4b). The results showed the longest time recorded until capture was 1.18s with an average of 1.11s. This accounted for 35% of the total average singularisation time.

The capture time of the leading particle was determined by the distance the particle was from the capture site and the particle's velocity. While increasing overall system pressures can increase particle velocity, and decrease time, the capture time can also be reduced more effectively by decreasing the distance. The initial distance of the leading particle before capture, had been identified as being effected by three processes. This can be seen in Fig. 7.7 where the particles move upstream and downstream over the course of singularisation, before finally moving to a location just before the capture process. The first process was the flush back process (Fig. 7.4c), where the period from when chamber F was opened until

chamber H was closed, determines one section of the distance. The second was the closure of chamber D where there was movement of the particles back downstream. The last process was termination, where the particles are transported upstream. This termination distance was determined by the delay between the closure of chamber D and F. By carefully controlling the switching delays in each of the sub-processes, the final resting location of the lead particle can be controlled, and the travel distances minimised.

There are however limits to how short these delays can be, as failure may result. The flush back process was determined by the need to transport the lagging particle outside of the main leading particle transport flow region. This has been previously discussed in Sect. 7.3.1.1, where failure occurred if particles lay within the main transport flow or in the turbulent region during flow establishment. The termination delay was limited by the need to prevent the lagging particles from flowing back downstream (The termination sequence has been previous discussed in Sect. 6.5.3). Further investigation of this region was inhibited by the short length of the optical channel. If a longer channel was able to be manufactured, investigation of these delays will yield the locations where increased likelihood of failure begins, and the potential to achieve the shortest capture distance.

Third Longest Contributing Process - Flow establishment till particle release The third longest process was the delay in the release of the leading particle. The current initial algorithm currently waits 0.71s before chamber C2 was opened, immediately releasing the particle into the main flow. The rationale for this delay was to minimize the effects of random turbulent effects and to wait for the flow to develop more before release. Although it may seem to be a simple operation it was found to account for 22.5% of the total singularisation time. This was quite a significant proportion, and most likely the process can be greatly reduced. Further testing will determine the minimum acceptable release time.

Remaining Contributing Process The other intermediate steps in the singularisation process contribute 2.4% to the overall process and therefore it was more

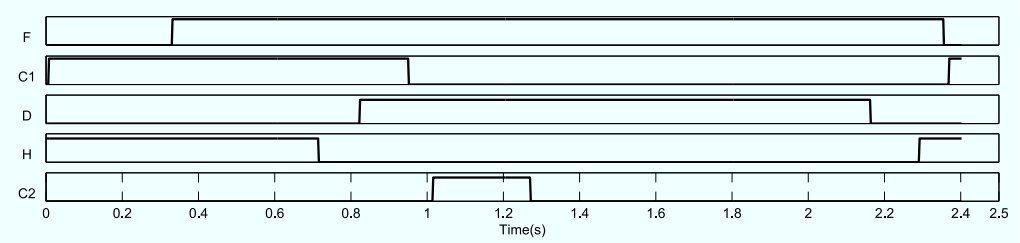

Figure 7.10 – *Timing diagram for valves of algorithm 2.*

effective to focus improvement on the described three processes.

7.3.2 Algorithm 2 - Reduced cycle time singularisation control algorithm

Algorithm 2 presented in this section was a control algorithm with shorter delays and valve switching times implemented with the suggested improvements described in the previous Sect. 7.3.1.2. The improvements include both the increase in overall system pressures and shorter delays. The overall system pressure in this setup has been increased to -6700Pa compared with -6000Pa in the first algorithm. The timing diagram of the valves during algorithm 2 is shown in Fig. 7.10.

The algorithm displayed similar dynamics to the initial algorithm. The movement patterns for the particles were similar to the results for the initial algorithm in Sect. 7.3.1, with the exception that the particles were moving at higher velocities and traversing shorter distances (Fig. 7.13). The longest singularisation time from the trials conducted was 2.03s while the shortest was 1.82s with an average cycle time of 1.93s (Fig. 7.12). This was an improvement by 39%. Once again the variations in time for the process were due to the varying capture times of the leading particle as all other process are predetermined.

Decomposing the singularisation process once again into separate processes the improvements in time can be analysed:

Longest Contributing Process - Transport of leading particle In algorithm 2 the longest contributing process was the transport of the leading particle downstream, which In the experimental setup was out directly into a Petri dish. The process

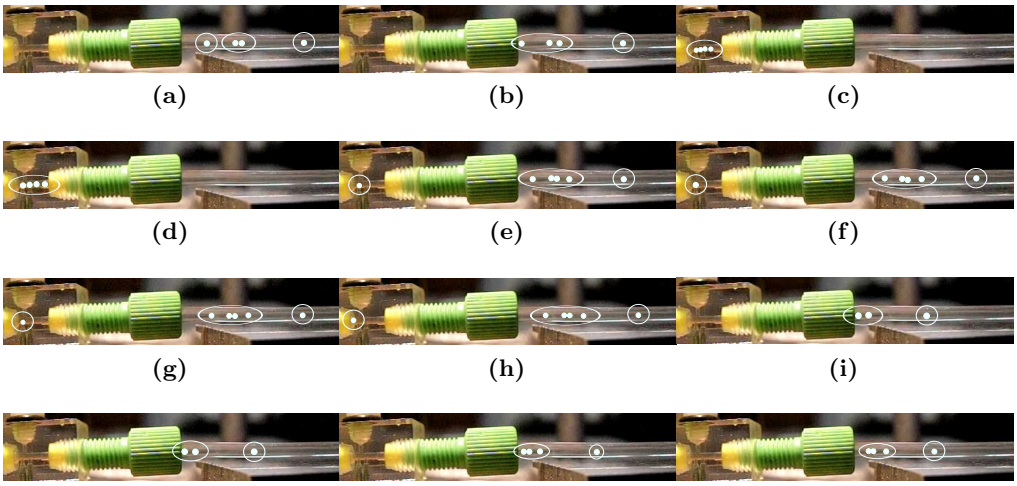

Figure 7.11 – *Frames showing key processes of the singularisation algorithm 2. (a)-(c) The capture of leading particle. (d)-(f) The transport of lagging particles upstream. (g)-(i) The transport of the leading particle to systems further downstream. (j)-(l) Termination process.*

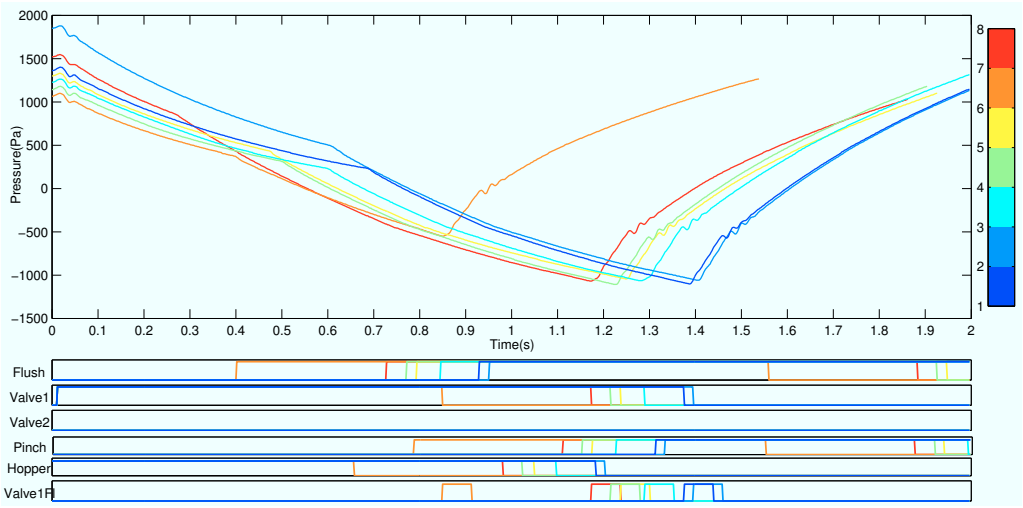

Figure 7.12 – *Pressure response of chamber C, and timing diagram of valves, during the singularisation cycle for algorithm 2. Eight singularisation cycles are illustrated which were performed continuously. Various capture times and thus varying cycles times can be seen.*

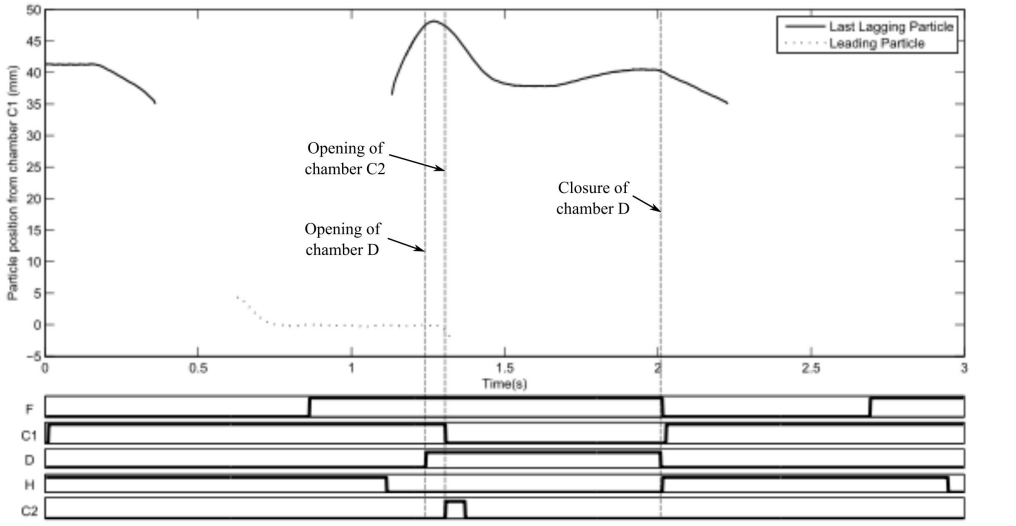

Figure 7.13 – *Typical displacement response of a lagging particle and the leading particle to the manipulation of fluid flow, during singularisation algorithm 2.*

to transport the leading particle had been reduced from 1.28s in the previous algorithm to 0.72s an improvement by 43%. This reduction in the flushing time was due to the decrease in the distance and higher particle velocities. The transport of the leading particles still contributed highly to the overall singularisation process contributing towards 37%.

Second Longest Contributing Process - Capture of lagging particles The time required to capture the lead particle is similar to the time required to transport the leading particle. The fastest trial captured the leading particle in 0.64s, while the longest cycle was 0.86s, with an average capture time of 0.74s. On average the capture of the lagging particle has been reduced by 34% accounting for 38% of the total singularisation process.

This decrease in the capture time was primarily due to decreasing the particles required travel distances. As previously discussed (Sect. 7.3.1.2) distances can be reduced by reducing the flush back period and reducing the termination period. In algorithm 2 the period from the opening of chamber F to the closure of chamber H has been reduced from 0.384s to 0.254s. This decrease in delay resulted in the reduction in the distance the lagging particles are flushed back. In a trial

(representative of typical particle movements) the last lagging particle was now transported upstream 47mm compared with 70mm in the previous algorithm (Fig. 7.13).

The particles were still observed to move downstream when chamber D was opened. The movement was somewhat consistent with the previous algorithm where the particles move downstream by approx 10mm. However, control over this distance was not known for certain.

The largest change to the distance has been at termination, when chamber D and chamber F are closed. In the previous algorithm the delay resulted in the particle being typically transported upstream by a further 25mm. Where in the current algorithm the particle movement was insignificant (<1mm) (Fig. 7.13).

Third Longest Contributing Process - Transport of leading particle The delay from when the transport flow is initiated (chamber F opened) to the release of the particle into the main transport stream (opening of chamber C1) has been reduced. This has been reduced by 38% from 0.71s to 0.44s and contributes towards 23% of the singularisation process. The contribution still remains high, but further experimentation should yield much lower release times and lower contributions.

7.4 Discussion

The presented device has demonstrated the ability to separate a single particle from a particle train. The fluidics device utilised hydrodynamic forces to manipulate particles within the flow. This method of manipulation did not rely on the physical properties of the particle nor labelling and was highly flexible. The device utilised a single trapping location with the sequential manipulation of fluid flow paths to achieve singularisation. The use of a single trapping location instead of two, was a significant improvement over the dual trapping method of singularisation presented in the previous chapter (Chapter 6). The new method improves upon throughput, parts count and reliability. A number of aspects were investigated which include the dynamics of the device, reliability and throughput.

In the first part of the investigation (Sect. 7.3.1) algorithm 1 showed singularisation efficiencies of 100%. The system may have had a singularisation success rate which was very accurate when compared with a similar reported device [123], however, it was relatively slow. This was due to the number of transitions and total fluid switches that occurred within the system, as opposed to concepts which utilised a continuous flow [124]. Occasional blockages were observed to occur and singularisation would fail, but these were not included in the singularisation success count, as it was not a problem with the operational principle of the device. These blockages were due to the diameter of the chamber, relative to the size of the particles. Blockages occurred at the point where the main chamber transitions from a diameter of 1.3mm to 1.6mm. These blockages were expected as the beads have an average diameter of 0.8mm, while the transition chamber was 1.6mm, this was 100% larger than the bead diameter. Previously reported devices [121] have suggested that 30-40% minimises the probability of these occurrences. The problem can be easily remedied by changing the diameter of the tubing such that a transition to 1.6mm is not required.

In the second part of the investigation, the throughput of the device and sub-processes which constitute the singularisation process was investigated. Investigation of algorithm 1 identified three lengthy processes which provided the most effective means of improving the cycle time. These were the transport of the leading particle to systems downstream, the capture of the leading particle and the release of the leading particle in to the main flow. By investigating the factors that determined the length for each of these processes the cycle time was reduced. A general improvement to all these process was to simply have a higher negative pressure. This would increase the flow rate and therefore the velocity of the particles. Other improvements for the first two processes included decreasing the distance the particles traverse.

The initial algorithm 1 showed that the transport of the leading particle contributed towards 40.6% of the total singularisation time and required 1.28s. Increasing the velocity of the particle and decreasing the distance from the device to the desired exit location was the best method of decreasing this time. In the

experimental setup used in algorithm 2 this was implemented and a reduction in time by 43% was achieved, however still contributing 37%.

Another large contributing process was the capture of the leading particle. It was found that the distance the lagging particles were transported to at the end of each singularisation process were excessive and significant reductions in time could be made. By ensuring the particles were positioned closer to the capture site, shorter capture times could be achieved. The final location of the lagging particles at end of singularisation, was determined by the net movement of the particles from a number of process, which in term was caused by the delays in the opening and closure of the valves. By carefully controlling the delays at each of the processes, the position of the particle at the end of the cycle could be controlled to rest at a location closer to the capture chamber. There was however, a limit that existed to how close this location was, where the particles in close vicinity to chamber F were themselves caught in the main transporting flow to the injection device. The distance was difficult to quantify as the optically clear length of the chamber was short. Future prototypes where different manufacturing methods can be employed will enable longer optically clear channels, enabling this investigation. By decreasing the delays as well as increasing the pressure in algorithm 2, the process was decreased by 34% from algorithm 1, while still contributing towards 38% of the singularisation process.

The third longest contributing process was the time from when chamber F was first opened to the release of the leading particle. The rationale for this delay was to ensure flow was properly developed in chamber F before the leading particle was released into the flow, thereby decreasing the random turbulent effects during the development of flow. In algorithm 1 the delay was 0.71s contributing towards 22.5% of the singularisation time, while in algorithm 2 this was deceased to 0.44s while still contributing towards 23% of the singularisation process. The simplicity of the process suggests that much shorter delays can be still achieved. Further investigations to determine the probability of failure versus decreasing delays will determine the limits of this process.

7.5 Summary

In this chapter a fluidics singularisation device utilising hydrodynamic forces for the gentle handling of particles was presented. The device utilised a single trapping site with closed loop feedback, in combination with manipulation of fluidic flow paths to achieve label-free singularisation. The simplicity of the fluidic structures can be easily transferred to micro-fabrication techniques to achieve structures on a much smaller scale if required. The single trap site improves upon, cycle time and reliability over previously developed devices in Chapter 5 and Chapter 6. The dynamics of the device were investigated and 100% singularisation accuracy with both algorithms was achieved. The only observed mode of failure was due to blockages at the point where the device chambers transitioned from 1.3mm to 1.6mm to match that of the tubing diameter. Throughput of the device was found to be predominately affected by the transport of the leading particle out of the device, and the capture time of the leading particle. Factors involved in the sub-processes were identified and in algorithm 2 throughput improvements were made. A recorded average throughput of 1.93s was achieved, however this throughput does not represent the speed limitations of the device, and much faster cycle times can still be achieved. The presented singularisation device has high accuracies which will enable the effective use in a wide range of biological applications including tissue assembly and has potential in handling and manipulation of rare cells. In the next chapter the injection device is presented which is connected downstream of the singularisation device and provides a method to deliver the particles into the lattice pores.

Chapter 8

Retractable Pore Expanding Spheroid Delivery Device

8.1 Introduction

The spheroid delivery system as described in the previous Chapter 3 consisted of two subsystems, the singularisation system and the injection system. In this chapter the latter is described. The main functional requirement of the injection system was to expand the lattice fibres, creating an unobstructed free path for the delivery of the spheroid into the pore spacing, thereby allowing the automated assembly of a three-dimensional (3D) tissue construct. The rationale for the approach requiring expansion and elastic deformation of the scaffold instead of the spheroids was to minimise the stresses exhibited on the spheroid, thereby decreasing the likelihood of damage to the cells.

Expanding the pore in the meso-scale was not a straight forward task. A literature search did not find a device with capabilities that expanded the pore with an effective mechanism. To the authors knowledge the device described in this chapter is a unique solution to the problem. The following sections describe the design problems and experiments conducted on the prototype. In Sect. 8.2 a brief description of a number of concepts are described along with design issues.

Section 8.3 describes the operational function of the injection device, experimental setup and general experimental procedures. Section 8.4 will present the results and discussion on the characterisation of the scaffold, the scaffold expansion analysis and the analysis of particle transport into the pore. Finally Sect. 8.5 will summarise the chapter in the development of the injection device.

8.2 Conceptualisation and design issues

The construct technique required spheroids to be incorporated into the scaffold lattice, while a holding mechanism prevented spheroid egress. This was realised through dimensional differences between the particle diameter and the pores size, which ensured a press fit occurred (Fig. 8.1(a)). To gently deliver the particle into the pore it was desirable to expand the pore, rather than to deform the spheroid.

A simple conceptual approach allowing the safe expansion of the scaffold's lattice fibres, was to use fingers attached to a movable stage which were able to move apart separately, expanding the lattice (Fig. 8.1(b)). However there were several shortcomings to this concept, as the strength required to expand the relatively stiff but elastic lattice fibres would require thick fingers. The thickness of the material needed to be kept to a minimum in order to reduce the degree of scaffold expansion, given that the device and the spheroid together must fit inside the pore spacing (Fig. 8.1(b)-(c)). Thus the lattice was required to expand and accommodate not only the spheroid, but also the expanding device material thickness.

The difficulty with minimising the wall thickness was a common problem associated among concepts utilising multiple separated expanding components. The concept with great potential in reducing the wall thickness of the device, was a sheath concept. The sheath would act as a smooth guide for the proceeding syringe to move through into the pore. This concept is illustrated in Fig. 8.1(d)-(e). The concept enabled much greater reductions in the wall thickness as the secondary monolithic solid cylindrical syringe would provide the expanding force. However the main difficulty with the concept, was in finding an appropriate cost

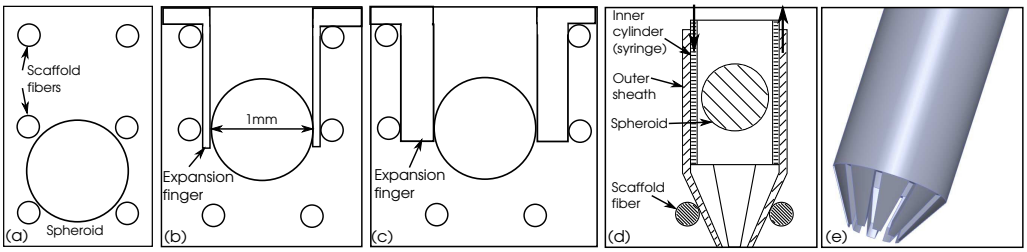

Figure 8.1 – *(a) Diagram showing the dimensional difference between the spheroid and fibre spacing. (b) Movable finger based concept showing ideal thickness. (c) Finger concept showing realistic wall thickness and excessive expansion required. (d) The sheath concept comprises of an outer sheath arranged in a conical shape with slots, and an inner solid tube. The sheath guides the assembly into the pore while the inner tube expands the sheath end. (e) 3D rendering of the device.*

effective method for manufacturing the sheath at such small scales. The concept was thus not deemed a viable option and further concepts were developed. A concept was finally conceived which had the desirable characteristics of minimising the wall thickness, and the potential to be fabricated using simple methods. The investigation and functionality of the final concept is further described in the following sections.

8.3 Method and Materials

8.3.1 Injection System

The main function of the injection system was to expand the lattice pore to a suitable size to ensure a particle could be reliably delivered into the spacing and have it remain fixed in place. As the system was dealing with a single particle, no additional mechanisms were required to ensure only a single particle was delivered into the pore space.

The injection system (Fig. 8.2) comprised functionally of two main components:

- The expanding rod (Fig. 8.2(1)).
- The thin outer sheath or nozzle (Fig. 8.2(2)).

The remaining components were for the support of the functional components. The fluidic chambers (Fig. 8.2(3)), bushing(4), retaining collar (5), the housing

(6) and the expanding rod linear actuator. For detailed mechanical drawings of the device refer to Appendix Fig. C.11.

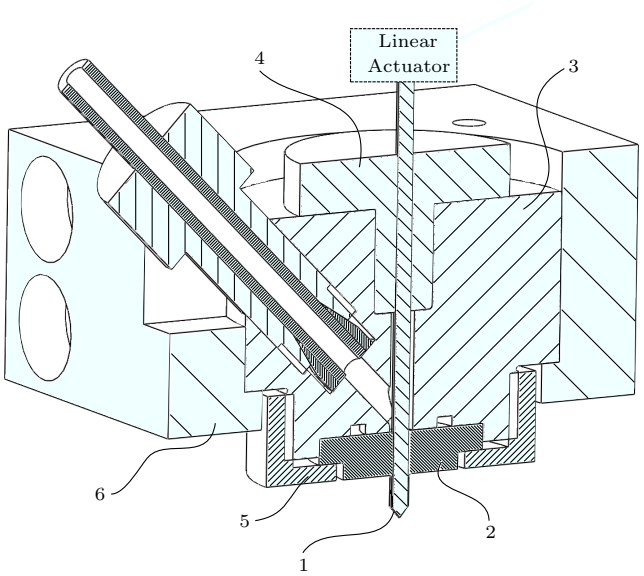

Figure 8.2 – *The injection device comprises of two main functional components which are the expanding rod (1) and outer sheath (2). The remaining are support components. These are the fluidic chambers block (3), bushing (4), retaining collar (5), the housing (6) and the linear actuator for the expanding rod. Functionality of the device is described in Sect. 8.3.1.*

Device functionality The principle concept in the expansion of the lattice fibres was the use of the outer sheath and the expanding rod. Together in a fixed configuration, the expanding rod and outer sheath form a relatively smooth outer profile. The expansion process is illustrated in Fig. 8.3. First the expanding rod and sheath advance towards the constrained lattice. The lattice fibres deform and slide along the outer profile and begin to expand (b). At a certain vertical displacement of the injection device, the fibres slide and transition from the expanding rod and rest on the outer sheath (c). The inner expanding rod is retracted (d), enabling a spheroid to be transported through the outer sheath. The spheroid is transported by a carrier fluid into the lattice pore (e), while the whole assembly is retracted from the lattice. The retraction of the device enables the lattice fibres to return to their original positions (f) entrapping the spheroid.

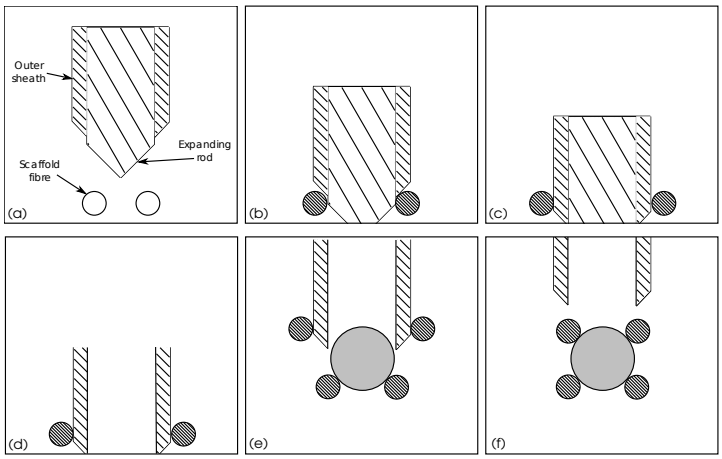

Figure 8.3 – *Injection concept - (a) The functional components of the injection device. The first process is the movement of the assembly down towards the lattice, where the lattice fibres are deformed and slide along the outer profile of the expanding rod (b). At a certain displacement of the device, the fibres slide and rest on the outer sheath (c). The expanding rod is retracted (d) enabling a spheroid to be delivered into the pore (e), while finally the whole assembly is retracted (f), entrapping the spheroid.*

8.3.2 Integrated scaffold deposition and particle injection system

The integrated platform for the fabrication of the scaffold and injection of the particle into a pore, consisted of all described subsystems in the preceding chapters (Fig. 8.4). The three-dimensional positioning system (Sect. 3.3.3) and the control system (Chapter 4) form the positioning and control platform for the scaffold deposition and spheroid injection heads. The singularisation device (Chapter 7) enabled a single particle to be delivered through to the injection device, thus fixing it in a defined location within the scaffold lattice. The singularisation system was connected to the injection system through a long length of tube and was located at a significantly different elevation. Due to the system specifications in terms of pressure, the system parameters which affected the flow rate are summarised in Table 8.1.

8.3.3 Scaffold Fabrication

Fabrication of the scaffold was produced using the general technique described by Woodfield et al. [17] with modifications to the equipment. These modifications were the introduction of an auger feed system (DL Technology) with associated 22

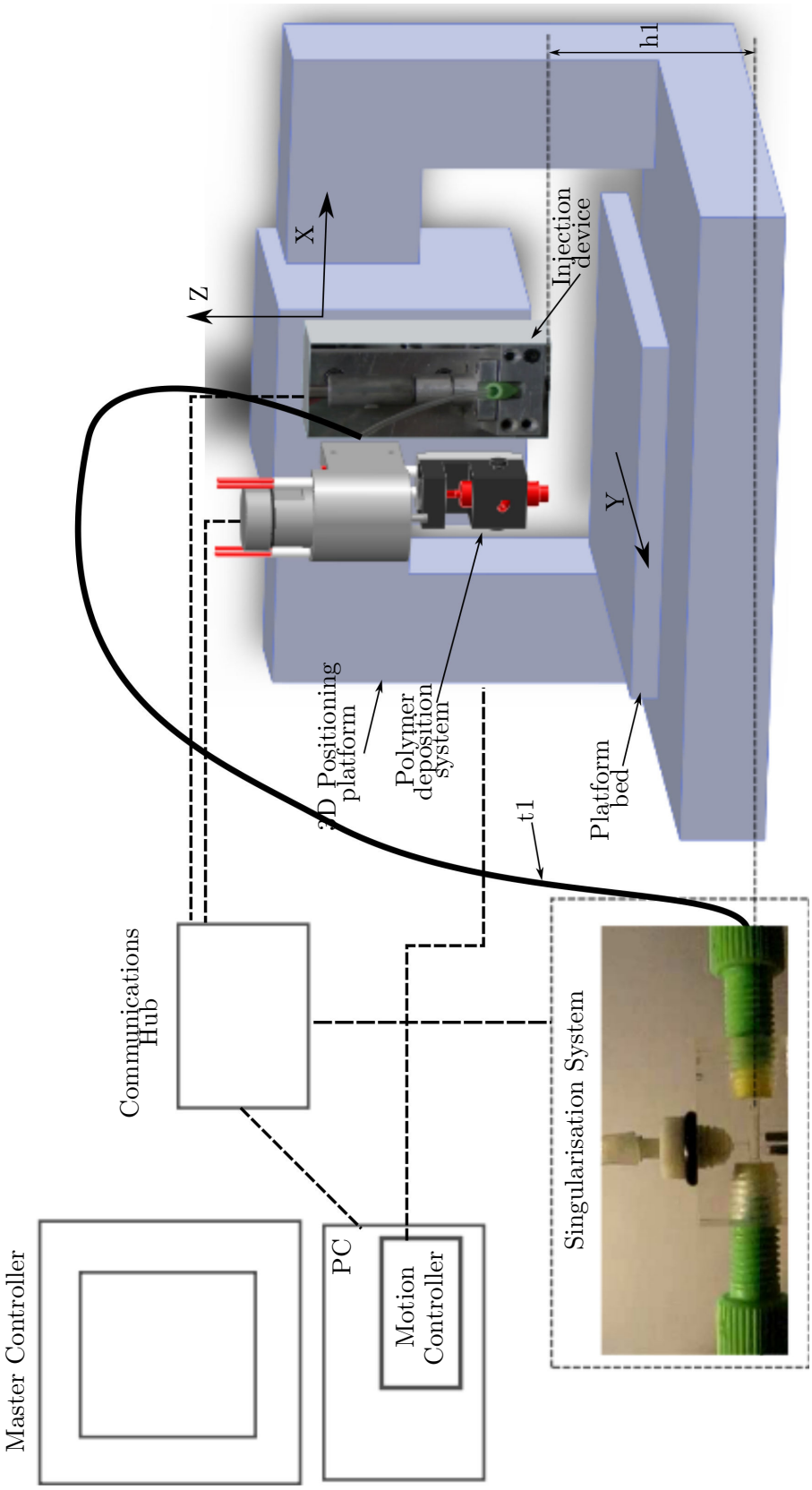

Figure 8.4 – *The setup consisted of a polymer fiber generation system, the singularisation system, 3D positioning platform and the injection system. They are connected to a common bus through the communications hub with high level control performed by the master controller. The injection and fiber generation systems are attached to the ZX stage while the bed moves in the Y axis allowing for all three axes control of the heads relative to the substrate.*

Table 8.1 – *Experimental setup parameters.*

Parameter	Property
Singularisiation system positve pressure	18100±10 Pa
Singularisation system negative pressure	-6670±10 Pa
h_1	0.40±0.01 m
l_1	1.515±0.005 m
Tube ID	1.6 mm

gauge nozzle. The setup consisted of a high pressure nitrogen tank connected to a heated reservoir. The pressurised reservoir contained the molten polymer and was connected to the auger feed system. The auger enabled much higher pressures to be attained with precise control over the flow rate. This was due to the coupling of the auger to a stepper motor (MDrive® 17 IMS) capable of 51200 steps per revolution, enabling precision control over the auger rotation. The high pressure generated by the auger also allowed for much smaller diameter nozzles to be used.

The polymer used in the fabrication of the scaffold was a co-polymer comprising a hydrophilic poly(ethylene glycol)-terephthalate (PEGT) and hydrophobic poly(butylene terephthalate) (PBT). The specific copolymer, Polyactive 300PEGT55PBT45 (PolyVation) had a PEG molecular weight of 300 g/mol and a PEGT:PBT weight percentage ratio of 55:45. By varying the amount and length of the PEGT and PBT composition, the co-polymer can be designed with specific properties such as swelling, degradability and mechanical strength [125].

The layup pattern of the scaffold was either a 0° or 90° fibre orientation. A layup pattern (0, 90, 0, 0, 90 ,0 ,0 ,90 ,0) having a total of 9 layers was used to create a structure with a range of pore sizes, and these fabrication process parameters are summarised in Table 8.2. Prior to use, the large scaffold was generally cut into a 3x5 pore size for visualisation purposes during the delivery of the particle.

8.3.4 Spheroid particle simulant

To provide an inexpensive and easily attained simulant to the spheroids, glass beads (Meyer Imports) were used. A group of 10 beads were selected and measured via

Table 8.2 – *Fiber deposition process parameters.*

Case	Pore spacing (mm)	Height offset (mm)	Temp(°C)	P (Bar)	Auger speed (RPM)	Traverse Speed (mm/sec)
1	1.1x1.1	0.3	200	2	10	350
2	1.2x1.2	0.3	200	2	10	350

Table 8.3 – *Glass bead diameter characterisation.*

Number of particles	Min (mm)	Max (mm)	Mean (mm)	Sd (mm)
10	0.93	1.01	0.95	0.02

an optical microscope. A summary of the measurement can be seen in Table 8.3.

8.3.5 Experimental Procedure

For the investigation of the successful particle delivery into the pore, all subsystems needed to be integrated. First the small section of the scaffold was glued onto the 3D positioning platform bed. The injection nozzle was manually positioned above the required pore, and manually advanced into the scaffold to the desired depth. This depth was to place the sheath tip directly at the centre of the pore in between the fibres of the scaffold (Fig. 8.5). Subsequently the injection process was started where the master controller initiated the singularisation system transporting a single particle towards the injection system. After a pre-set calibrated time the singularisation system broadcasted a message which was acknowledged by the master controller, commanding the positioning system to withdraw the injection device. This pre-set time needed to be calibrated through experimentation to guarantee the exit of the particle. Fluid flow was maintained 1s after withdrawal. This manual and automated process was repeated for each pore. After experimentation the injected beads were removed from the scaffold and reused.

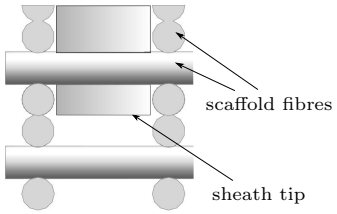

Figure 8.5 – *Illustration showing the placement of the sheath in the center of the two spacer fibers.*

8.4 Results and Discussion

8.4.1 Scaffold Architecture

The architecture of the scaffold had implications on both the mechanical, biological, and assembly process properties of the 3D construct. The architecture can affect the level of interaction between the fibres and the particle during the delivery, in addition to the particles final resting position and retention.

The main function in terms of assembly for the scaffold architecture was to confine a particle into a predetermined three-dimensional location to achieve complex 3D constructs. Confinement of the particle while retaining high interconnectivity can be achieved by the 3D layer-by-layer fabrication of pores. The pores in general were regular and "box" shaped which aided in the expansion process and access to the inner pores.

The general scaffold architecture consisted of 3D printed fibres with a fibre spacing less than that of the diameter of the target particles. This ensured a frictional fit between the particle and the fibres, thus preventing the particle egress from the scaffold. With this architecture the scaffold fibres are at a close proximity to the particle, greater contact area occurs, and a higher pore fill factor could be achieved. However the effects of these factors on actual spheroids have not been investigated and will be the focus of future work.

Characterisation Using the described fabrication technique and process parameters (Table 8.2) scaffolds were fabricated and characterised via an optical microscope. The process produced repeatable, regular deposition of fibres which were well

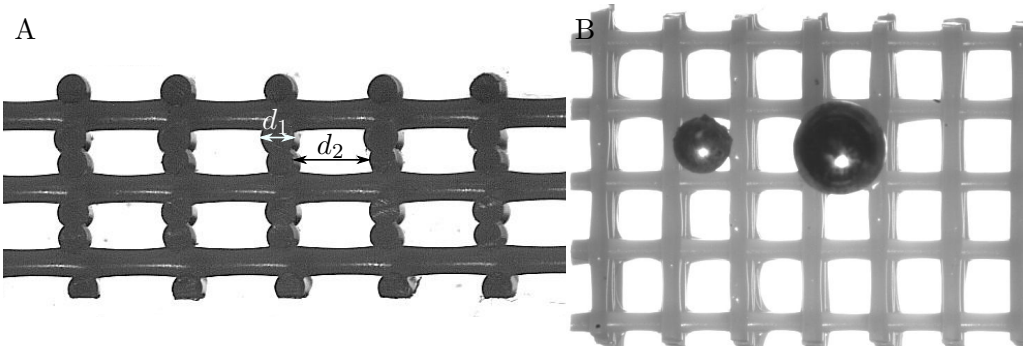

Figure 8.6 – *Optical microscope images of the surface and cross section of the 1.2mmx1.2mm scaffolds. (A) Cross section of the scaffold showing the parameters of the fiber diameter (d_1) and pore spacing (d_2). (B) Surface view with the simulant particle placed on top and larger reference particle (ϕ1.59mm).*

Table 8.4 – *Scaffold Architecture Characterisation.*

Scaffold pore architecture	Average pore size	Average fibre diameter
1.1 mmx1.1 mm	0.42±0.03 mm	0.645±0.03 mm
1.2 mmx1.2 mm	0.82±0.03 mm	0.33±0.03 mm

bonded with straight fibers deposited on top of underlying spaced fibers, yielding no significant drooping. The scaffolds were successfully fabricated to accurately replicate the desired general scaffold architecture and geometry as shown in Fig. 8.6(a,b).

Scaffold sections were taken for each experimental specimen, for the characterisation of the physical geometry (Fig. 8.6(a)). Results showed minor variations existed in both the fibre diameter and the pore size (Table 8.4). In the case of scaffolds with a 1.2mm fibre spacing the variations in the pore spacing was up to 5% of the deposited fibre spacing. It is worthwhile to note that in the illustrated example the bottom layer was significantly offset from the remainder of the fibers. The results also showed that deposition of scaffolds with a 1.1mm fibre spacing had a fiber diameter which was 95% larger than the fiber diameter of the 1.2mm scaffold, but uncertainty remained the same. The polymer for the 1.1mm scaffold was also notably much darker than the 1.2mm scaffold.

The geometric distribution in pore size exhibited in the fabrication process

were expected, but the distribution from the mean value in both the particle diameter and pore spacing need to be considered. For a high probability of particle retention, the particle diameter distribution must be below the pore spacing distribution. Overlapping of the distribution increases the probability of the pore being larger than the particle, thus egress. While greater separation between the particle diameter distributions will require greater expansion of the pore. A balance will need to be reached between an acceptable level of expansion and particle egress probability. The distribution of the particle diameter may be further refined if a sorting device is introduced at the singularisation stage. The characterisation results of the scaffold geometric distribution and the test particles showed there should be a low probability of particle egress.

The cause of the variations in the scaffold may be attributed to the movement of the specimen on the platform bed during the printing process. In Fig. 8.6 the significant shift was most likely to have resulted from the specimen being knocked during the deposition process. Significant vibrations were also observed during the movement of the bed in the Y axis which may have caused the specimen to move on the platform. Proper restraint of the specimen with additional dampening material should eliminate this problem. Even with this problem an uncertainty of ± 0.03 mm was achieved which was similar to the accuracy of the positioning platform, having a resolution of ± 0.02 mm with a repeatability of ± 0.01 mm. The uncertainty value was also close to values reported by other studies [17, 126].

Significant differences in the fiber diameter between the 1.1mm case and the 1.2mm were found, although the same process parameters were used. The likely explanation for this was due to the deposition of the highly degraded polymer. In the 1.1mm case the polymer was observed to be significantly darker indicating signs of degradation. The degradation of the polymer would have led to a decrease in the dynamic viscosity [127], leading to a higher flow rate Q. The fiber width is related to Q by the following equation [128],

$$Q = ahv_o \tag{8.1}$$

Where a is the line or fiber width, h the height of the fiber and v_o the velocity of the substrate with respect to the nozzle. Assuming the product of the width and height can be used to estimate the cross-sectional area of the deposited structure. The equation shows that an increase in Q (due to a decrease in viscosity) with the same v_o will lead to an increase in the cross-sectional area which confirms what has occurred. Equation 8.1 also indicates that for greater accuracy over the fiber width, parameters involved in the determination of Q and the velocity of the nozzle, relative to the substrate, need to be kept constant and well controlled. These are important considerations if more accurate pore geometries are desired and also in extended printing sessions.

8.4.2 Particle delivery through device investigation

To investigate the reliability of delivering a single particle through the injection device, the probability of the particle exiting the nozzle into an open container was investigated.

In all trials the particles successfully exited the device, indicating that blockages or obstructions within the device was unlikely. Results show there was large variability in the exit time of the beads from the sheath. The average exit time was 9.0±0.5 s. The variability was likely caused by the particles being in contact with the side-walls. As the particles were more dense than the carrier fluid, there was a high likelihood of the particle coming into contact with the bottom of the tube wall as it travelled. Due to the long length of tubing from the singularisation device to the injection system and the frequency of contact, the total contact time with the side wall may be relatively high. This process was random and may account for the variability in the exit time of the bead. In the ideal setup, the singularisation device should be located much closer to the injection device, significantly reducing the total transport time and absolute variability in time.

A factor that may need consideration is the increased fluid resistance once the sheath is inside the scaffold. The current experimental setup where the exit was into an open container would exhibit the lowest resistance, thus would

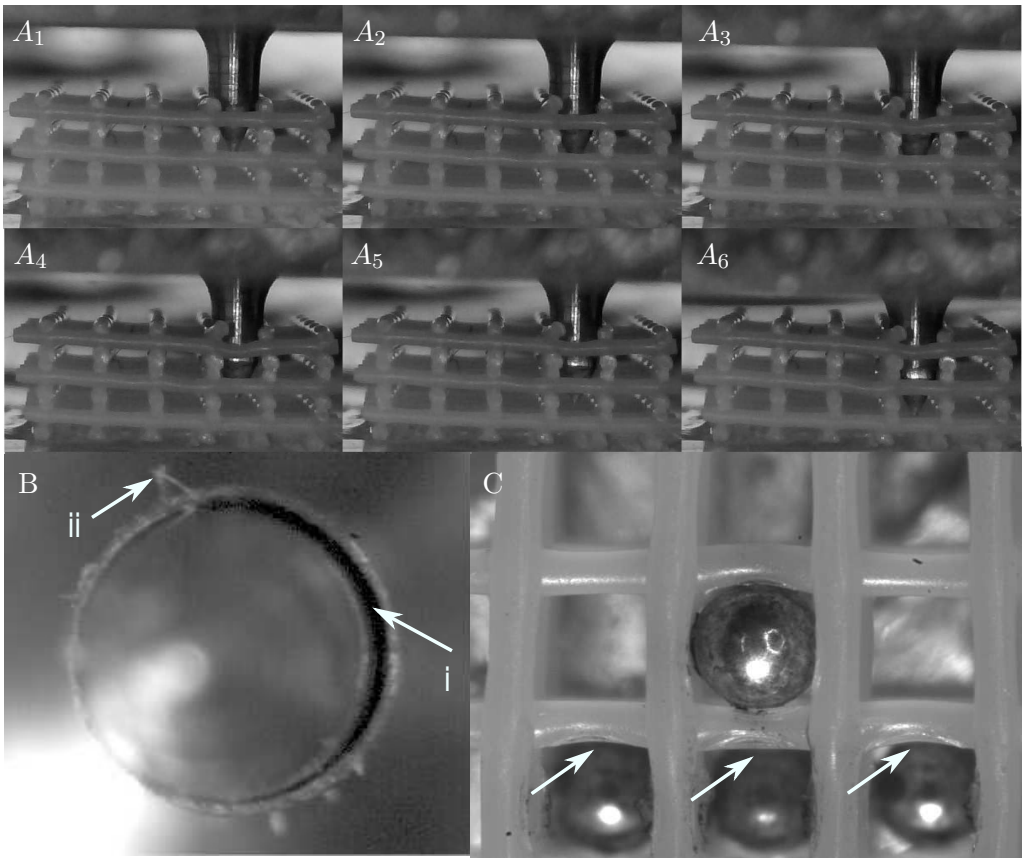

Figure 8.7 – *Images of device entry and pore expansion process. ($A_1 - A_6$) Images showing the entry of the injection device into the pore with visible scaffold deformation. (B) High clearance fit between the expanding rod and the outer sheath (i), with remnants of the scaffold attached to the sheath (ii). (C) Minor signs of damage to the scaffold fibers after device insertion and expansion.*

incorrectly represent the conditions found in injecting into the scaffold. The fluid resistance may also depend on the depth of the nozzle in the scaffold and scaffold size, as the fluid will be required to travel through larger pore networks before reaching atmosphere. However, an advantage with the scaffold architecture is 100% interconnectivity between pores, which helps to minimise these effects. The increased fluid resistance can simply be countered by a higher system pressure which maintains the fluid flow rate.

8.4.3 Sheath-rod entry and pore expansion

Scaffold Damage The successful expansion and retraction of the scaffold fibres was an essential process for the successful delivery of a bead into the pore location and particle retention. Permanent deformation or damage to the scaffold may effect the fibres ability to return to its resting position, thus particle retention ability. In all trials the entry of the assembly did not cause significant damage to the scaffold, and lattice fibres remained bonded for the 1.2mm scaffold through to the 1.1mm scaffold. Damage to the scaffold was only observed with slight tearing of the fibres. Under high magnification minor tearing could be observed near the midpoints of the fibres (Fig. 8.7(c)). In addition signs of damage could be observed in Fig. 8.7(b) where remnants of the scaffold can be seen attached to the outer sheath. The cause of damage was likely attributed to the fit between the outer sheath and the expanding rod. The clearances between the outer-sheath and the inner expanding rod were not as low as conceptualised, thus a smooth outer profile was not realised. Instead sharp edges may be exposed to the scaffold as the assembly moves down. The loose fit can be observed in Fig. 8.7(b), where dark shadows can be seen due to the clearances between the outer sheath and expanding rod. The problem with the relatively high clearance fit could be solved with higher precision manufacturing methods to realise a smooth outer profile.

Sheath Placement The experimental procedure for sheath positioning was to place the sheath in between the two spacer fibers. When the robotic positioning platform was commanded to the desired depth, variations in the relative position to the fibres was observed. The deformation of the scaffold during the insertion of the assembly can be seen in Fig. 8.7($A_1 - A_6$). The variations were due to the elasticity of the scaffold structure. The deformation (or compression) of the scaffold in the z axis caused the variations in the relative positioning of the outer sheath to the scaffold fibres. A possible solution is to move the sheath to a depth further than the required position, then move back to the desired position. This solution may help as the forces against the fibres are less while the sheath is retracted, due to the fibres only sliding along the sheath. The problem may also be less pronounced once a smooth external profile is achieved, allowing the fibres

Table 8.5 – *Device withdrawal investigation.*

Case	Singularisation positive pressure (Pa)	Transport time (s)	Withdrawal velocity (mm/sec)
1	18100	20	150
2	18100	10.5	3000

to slide more readily during the device insertion.

Expansion and sheath wall thickness The expansion process was dependent on the dimensional difference between the pore size, particle, plus the constant wall thickness of the sheath. By minimising the wall thickness of the sheath the device was able to achieve the required expansions without the addition of unnecessary expansions due to the thickness of the sheath side walls. At smaller scales the expansion requirements due to the wall thickness of the sheath may become more pronounced, thus minimisation is advantageous.

Minimisation of the wall thickness was greatly simplified due to the conceptual utilisation of the solid core and a solid one piece cylindrical sheath. Given a low clearance fit between the outer sheath and centre expanding rod, the solid centre can provide additional support to the sheath during the insertion process. The one piece cylindrical sheath compared with other mentioned concepts (Sect. 8.2) provides excellent utilisation of the material. Both these factors in addition to the selection of a material with higher properties aid in the minimisation of the wall thickness, as well as the extension of the sheath to access deeper layers if required.

8.4.4 Particle delivery into pore and sheath withdrawal

The probability of successfully delivering a particle into the pore was investigated with various withdrawal speeds. The results show the device withdrawal speed does not affect the probability of successfully delivering a bead into the pore, but does affect the probability of the particle's position within the pore.

Table 8.6 – *Device withdrawal investigation.*

Case	Withdrawal velocity (mm/sec)	Bead Located Bottom	Located Middle	Located Top
1	150	20%	30%	50%
2	3000	60%	0 %	40%

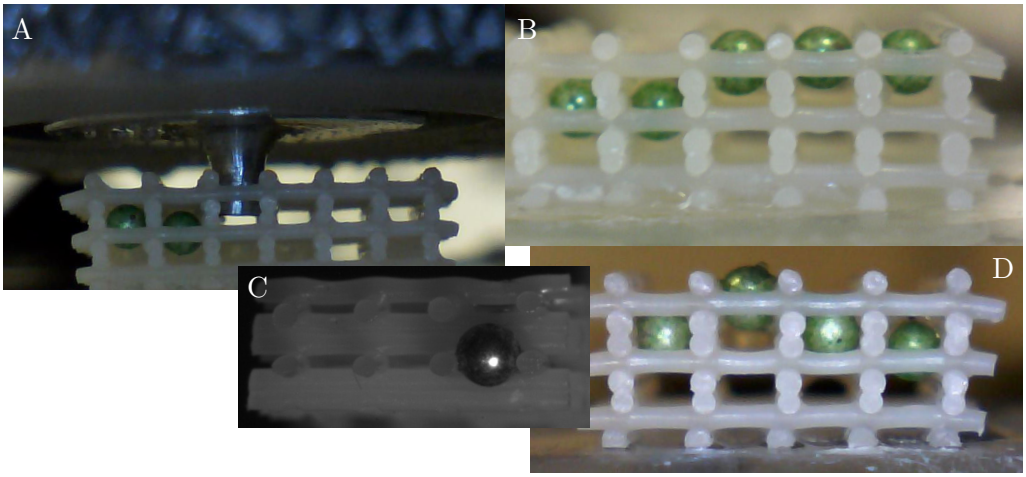

Figure 8.8 – *Images of the particle position within the pore after sheath withdrawal and particle transport. (A) Position of the sheath relative to pore before withdrawal process. (B) Sample of transported particles after slow withdrawal speeds. (D) Sample of transported particles after fast withdrawal speeds. (C) Cross section of the scaffold showing the large fiber spacing relative to the particle diameter.*

Particle Positioning The variations in particle position after delivery can be seen in Fig. 8.8(b,d). The particles were found to be generally located in the top, middle and bottom positions. It was found that there was a higher probability of the particle being located at the top position with slow withdrawal speeds. While at high withdrawal speeds there was a higher probability of the particles being located at the bottom of the pore. The probability of particle location within the pore is summarised in Table 8.5 for the two withdrawal speeds. In both cases the particle was constrained within the pore. The issue with the particle being located near the top position with slow withdrawal speeds may be minor as the high withdrawal speeds gave a better representation of the actual operating conditions.

The variations in the positioning of the particle was also illustrative of the level of influence the scaffold architecture had on the placement of the beads. In

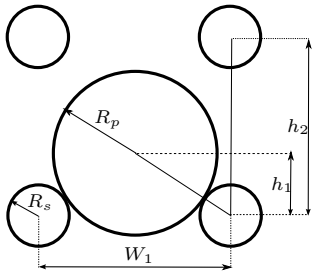

Figure 8.9 – *Particle position model.*

all cases the particle was constrained within the top and bottom layers, and in the majority of cases it was located either in the top position or the bottom. The dimensional difference causing the particle to come to rest at the bottom of the pore can be seen in Fig. 8.8c. Here the particle can be seen resting on top of the fibres and is positioned at the bottom of the pore. The same principle of confinement occurs for particle located at the top of the pore.

The particle position relative to the pore can be determined by pore geometry which can be characterised by the height and width. Referring to the diagram Fig. 8.9, and assuming circular cross-sections for both the particle and fibers, the following equation describes the likely resting position of the particle.

$$h_1 = \sqrt{(R_p + R_s)^2 - (\frac{W_1}{2})^2} \tag{8.2}$$

$$\text{height ratio} = \frac{h_1}{h_2} \tag{8.3}$$

$$\text{height ratio} = \frac{\sqrt{(R_p + R_s)^2 - (\frac{W_1}{2})^2}}{h2} \tag{8.4}$$

Where R_p is the radius of the particle, R_s the radius of the scaffold fiber, W_1 the width of the pore, h_2 the height of the pore, and $h1$ the height of the particle relative to the bottom of the pore. When the height ratio is equal to 0.5 the particle is positioned in the middle of the pore,

$$\frac{\sqrt{(R_p + R_s)^2 - (\frac{W_1}{2})^2}}{h2} = 0.5 \tag{8.5}$$

It can be seen that there are an infinite number of solutions which satisfy this equation. The best combination will be one where W_1 is large, as this will enable lower pore expansion and therefore minimise damage to the scaffold. The value of h_2 was also restricted to multiples of the fiber diameter. The large values of W_1 may result in the particle protruding from the pore, in which case, modifications to the scaffold architecture will need to take place to account for this, namely an additional spacing layer. Applying Eq. 8.4 to the previously characterised scaffold and particles, a position ratio of 0.28 is given. This indicated that the center of the particle should rest at a position slightly above or below a quarter of the pore height, which verifies the positional limits observed in the results. The ratio shows that the particle was not fully constrained and defines the upper and lower bounds to the particle position distribution within the pore.

Particle holding force After the particle was delivered into the pore a series of simple qualitative tests were carried out to determine the level of the holding force. A series of forceful taps and flushing of compressed air to the back of the lattice did not yield noticeable movement of the particle within the pore. This indicated the high retention forces against the particle was present, which is desirable if the construct is to be implanted shortly after assembly. However, the high retention force may not be such an issue during culture and incubation as drag forces generated from fluid flow are typically low. The flexibility of the entire process also enables the architecture to be easily adjusted to provide the desired level of holding forces, either throughout the scaffold or in specific regions.

8.5 Summary

In this chapter a unique injection device was presented after an exhaustive generation of concepts. The injection device utilised a thin cylindrical outer sheath in combination with a retractable expanding rod to solve the problem of expanding the lattice fibres, while enabling the delivery of a particle through the device. The characterisation of the scaffold has shown that variability existed

in the pore spacing and to achieve a high probability of particle retention the diameter distribution of the particle must lie below the spacing distribution of the pore.

Particle transport through the device alone was investigated and tests have shown that blockages do not occur, with the particles being able to exit the device in all trials. The particle delivery time from the singularisation device was found to vary considerably relative to the other process times. The likely cause was due to the particles random contact time with the tube walls during its long travel time. This variability will be negligible once the singularisation device is located next to the injection device in the actual application. The transport time or system pressure may also need to be increased when transporting the particle into the scaffold. This is due to the increased fluid resistance which may be encountered as the fluid exits through the scaffold pore network, compared with the test conditions.

The entry of the injection device into the scaffold did not result in significant damage to the overall scaffold structure, however, minor damage to the fibres were observed. This was due to the high clearances between the expanding rod and outer sheath, resulting in large exposed edges.

During insertion, deformation of the scaffold in the z axis was observed, resulting in variability in the positioning of the sheath relative to the scaffold fibres. A possible solution would be to advance further than the desired depth, then move back to the desired position. This may result in more accurate positioning as the fibres experience lower forces during retraction than insertion. The issue may not be as significant once a high precision, low clearance fit is formed between the sheath and rod, yielding a smooth outer profile.

The probability of successfully delivering a particle into the pore was found to be unaffected by the withdrawal speed, however, it did affect the particle's position within the pore. With slow withdrawal speeds the particle was found to have a higher probability of being located at the top of the pore, while fast withdrawal speeds at the bottom of the pore. Variability of the particle position can be attributed to the lack of tight confinement exhibited on the particle by

the scaffold architecture. The confinement of the particle position within the pore was also investigated using a simple geometric model. The model has shown many solutions existing for full confinement of the particle and locating it in the middle of the pore. The most practical solution is one where the pores are wide, minimising the neccessary expansion, thus reducing the risk of damage to the scaffold.

The chapter has presented a concept and prototype for the expansion and delivery device and has brought together all the systems previously described in the thesis to achieve successful delivery of a single particle into a pore. The next chapter will provide conclusions to the work presented in this thesis and make recommendations for directions of future work based on the results.

Chapter 9

Conclusions and Future Work

9.1 Conclusion

The work described in this thesis has contributed towards the fully integrated automation of a novel 3D tissue assembly technique for tissue engineering application or high-throughput screening of cell or tissue function in 3D and addressed a number of limitations with the current state of the art construct technologies.

A framework and systems architecture for the automation of the tissue assembly process was developed, and five main subsystems were conceptualised: the singulation device and injection device subsystems forming the spheroid delivery system, the scaffold deposition system, 3D positioning system and the control systems. The modular architecture of the system, enabled independent development, verification; and minimised coupling.

The control system developed, was a decentralised scheme, where specific tasks were delegated to the specific control board, with the main controller implemented on a PC. Each control board had the capability to sense and control the process, with algorithms implemented in software, providing high flexibility. A simple communications protocol was implemented around the Modbus standards and enabled intercommunication of the individual distributed control modules. The modular architecture of the control systems enabled independent testing, while the decentralised control approach eased integration.

The development of the singulation devices provided many challenges, as a device with 100% singulation accuracy, and gentle handling methods was required. Three prototypes were developed ranging from mechanical to fluidic manipulation methods.

The first prototype utilised a mechanical mechanism and was found to operate correctly, when the operator controlled and actuated the loading of test particles into the singulation chamber. However when automated methods were employed, failure occurred. This was due to the inability of the system to accurately control the position of the alginate test particle within the chamber, where the extension of the separation rod would severe the particle against the juncture of the loading and singulation chamber. In the actual application, cartilage or micro-tissue spheroids would be utilised which would be more robust than the test alginate beads, and may be more resilient to tearing. However since the potential for damage existed, other more gentle methods of handling were sought, which would enable the handling of more delicate tissues in the future.

In the fluidic prototypes, a method utilising more gentle hydrodynamic forces for separation was conceptualised, developed and verified. It was found that careful sequential timing of valves in all sub-processes were required to manipulate the flows to minimise or eliminate the establishment of undesirable fluid flow paths. Failure at any of the key stages of the sub-processes would result in the failure for the entire singulation cycle.

The capture of the second particle proved to be the most challenging, and trials found the capture of the second particle was not guaranteed, and instead a variety of factors influenced it. The cause for the release was found to be due to the forces exerted by the lagging particles as they were obstructed by the trapped particle, both in collisions and in the constant drag forces being exerted. This was discovered to be due to the substantial leakage flows, relative to flow into the second trapping chamber, or the fluid flow flux ratio.

It was found that a large flow flux ratio, at the moment the second particle was captured, greatly increased the probability of successfully retaining the second particle. The profile of the flow ratio was not a constant value and was dynamic

as the flow developed, thus time considerations were required. By decreasing the leakage flow into the first chamber and enabling longer flow development times, a capture probability of 88% was reached. Further decreases in the fluid flow ratio resulted in failure, with the early release of the leading particle.

A second prototype was later conceptualised and developed utilising the knowledge gained from the first prototype. The issues with fluid fluxes affecting the capture of the second particle were eliminated altogether, through the capture and use of a single particle. This greatly improved the throughput, and the capture and singularisation accuracy. Characterisation of the process, identified all sub-processes responsible for improving the throughput of the device, while retaining 100% singulation efficiency. The device was able to achieve a throughput of 1Hz, however this was not a limit of the device and higher throughput is still possible.

The injection device was required for the delivery of the spheroid into the scaffold lattice pore. A prototype was developed for the concept, and verified. The concept was able to successfully expand the pore and enable an unobstructed path for the delivery of the particle, while minimising damage to the scaffold. Within the pore geometries investigated, 100% delivery success was achieved. The concept proved to be a simple and effective mechanism.

All key electro-mechanical subsystems required for the automation of the tissue assembly process have been conceptualised, developed and verified to perform their required functions, providing proof of concept and great insight into the devices operational mechanisms. The development of the novel singulation devices, and injection device to solve the unique problem associated with automating the tissue construct process, will now enable the further integration of the subsystems with more conventional and mature positioning systems.

9.2 Future Work

9.2.1 Singularisation Device

The process to capture and release the particle in a high throughput manner was not as simple as it first seemed and would have benefited from fluid flow visualisation techniques such as particle image velocimetry (PIV), now that important aspects have been identified, along with thorough instrumentation of the fluid pressures within the device. Furthermore an up-scaled model with similitude analysis technique will be beneficial.

9.2.2 Injection Device

The injection device has been validated to perform well. However, more accurate fabrication processes and the utilisation of higher strength materials will enable reductions in the sheath thickness and smaller clearance fits, further enhancing performance.

9.2.3 Full Systems Integration

An issue limiting the complete integration of the setup was the inability to establish two way communications with the printer. Thus timely coordination of the positioning devices and delivery devices was difficult. The purchase of a motion control board supporting the control of external devices through G-code, or the development of a custom motion control board will enable full integration.

9.2.4 Device testing with actual micro-tissue

The tests have provided proof of concept and verification for the glass beads used in the fluidics based singulation device and injection system. However, further verification will be required for the device performances with actual desired target micro-tissue to be assembled.

9.2.5 Sterile Operating Conditions

Ultimately if verification of the system processes on the viability of spheroids and cells is to be performed, sterile operating conditions will be required. The simplest solution would be to place the functional systems within a conventional laminar flow hood. However the current size and weight of the positioning system may not be easily accommodated, and a smaller replacement may be required. Alternatively an enclosure could be constructed, with high-efficiency particulate arresting (HEPA) filtered air maintaining a constant positive pressure within the enclosure.

9.2.6 Construct Technologies

With the elimination of the manual assembly process much higher resolutions can be explored if smaller spheroids are utilised. Due to the inherent simplicity of the developed devices they are amendable for downscaling. This may allow for even more complex 3D constructs to be achieved, such as the formation of multiple cell type channels, not limited by diffusional limits.

9.3 Final Comments

Tissue engineering holds great promise in providing a solution to the current shortage of replacement tissue and organs. The automation of the novel construct technique which addresses a number of limitations currently present in the state of art construct technologies, will enable the realisation and investigation of more complex constructs, unachievable with current manual processes. The realisation of such constructs will enable features more closely mimicking those of tissue within the body, and may provide the necessary signals and micro-environment to enable the correct regulation in the remodelling and formation of complex functional tissue. This may one day lead to 3D printing or assembly of viable replacement tissue and whole organs, or accurate in vitro model systems for laboratory testing.

Bibliography

[1] B. Lalan, M. Pomerantseva, and M. Vacanti, "Tissue engineering and its potential impact on surgery," *World Journal of Surgery*, vol. 25, no. 11, pp. 1458–66, Nov. 2001.

[2] R. Skalak and C. Fox, *Tissue engineering: proceedings of a workshop, held at Granlibakken, Lake Tahoe, California, February 26-29, 1988.* Alan R. Liss, 1988, vol. 107.

[3] T. B. F. Woodfield, J. M. Bezemer, J. S. Pieper, C. A. van Blitterswijk, and J. Riesle, "Scaffolds for tissue engineering of cartilage," *Critical Reviews in Eukaryotic Gene Expression*, vol. 12, no. 3, pp. 209–236, 2002.

[4] L. G. Griffith and G. Naughton, "Tissue Engineering–Current challenges and expanding opportunities," *Science*, vol. 295, no. 5557, pp. 1009 –1014, Feb. 2002.

[5] F. Pampaloni, E. G. Reynaud, and E. H. K. Stelzer, "The third dimension bridges the gap between cell culture and live tissue," *Nature Reviews Molecular Cell Biology*, vol. 8, no. 10, pp. 839–845, Oct. 2007.

[6] R. Lanza, R. Langer, and J. Vacanti, *Principles of Tissue Engineering, 3rd Edition*, 3rd ed. Academic Press, Aug. 2007.

[7] R. Langer and J. Vacanti, "Tissue engineering," *Science*, vol. 260, no. 5110, pp. 920 –926, May 1993.

[8] B. Guillotin and F. Guillemot, "Cell patterning technologies for organotypic tissue fabrication," *Trends in Biotechnology*, vol. 29, no. 4, pp. 183–190, Apr. 2011.

[9] C. Hagios, A. Lochter, and M. J. Bissell, "Tissue architecture: the ultimate regulator of epithelial function?" *Philosophical Transactions of the Royal Society of London. Series B: Biological Sciences*, vol. 353, no. 1370, pp. 857–870, Jun. 1998.

[10] M. P. Lutolf and J. A. Hubbell, "Synthetic biomaterials as instructive extracellular microenvironments for morphogenesis in tissue engineering," *Nat Biotech*, vol. 23, no. 1, pp. 47–55, Jan. 2005.

[11] C. M. Nelson and M. J. Bissell, "Of extracellular matrix, scaffolds, and signaling: Tissue architecture regulates development, homeostasis, and cancer," *Annual review of cell and developmental biology*, vol. 22, pp. 287–309, 2006, PMID: 16824016 PMCID: 2933192.

[12] E. A. Phelps and A. J. García, "Engineering more than a cell: vascularization strategies in tissue engineering," *Current Opinion in Biotechnology*, vol. 21, no. 5, pp. 704–709, Oct. 2010.

[13] M. Lovett, K. Lee, A. Edwards, and D. L. Kaplan, "Vascularization strategies for tissue engineering," *Tissue Engineering Part B: Reviews*, vol. 15, no. 3, pp. 353–370, Sep. 2009.

[14] T. Kaully, K. Kaufman-Francis, A. Lesman, and S. Levenberg, "Vascularization–the conduit to viable engineered tissues," *Tissue Engineering. Part B, Reviews*, vol. 15, no. 2, pp. 159–169, Jun. 2009, PMID: 19309238.

[15] B. R. Ringeisen, B. J. Spargo, and P. K. Wu, Eds., *Cell and Organ Printing*, 1st ed. Springer, Sep. 2010.

[16] G. Chen, T. Ushida, and T. Tateishi, "Scaffold design for tissue engineering," *Macromolecular Bioscience*, vol. 2, no. 2, pp. 67–77, Feb. 2002.

[17] T. Woodfield, J. Malda, J. de Wijn, F. Péters, J. Riesle, and C. van Blitterswijk, "Design of porous scaffolds for cartilage tissue engineering using a three-dimensional fiber-deposition technique," *Biomaterials*, vol. 25, no. 18, pp. 4149–4161, Aug. 2004.

[18] S. Lee, H. Kang, J. K. Park, J. Rhie, S. K. Hahn, and D. Cho, "Application of microstereolithography in the development of three-dimensional cartilage regeneration scaffolds," *Biomedical Microdevices*, vol. 10, no. 2, pp. 233–241, Apr. 2008, PMID: 17885804.

[19] A. Mata, E. J. Kim, C. A. Boehm, A. J. Fleischman, G. F. Muschler, and S. Roy, "A three-dimensional scaffold with precise micro-architecture and surface micro-textures," *Biomaterials*, vol. 30, no. 27, pp. 4610–4617, Sep. 2009.

[20] H. Zhang, E. Burdet, A. N. Poo, and D. W. Hutmacher, "Microassembly fabrication of tissue engineering scaffolds with customized design," *IEEE Transactions on Automation Science and Engineering*, vol. 5, no. 3, pp. 446–456, Jul. 2008.

[21] B. S. Schon, K. Schrobback, M. Ven, S. Stroebel, G. J. Hooper, and T. B. F. Woodfield, "Validation of a high-throughput microtissue fabrication process for 3D assembly of tissue engineered cartilage constructs," *Cell and Tissue Research*, Feb. 2012.

[22] F. P. Melchels, J. Feijen, and D. W. Grijpma, "A review on stereolithography and its applications in biomedical engineering," *Biomaterials*, vol. 31, no. 24, pp. 6121–6130, Aug. 2010.

[23] D. W. Hutmacher, M. Sittinger, and M. V. Risbud, "Scaffold-based tissue engineering: rationale for computer-aided design and solid free-form fabrication systems," *Trends in Biotechnology*, vol. 22, no. 7, pp. 354–362, Jul. 2004.

[24] C. Liu, Z. Xia, and J. Czernuszka, "Design and development of Three-Dimensional scaffolds for tissue engineering," *Chemical Engineering Research and Design*, vol. 85, no. 7, pp. 1051–1064, 2007.

[25] I. Martin, D. Wendt, and M. Heberer, "The role of bioreactors in tissue engineering," *Trends in Biotechnology*, vol. 22, no. 2, pp. 80–86, Feb. 2004, PMID: 14757042.

[26] H. Dietmar W., "Scaffolds in tissue engineering bone and cartilage," *Biomaterials*, vol. 21, no. 24, pp. 2529–2543, Dec. 2000.

[27] J. Rouwkema, N. C. Rivron, and C. A. van Blitterswijk, "Vascularization in tissue engineering," *Trends in Biotechnology*, vol. 26, no. 8, pp. 434–441, Aug. 2008.

[28] T. P. Richardson, M. C. Peters, A. B. Ennett, and D. J. Mooney, "Polymeric system for dual growth factor delivery," *Nature Biotechnology*, vol. 19, no. 11, pp. 1029–34, Nov. 2001.

[29] M. W. Laschke, Y. Harder, M. Amon, I. Martin, J. Farhadi, A. Ring, N. Torio-Padron, D. Junker, C. Carvalho, M. Heberer, and B. Vollmar, "Angiogenesis in tissue engineering: Breathing life into constructed tissue substitutes," *Tissue Engineering*, vol. 12, no. 8, pp. 2093–104, Aug. 2006.

[30] A. H. Zisch, M. P. Lutolf, and J. A. Hubbell, "Biopolymeric delivery matrices for angiogenic growth factors," *Cardiovascular Pathology: The Official Journal of the Society for Cardiovascular Pathology*, vol. 12, no. 6, pp. 295–310, Dec. 2003, PMID: 14630296.

[31] R. R. Chen, E. A. Silva, W. W. Yuen, and D. J. Mooney, "Spatio-temporal VEGF and PDGF delivery patterns blood vessel formation and maturation," *Pharmaceutical Research*, vol. 24, no. 2, pp. 258–264, Feb. 2007, PMID: 17191092.

[32] R. K. Jain, P. Au, J. Tam, D. G. Duda, and D. Fukumura, "Engineering vascularized tissue," *Nature Biotechnology*, vol. 23, no. 7, pp. 821–823, Jul. 2005.

[33] J. Rouwkema, J. D. Boer, and C. A. V. Blitterswijk, "Endothelial cells assemble into a 3-Dimensional prevascular network in a bone tissue engineering construct," *Tissue Engineering*, vol. 12, no. 9, pp. 2685–2693, Sep. 2006.

[34] R. E. Unger, A. Sartoris, K. Peters, A. Motta, C. Migliaresi, M. Kunkel, U. Bulnheim, J. Rychly, and C. James Kirkpatrick, "Tissue-like self-assembly in cocultures of endothelial cells and osteoblasts and the formation of microcapillary-like structures on three-dimensional porous biomaterials," *Biomaterials*, vol. 28, no. 27, pp. 3965–3976, Sep. 2007.

[35] J. M. Kelm, V. Djonov, S. P. Hoerstrup, C. I. Guenter, L. M. Ittner, F. Greve, A. Hierlemann, C. D. Sanchez-Bustamante, J. Perriard, E. Ehler, and M. Fussenegger, "Tissue-transplant fusion and vascularization of myocardial microtissues and macrotissues implanted into chicken embryos and rats," *Tissue Engineering*, vol. 12, no. 9, pp. 2541–2553, Sep. 2006, PMID: 16995787.

[36] J. T. Borenstein, M. M. Tupper, P. J. Mack, E. J. Weinberg, A. S. Khalil, J. Hsiao, and G. García-Cardeña, "Functional endothelialized microvascular networks with circular cross-sections in a tissue culture substrate," *Biomedical Microdevices*, vol. 12, no. 1, pp. 71–79, Sep. 2009.

[37] T. P. Kraehenbuehl, L. S. Ferreira, P. Zammaretti, J. A. Hubbell, and R. Langer, "Cell-responsive hydrogel for encapsulation of vascular cells," *Biomaterials*, vol. 30, no. 26, pp. 4318–4324, Sep. 2009, PMID: 19500842.

[38] G. Y. Huang, L. H. Zhou, Q. C. Zhang, Y. M. Chen, W. Sun, F. Xu, and T. J. Lu, "Microfluidic hydrogels for tissue engineering," *Biofabrication*, vol. 3, no. 1, p. 012001, Mar. 2011.

[39] A. Khademhosseini, R. Langer, J. Borenstein, and J. P. Vacanti, "Microscale technologies for tissue engineering and biology," *Proceedings of the National Academy of Sciences of the United States of America*, vol. 103, no. 8, pp. 2480 –2487, Feb. 2006.

[40] M. P. Cuchiara, A. C. Allen, T. M. Chen, J. S. Miller, and J. L. West, "Multilayer microfluidic PEGDA hydrogels," *Biomaterials*, vol. 31, no. 21, pp. 5491–5497, Jul. 2010.

[41] A. P. Golden and J. Tien, "Fabrication of microfluidic hydrogels using molded gelatin as a sacrificial element," *Lab Chip*, vol. 7, no. 6, pp. 720–725, Mar. 2007.

[42] C. Fidkowski, M. R. Kaazempur-Mofrad, J. Borenstein, J. P. Vacanti, R. Langer, and Y. Wang, "Endothelialized microvasculature based on a biodegradable elastomer," *Tissue Engineering*, vol. 11, no. 1-2, pp. 302–309, Jan. 2005.

[43] Y. Ling, J. Rubin, Y. Deng, C. Huang, U. Demirci, J. M. Karp, and A. Khademhosseini, "A cell-laden microfluidic hydrogel," *Lab Chip*, vol. 7, no. 6, pp. 756–762, May 2007.

[44] J. H. Park, B. G. Chung, W. G. Lee, J. Kim, M. D. Brigham, J. Shim, S. Lee, C. M. Hwang, N. G. Durmus, U. Demirci, and A. Khademhosseini, "Microporous cell-laden hydrogels for engineered tissue constructs," *Biotechnology and Bioengineering*, vol. 106, no. 1, pp. 138–148, May 2010.

[45] K. M. Chrobak, D. R. Potter, and J. Tien, "Formation of perfused, functional microvascular tubes in vitro," *Microvascular Research*, vol. 71, no. 3, pp. 185–196, May 2006.

[46] K. Y. Lee and D. J. Mooney, "Hydrogels for tissue engineering," *Chem. Rev.*, vol. 101, no. 7, pp. 1869–1880, 2001.

[47] J. L. Drury and D. J. Mooney, "Hydrogels for tissue engineering: scaffold design variables and applications," *Biomaterials*, vol. 24, no. 24, pp. 4337–4351, Nov. 2003.

[48] K. T. Nguyen and J. L. West, "Photopolymerizable hydrogels for tissue engineering applications," *Biomaterials*, vol. 23, no. 22, pp. 4307–4314, Nov. 2002.

[49] E. Donald L, "Bottom-up tissue engineering," *Current Opinion in Biotechnology*, vol. 22, no. 5, pp. 674–680, Oct. 2011.

[50] K. Jakab, C. Norotte, F. Marga, K. Murphy, G. Vunjak-Novakovic, and G. Forgacs, "Tissue engineering by self-assembly and bio-printing of living cells," *Biofabrication*, vol. 2, p. 022001, Jun. 2010.

[51] A. Khademhosseini and R. Langer, "Microengineered hydrogels for tissue engineering," *Biomaterials*, vol. 28, no. 34, pp. 5087–5092, Dec. 2007.

[52] R. Gauvin and A. Khademhosseini, "Microscale technologies and modular approaches for tissue engineering: Moving toward the fabrication of complex functional structures," *ACS Nano*, vol. 5, no. 6, pp. 4258–4264, 2011.

[53] J. G. Fernandez and A. Khademhosseini, "Micro-Masonry: construction of 3D structures by microscale Self-Assembly," *Advanced Materials*, vol. 22, no. 23, pp. 2538–2541, Jun. 2010.

[54] F. Yanagawa, H. Kaji, Y. Jang, H. Bae, D. Yanan, J. Fukuda, H. Qi, and A. Khademhosseini, "Directed assembly of cell-laden microgels for building porous three-dimensional tissue constructs," *Journal of Biomedical Materials Research Part A*, vol. 97A, no. 1, pp. 93–102, Apr. 2011.

[55] A. P. McGuigan and M. V. Sefton, "Vascularized organoid engineered by modular assembly enables blood perfusion," *Proceedings of the National Academy of Sciences of the United States of America*, vol. 103, no. 31, pp. 11 461–11 466, Aug. 2006, PMID: 16864785.

[56] Y. Du, E. Lo, S. Ali, and A. Khademhosseini, "Directed assembly of cell-laden microgels for fabrication of 3D tissue constructs," *Proceedings of the National Academy of Sciences*, vol. 105, no. 28, pp. 9522 –9527, Jul. 2008.

[57] N. N. Kachouie, Y. Du, H. Bae, M. Khabiry, A. F. Ahari, B. Zamanian, J. Fukuda, and A. Khademhosseini, "Directed assembly of cell-laden hydrogels for engineering functional tissues," *Organogenesis*, vol. 6, no. 4, pp. 234–244, Oct. 2010.

[58] B. Liu, Y. Liu, A. K. Lewis, and W. Shen, "Modularly assembled porous cell-laden hydrogels," *Biomaterials*, vol. 31, no. 18, pp. 4918–4925, Jun. 2010.

[59] Y. Du, M. Ghodousi, H. Qi, N. Haas, W. Xiao, and A. Khademhosseini, "Sequential assembly of cell-laden hydrogel constructs to engineer vascular-like microchannels," *Biotechnology and Bioengineering*, vol. 108, no. 7, pp. 1693–1703, Jul. 2011, PMID: 21337336.

[60] F. Guillemot, V. Mironov, and M. Nakamura, "Bioprinting is coming of age: report from the international conference on bioprinting and biofabrication in bordeaux (3B'09)," *Biofabrication*, vol. 2, p. 010201, Mar. 2010.

[61] B. Guillotin, A. Souquet, S. Catros, M. Duocastella, B. Pippenger, S. Bellance, R. Bareille, M. Rémy, L. Bordenave, J. Amédée, and F. Guillemot, "Laser assisted bioprinting of engineered tissue with high cell density and microscale organization," *Biomaterials*, vol. 31, no. 28, pp. 7250–7256, Oct. 2010.

[62] T. Boland, T. Xu, B. Damon, and X. Cui, "Application of inkjet printing to tissue engineering," *Biotechnology Journal*, vol. 1, no. 9, pp. 910–917, Sep. 2006.

[63] C. C. Chang, E. D. Boland, S. K. Williams, and J. B. Hoying, "Direct-write bioprinting three-dimensional biohybrid systems for future regenerative

therapies," *Journal of Biomedical Materials Research Part B: Applied Biomaterials*, vol. 98B, no. 1, pp. 160–170, Jul. 2011.

[64] X. Cui and T. Boland, "Human microvasculature fabrication using thermal inkjet printing technology," *Biomaterials*, vol. 30, no. 31, pp. 6221–6227, Oct. 2009, PMID: 19695697.

[65] Y. Nishiyama, M. Nakamura, C. Henmi, K. Yamaguchi, S. Mochizuki, H. Nakagawa, and K. Takiura, "Development of a Three-Dimensional bioprinter: Construction of cell supporting structures using hydrogel and State-Of-The-Art inkjet technology," *Journal of Biomechanical Engineering*, vol. 131, no. 3, pp. 035 001–6, Mar. 2009.

[66] W. C. Wilson Jr. and T. Boland, "Cell and organ printing 1: Protein and cell printers," *The Anatomical Record Part A: Discoveries in Molecular, Cellular, and Evolutionary Biology*, vol. 272A, no. 2, pp. 491–496, Jun. 2003.

[67] M. Nakamura, Y. Nishiyama, C. Henmi, S. Iwanaga, H. Nakagawa, K. Yamaguchi, K. Akita, S. Mochizuki, and K. Takiura, "Ink jet Three-Dimensional digital fabrication for biological tissue manufacturing: Analysis of alginate microgel beads produced by ink jet droplets for three dimensional tissue fabrication," *Journal of Imaging Science and Technology*, vol. 52, no. 6, p. 060201, 2008.

[68] B. R. Ringeisen, C. M. Othon, J. A. Barron, D. Young, and B. J. Spargo, "Jet-based methods to print living cells," *Biotechnology Journal*, vol. 1, no. 9, pp. 930–948, Sep. 2006, PMID: 16895314.

[69] F. Guillemot, A. Souquet, S. Catros, and B. Guillotin, "Laser-assisted cell printing: principle, physical parameters versus cell fate and perspectives in tissue engineering," *Nanomedicine*, vol. 5, no. 3, pp. 507–515, Apr. 2010.

[70] N. R. Schiele, D. T. Corr, Y. Huang, N. A. Raof, Y. Xie, and D. B. Chrisey, "Laser-based direct-write techniques for cell printing," *Biofabrication*, vol. 2, p. 032001, Sep. 2010.

[71] D. J. Odde and M. J. Renn, "Laser-guided direct writing for applications in biotechnology," *Trends in Biotechnology*, vol. 17, no. 10, pp. 385–389, Oct. 1999, PMID: 10481169.

[72] T. Boland, V. Mironov, A. Gutowska, E. A. Roth, and R. R. Markwald, "Cell and organ printing 2: Fusion of cell aggregates in three-dimensional gels," *The Anatomical Record Part A: Discoveries in Molecular, Cellular, and Evolutionary Biology*, vol. 272A, no. 2, pp. 497–502, Jun. 2003.

[73] W. Lee, V. Lee, S. Polio, P. Keegan, J. Lee, K. Fischer, J. Park, and S. Yoo, "On-demand three-dimensional freeform fabrication of multi-layered hydrogel scaffold with fluidic channels," *Biotechnology and Bioengineering*, vol. 105, no. 6, pp. 1178–1186, Apr. 2010.

[74] P. J. Schaner, N. D. Martin, T. N. Tulenko, I. M. Shapiro, N. A. Tarola, R. F. Leichter, R. Carabasi, and P. J. DiMuzio, "Decellularized vein as a potential scaffold for vascular tissue engineering," *Journal of Vascular Surgery*, vol. 40, no. 1, pp. 146–153, Jul. 2004.

[75] D. Pham and R. Gault, "A comparison of rapid prototyping technologies," *International Journal of Machine Tools and Manufacture*, vol. 38, no. 10-11, pp. 1257–1287, Oct. 1998.

[76] C. M. Smith, A. L. Stone, R. L. Parkhill, R. L. Stewart, M. W. Simpkins, A. M. Kachurin, W. L. Warren, and S. K. Williams, "Three-Dimensional BioAssembly tool for generating viable Tissue-Engineered constructs," *Tissue Engineering*, vol. 10, no. 9-10, pp. 1566–76, Sep. 2004.

[77] N. E. Fedorovich, I. Swennen, J. Girones, L. Moroni, C. A. van Blitterswijk, E. Schacht, J. Alblas, and W. J. A. Dhert, "Evaluation of photocrosslinked

lutrol hydrogel for tissue printing applications," *Biomacromolecules*, vol. 10, no. 7, pp. 1689–1696, 2009.

[78] J. Shim, J. Y. Kim, M. Park, J. Park, and D. Cho, "Development of a hybrid scaffold with synthetic biomaterials and hydrogel using solid freeform fabrication technology," *Biofabrication*, vol. 3, p. 034102, Sep. 2011.

[79] W. Wu, A. DeConinck, and J. A. Lewis, "Omnidirectional printing of 3D microvascular networks," *Advanced Materials*, vol. 23, no. 24, pp. H178–H183, Jun. 2011.

[80] V. Mironov, R. P. Visconti, V. Kasyanov, G. Forgacs, C. J. Drake, and R. R. Markwald, "Organ printing: tissue spheroids as building blocks," *Biomaterials*, vol. 30, no. 12, pp. 2164–2174, Apr. 2009, PMID: 19176247.

[81] K. Jakab, C. Norotte, B. Damon, F. Marga, A. Neagu, C. L. Besch-Williford, A. Kachurin, K. H. Church, H. Park, V. Mironov, R. Markwald, G. Vunjak-Novakovic, and G. Forgacs, "Tissue engineering by Self-Assembly of cells printed into topologically defined structures," *Tissue Engineering Part A*, vol. 14, no. 3, pp. 413–421, Mar. 2008.

[82] C. Norotte, F. S. Marga, L. E. Niklason, and G. Forgacs, "Scaffold-free vascular tissue engineering using bioprinting," *Biomaterials*, vol. 30, no. 30, pp. 5910–5917, Oct. 2009.

[83] W. Lee, J. C. Debasitis, V. K. Lee, J. Lee, K. Fischer, K. Edminster, J. Park, and S. Yoo, "Multi-layered culture of human skin fibroblasts and keratinocytes through three-dimensional freeform fabrication," *Biomaterials*, vol. 30, no. 8, pp. 1587–1595, Mar. 2009.

[84] M. Radisic, H. Park, F. Chen, J. E. Salazar-Lazzaro, Y. Wang, R. Dennis, R. Langer, L. E. Freed, and G. Vunjak-Novakovic, "Biomimetic approach to cardiac tissue engineering: oxygen carriers and channeled scaffolds," *Tissue Engineering*, vol. 12, no. 8, pp. 2077–2091, Aug. 2006, PMID: 16968150.

[85] T. B. F. Woodfield, M. Guggenheim, B. von Rechenberg, J. Riesle, C. A. van Blitterswijk, and V. Wedler, "Rapid prototyping of anatomically shaped, tissue-engineered implants for restoring congruent articulating surfaces in small joints," *Cell Proliferation*, vol. 42, no. 4, pp. 485–497, Aug. 2009, PMID: 19486014.

[86] A. Kossiakoff and W. N. Sweet, *Systems Engineering Principles and Practice*, 1st ed. Wiley-Interscience, Dec. 2002.

[87] D. M. Buede, *The Engineering Design of Systems: Models and Methods*. Wiley-Interscience, Dec. 1999.

[88] M. W. Maier, *The Art of Systems Architecting, Third Edition*, 3rd ed. CRC Press, Jan. 2009.

[89] R. W. Johnson, *The handbook of fluid dynamics*. Springer, 1998.

[90] R. Weinreich and G. Buchgeher, "Paving the road for formally defined architecture description in software development," in *Proceedings of the 2010 ACM Symposium on Applied Computing*, ser. SAC '10. New York, NY, USA: ACM, 2010, p. 2337–2343.

[91] N. S. Nise, *Control Systems Engineering*, 6th ed. Wiley, Dec. 2010.

[92] F. Lian, J. R. Moyne, and D. M. Tilbury, "Performance evaluation of control networks: Ethernet, ControlNet, and DeviceNet," *IEEE Control Systems*, vol. 21, no. 1, pp. 66–83, Feb. 2001.

[93] S. MacKay, E. Wright, and D. Reynders, *Practical Industrial Data Networks: Design, Installation and Troubleshooting*. Newnes, Apr. 2004.

[94] J. D. Decotignie, "Ethernet-Based Real-Time and industrial communications," *Proceedings of the IEEE*, vol. 93, no. 6, pp. 1102–1117, Jun. 2005.

[95] L. L. Peterson and B. S. Davie, *Computer Networks: A Systems Approach, Fourth Edition*, 4th ed. Morgan Kaufmann, Mar. 2007.

[96] M. P. Clark, *Data Networks, IP and the Internet: Protocols, Design and Operation*, 1st ed. Wiley, Mar. 2003.

[97] MODBUS.org, "Modbus serial line protocol and implementation guide v1.02," Dec. 2006. [Online]. Available: http://www.modbus.org/docs/Modbus_over_serial_line_V1_02.pdf

[98] P. Koopman and T. Chakravarty, "Cyclic redundancy code (CRC) polynomial selection for embedded networks," in *2004 International Conference on Dependable Systems and Networks*. IEEE, Jul. 2004, pp. 145– 154.

[99] Modbus-IDA, "MODBUS application protocol specification v1.1b," Dec. 2006. [Online]. Available: http://www.modbus.org/docs/Modbus_Application_Protocol_V1_1b.pdf

[100] R. Pallás-Areny and J. G. Webster, *Sensors and Signal Conditioning, 2nd Edition*, 2nd ed. Wiley-Interscience, Nov. 2000.

[101] A. Doboli and E. H. Currie, *Introduction to Mixed-Signal, Embedded Design*, 1st ed. Springer, Dec. 2010.

[102] S. Franco, *Design with Operational Amplifiers and Analog Integrated Circuits*, 3rd ed. McGraw-Hill Science/Engineering/Math, Aug. 2001.

[103] T. Instruments, "Low-Power, Single-Supply, CMOS instumentation amplifiers (Rev. c)," Apr. 2005. [Online]. Available: http://www.ti.com/lit/gpn/ina2331

[104] C. D. Motchenbacher and J. A. Connelly, *Low-Noise Electronic System Design*, 1st ed. Wiley-Interscience, Jun. 1993.

[105] M. E. V. Valkenburg and M. E. V. Valkenburg, *Analog Filter Design*. Oxford University Press, USA, Jun. 1995.

[106] R. Raut and M. N. S. Swamy, *Modern Analog Filter Analysis and Design: A Practical Approach*, 1st ed. Wiley-VCH, Dec. 2010.

[107] S. Winder, *Analog and Digital Filter Design, Second Edition*, 2nd ed. Newnes, Oct. 2002.

[108] R. G. Lyons, *Understanding Digital Signal Processing*, 1st ed. Pearson Education, Nov. 1996.

[109] R. Sallen and E. Key, "A practical method of designing RC active filters," *IRE Transactions on Circuit Theory*, vol. 2, no. 1, p. 74–85, 1955.

[110] A. J. Hand, T. Sun, D. C. Barber, D. R. Hose, and S. MacNeil, "Automated tracking of migrating cells in phase-contrast video microscopy sequences using image registration," *Journal of Microscopy*, vol. 234, no. 1, pp. 62–79, Apr. 2009, PMID: 19335457.

[111] K. Li, E. D. Miller, M. Chen, T. Kanade, L. E. Weiss, and P. G. Campbell, "Computer vision tracking of stemness," in *5th IEEE International Symposium on Biomedical Imaging: From Nano to Macro, 2008. ISBI 2008.* IEEE, May 2008, pp. 847–850.

[112] A. Saad, W. Chiu, and P. A. Thuman-Commike, "Multiresolution approach to automatic detection of spherical particles from electron cryomicroscopy images," in *1998 International Conference on Image Processing, 1998. ICIP 98. Proceedings.* IEEE, Oct. 1998, pp. 846–850 vol.3.

[113] O. Ronneberger, Q. Wang, and H. Burkhardt, "Fast and robust segmentation of spherical particles in volumetric data sets from brightfield microscopy," in *5th IEEE International Symposium on Biomedical Imaging: From Nano to Macro, 2008. ISBI 2008.* IEEE, May 2008, pp. 372–375.

[114] J. Schaffer, A. Saxena, J. Sanders, S. Antolovich, and S. Warner, *Science and Design of Engineering Materials*, 2nd ed. McGraw-Hill Science/Engineering/Math, Dec. 2000.

[115] C. Tsao and D. DeVoe, "Bonding of thermoplastic polymer microfluidics," *Microfluidics and Nanofluidics*, vol. 6, no. 1, pp. 1–16, Jan. 2009.

[116] M. T. Koesdjojo, C. R. Koch, and V. T. Remcho, "Technique for microfabrication of Polymeric-Based microchips from an SU-8 master with Temperature-Assisted vaporized organic solvent bonding," *Analytical Chemistry*, vol. 81, no. 4, pp. 1652–1659, Feb. 2009.

[117] D. Ogonczyk, J. Wegrzyn, P. Jankowski, B. Dabrowski, and P. Garstecki, "Bonding of microfluidic devices fabricated in polycarbonate," *Lab on a Chip*, vol. 10, no. 10, pp. 1324–1327, 2010.

[118] S. F. Ibrahim and G. Engh, "Flow cytometry and cell sorting," in *Cell Separation*, A. Kumar, I. Y. Galaev, and B. Mattiasson, Eds. Berlin, Heidelberg: Springer Berlin Heidelberg, 2008, vol. 106, pp. 19–39.

[119] J. F. Leary, "Ultra high-speed sorting," *Cytometry Part A*, vol. 67A, no. 2, pp. 76–85, Oct. 2005.

[120] A. A. S. Bhagat, H. Bow, H. W. Hou, S. J. Tan, J. Han, and C. T. Lim, "Microfluidics for cell separation," *Medical & Biological Engineering & Computing*, Apr. 2010.

[121] S. Kobel, A. Valero, J. Latt, P. Renaud, and M. Lutolf, "Optimization of microfluidic single cell trapping for long-term on-chip culture," *Lab on a Chip*, vol. 10, no. 7, p. 857, 2010.

[122] J. Nilsson, M. Evander, B. Hammarström, and T. Laurell, "Review of cell and particle trapping in microfluidic systems," *Analytica Chimica Acta*, vol. 649, no. 2, pp. 141–157, Sep. 2009, PMID: 19699390.

[123] F. Guillemot, A. Souquet, S. Catros, B. Guillotin, J. Lopez, M. Faucon, B. Pippenger, R. Bareille, M. Rémy, S. Bellance, P. Chabassier, J. Fricain, and J. Amédée, "High-throughput laser printing of cells and biomaterials for tissue engineering," *Acta Biomaterialia*, vol. 6, no. 7, pp. 2494–2500, Jul. 2010.

[124] A. Lenshof and T. Laurell, "Continuous separation of cells and particles in microfluidic systems," *Chemical Society Reviews*, vol. 39, no. 3, p. 1203, 2010.

[125] J. Malda, T. B. F. Woodfield, F. van der Vloodt, C. Wilson, D. E. Martens, J. Tramper, C. A. van Blitterswijk, and J. Riesle, "The effect of PEGT/PBT scaffold architecture on the composition of tissue engineered cartilage," *Biomaterials*, vol. 26, no. 1, pp. 63–72, Jan. 2005, PMID: 15193881.

[126] L. Moroni, J. de Wijn, and C. van Blitterswijk, "3D fiber-deposited scaffolds for tissue engineering: Influence of pores geometry and architecture on dynamic mechanical properties," *Biomaterials*, vol. 27, no. 7, pp. 974–985, Mar. 2006.

[127] F. Samperi, C. Puglisi, R. Alicata, and G. Montaudo, "Thermal degradation of poly(ethylene terephthalate) at the processing temperature," *Polymer Degradation and Stability*, vol. 83, no. 1, pp. 3–10, Jan. 2004.

[128] "Microsyringe-Based deposition of Two-Dimensional and Three-Dimensional polymer scaffolds with a Well-Defined geometry for application to tissue engineering," *Tissue Engineering*, vol. 8, no. 6, pp. 1089–98, 2002.

Appendices

Appendix A

Hardware

A.0.1 Singularisation Board

A.0.2 Communications Hub

A.0.3 Pressure Regulator

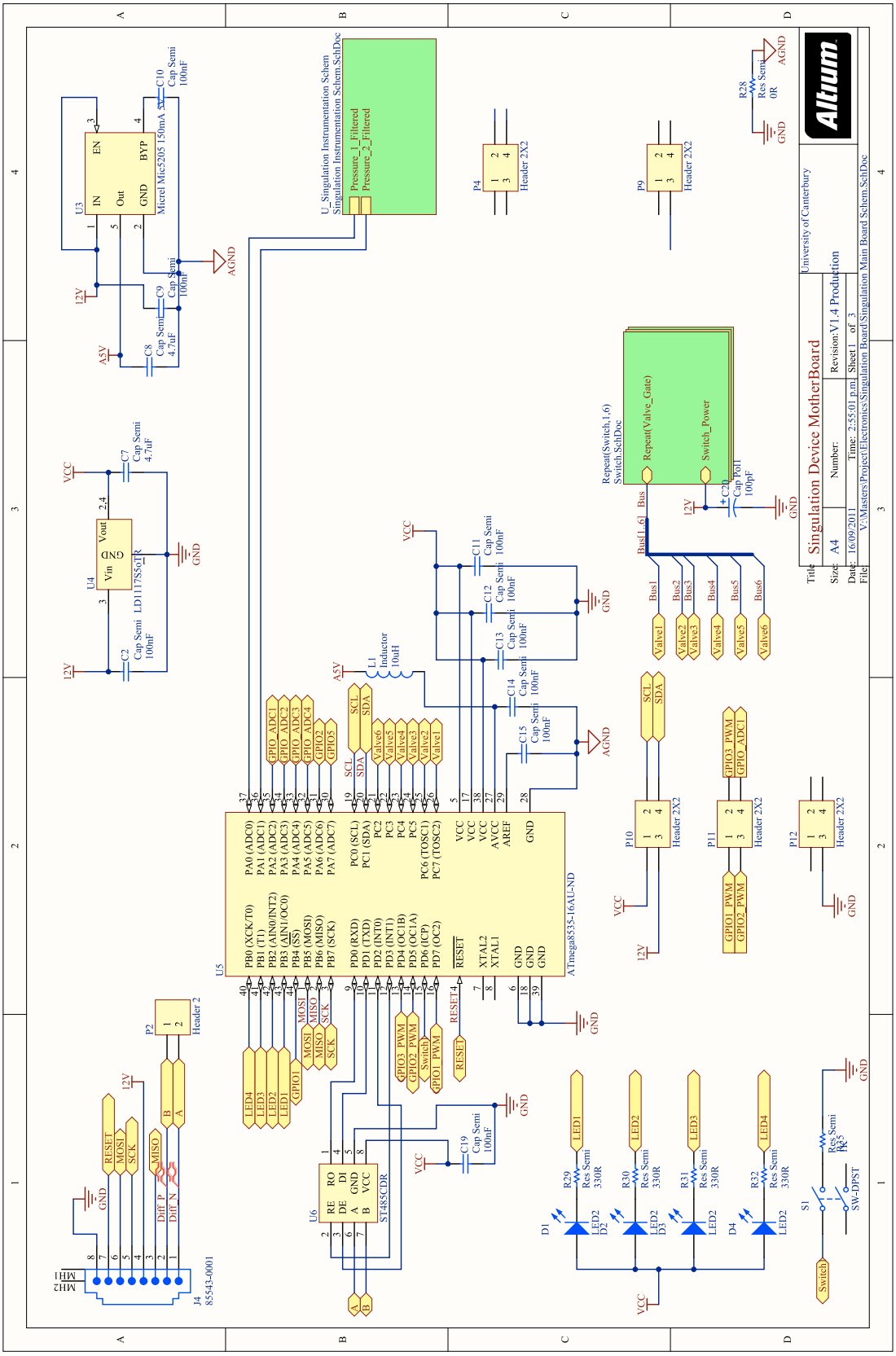

Figure A.1 – *Singularisation board main schematic.*

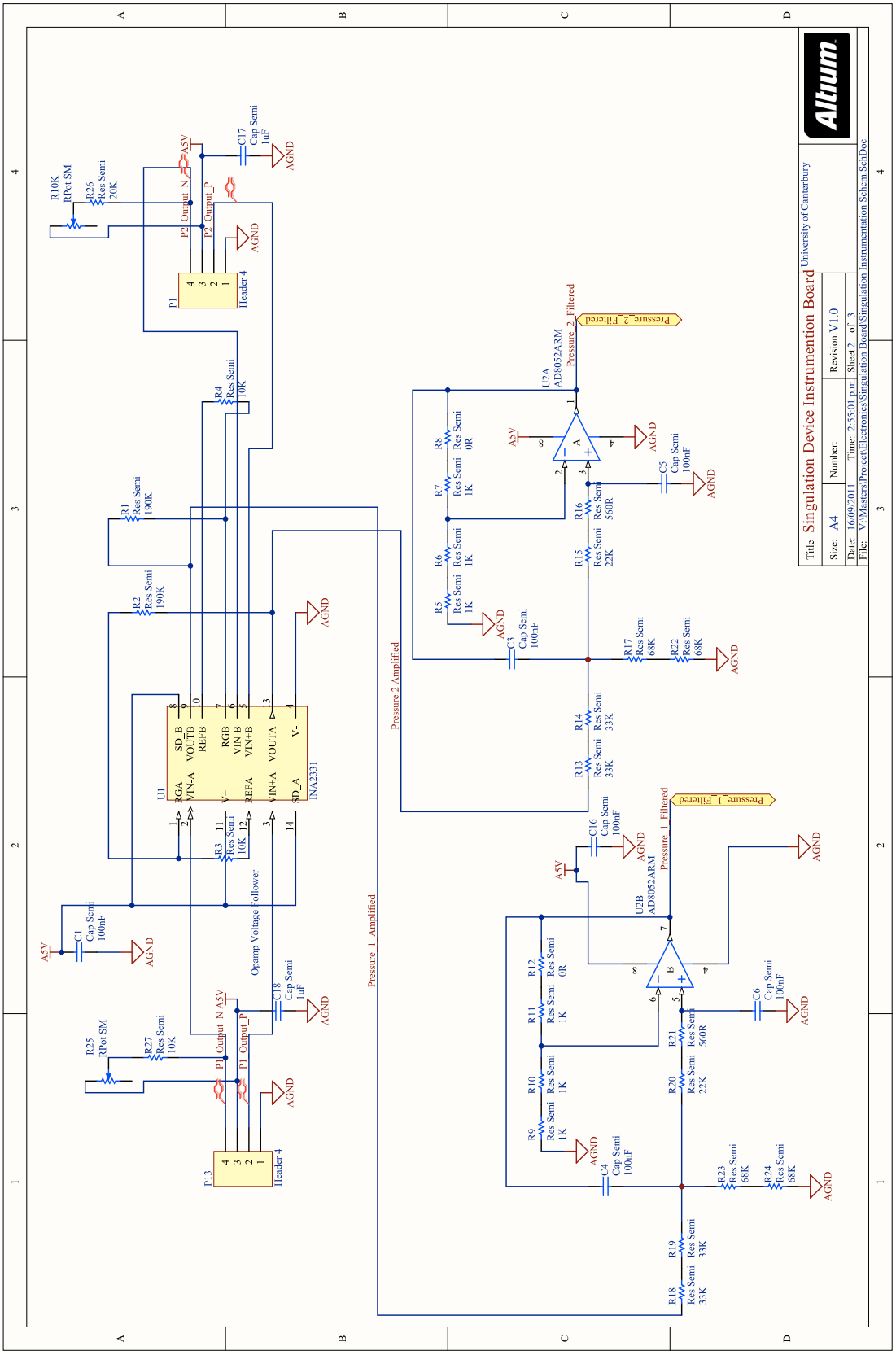

Figure A.2 – *Singularisation board signal conditioning schematic.*

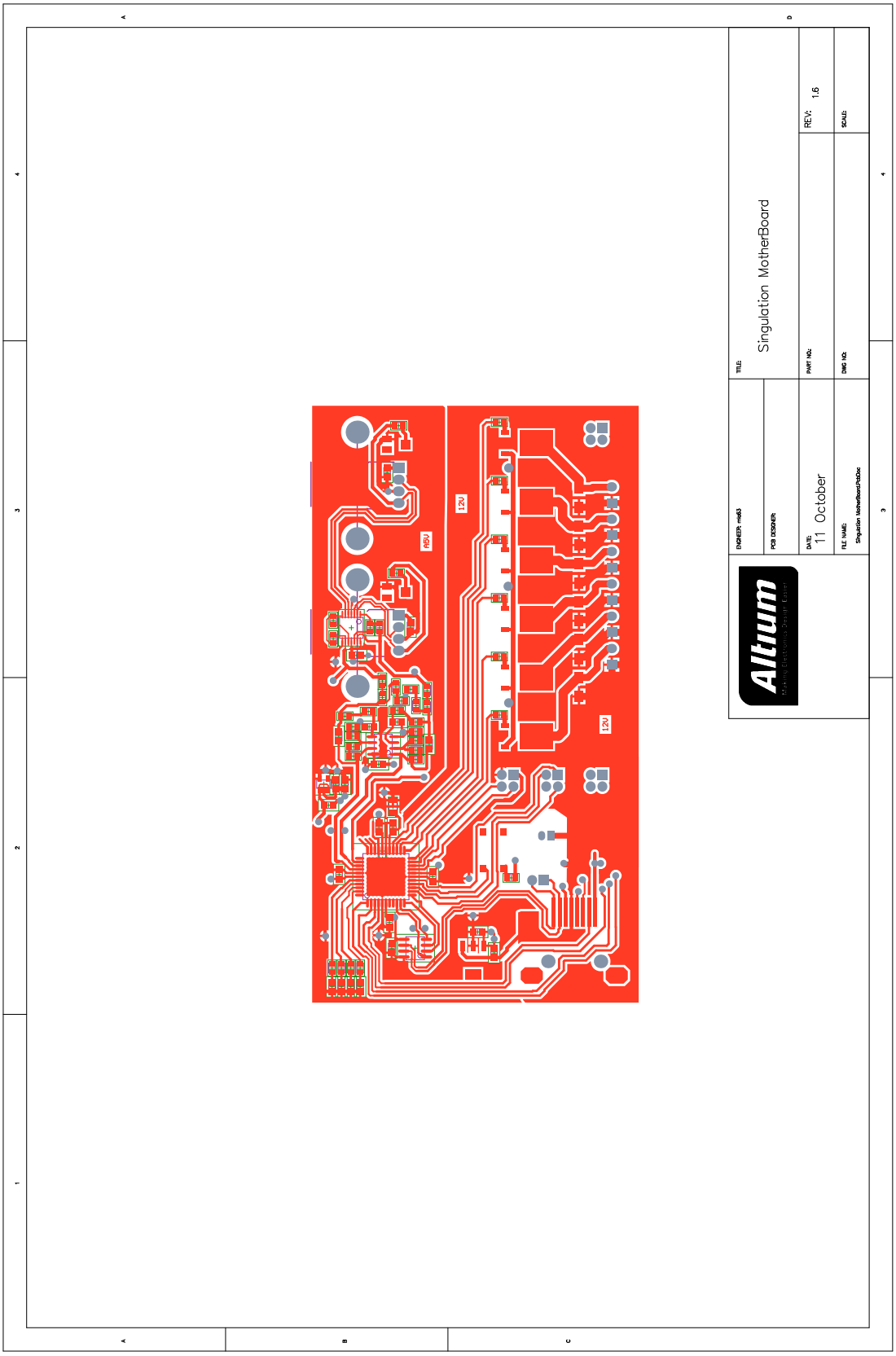

Figure A.3 – *Top PCB layer of singularisation board.*

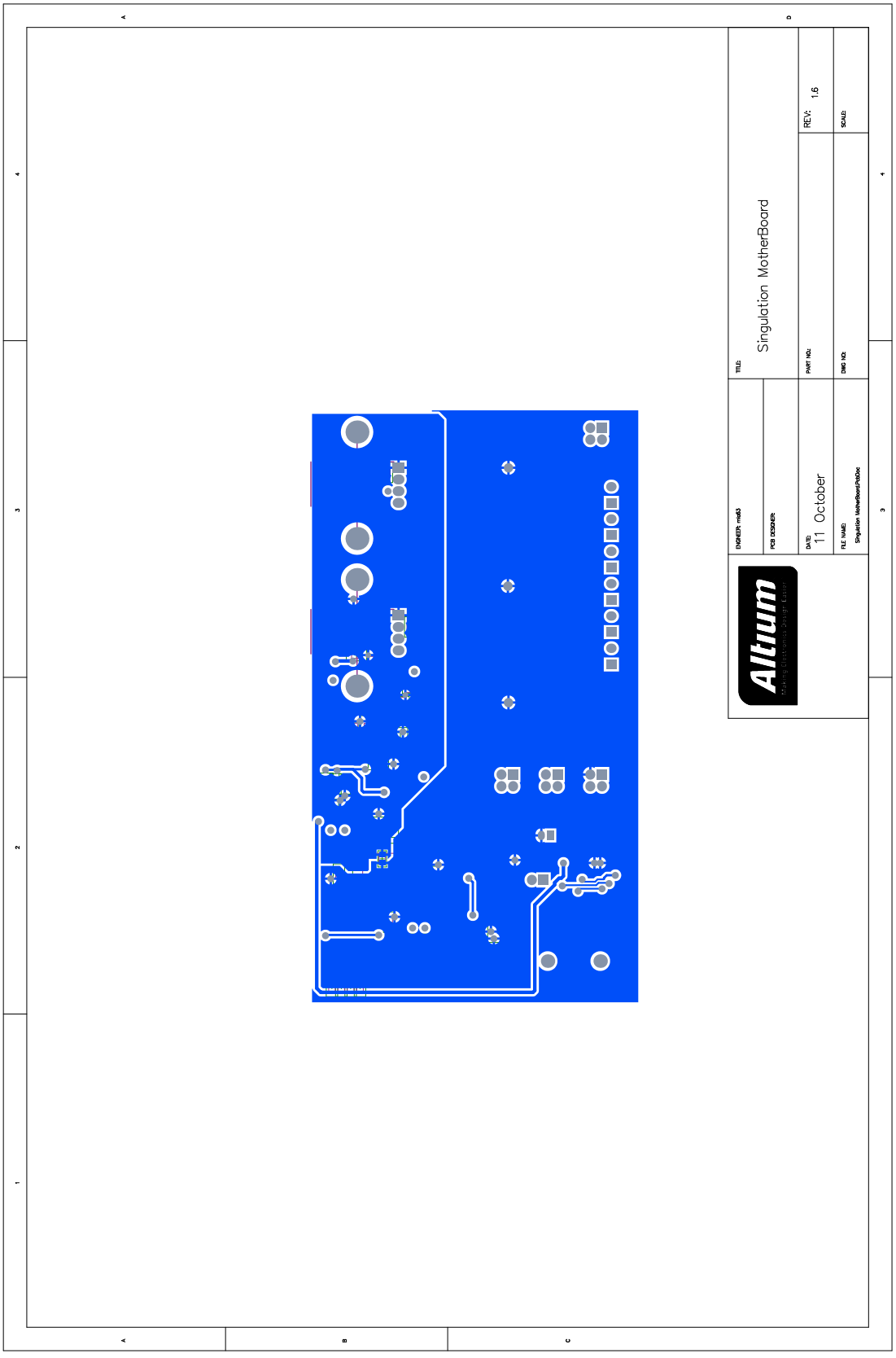

Figure A.4 – *Bottom PCB layer of singularisation board.*

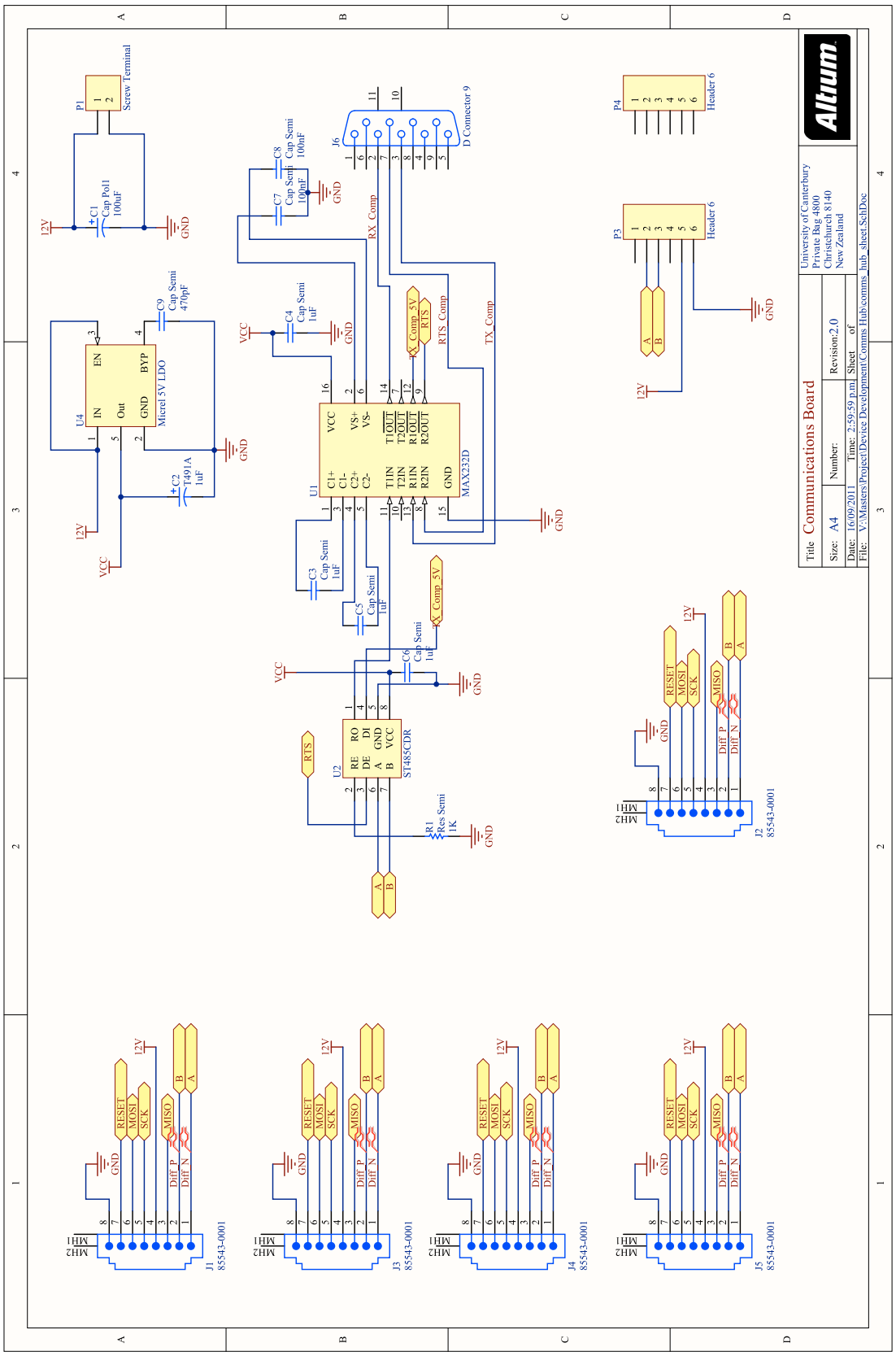

Figure A.5 – *Communications hub schematic. The communications hub provides translation from the RS-485 to RS-232 physical layer, in addition to enable the physical linking of devices to the bus.*

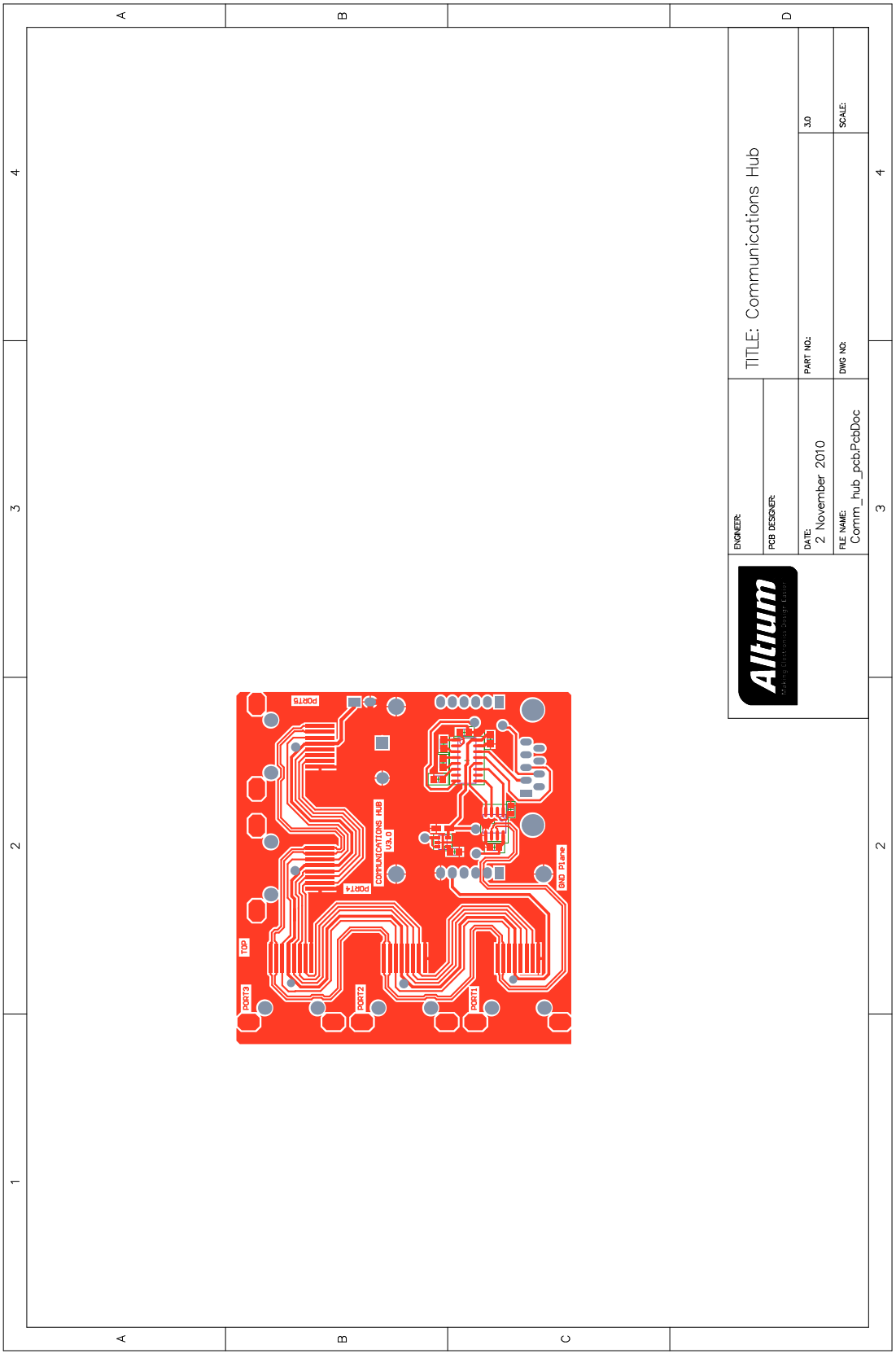

Figure A.6 – *Communication hub PCB top layer.*

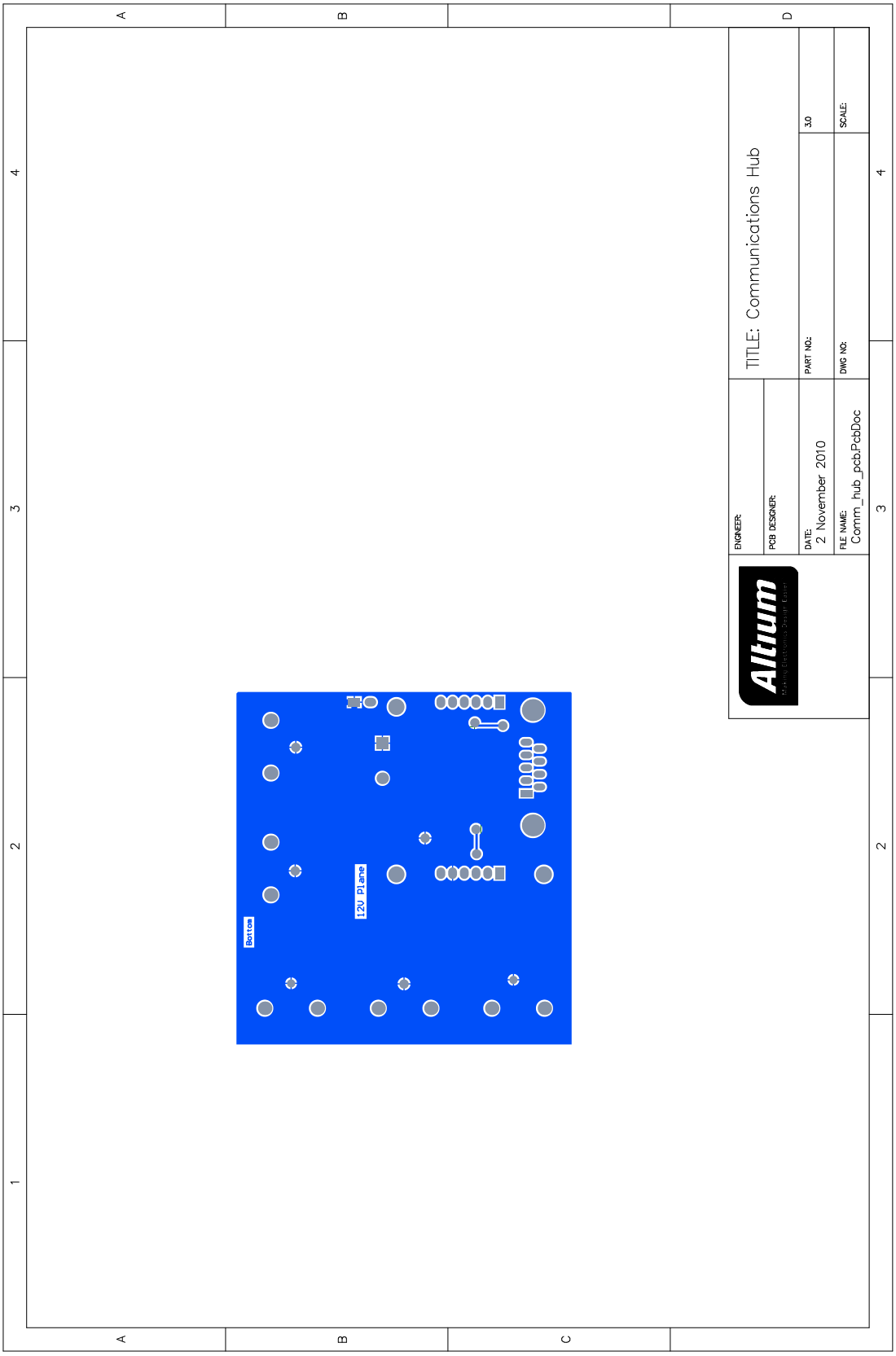

Figure A.7 – *Communication hub PCB bottom layer.*

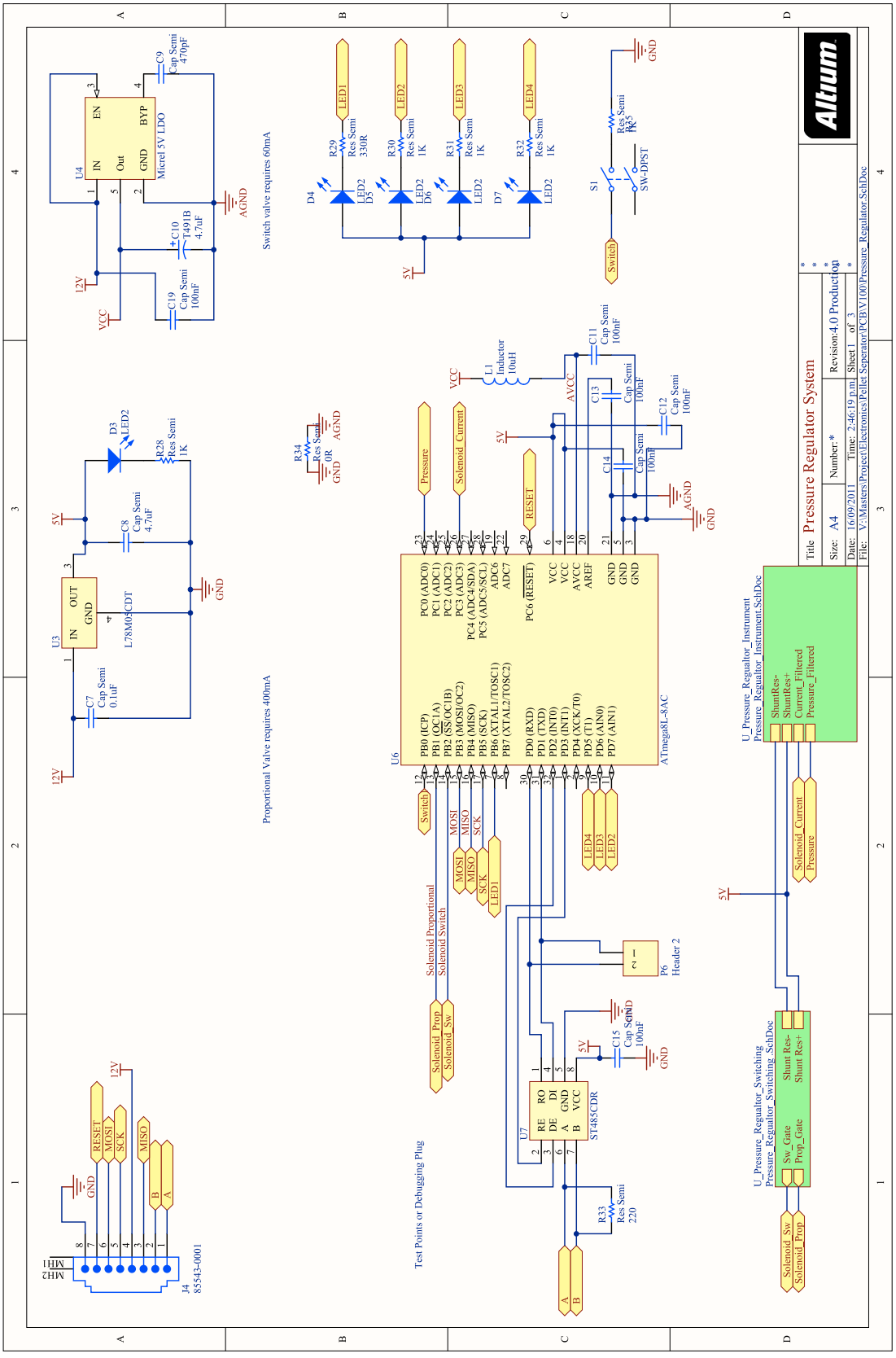

Figure A.8 – *Pressure regulator main schematic.*

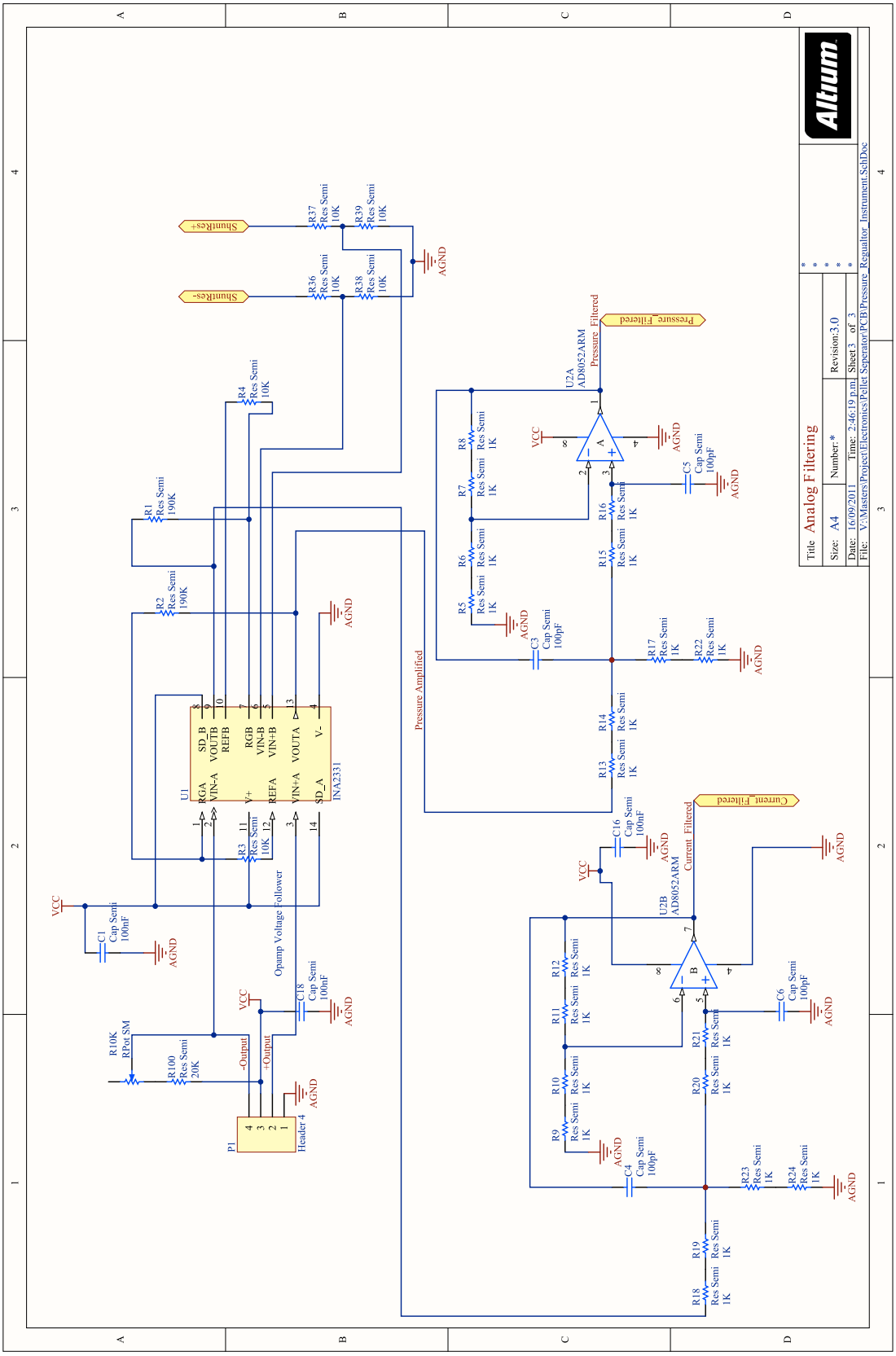

Figure A.9 – *Pressure regulator signal conditioning schematic.*

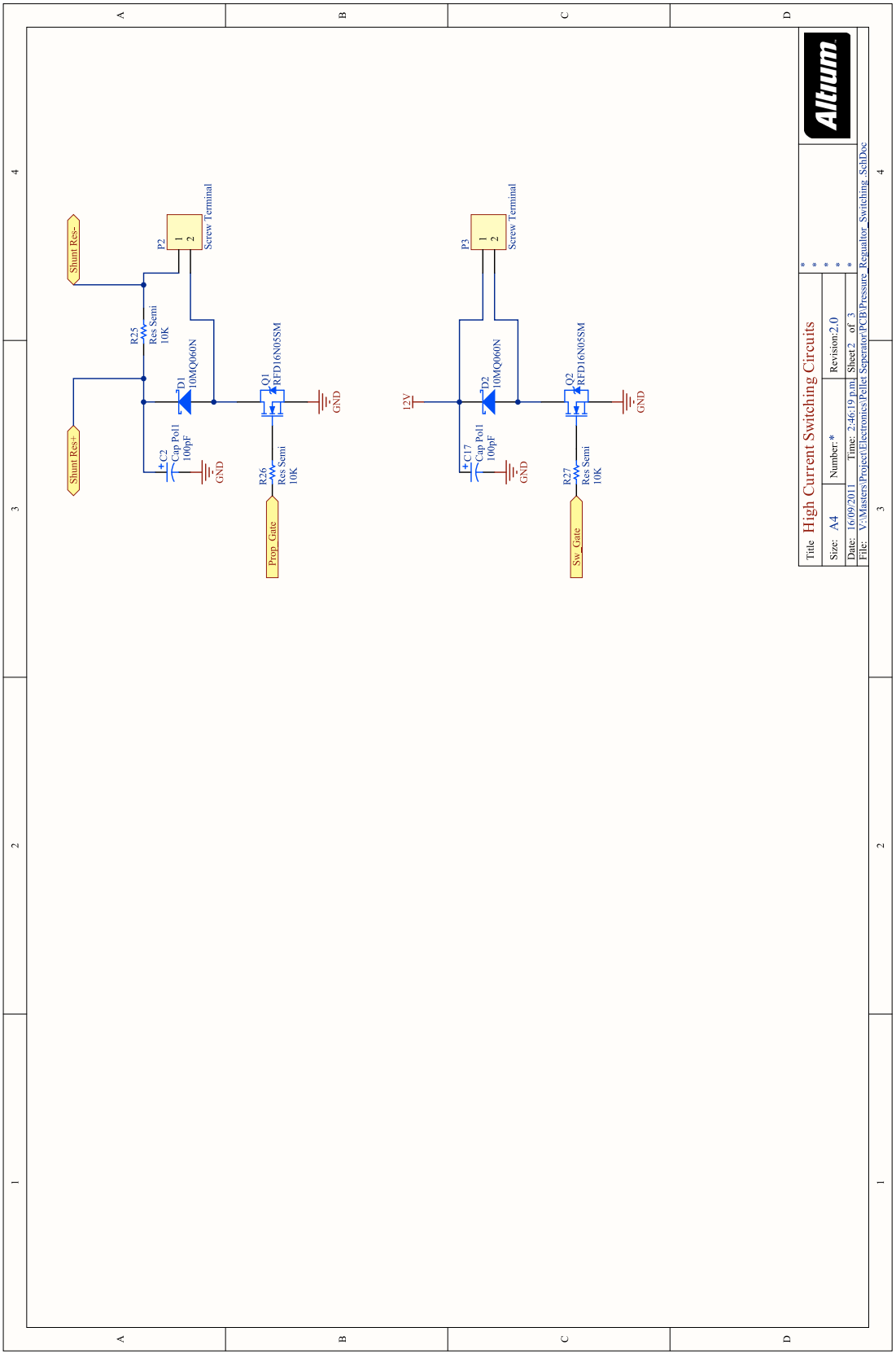

Figure A.10 – *Pressure regulator solid state switch schematic.*

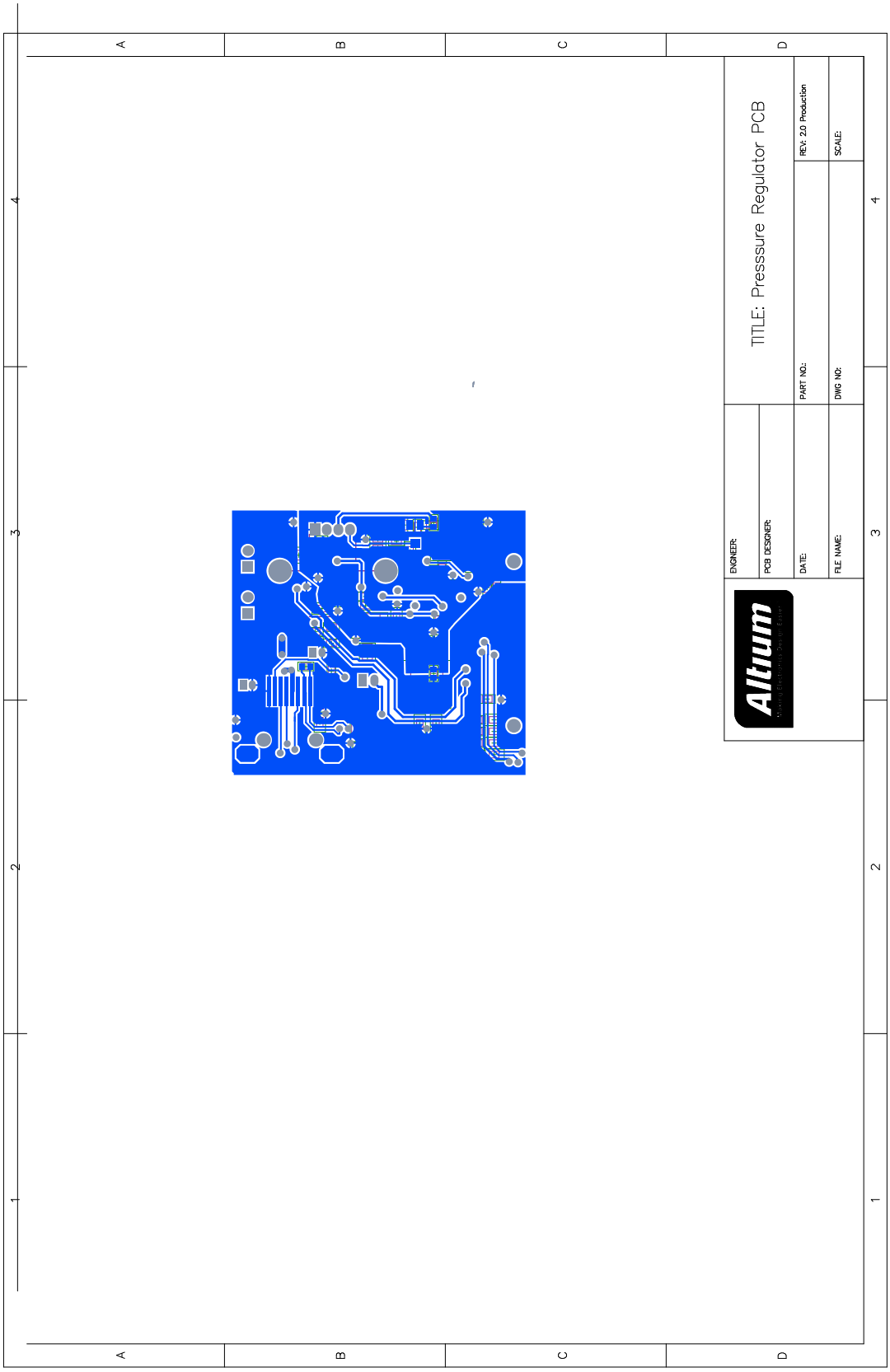

Figure A.11 – *Pressure regulator PCB bottom layer.*

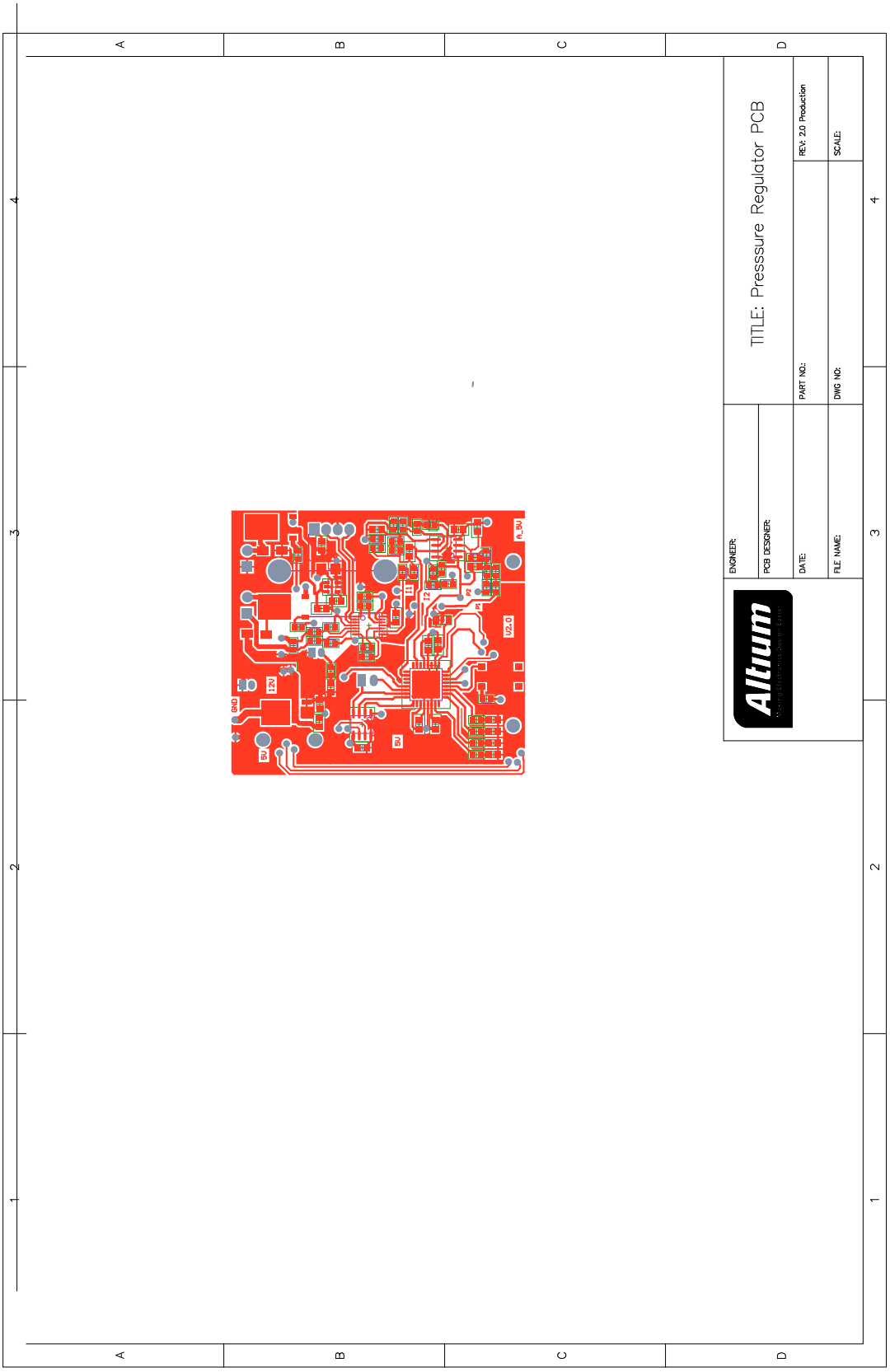

Figure A.12 – *Pressure regulator PCB top layer.*

Appendix B

Software

B.0.4 Data Link Layer

B.0.5 Application Layer

B.0.6 Message Functions

B.0.7 Singularisation Board

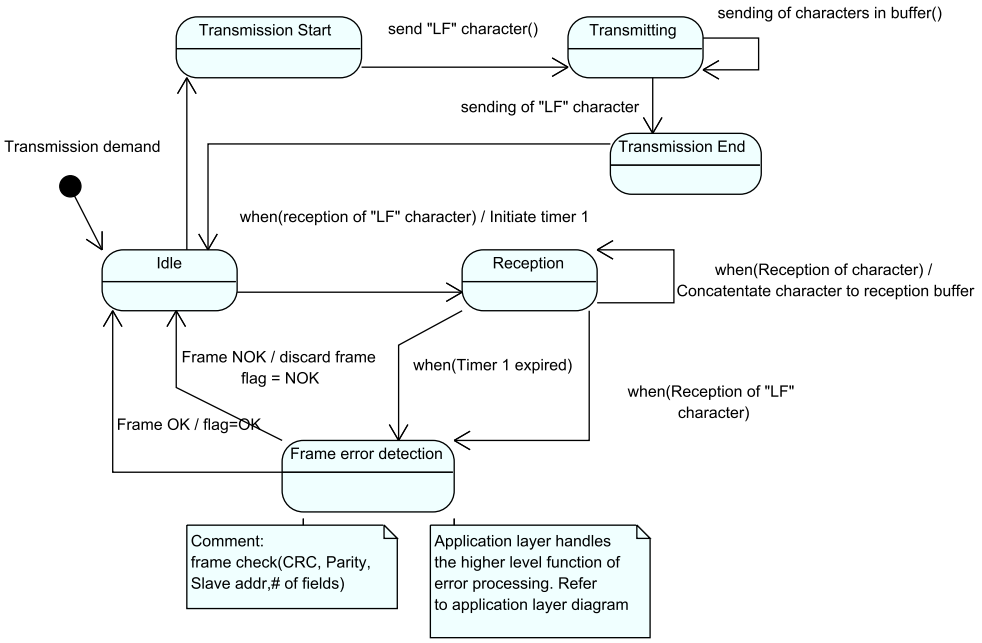

Figure B.1 – *Datalink State Behaviour.*

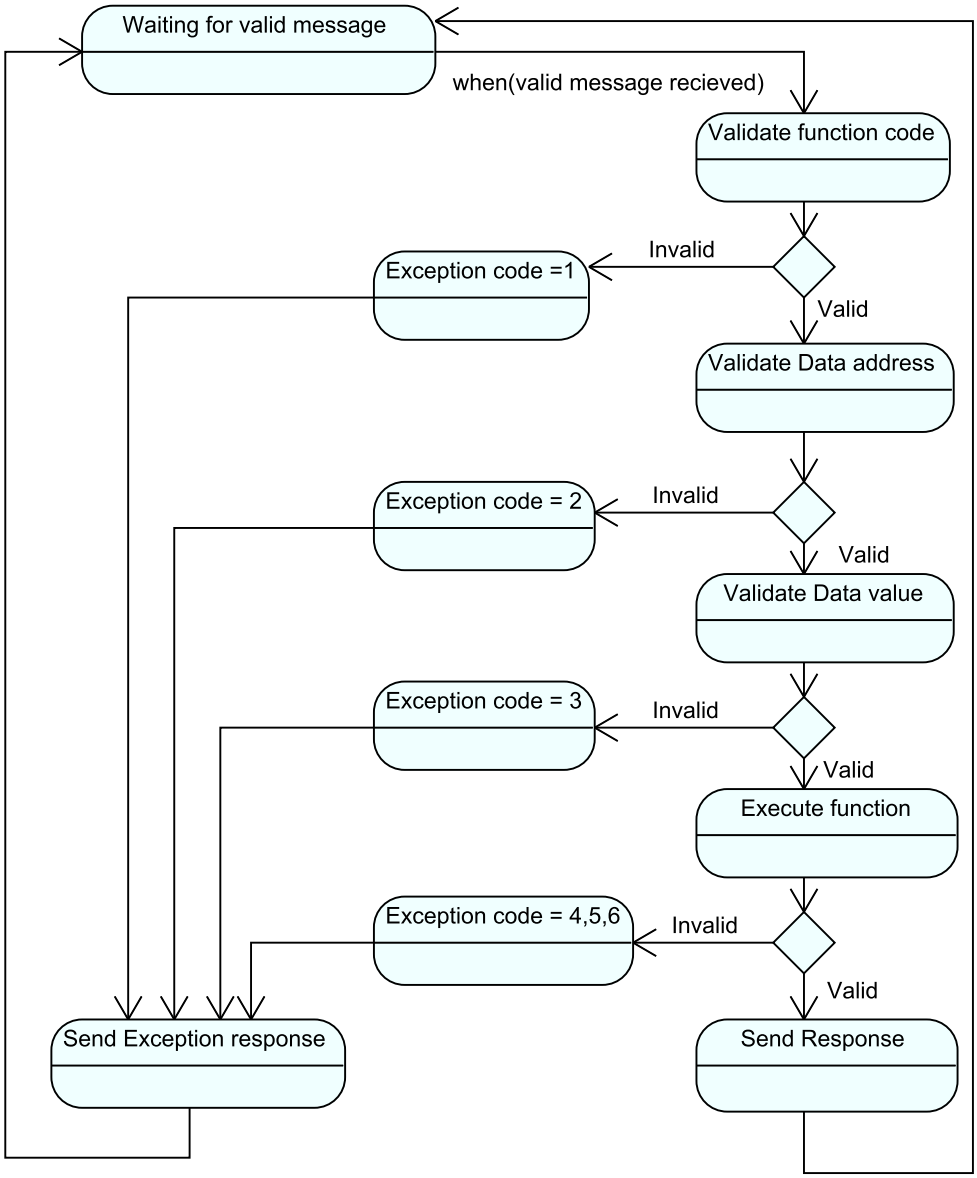

Figure B.2 – *Application Layer for reception of message.*

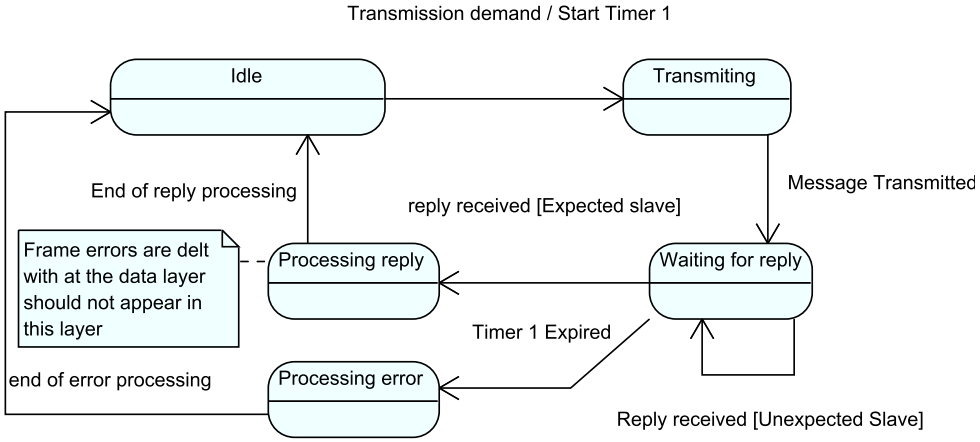

Figure B.3 – *Application Layer for transmission of message.*

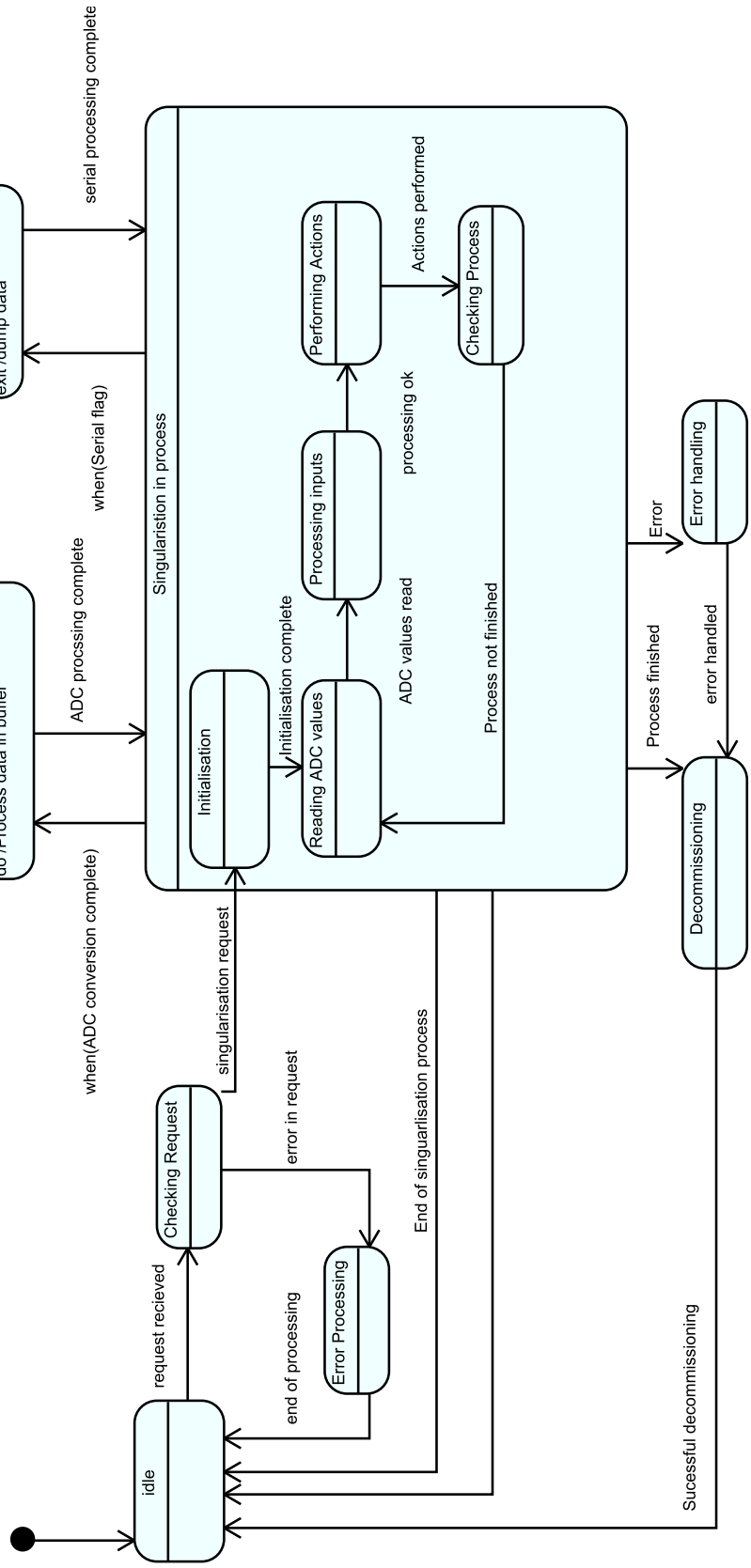

Figure B.4 – *High level state diagram of the software in the singularisation board.*

Appendix C

Mechanical Drawings

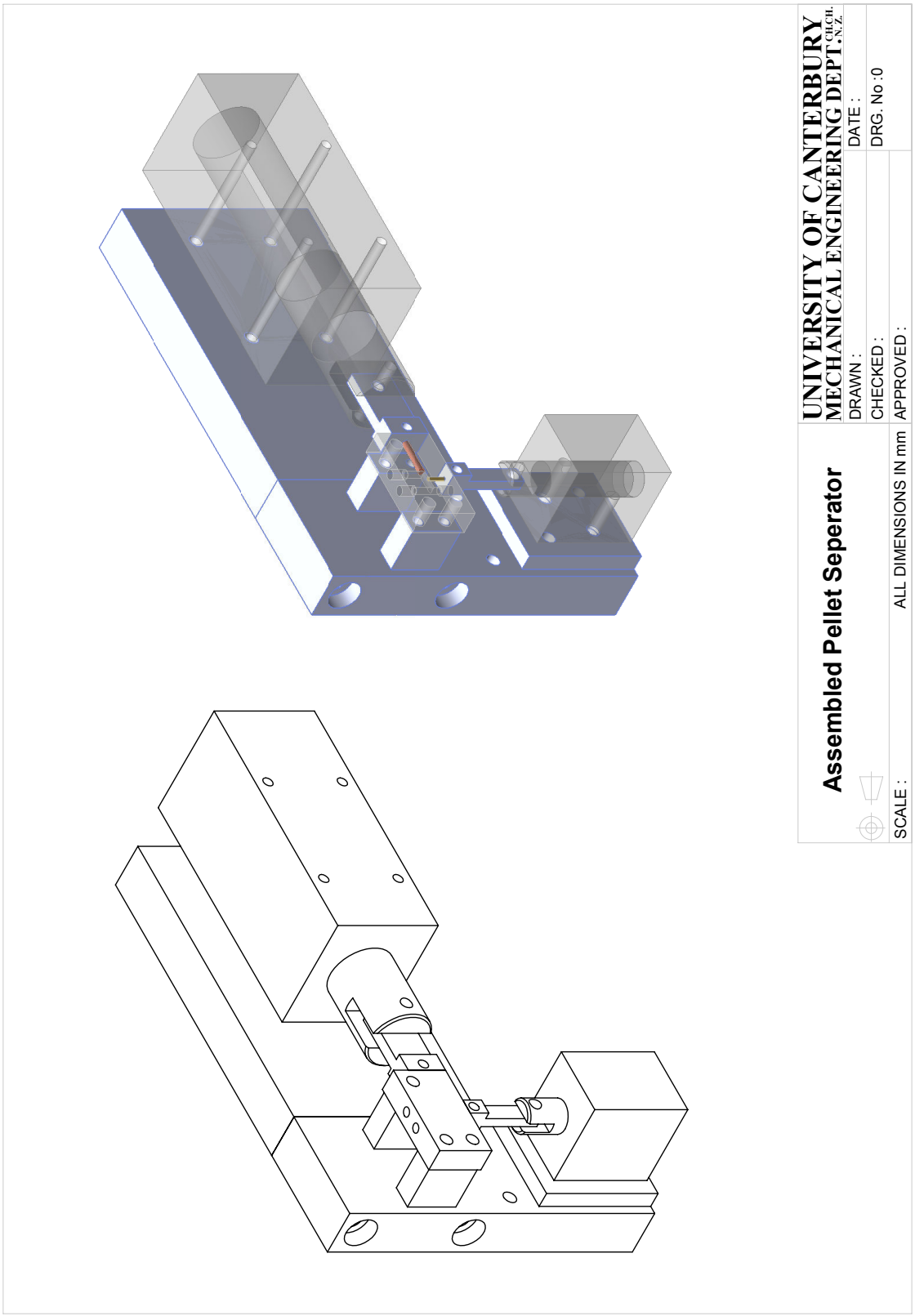
UNIVERSITY OF CANTERBURY
MECHANICAL ENGINEERING DEPT. CHCH. N.Z.
Assembled Pellet Seperator
DRAWN :
DATE :
CHECKED :
DRG. No :0
SCALE :
ALL DIMENSIONS IN mm
APPROVED :

Figure C.1 –

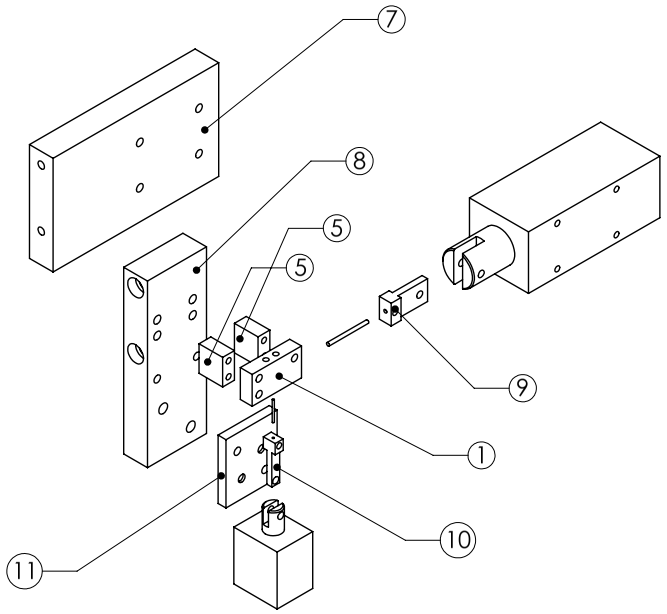

ITEM NO.	PART NUMBER	DESCRIPTION	Retracted/QTY.
1	Block		1
5	Block Spacer		2
7	Large Plate		1
8	Small Plate		1
9	Large Solenoid Coupling		1
10	Small Solenoid Coupling		1
11	Solenoid Spacer		1

Pellet Seperator Exploded

SCALE : ALL DIMENSIONS IN mm

UNIVERSITY OF CANTERBURY
MECHANICAL ENGINEERING DEPT. CH.CH. N.Z.

DRAWN : DATE :
CHECKED : DRG. No :1
APPROVED :

Figure C.2 –

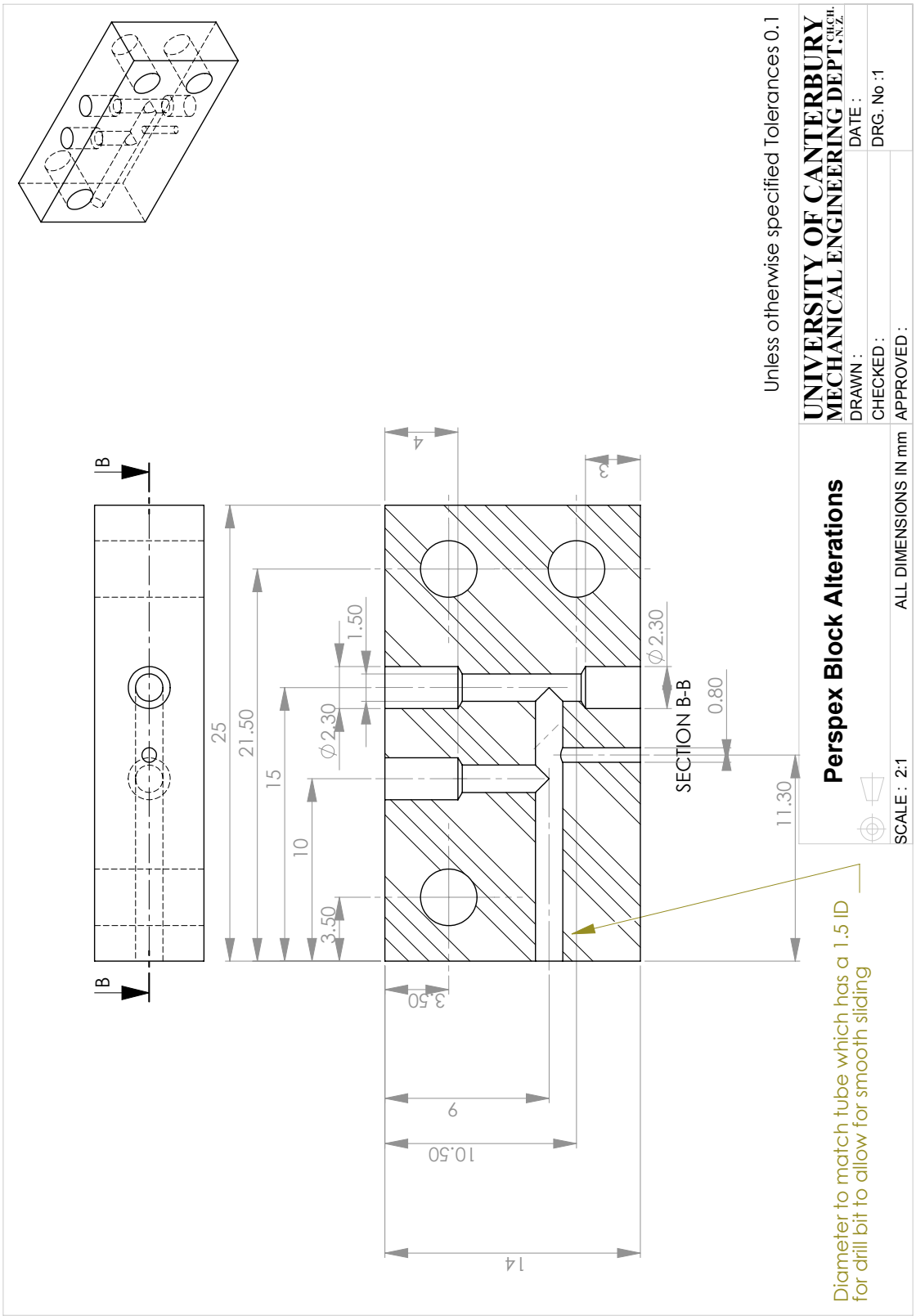
Unless otherwise specified Tolerances 0.1
UNIVERSITY OF CANTERBURY
MECHANICAL ENGINEERING DEPT. N.Z.
DRAWN :
DATE :
CHECKED :
DRG. No :1
APPROVED :
SCALE : 2:1
ALL DIMENSIONS IN mm
Perspex Block Alterations
SECTION B-B
B
B
25
21.50
15
10
3.50
1.50
Ø 2.30
Ø 2.30
0.80
11.30
4
3
3.50
9
10.50
14
Diameter to match tube which has a 1.5 ID
for drill bit to allow for smooth sliding

Figure C.3 –

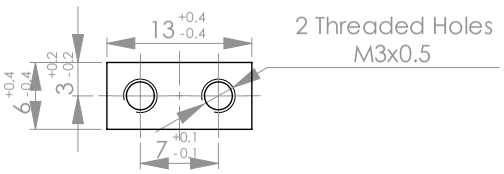

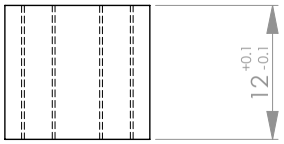

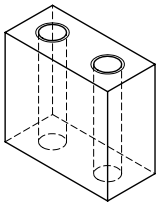

Unless otherwise specified Tolerances 0.1
Material: Aluminium

Block Spacer		**UNIVERSITY OF CANTERBURY** MECHANICAL ENGINEERING DEPT. CH.CH. N.Z.	
		DRAWN :	DATE :
		CHECKED :	DRG. No :1
SCALE : 2:1	ALL DIMENSIONS IN mm	APPROVED :	

Figure C.4 –

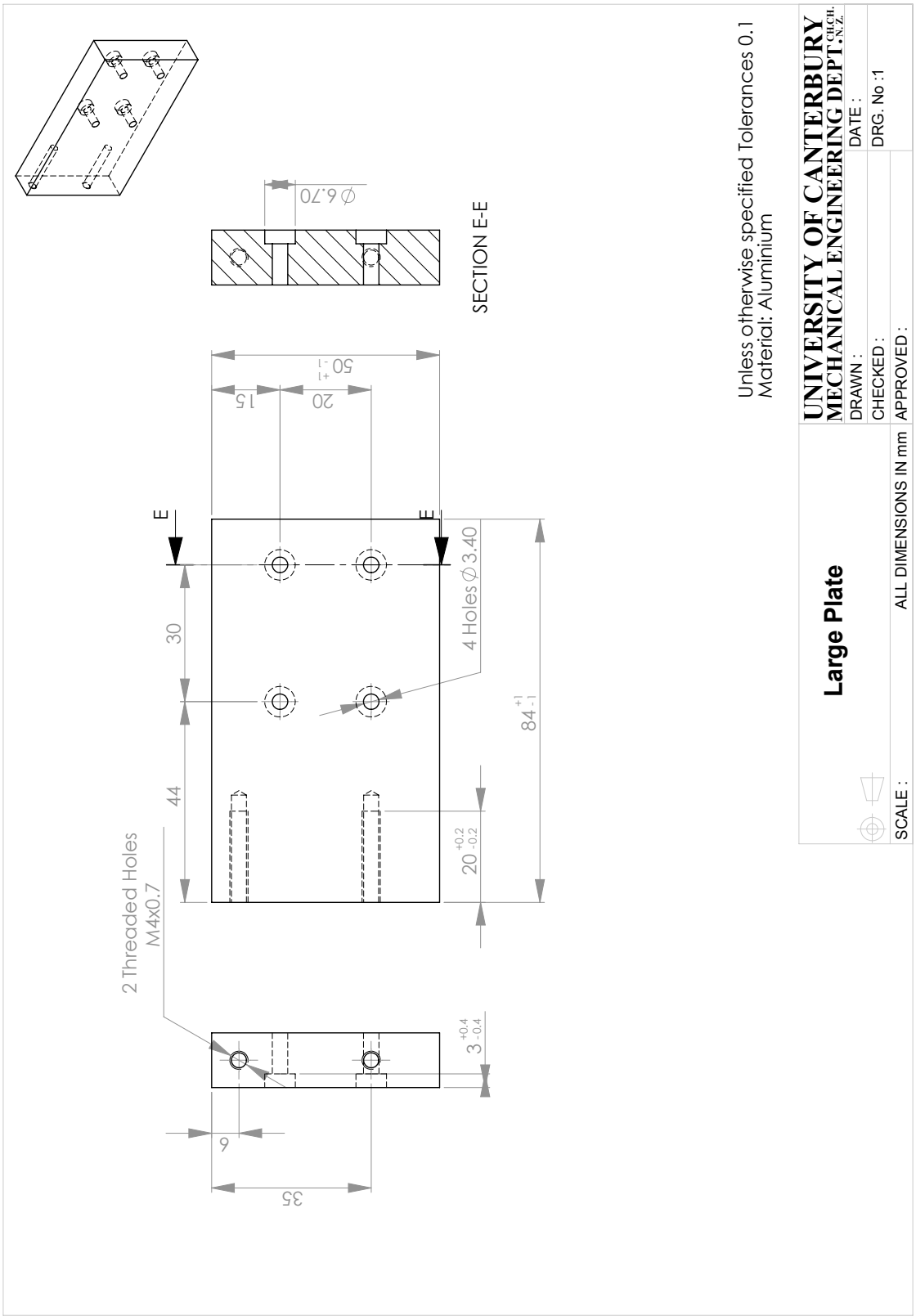
Unless otherwise specified Tolerances 0.1
Material: Aluminium
UNIVERSITY OF CANTERBURY
MECHANICAL ENGINEERING DEPT. N.Z.
Large Plate
DRAWN :
DATE :
CHECKED :
DRG. No :1
SCALE :
ALL DIMENSIONS IN mm
APPROVED :
SECTION E-E
Ø6.70
50 +1 -1
15
20
E
E
30
44
4 Holes Ø3.40
84 +1 -1
20 +0.2 -0.2
2 Threaded Holes
M4x0.7
3 +0.4 -0.4
6
35

Figure C.5 –

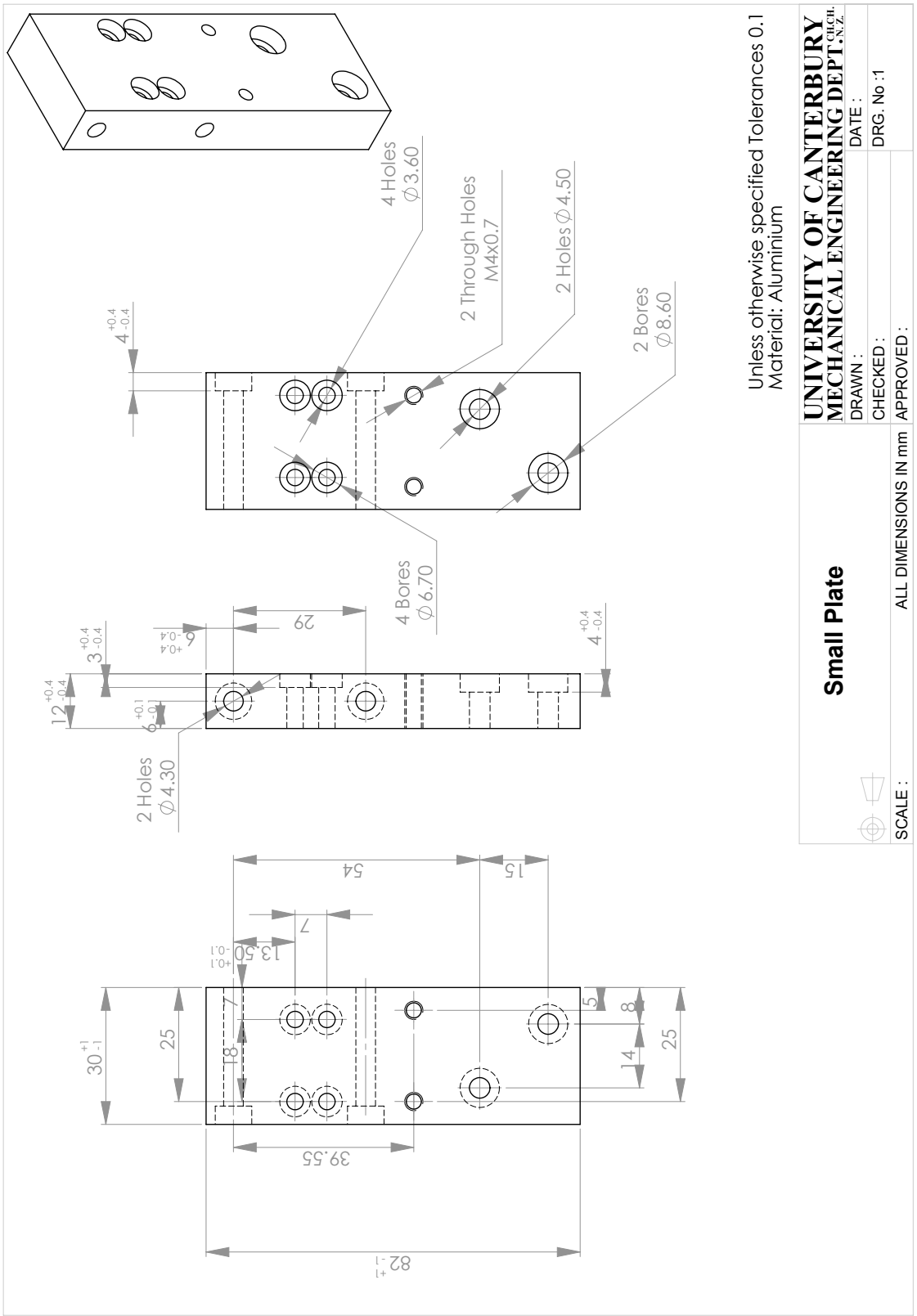
Unless otherwise specified Tolerances 0.1
Material: Aluminium
UNIVERSITY OF CANTERBURY
MECHANICAL ENGINEERING DEPT. CHCH. N.Z.
Small Plate
DRAWN :
DATE :
CHECKED :
DRG. No :1
SCALE :
ALL DIMENSIONS IN mm
APPROVED :
4 Holes Ø3.60
2 Through Holes M4x0.7
2 Holes Ø4.50
2 Bores Ø8.60
4 Bores Ø6.70
2 Holes Ø4.30
82
39.55
54
15
25
30
18
13.50
7
29
12
3
6
4

Figure C.6 –

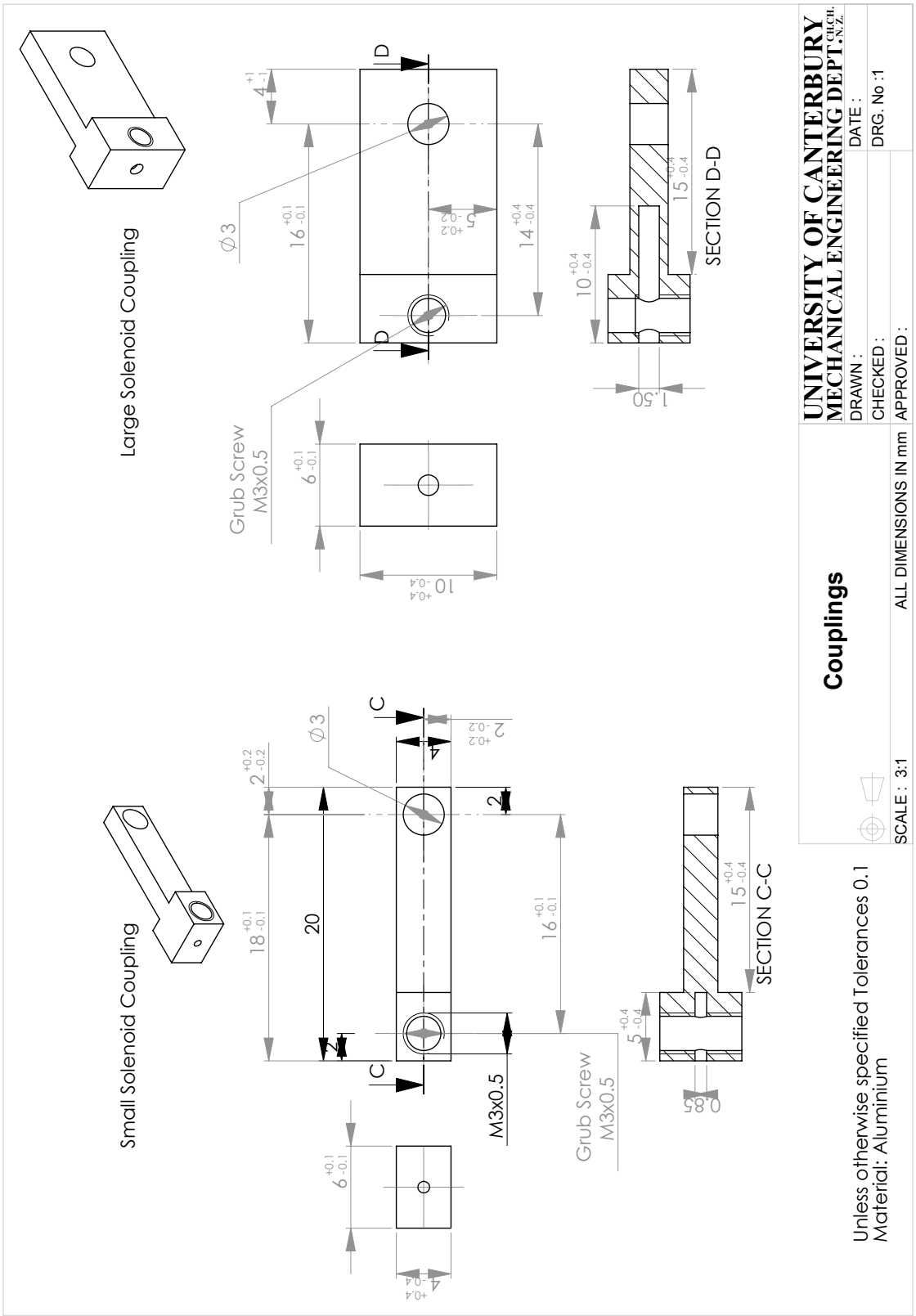
Large Solenoid Coupling
Small Solenoid Coupling
Grub Screw M3x0.5
Grub Screw M3x0.5
M3x0.5
SECTION D-D
SECTION C-C
Couplings
UNIVERSITY OF CANTERBURY
MECHANICAL ENGINEERING DEPT. N.Z.
DRAWN :
DATE :
CHECKED :
DRG. No :1
APPROVED :
SCALE : 3:1
ALL DIMENSIONS IN mm
Unless otherwise specified Tolerances 0.1
Material: Aluminium

Figure C.7 –

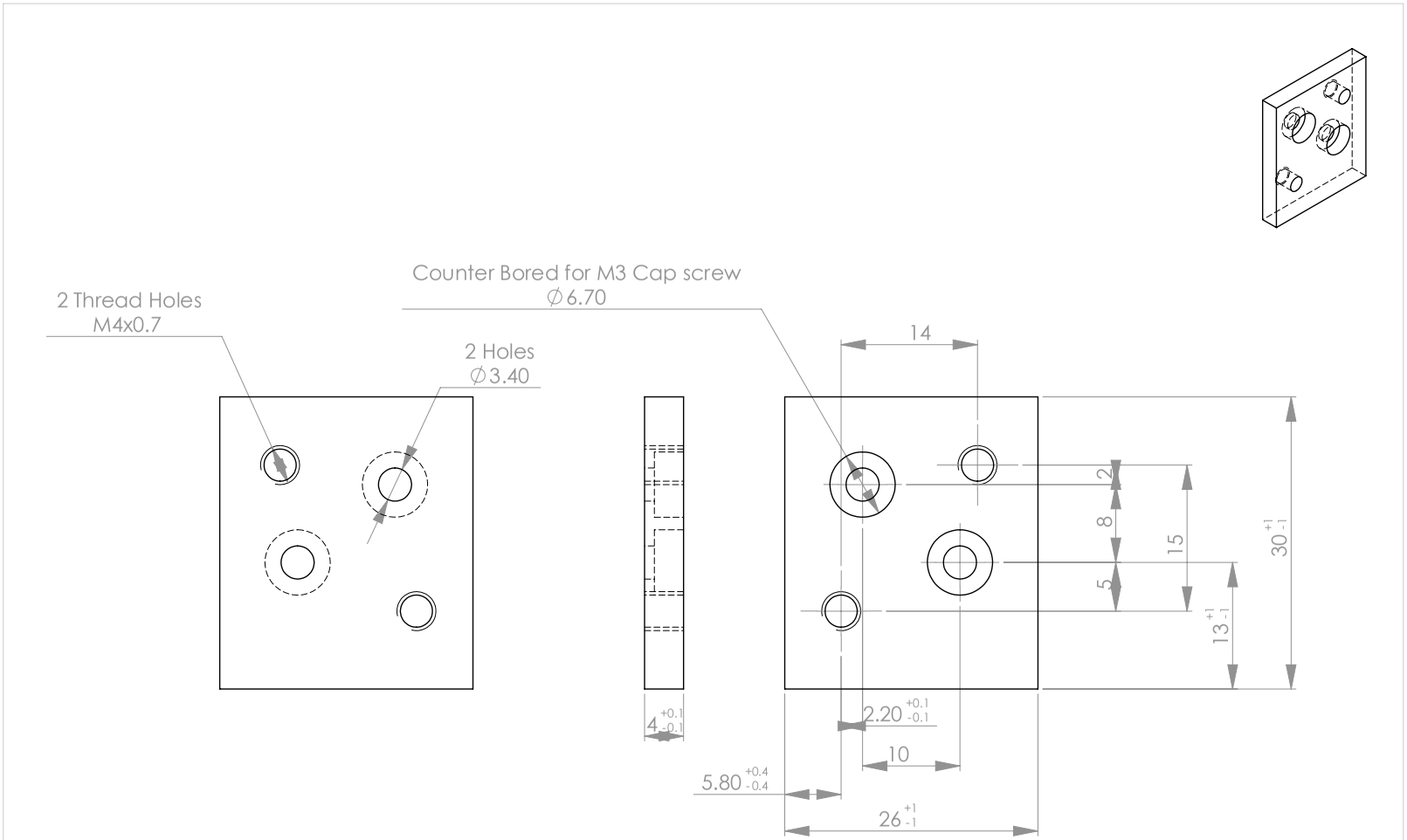
2 Thread Holes
M4x0.7
Counter Bored for M3 Cap screw
∅6.70
2 Holes
∅3.40
14
2
8
15
5
30 +1 -1
13 +1 -1
4 +0.1 -0.1
2.20 +0.1 -0.1
10
5.80 +0.4 -0.4
26 +1 -1
Unless otherwise specified Tolerances 0.1
Material: Aluminium
Solenoid Spacer
SCALE :
ALL DIMENSIONS IN mm
UNIVERSITY OF CANTERBURY
MECHANICAL ENGINEERING DEPT. CH.CH. N.Z.
DRAWN :
DATE :
CHECKED :
DRG. No :1
APPROVED :

Figure C.8 –

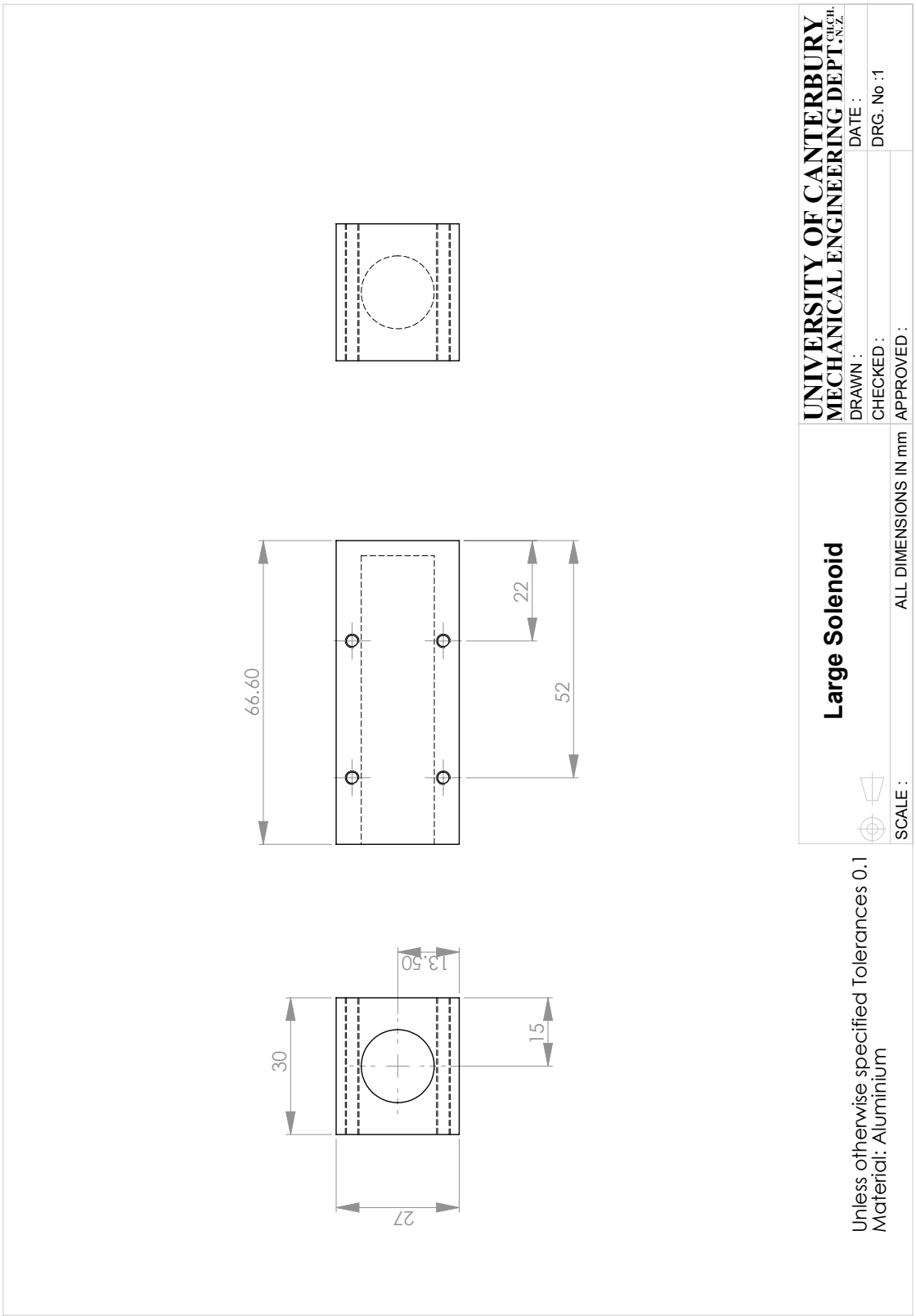
66.60
22
52
13.50
30
15
27
Large Solenoid
UNIVERSITY OF CANTERBURY
MECHANICAL ENGINEERING DEPT. CHCH. N.Z.
DRAWN :
DATE :
CHECKED :
DRG. No :1
SCALE :
ALL DIMENSIONS IN mm
APPROVED :
Unless otherwise specified Tolerances 0.1
Material: Aluminium

Figure C.9 –

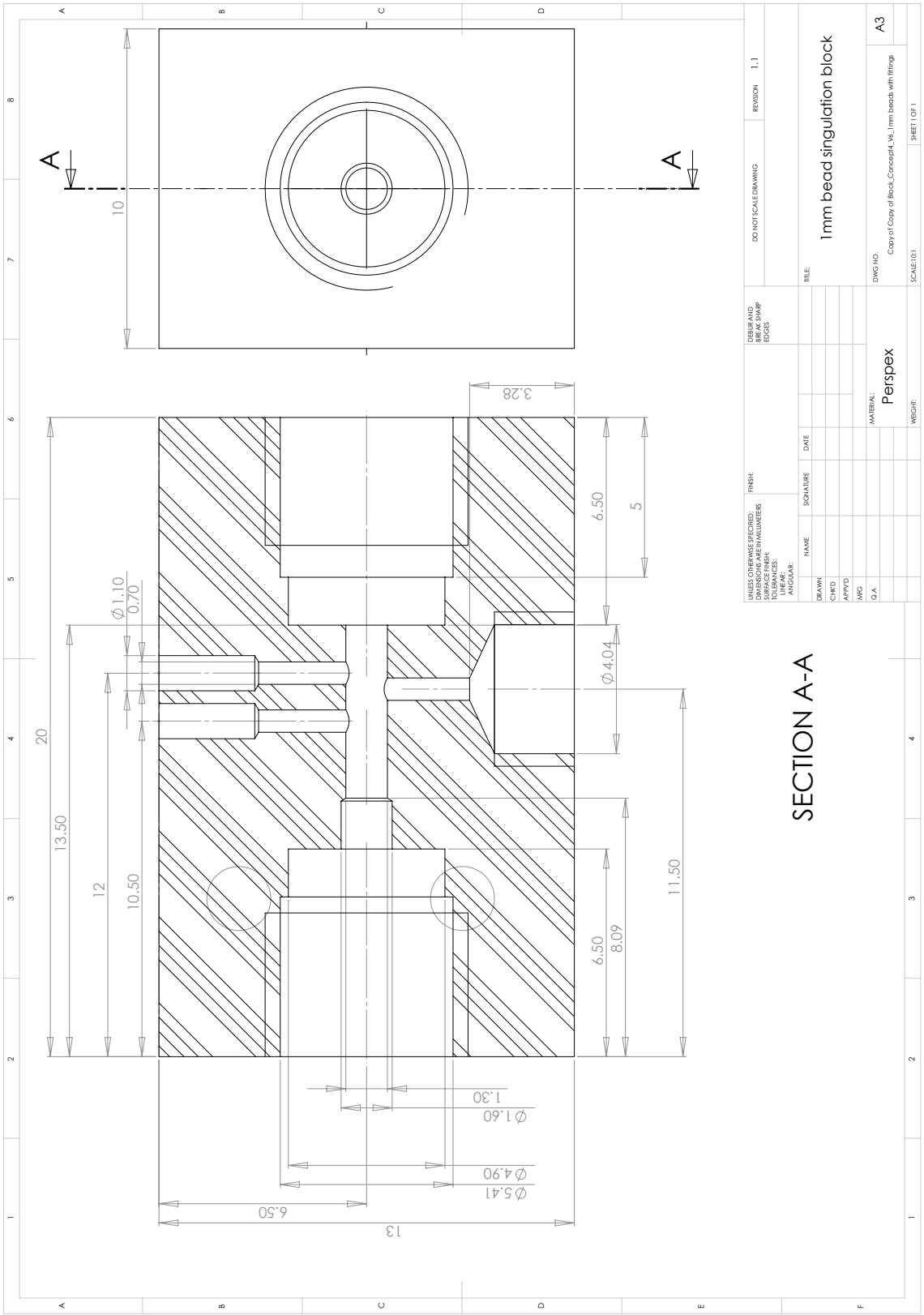

Figure C.10 – *Fluidics device.*

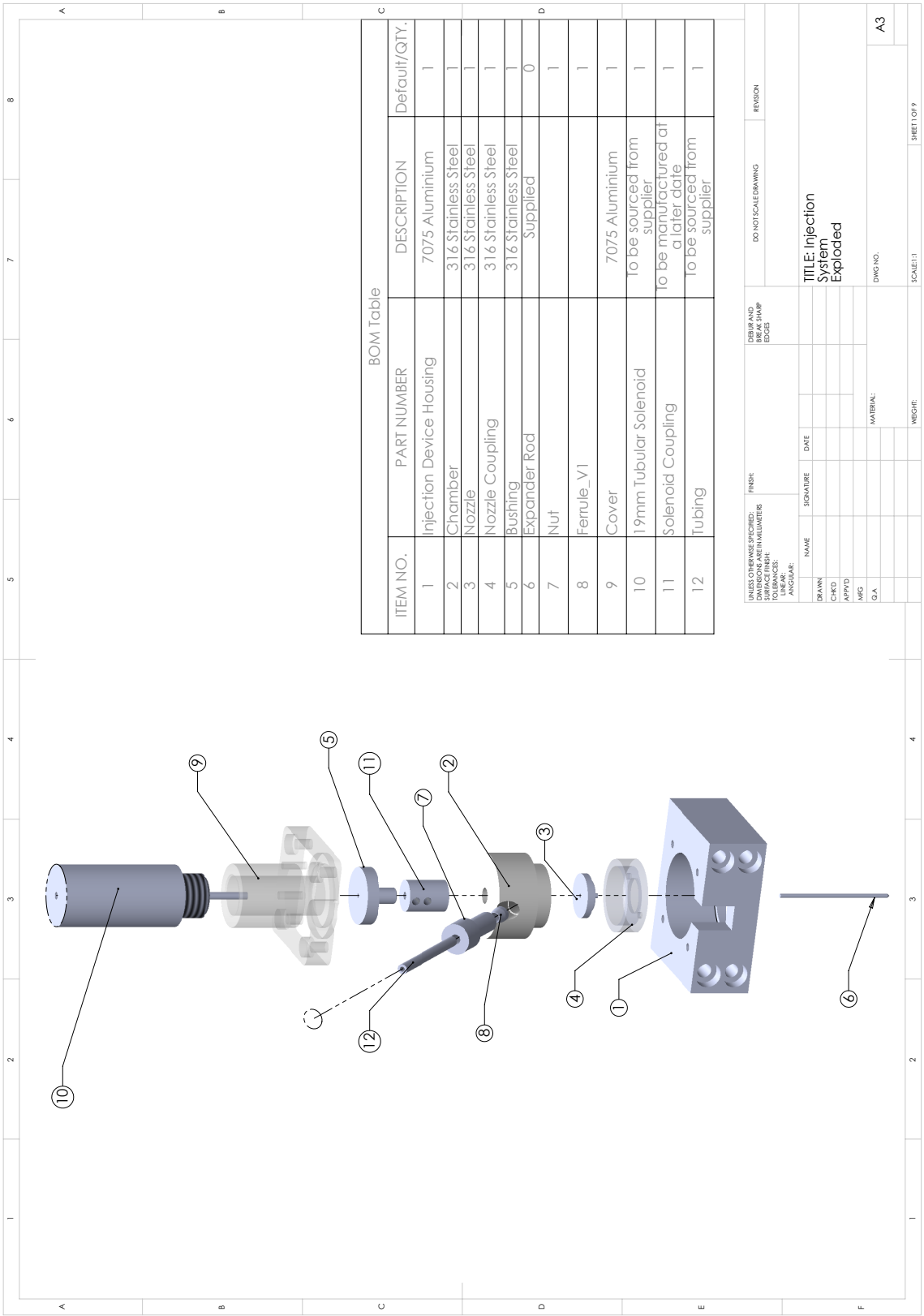

Figure C.11 – *Injection device components.*

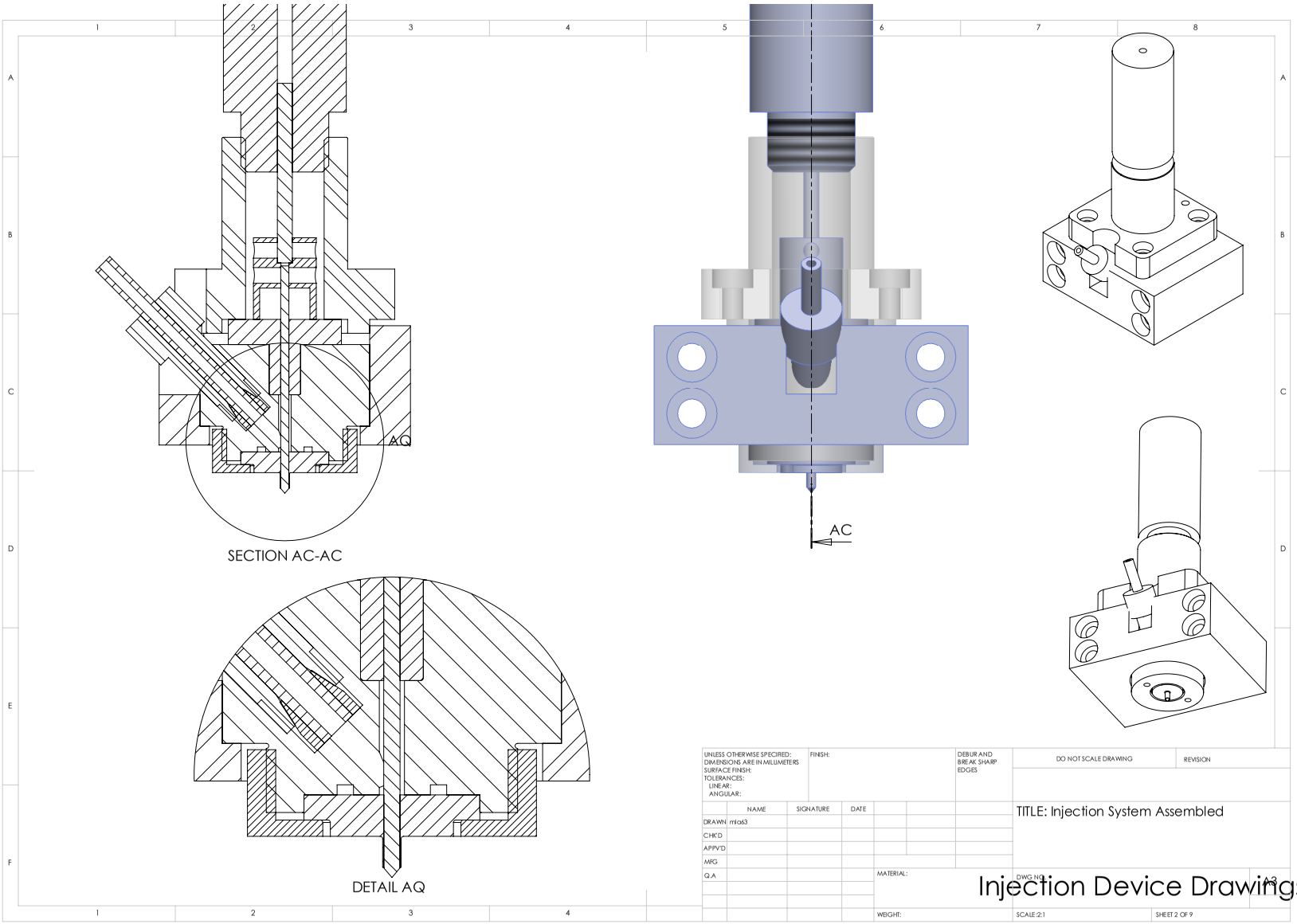

Figure C.12 – *Injection device assembled.*

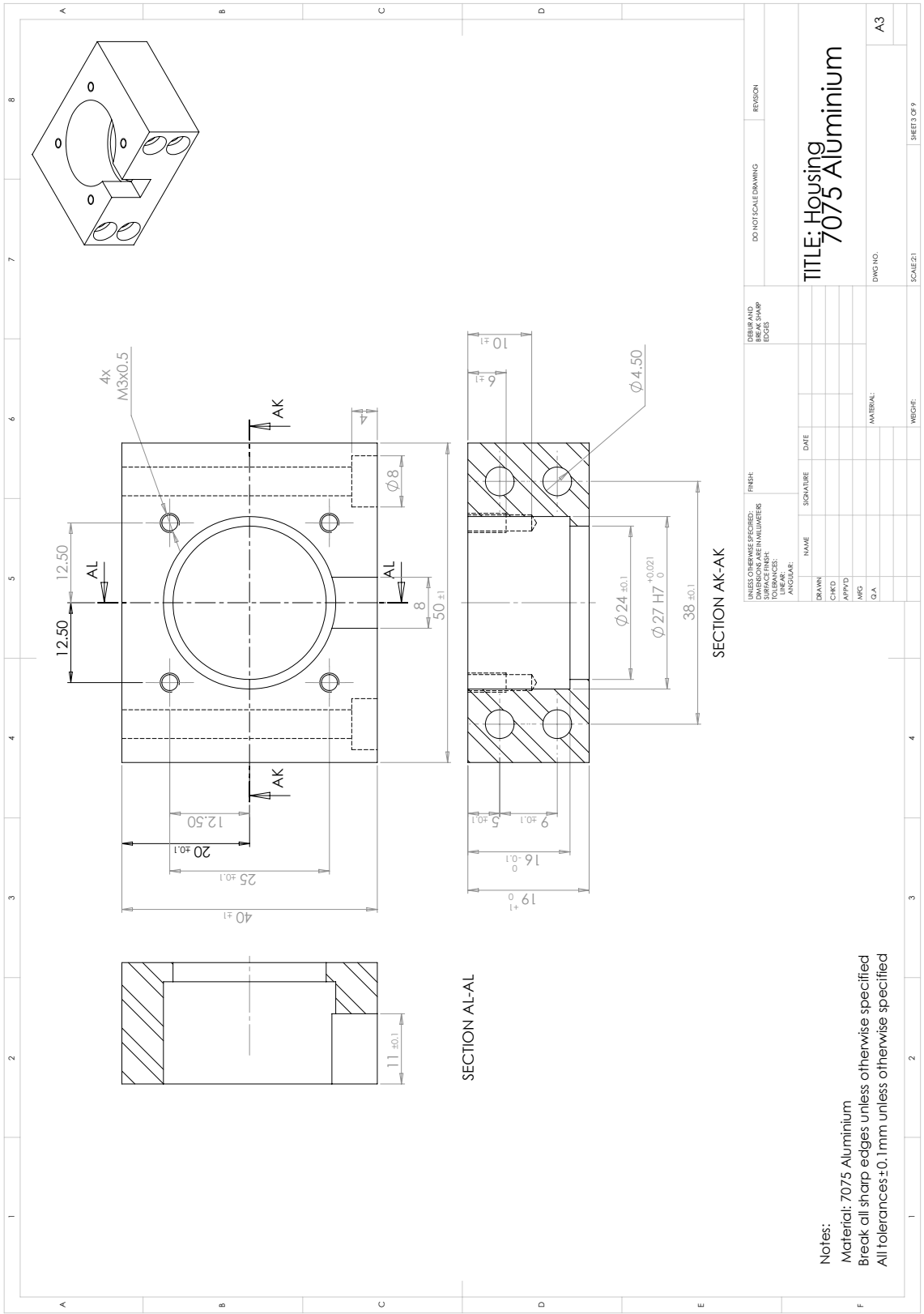
TITLE: Housing
7075 Aluminium
A3
SECTION AK-AK
SECTION AL-AL
4x M3x0.5
Notes:
Material: 7075 Aluminium
Break all sharp edges unless otherwise specified
All tolerances±0.1mm unless otherwise specified

Figure C.13 –

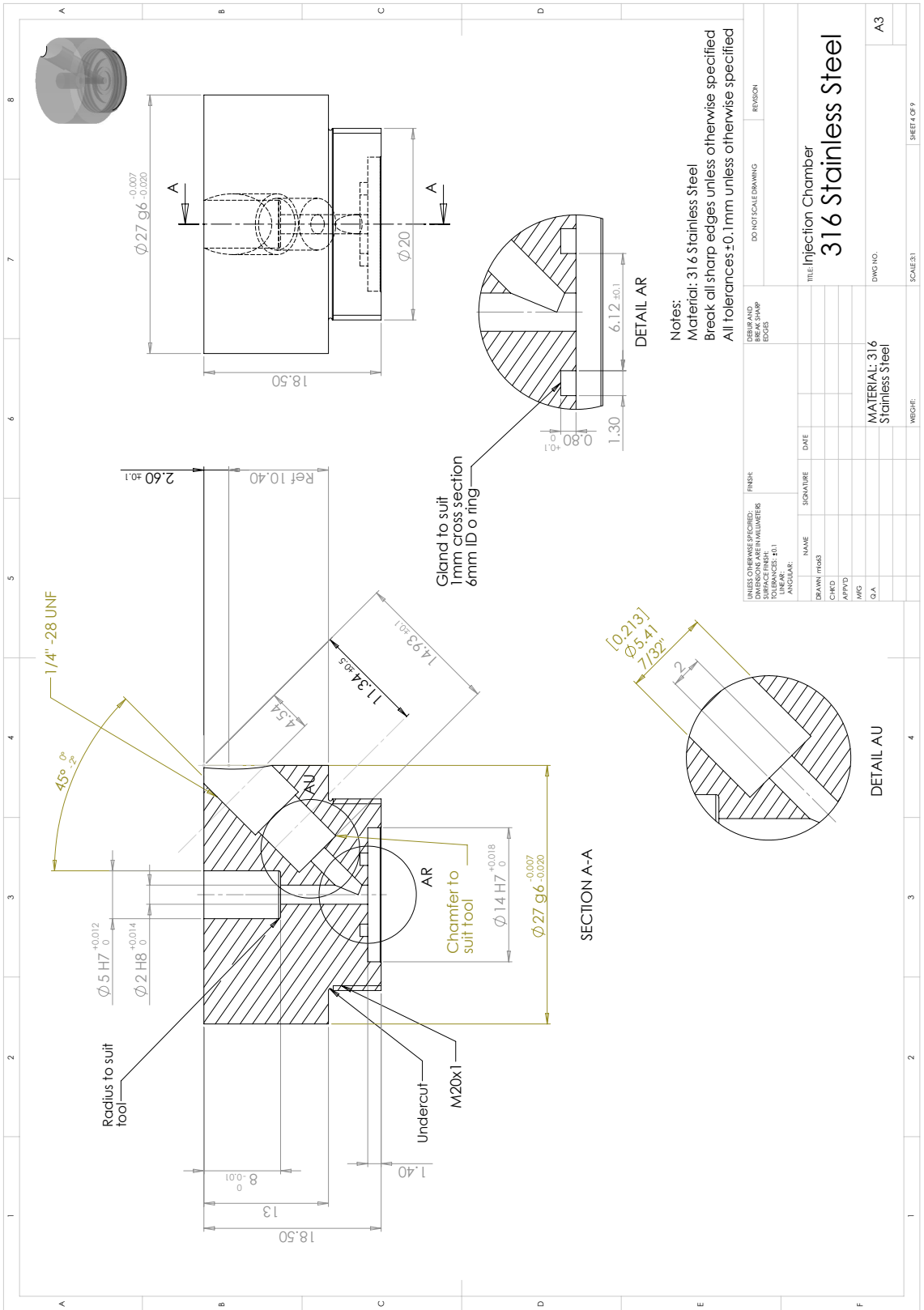
Notes:
Material: 316 Stainless Steel
Break all sharp edges unless otherwise specified
All tolerances ±0.1mm unless otherwise specified
Injection Chamber
316 Stainless Steel
MATERIAL: 316 Stainless Steel
A3
SECTION A-A
DETAIL AR
DETAIL AU
Gland to suit
1mm cross section
6mm ID o ring
1/4" -28 UNF
45°
Radius to suit tool
Undercut
M20x1
Chamfer to suit tool
AR
AU
18.50
13
8
1.40
2.60
Ref 10.40
4.54
11.34
14.92
6.12
1.30
0.80
Ø20
Ø27 g6
Ø14 H7
Ø5 H7
Ø2 H8
[0.213]
Ø5.41
7/32"
2

Figure C.14 –

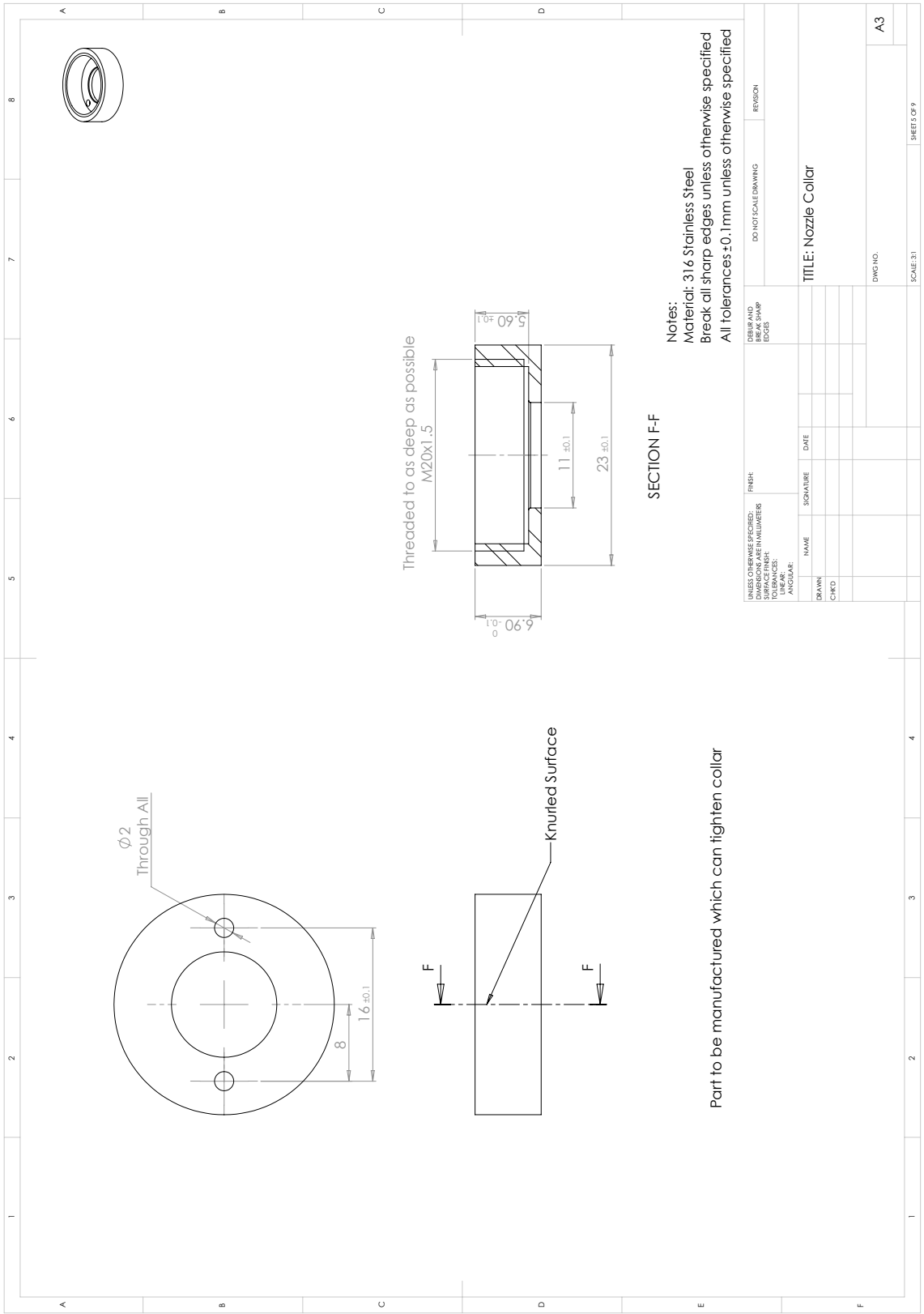
Ø2
Through All
8
16 ±0.1
F
F
Knurled Surface
Threaded to as deep as possible
M20x1.5
6.90 +0.1 0
5.60 +0.1
11 ±0.1
23 ±0.1
SECTION F-F
Notes:
Material: 316 Stainless Steel
Break all sharp edges unless otherwise specified
All tolerances ±0.1mm unless otherwise specified
Part to be manufactured which can tighten collar
TITLE: Nozzle Collar
DWG NO.
A3
SCALE: 3:1
SHEET 5 OF 9
DO NOT SCALE DRAWING
REVISION
DEBUR AND BREAK SHARP EDGES
FINISH:
UNLESS OTHERWISE SPECIFIED:
DIMENSIONS ARE IN MILLIMETERS
SURFACE FINISH:
TOLERANCES:
LINEAR:
ANGULAR:
NAME
SIGNATURE
DATE
DRAWN
CHK'D

Figure C.15 –

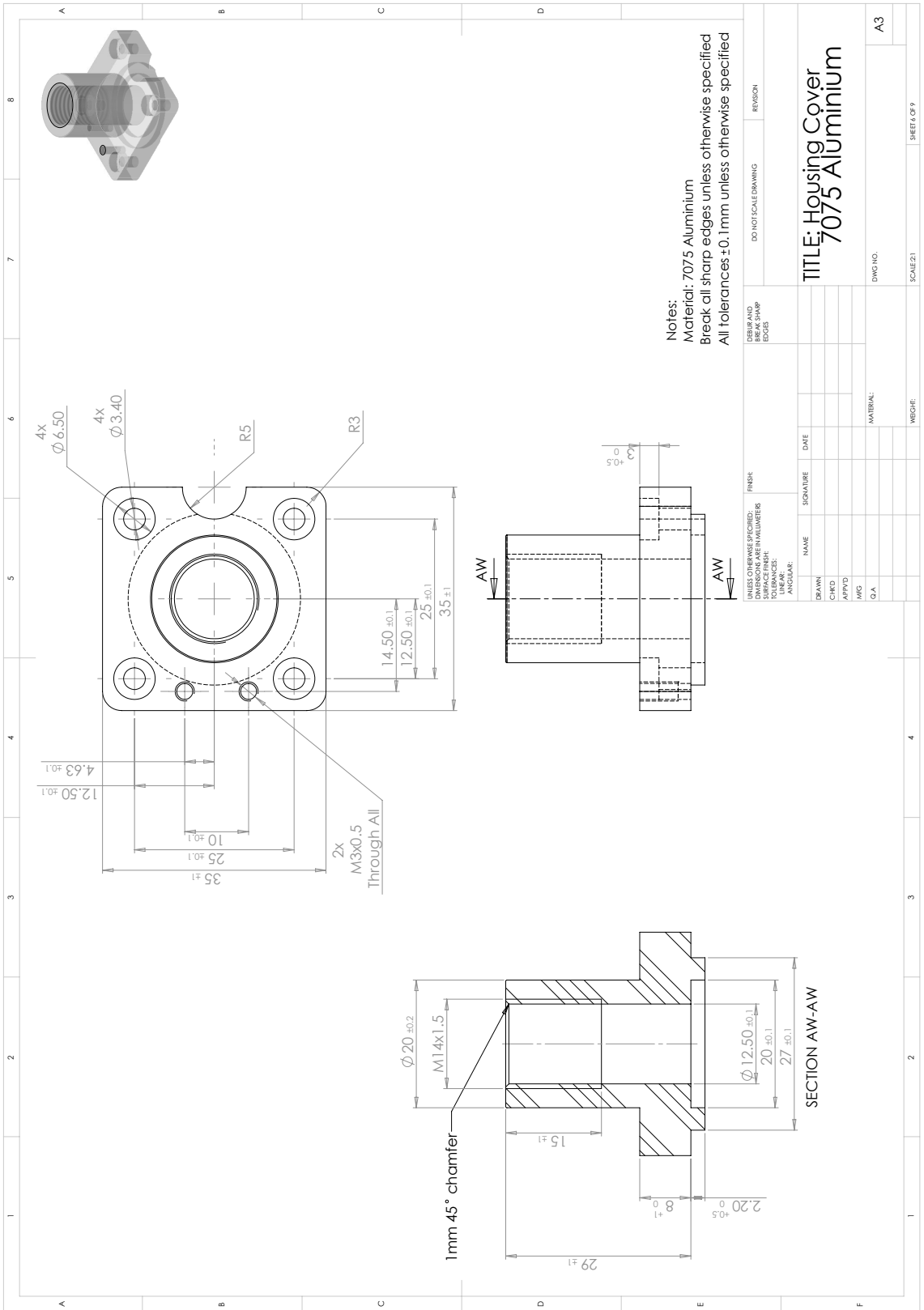
Notes:
Material: 7075 Aluminium
Break all sharp edges unless otherwise specified
All tolerances ±0.1mm unless otherwise specified
TITLE: Housing Cover
7075 Aluminium
A3
SECTION AW-AW
1mm 45° chamfer
4x Ø6.50
4x Ø3.40
R5
R3
2x M3x0.5 Through All
Ø20 ±0.2
M14x1.5
Ø12.50 ±0.1
20 ±0.1
27 ±0.1
15 ±1
29 ±1
2.20 +0.5 0
8 +1 0
14.50 ±0.1
12.50 ±0.1
25 ±0.1
35 ±1
AW
AW

Figure C.16 –

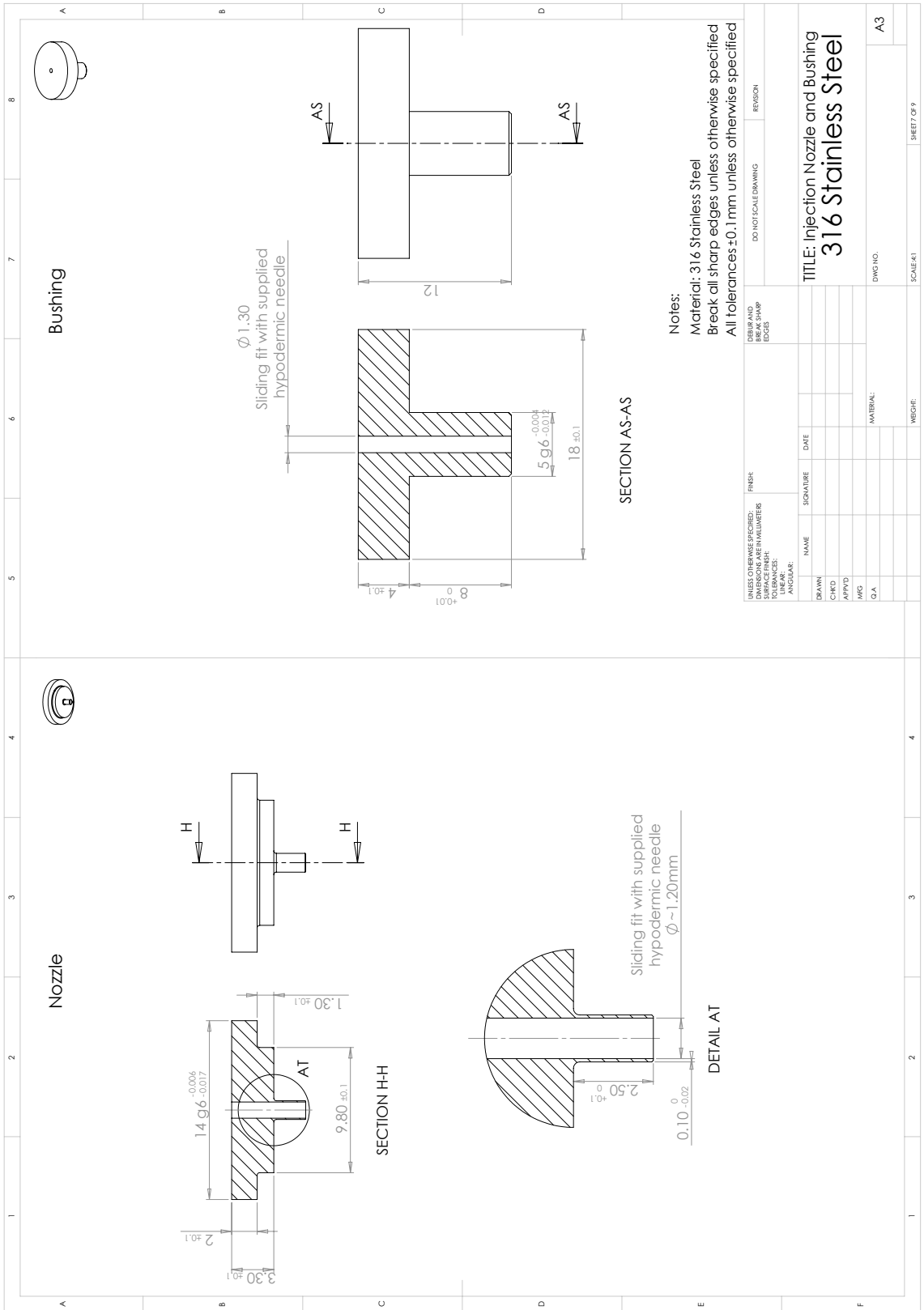
Bushing
Nozzle
SECTION AS-AS
SECTION H-H
DETAIL AT
Notes:
Material: 316 Stainless Steel
Break all sharp edges unless otherwise specified
All tolerances ±0.1 mm unless otherwise specified
TITLE: Injection Nozzle and Bushing
316 Stainless Steel
A3

Figure C.17 –

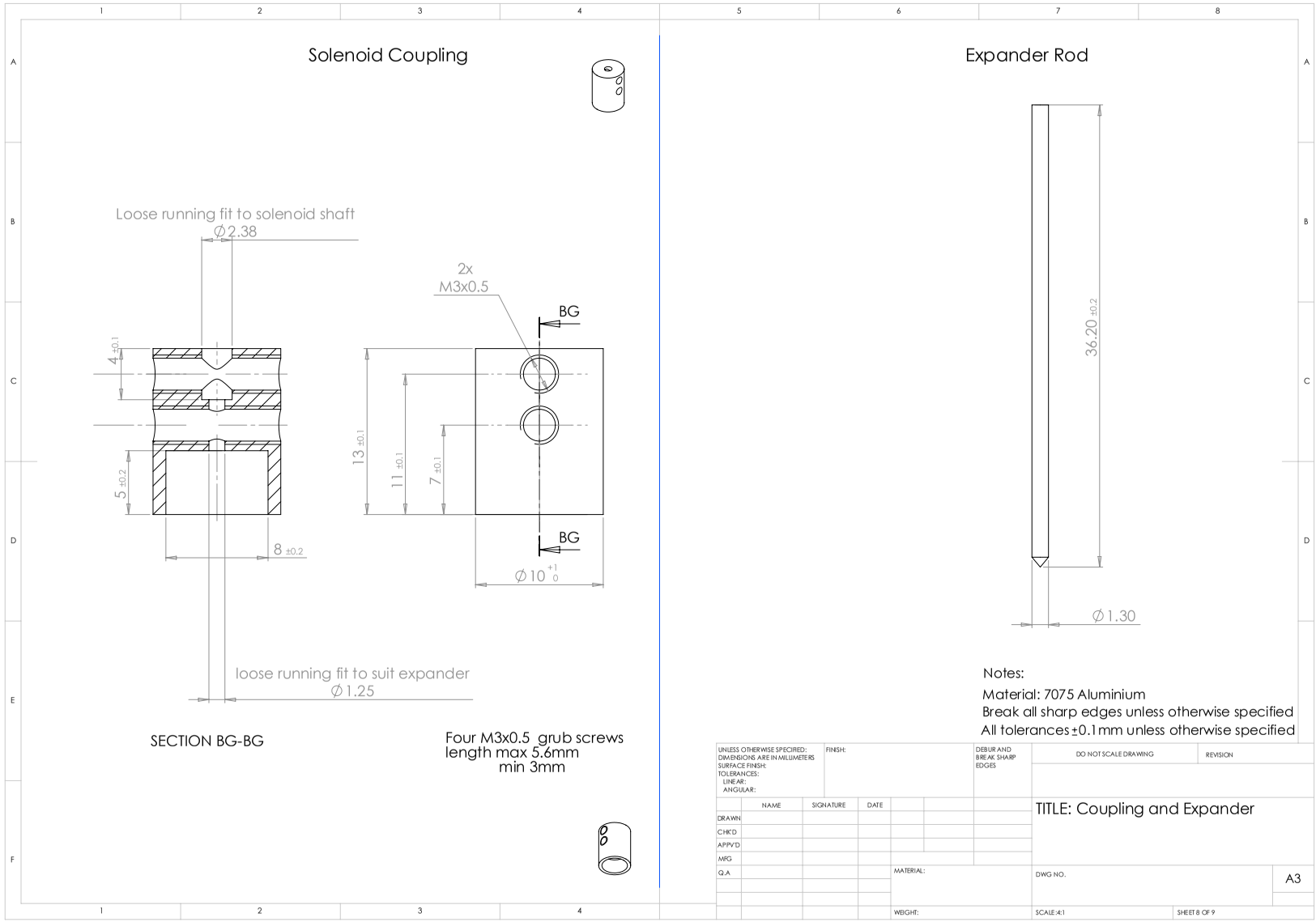
Solenoid Coupling
Loose running fit to solenoid shaft
∅2.38
2x
M3x0.5
BG
BG
4 ±0.1
5 ±0.2
8 ±0.2
13 ±0.1
11 ±0.1
7 ±0.1
∅10 +1 0
loose running fit to suit expander
∅1.25
SECTION BG-BG
Four M3x0.5 grub screws
length max 5.6mm
min 3mm
Expander Rod
36.20 ±0.2
∅1.30
Notes:
Material: 7075 Aluminium
Break all sharp edges unless otherwise specified
All tolerances ±0.1mm unless otherwise specified
UNLESS OTHERWISE SPECIFIED:
DIMENSIONS ARE IN MILLIMETERS
SURFACE FINISH:
TOLERANCES:
LINEAR:
ANGULAR:
FINISH:
DEBUR AND BREAK SHARP EDGES
DO NOT SCALE DRAWING
REVISION
NAME
SIGNATURE
DATE
DRAWN
CHK'D
APPV'D
MFG
Q.A
TITLE: Coupling and Expander
MATERIAL:
DWG NO.
A3
WEIGHT:
SCALE:4:1
SHEET 8 OF 9

Figure C.18 –